Safety and reliability assessment of managed pressure drilling in well control operations

By

©Idris Olusola Sule

A thesis submitted to the School of Graduate Studies
In partial fulfillment of the requirements for the degree of

Doctor of Philosophy

Faculty of Engineering and Applied Science

Memorial University of Newfoundland

July 2019

St. John's, Newfoundland, Canada

Dedicated to

Almighty Allah for His provision of blessings, guidance, and wisdom

Abstract

Managed pressure drilling (MPD) is a technique utilized in drilling to manage annular pressure, hold reservoir influx, and divert mud returns away safely from the rig floor through a closed loop system. Thus, MPD plays key roles in well control operations and in drilling deepwater wells. However, despite the operational, safety, and economic benefits, limited information is available on understanding the complexity of MPD system. Furthermore, the oil and gas industry currently relies on a flow monitoring system for earlier kick detection but faces severe flaws and limited progress has been made on approach that monitors kick from downhole due to the complexity of offshore drilling operations. Thus, the main objective of this research is to assess the safety and reliability of MPD. In this research, following novel contributions have been made: several dynamic downhole drilling parameters have been identified to enhance earlier kick detection technique during drilling, including about 33 – 89% damping of bit-rock vibrations due to gas kick; a reliability assessment model has been developed to estimate the failure probability of an MPD system as 5.74%, the assess the increase in reliability of kick control operation increases from 94% to 97% due to structural modification of the MPD components, identify that MPD operational failure modes are non-sequential, and identify that an MPD control system is the most safety-critical components in an MPD system; an automated MPD control model, which implements a nonlinear model predictive controller (NMPC) and a two-phase hydraulic flow model, has been developed to perform numerical simulations of an MPD operation; and lastly, an integrated dynamic blowout risk model (DBRM) to assess the safety during an MPD operation has been developed and its operation involves three key steps: a dynamic Bayesian network (DBN) model, a numerical simulation of an MPD control operation, and dynamic risk analysis to assess the safety of the well control operation as drilling conditions change over time. The DBRM also implemented novel kick control variables to assess the success / failure of an MPD operation, i.e. its safety, and are instrumental in providing useful information to predict the performance of / diagnose the failure of an MPD operation and has been successfully applied to replicate the dynamic risk of blowout risk scenarios presented in an MPD operation at the Amberjack field case study from the Gulf of Mexico.

Keywords: Kick indicators, Dynamic Bayesian Network, MPD, Reliability, NMPC, automation, Pressure control, Flow control, Blowout, drilling

Acknowledgments

This thesis would not have been possible without the guidance and unending support of several individuals.

First and foremost, I would seize this opportunity to thank my wife for all her sacrifices, caring, love, patience to stick with me through the thin and thick, and for being the neck that supports the head. Boundless gratitude to my two adorable boys for their understanding, especially when daddy is too busy to play. This gratitude is also extended to my mom for her prayers to be successful, my ailing mother-in-law for her prayers and my brothers and sisters, friends, and relatives for their love and prayers.

Deep and profound gratitude to my supervisors, Dr. Faisal Khan, and Dr. Stephen Butt, firstly for giving me the opportunity to work with you and for your patience, guidance, direction, support and encouragement, especially during the challenging times, to accomplish my Ph.D. research work. I am expressing deep gratitude to Dr. Syed Imtiaz for being a member of my supervisory committee and for all your advice on progressing through my research. My deep appreciation also goes to Dr. Ming Yang for his advice, support, and contributions towards this research. I have benefitted greatly and learned from all your advice and seasoned expertise in my research field.

Thank you.

Table of Contents

List of Figures

List of Tables

Nomenclature

Acronym		*Notation*	
2TBN	Two time-slice temporal Bayesian Network	q_{bb}	Backpressure pump flow rate [LPM]
BHP	Bottomhole pressure	P_{bh} , P_{bh}^{set}	Bottomhole pressure and bottomhole pressure setpoint [psi / Bar]
BE	Basic event	β_d β_a	Bulk modulus in the drillstring and annulus [psi / Bar]
BT	Bow-tie	P_c	Choke or surface backpressure [psi / Bar]
BN	Bayesian network	u_c	Choke valve opening input $u_c \in [0,1]$
CBHP	Constant bottomhole pressure	Z_t^i	Components variables at *i*-th node and time-slice *t*,
CPT	Conditional probability tables	ρ	Density [kg/m^3]
DBN	Dynamic Bayesian Network	$\bar{\beta}$	Effective bulk modulus [psi / Bar]
DBRM	Dynamic Blowout Risk Model	P_{frac}	Formation fracture pressure [psi / Bar]
DAPC	Dynamic Annular Pressure Control	P_{pore}	Formation pore pressure [psi / Bar]
ECD	Equivalent circulating density	F_a F_d	Friction factor in the annulus and drillstring
ET	Event Tree	χ_g , χ_L	Gas and liquid mass fractions
FT	Fault Tree	α_g , α_l	Gas and liquid volume fractions
MPD	Managed Pressure Drilling	μ	Mean
NMPC	Nonlinear model predictive controller	N	Number of random variables in Z_t^i
NPT	Non-productive time	$Pa(Z_t^i)$	Parents of Z_t^i
NRV	Non-return valve	k_b	Permeability factor [m^3/sPa]
PRV	Pressure relief valves	P_p	Pump pressure [psi / Bar]
PWD	Pressure while drilling	q_p q_b q_c	Pump, bit, choke flow rates [LPM]
RCD	Rotating control device	P	Probability
SB	Safety barrier	q_{res}	Reservoir influx [BPM]
TE	Top event	q_{inf}^{limit}	Reservoir influx limit [BPM]
		c_G^2, c_L^2	Square of speed of sound in gas and liquid phases [m^2/s^2]
		σ	Standard deviation
		h_{TVD}	Total vertical depth [ft]

Chapter 1 Introduction

1.1 Background

Well control practices have been an integral part of drilling operation planning and strategies in oil and gas exploration and production projects. Thus, there has been an evolution of techniques implemented in parallel with technological advancement assimilated by the industry. For instance, by early 80's, kick (an undesired formation influx into wellbore) detection techniques relied on pit gain and delta flow tracking flow sensors, and by late '80s, significant improvement to sensing devices with reduced false alarms and capability of performing acoustic analysis for faster detection and smaller influx size (0.5 bbl) were made (Lage et al., 1994). Nowadays, the complex nature of oil and gas prospects, which have drifted further into the deepwater, makes this technique inadequate. Meanwhile, a flow check procedure is favoured over the traditional pit gain system for kick detection due to their poor reliability, especially in high permeability formations in deepwater wells where the fracture gradients are typical and the additional volume of gas produced during flow check can be significant (Lage et al., 1994). Shut-in procedures are normally implemented, with activation of blowout preventers, to prevent the escalation of kick event and to circulate the influx out of well.

Typically, well control operation is implemented in two stages. The primary stage is based on preventing kick, and it is conventionally achieved by maintaining the bottomhole pressure more than the formation pore pressure (overbalanced drilling) using a mud weight. The secondary stage is activated to prevent the escalation of kick event into a blowout incident using a blowout preventer (BOP) system. Well blowout results in catastrophic consequences, including personnel injuries and/or fatalities, environmental pollution, loss of assets, and fines (Rice et al, 1987).

Drilling operation is becoming more complex, especially in the offshore operation, and faces many operational challenges, including well control. This is even more significant considering that most remaining prospects for hydrocarbon resources are either driving exploration into deepwater (Graham et al., 2011) or that the existing ones are presented with narrow drilling windows between the pore pressure and the fracture gradient be due to reservoirs depletion or depth. The narrow margins are most prominent in deepwater applications where much of the overburden is seawater (Malloy and McDonald, 2008). Deyab et al., (2018) documented a series of offshore accidents that have stemmed from the loss of well control due to the failure of equipment that is particularly subjected to offshore harsh environmental conditions. These extreme drilling environments heighten geological uncertainty as their complexity are becoming the norm in todays drilling operations. Issues such as, well control incidents, are periodically encountered and can increase operational costs (e.g. lengthy non-productive time - NPT) and risks of operations, especially when relying on conventional primary well control to prevent kick occurrence.

The conventional drilling method merely relies on mud pump flow rates and mud weight to manage the wellbore annular pressure. These methods have been shown to be inadequate in controlling or monitoring wellbore pressure since any pressure events could lead to frequent well shut-in – this condition is termed as “kick-stuck-kick-stuck” scenario. For instance, a small influx to the wellbore (or outflux to the formation) can become significantly uncontrollable quickly and could be consequential to a blowout occurrence. This brings loss not only to the operational assets but human lives. Even the benefits of Underbalanced Drilling (UBD) technology, which includes reservoir damage prevention and increase in the rate of penetration, still present challenges from operational and safety perspectives for offshore applications due to well continuously being flown

to the surface while drilling (Gala and Toralde, 2011). As a result, the oil and gas industry are increasingly adopting "managed pressure drilling" (MPD) practices, which provides safe, efficient, and economical drilling operation while avoiding continuous flow to surface (Gala and Toralde, 2011; Rohani, 2012; Malloy and McDonald, 2008; Kok and Tercan, 2012).

The purpose of an MPD is to control annular frictional pressure losses especially in the fields where pore pressure and fracture pressure gradient have a close margin (narrow drilling window). Because MPD operation is a closed system, influxes and losses are detected instantaneously. This is due to more precise control of the annular wellbore pressure profiles and thus, enhances the safety of rig personnel and equipment in everyday drilling operations. Additionally, MPD operations improve drilling economics by reducing excessive drilling mud costs and reducing drilling-related non-productive time (NPT) as well as enabling the drilling of many declared non-drillable/uneconomical wells.

Many case studies are available on MPD system and techniques that detail its operational advantages, such as precise BHP control, influx management, and economic benefits (Vieira et al.,2008; Grayson, 2009; Nas, 2010; Driedger et al., 2013; Oyovwevotu et al., 2014). Whereas only a few studies explore the safety benefits of an MPD in terms of assessing the risks levels in conventional drilling practice compared to MPD techniques (Grayson and Gans, 2012; Handal A. and Øie, 2013; Gabaldon et al., 2014; Zan and Bicke, 2014; Abimbola et al., 2015). The significance of safety benefits that MPD technologies bring to conventional drilling can be measured or assessed through the boost in safety barrier of conventional primary well control, especially in deepwater drilling. However, limited studies on safety analysis of MPD operations

may be influenced by its limited understanding causing many oil and gas operators to have reluctance in adopting the technology. For instance, there are no clear standards of quantifying the acceptable influx that an MPD system can take to consider the operation safe. Additionally, the operational and economic benefits are well touted by the technology providers, but limited information is available on the complexity of the MPD system and the operational interactions among its components. Thus, more research should be devoted to understanding the complexity of the MPD system and operations as a primary well control safety barrier element to facilitate the development of safety and reliability models that will be inclusive.

1.2 Research scope and objectives

This research aims to assess the dynamics of an MPD system operation and control, and model their failure scenarios, in addition to the safety, reliability, and control system involved in its execution. The reliability assessment of an MPD operation will focus not only on identifying the most safety critical equipment of the MPD system but also in achieving a better understanding of the components' interactions during operation and their modes of failure. Additionally, the research also aims at developing an MPD simulator that implements an advanced control scheme and hydraulic model to numerically perform failure simulations of an MPD operation, develops an approach to interpret failure data using logical description, and develops dynamic risk assessment tool to assess safety of blowout scenarios in an MPD operation.

Furthermore, because an MPD system is primarily employed as part of a well control operation during drilling, the current research also explores other measures, such as earlier kick detection parameters to enhance the kick detection techniques. In summary, the main objective of this

research is to develop an advanced risk assessment methodology to assess the safety and reliability of managed pressure drilling operation and this can be sub-divided as follows:

- To explore and identify downhole drilling parameters for earlier kick indicators as measures of enhancing kick detection techniques during drilling
- To develop an understanding of the components' interactions in an MPD system and their modes of failure
- To identify the safety critical components/equipment of an MPD system
- To develop a numerical model for simulating an MPD control operation and assessing the design limitations and robustness of an MPD system.
- To develop an integrated dynamic risk assessment tool for assessing the safety during an MPD operation
- develop a comprehensive well control tool for field applications

1.3 Novel contributions

This research has novel contributions in the safety and reliability assessment of well control operations during drilling; specifically, by enhancing kick detection techniques and assessing the reliability and safety of a managed pressure drilling in kick control operations. Figure 1.1 illustrates the summary of contributions. Thus, these novel contributions will have significant benefits to the oil and gas exploration and production companies/contractors, particularly in the deepwater drilling where well control operation is a key component of drilling safety, that includes a safety and reliability management tool for managed pressure drilling systems in conjunction with a robust early kick detection technology.

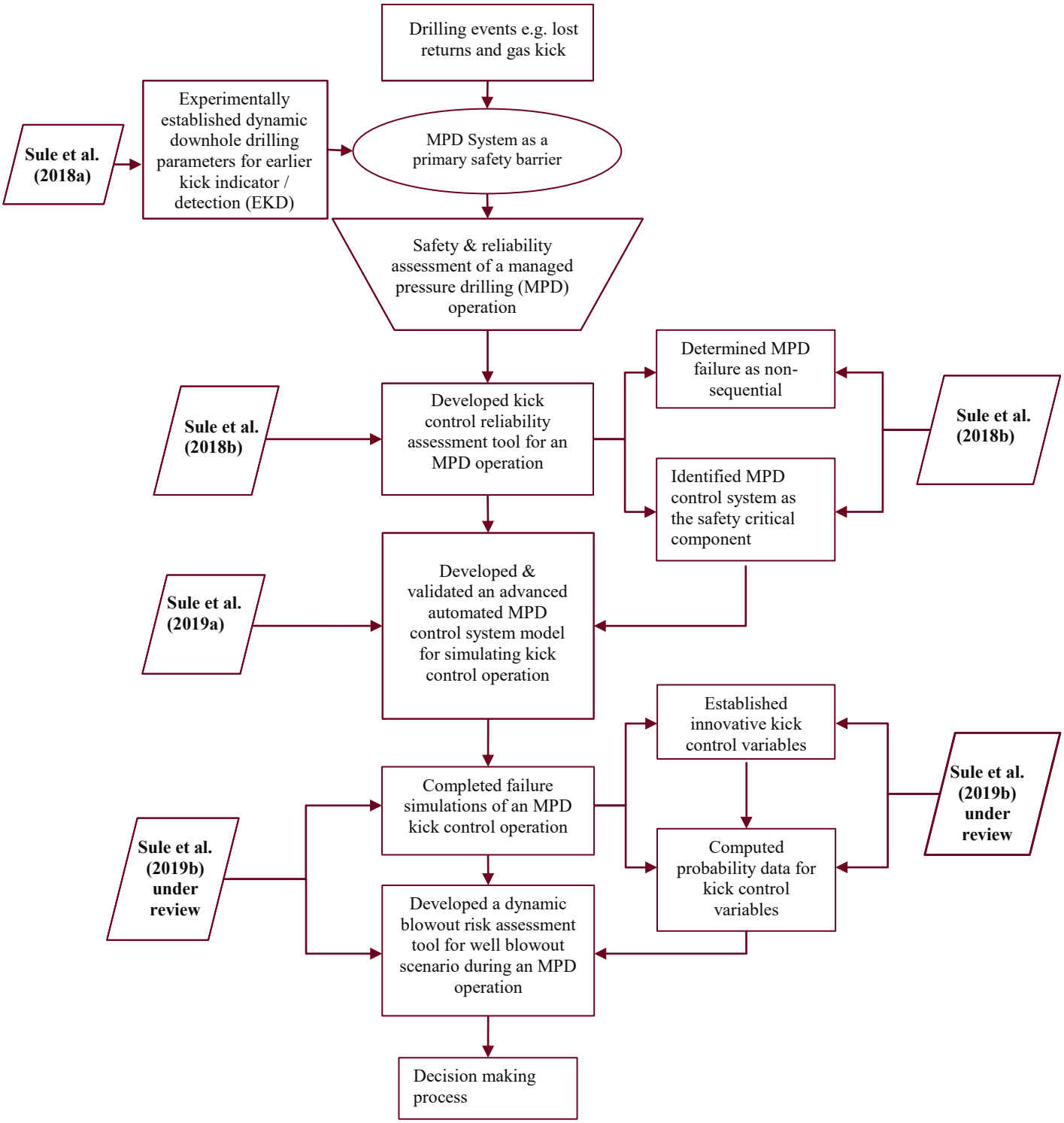

Figure 1.1: Safety and reliability assessment model for a managed pressure drilling in well control operation

1.4 Structure of this Thesis

The thesis has the following structure:

- **Chapter 2** focuses on the literature review of managed pressure drilling (MPD) system and operation as an unconventional primary well control safety barrier element citing both industry and academic literature. It also highlights various MPD techniques and control applications, common equipment involved, safety and economic benefits, and common risk assessment methods in relation to an MPD operation.
- **Chapter 3** focuses on the experimental investigation of dynamic drilling parameters to enhance the earlier kick detection indicators during drilling. The findings provide new improvement into kick detection techniques. This chapter has been published in the published in the *Journal of Petroleum Exploration and Production Technology (2018);* *https://doi.org/10.1007/s13202-018-0510-z*
- **Chapter 4** performs a comprehensive failure analysis of a managed pressure drilling system during kick control operation to identify its modes of failure, most safety-critical component, and reliability on kick control operation. This chapter is published in the *Journal of loss prevention in processing industries (2018); Vol. 52 pp. 7–20.* *https://doi.org/10.1016/j.jlp.2018.01.007*
- **Chapter 5** presents an advanced and robust control model for an MPD control system, which implements a nonlinear model predictive controller and a two-phase flow hydraulic model. This provides flexibility to perform numerical simulation of an MPD kick control operation and have been validated using a field case study and laboratory experiments. This chapter 5 has been published in the *Journal of Petroleum Science and Engineering, Vol. 174 pp 1223-1235* https://doi.org/10.1016/j.petrol.2018.11.046

- **Chapter 6** presents an advanced dynamic blowout risk model (DBRM) to assess the safety during the managed pressure drilling operation. The DBRM involves three key steps: a dynamic Bayesian network (DBN) model, a numerical simulation of an MPD kick control operation, and dynamic risk analysis; and implements a novel approach for simulating an MPD failure and assessing the dynamic risk of a blowout. This chapter is under review in the *Journal of Petroleum Science and Engineering* for publication.
- **Chapter 7** highlights the conclusions and contributions made by this research and suggests recommendations for future research on this topic.

Chapter 2 : Literature Review

2.1 Managed pressure drilling improves well control operation

Generally, well control is one of the key important operations that contribute to successful drilling; however, this operation is more complex and challenging in deepwater drilling. Well control is categorized in to primary and secondary well controls. Primary well control is accomplished by hydrostatic pressure from the drilling mud weight that counterbalances the wellbore pressure. The required hydrostatic pressure by the drilling fluid overbalances the formation pressure to prevent kick or loss of circulation. However, when the primary well control fails due to uncontained formation pressure (kick) or loss of circulation, secondary well control is initiated. Secondary well control is mainly performed by the blowout preventers (BOP), a system that functions to prevent uncontrollable fluid influx into wellbore or blowout of formation fluid to the surface. This conventional drilling practice uses the hydrostatic pressure exerted by mud weight as the main well control barrier to keep the wellbore balanced when not circulating. Mathematically, this is expressed as:

$$P_{MW} \geq P_b \quad (statc\ condition) \tag{2.1}$$

Where P_{MW} is hydrostatic pressure exerted by mud weight and P_b is the bottomhole pressure.

When the pump is activated to resume circulation, the hydraulic system becomes dynamic and annular friction pressure (AFP), created by the motion of the drilling fluid along the entire wellbore depth against the outside diameters of the entire length of the drill string, is introduced. The mud weight and mud pump flow rates are used to primarily control annular pressure. Mathematically, this is expressed as:

$$P_b = P_{MW} + AFP \quad (dynamic\ condition) \tag{2.2}$$

Problems arise with this drilling method when the well has a narrow drilling window, such as in re-entry of partially depleted reservoirs or deepwater, which is common in oil and gas fields today. In this case, annular pressures are challenging to control due to kick-loss-kick-loss scenarios. Thus, any delays in detecting the influx and reacting could lead to a blowout incident. The well control management process can be highly time-consuming and leads to very costly non-productive time.

Underbalanced drilling operation on the other hand, uses a closed hydraulic system with appropriate equipment and controls to intentionally lower bottomhole pressure below the reservoir (pore) pressure *(P_{pore})* to induce influx into the wellbore with the aim to protect, and preserve reservoir from damage in addition to increasing rate of penetration (ROP). Mathematically, this is expressed as follows:

$$P_b < P_{pore} \tag{2.3}$$

Because this method allows influxes traveling up to the surface, many operators are skeptical in adopting underbalanced techniques, especially in offshore fields due to regulatory restrictions against gas flaring, wellbore instability potential, safety concerns exposing toxic gas release to the surface in high pressure environments, and cost (Birkeland et al., 2009).

However, managed pressure drilling, which is defined, by the International Association of Drilling Contractors (IADC), as an adaptive drilling process used to precisely control the annular pressure profile throughout the wellbore with intention to avoid continuous influx of formation fluids to the surface as well as employing appropriate process to safely contain any influx incidental to the operation events (Malloy and McDonald, 2008). Alternatively, an overbalanced drilling where a constant or correct bottomhole pressure is being maintained in a closed system by using a

combination of backpressure, mud weight, and equivalent circulating density (ECD) can be termed as MPD (Gala and Toralde, 2011). MPD operation uses the closed hydraulic system with the ability to monitor and control backpressure, fluid density, fluid rheology, circulating friction, and/or annular fluid volume; hence may allow faster corrective action to address any pressure events (Malloy and McDonald, 2008). When running an MPD operation backpressure can be applied on the wellbore annulus via a rotating control device (RCD) to control the bottomhole pressure during drilling or in a static condition. The backpressure can be manually or automatically controlled by choke settings; hence, provides a timely control of kicks and mud loss. These can be expressed mathematically as follows:

$$P_b = P_{MW} + ECD + \text{Back pressure} \qquad \text{(during drilling)} \tag{2.4}$$

$$P_b = P_{MW} + \text{Back pressure} \qquad \text{(during static condition)} \tag{2.5}$$

During static condition, the choke is used to add backpressure when drilling stops to maintain the bottomhole pressure instead of pumping heavier mud downhole.

2.2 Managed pressure drilling equipment

An oil rig that is either proactively and reactively configured to run MPD system is equipped with several key components, including rotating control device (RCD), non-return valves, drilling choke manifold, MPD control system, and backpressure pump as shown in Figure 2.1. These are described below:

- **Rotating control device** - (also called rotating control head) primarily functions to divert flow away from the rig floor and is mostly located atop of the annular preventer and complements the rig standard blowout preventer (BOP) stack. During operation, it forms a frictional seal around the drill pipe ball to create the closed-loop drilling system and allow backpressure to

be applied on the annulus to maintain well control. The design ratings and size are drilling application specific and are available in static pressure of 1000, 2500, and 5000 psi (Halliburton, 2016).

- **MPD choke manifold** - is a pressure regulator of MPD system that serves to control the wellhead pressure to the desired set point. Its openings are constantly adjusting to a changing flow rate through the chokes to maintain the desired downhole pressure. The choke manifold is available in many trim sizes as well as in automatic or manual controls. *A manual choke* allows the designated rig crew to control the backpressure manually with hydraulic control panel or by means of a software application. While the *automatic choke* is controlled by electronic monitoring equipment that has the quickness and precision required to adjust the back pressure to maintain desired downhole pressure. Many manifolds available today can also feature as early kick detection (EKD) with the use of a flow meter (Gala and Toralde, 2011).
- **Non-return valves (NRV)** – serves to prevent backward flow from the well up the drill string when applying back pressure on the annulus. They are normally installed in the bottomhole assembly (BHA) and it is recommended to install two or more NRVs to increase the redundancy with one located at the end of BHA and least another one located in the top of drilling string to aid bleeding of pressure; hence, increases the operational safety (Stødle et al., 2013).
- **Back pressure pump (BPP)** – is installed or available for MPD operation to maintain wellhead pressure throughout the drilling operation. Typical MPD system uses BPP to provide fluid supply and adequate flow to maintain the choke in a situation where the mud flow decreases in volume that the choke is not able to create the needed back pressure. In this case, the choke may not provide adequate backpressure, hence, the extra boost can be automatically

supplied by the BPP, which in part serves as a redundancy to mud pump failure or human error (Stødle et al., 2013).

- **Optional Equipment** – are more other specialized equipment important for specific MPD applications. According to IADC (2014), other key enabling equipment, either individually or in performance with other equipment to practice MPD operations includes downhole deployment valves (DDV), mud/gas separators of adequate capacity, nitrogen production units etc.

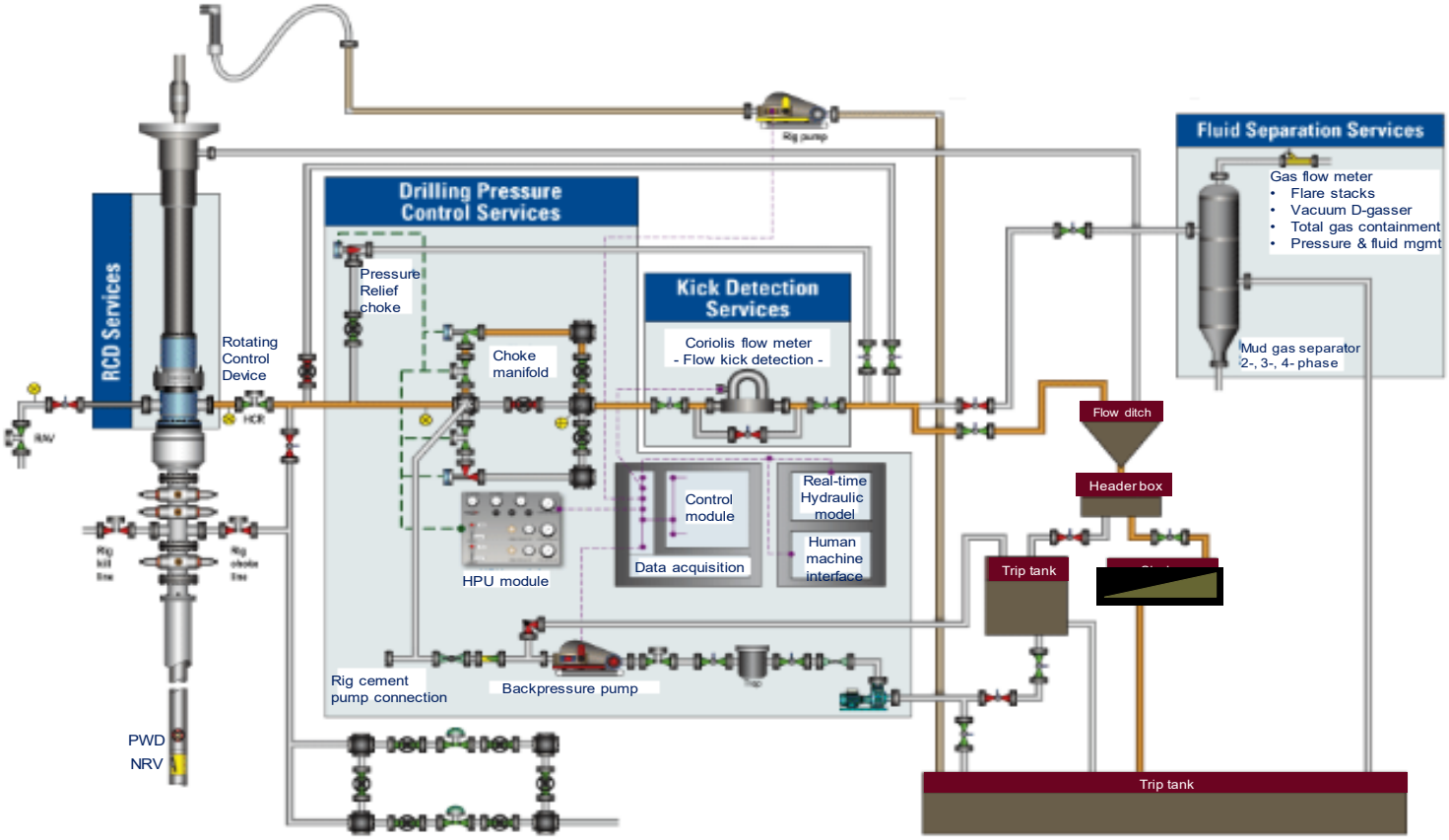

Figure 2.1: Generic MPD process flow system (Source: Schlumberger)

2.3 Managed Pressure Drilling Techniques

There are four basic MPD techniques that are well specific and are: constant bottomhole pressure drilling (CBHD), pressurized mud cap drilling (PMCD), dual-gradient drilling (DGD) method, and return flow control (RFC)-HSE method. According to IADC (2014), CBHP and PMCD have been safely and effectively practiced globally on prospects believed un-drillable with conventional method due to safety, economic or technical reasons. However, RFC-HSE method is just starting to be recognized as maybe a better way to drill some prospects that could be drilled conventionally and while DGD is still in its infancy, there have been hundreds of riser-less DGD applications, DGD with a marine riser, and subsea BOP.

2.3.1 Constant Bottomhole Pressure Drilling (CBHD)

It is uniquely suited for environments with narrow pressure window (Hannegan, 2006) such as the deepwater wells, and regarded as the most commonly practiced managed pressure drilling technique IADC (2014). The bottomhole pressure is regulated and maintained nearly constant and within a predefined pressure window imposed by the pore pressure and fracture pressure. Essentially, the backpressure can be applied or relieved in the annulus via choke manifold to achieve the pressure control in the wellbore (Gala and Toralde, 2011). CBHP technique has the potential to reduce the number of casing strings, hence reducing drilling costs. This MPD technique uses hydraulics models to establish wellhead pressure and maintains a suitable equivalent circulating density (ECD), annulus pressure gradient, and annulus ECD at a selected location in the wellbore. All CBHP systems, which include the dynamic annular pressure control (DAPC) @balance system by Schlumberger (see Figure 3.1), Weatherford MPD technology, and GeoBalance® Managed Pressure Drilling (MPD) by Halliburton, perform these three objectives. Unlike the DAPC control system, Weatherford MPD technology utilizes the Microflux® control

system while Halliburton MPD uses the combination of an Automated Choke Control System, a GeoBalance® Sentry™ Data Acquisition and the Halliburton INSITE Anywhere® GeoBalance® system.

2.3.2 Pressurized mud cap drilling (PMCD)

It is an MPD technique that is suited for fractured formations where severe loss of circulation can occur. Its operation involves drilling with no returns to surface and an annulus fluid column, assisted by the surface backpressure, is maintained above a formation pressure capable of accepting fluid and cuttings (Gala and Toralde, 2011). PMCD deals with loss circulation by first pumping sacrificial (lighter) mud to drill the depleted zone and then heavier mud to force the fluid into the loss zone and prevent influx gas from coming to the surface (Hannegan, 2006; Terwogt et al., 2005). Drilling operation keeps any influx and sacrificial fluid into the depleted zone. Also, in addition to RCD and other MPD equipment, PMCD requires a flow spool to be installed below the RCD to allow fluid to be pumped into the annulus (Rohani, 2012). Weatherford MPD technology, which utilizes the Microflux® control system, can be configured to run in a PMCD mode.

2.3.3 Dual Gradient Drilling (DGD)

It is an MPD technique that involves drilling with two different fluid-density gradients; such that the lighter fluid (e.g. seawater) is above the seafloor (or upper portion of the wellbore) and the heavier fluid is below the mud line (Abimbola et al., 2015; Rohani, 2012) to deliver the same bottomhole pressure that normally achieved by a single fluid gradient (Smith et al., 2001). This setup can be achieved by installing an RCD above the mudline to divert the return mud away from the riser through a return line to the surface and fill the riser with lightweight fluid. This technique has only been practiced in the deepwater operation where the total mud column in the marine riser

can create substantial overbalance in the well (Stødle et al., 2013) and its implementation eliminates the impact of water depth on the mudline. The need for DGD technology emerged out of the concept to reduce the riser weight and mud volumes, especially in an ultra-deepwater operation where there is reduced fracture gradient of formations below the mudline (Smith et al., 2001).

2.3.4 Return Flow Control (RFC) / HSE technique

RFC/HSE technique is considered as a passive variation of MPD system in that the technique does not involve any control of the annular pressure but diverts annulus returns away from the rig floor, while drilling using conventional method, to prevent any gas exposure to the rig floor. RFC technique requires the installation of two hydraulic valves, a conventional flow line to the shakers, and a flow line to the rig choke manifold in addition to the RCD to achieve these objectives (Rohani, 2012).

2.4 MPD control algorithms

In an automated MPD system, a combination of hydraulic model and control system is used to automatically control downhole pressure during drilling operations (Godhavn 2010; Godhavn et al., 2011). The key objective of an MPD is to accurately control the downhole pressure by regulating the backpressure to compensate for annular pressure fluctuations. Thus, in an automated MPD system, the automatic operation of the choke manifold is performed by a control system, which typically consists of two main parts: a hydraulic model (to estimate the downhole pressure in real-time) and a controller scheme (to automates the choke manifold to maintain the desired choke pressure). The hydraulic models can be simple or advanced, although the latter is more

challenging and complex (Kaasa et al., 2011) and the controller ranges from proportional integral derivative (PID) controller scheme to a non-linear model predictive controller (NMPC).

PID controller utilizes feedback and feed-forward control actions to control the choke pressure, whereby the feed-forward loop compensates for disturbances gain and the closed loop feedback compensates for error and maintain system equilibrium. To improve the performance and the capabilities of kick estimation and automatic well control system, Zhou et al. (2010) presents adaptive observers for estimating the flow rates through the well and the reservoir pore pressure for improved kick management using a PI controller. Zhou et al. (2011) presents an MPD automatic control procedure, which uses a switched control scheme and a PI controller that, on one hand, regulates the annular pressure in the well during drilling and on the other hand, attenuates kick in the event of a reservoir influx. Godhavn et al. (2011) presents a nonlinear model-based control scheme and observers to improve pressure control during MPD operations using a feedback linearization method. Hague et al. (2013) utilizes a switched control concept in controlling bottomhole pressure; whereby an MPD system controller manipulates the choke and backpressure pump by switching between a combination of pressure and flow control when there is no influx, and pure flow control when a kick is detected.

However, most processing systems are nonlinear; thus, making the PID controller insufficient, in some cases, to capture the nonlinearity of the system. Furthermore, another important aspect of an MPD control model is the accuracy of estimating the choke pressure, bottomhole pressure and kick size. Unfortunately, this topic has not been adequately addressed in most MPD control model simulations and only a few studies have sparsely discussed the effects of gas-phase influx in their MPD control simulator (Zhou et al., 2011; Kaasa et al., 2011; Aarsnes et al., 2016).

2.5 MPD Contributions to drilling

Two of the primary contributions of MPD are the reduction in drilling costs due reduction in NPT and increase in safety due to additional primary well control barrier it provides. In deepwater operations, many projects would not be economically viable without MPD techniques (Haghshenas et al., 2013). Many studies are available on MPD system and techniques that detail its operational advantages, including a precise BHP control, influx management, and economic benefits, including Driedger et al., (2013) on how MPD system enabled Talisman Energy to drill to the target depth through overcoming multiple abnormal pressure zones due to its features in early influxes and losses detection, dynamic equivalent mud weight management, maintenance of bottomhole pressure during static conditions.

However, only a few studies explore the safety assessment of an MPD in well control operation. The significance of safety benefits that MPD technologies bring to conventional drilling can be measured or assessed through the boost in safety barrier of conventional primary well control, especially in deepwater drilling. For instance:

Grayson and Gans (2012) examined the key elements of a closed-loop circulating system (including RCD and MPD influx control) and concluded that it increases the well control barrier layers and efficiency of drilling operations. They used the PRA model to compare the risk levels in using pen loop system (conventional well control) and closed loop system (MPD). They developed a blowout scenario using a fault tree model for each system in which they factored in human errors probability (HEP). The fault tree model for the MPD system depicts the ability of the MPD system to diagnose and mitigate influx based on the combination of HEP, MPD control

system, and the hardware system. Their analyses show that the additions of MPD and RCD into well control barrier layer reduced the possible risk of a blowout by almost 500%.

Handal A. and Øie (2013) performed safety barrier analysis and structured hazard identification of MPD system to identify its safety critical equipment due to the complexity that MPD pressure control equipment and MPD control system bring to well control. As a result, the authors focused their analysis on primary well barrier system with MPD pressure control equipment (mud + MPD system), which defers from the conventional primary well barrier configuration. They used FTA to illustrate the how failure in MPD pressure control equipment may be critical to BHP exceeding pressure limits of exposed formations and failure of MPD control system may lead to loss of well control.

Gabaldon et al. (2014) used well control barrier envelopes to describe how MPD improves influx management and prevent unnecessary shut-in or, in the worst case, blowout. They defined the primary safety barrier elements in conventional drilling to include drilling mud, casing, and cement while in MPD system, it includes: MPD equipment (e.g. RCD, choke manifold, back pressure pump, MPD control system etc.) in addition to conventional primary barrier elements. The secondary barrier envelope (SBE) include elements in the primary envelopes as well as BOP, choke line, kill lines and manifold for both MPD and Conventional drilling.

Zan and Bicke (2014) developed a probabilistic risk analysis (PRA) model to quantify the probability of a well control incident (WCI) in conventional drilling and how the WCI can be mitigated by MPD system. Their model translated the qualitative assessments in 2008 DOI MMS report into the quantitative assessment. Based on assumed probabilities for each deviation categories developed in their model, they obtained WCI probability of [0.0085]. This value was

reduced by 20% when MPD was implemented (i.e. the probability of WCI reduced to $[1.7 \times 10^{-3}]$). Handal A. and Øie (2013) performed barrier analysis and structured hazard identification of MPD system to identify its safety critical equipment due to the complexity that MPD pressure control equipment and MPD control system bring to well control.

According to Handal and Øie (2013), MPD systems, from a risk-based perspective, introduce both advantages (such as improved control of the BHP and enhanced well control) and challenges. The challenges stem from the fact that varieties of pressure control equipment are used to precisely adjust wellbore pressures, which in turns are controlled by an MPD control system. The applications of MPD have been seen to be common in areas (or prospects) where well control have been most challenging, un-drillable and conventionally drilling wells have failed or grossly exceeded budgets (Kok and Tercan, 2012; Handal and Øie, 2013).

Limited studies are available in assessing the operational failure of constant bottomhole pressure techniques of MPD. Abimbola et al. (2015) identified MPD control system, Rig pump, and RCD as the safety-critical equipment. However, a further investigation by Sule et al. (2018b) identified, in addition to MPD control system being the most safety-critical component, that the failure of MPD operation can occur via several scenarios in a non-sequential manner. These studies bring MPD control system, which can be classified as a form of automated drilling technology, under the microscope of safety and reliability investigation. To capture the nonlinearity in an MPD control system, Nygaard and Nævdal (2006); Breyholtz and Aamo (2008); Nandan and Imtiaz (2016); Park (2018) have implemented nonlinear model predictive controller (NMPC) in their control model. However, their hydraulic models are based on single-phase liquid flow, and did not

capture the multiphase-flow nature of the reservoir fluid. For instance, gas kick incident is particularly severe and challenging to manage, especially in a deepwater drilling. Unfortunately, this topic has not been adequately addressed in most MPD control model simulations and only few studies have indicated the effects of gas-phase influx in their MPD control simulator. Zhou et al. (2011) noted that because their model does not account for gas-phase, the estimation of reservoir fluid that contains gas-phase will cause considerable modelling error in influx size. As discussed in Kaasa et al. (2011), an influx of liquid and gas mixture into the annulus will cause the bulk modulus in the annulus to drop; thus, affect the model estimation of influx size and/or the casing pressure if the gas-phase of the reservoir influx is not considered.

2.6 Safety and reliability assessment techniques

Many risk assessment techniques have been proposed for oil and gas and chemical process operations. Khan (2001) presented most notable risk analysis techniques, including quantitative risk analysis and probabilistic safety analysis. Process safety, in the oil and gas operations, is typically assessed using various risk and reliability analysis tools to identify the critical failure components of the system and capture the level of risk (consequence) associated with the failure. Many reliability and risk analysis tools for offshore operations and chemical processes have been covered in the literature (Haver et al., 2001; Khan, 2001; Khan et al., 2002; Espen et al., 2011; Khakzad et al., 2012; Dikis et al., 2016). Khan (2001) presented the most notable risk analysis tools, including quantitative risk analysis and probabilistic safety analysis.

The quantitative risk analysis (QRA) technique, which comprises of four stages (from initial to final): hazard identification, frequency estimation, consequence analysis and measure of risk, can be performed using several diagnostic tools, including the fault tree analysis (FTA), event tree

analysis (ETA), and Bow-tie (BT). Fault Tree Analysis (FTA) is a deductive failure-based approach, and the most common probabilistic techniques used in system risk and reliability assessment (NASA, 2002). FTA starts with an undesired event, such as failure of the main equipment, and then determines its causes using a systematic, backward-stepping process (NASA, 2002). The quantification of an FT allows the determination of reliability parameters of interest for design improvement (NASA, 2002). FT can be evaluated either qualitatively to provide useful information on the causes of an undesired (top) event through gates or quantitatively to provide information on the failure probability of the top event occurrence and all the intermediate events given the knowledge of all basic events (NASA, 2002; Abimbola et al., 2015).

ETA is an inductive procedure that shows, in sequence, all possible outcomes resulting from an initiating event and additional (pivotal) events, considering whether the installed safety barriers are functioning or not (Rausand and Høyland, 2004). It can identify all potential accident scenarios and their sequences in a complex system and determine the probabilities of various outcomes resulting from the initiating event. The Bow-tie (BT) is one of the common and effective graphical method used in a risk evaluation to analyze and assess the consequences of causal relationships in high-risk scenarios, such as a blowout. The BT is constructed by connecting a fault tree top event to one or more elements of the event tree. However, these conventional risk assessment techniques, including Fault Tree (FT), Event Tree (ET), and Bow-Tie (BT) are incapable of capturing the dynamic effects of operational risks, such as change in well conditions due kick or sudden failure of equipment during drilling operations, and inability to assess the sequential dependencies among process variables in risk estimations (Barua et al., 2016; Khakzad, et al., 2012; Ferdous, et al., 2010).

Bayesian network (BN), however, is a more flexible modelling approach that is capable of performing both forward and backward analyses uniquely suitable for dynamic risk and safety analyses using conditional probabilities and probability reasoning to describe the causal influence relationships among dependent and independent variables (Bobbio et al., 2001; Khakzad et al., 2011, 2013; Cai et al., 2013; Barua et al., 2016; Sule et al., 2018b). The BN model, which is originated from the field of artificial intelligence (Langset and Portinale, 2007), have been developed to overcome the modeling deficiencies exhibited in FT, ET, and BT risk analysis techniques (Cai et al., 2012, 2013) and have been explicitly covered in the literature (Khakzad et al., 2011, 2013; Abimbola et al., 2015; Bhandari et al., 2015; Pui et al., 2017; Sule et al., 2018b). BN models can analyze the influence of dynamic risk variables such as drilling conditions (Wu et al., 2016). However, BN model is only restricted to one step posterior analysis and are not capable of explicitly modeling the changes in events likelihoods or relationship over time.

Thus, a dynamic Bayesian Network (DBN), which is a temporal extension of BN capable of modeling influences over time, has been developed to address the dynamic restrictions in the BN models (Murphy, 2002; Cai et al., 2013; Wu et al., 2016). The DBN models have been used in many probabilistic analyses of dynamic systems and operations across many industries, including oil and gas, process, manufacturing, computing etc. For instance, Cai et al., (2013) in quantitative risk assessment of human factors on offshore blowouts; Wu et al., (2016) in prediction and diagnosis of offshore drilling incidents; Dong C. and Yue H. (2016) in identification of functional connections in Biological neural networks; Amin et al., (2018) in dynamic availability assessment of safety-critical systems; Zhu et al., (2019) in Fatigue damage assessment of orthotropic steel deck; Luque and Straub (2019) in optimal inspection strategies for structural systems.

Chapter 3 : Experimental investigation of gas kick effects on dynamic drilling parameters

Preface

This chapter presents the experimental investigation of dynamic drilling parameters to enhance the earlier kick detection indicators during drilling. The findings provide new improvement into kick detection techniques, including the damping effects of drilling vibrations due to gas kick. A paper version of this chapter has been published in the ***Journal of Petroleum Exploration and Prod Technol (2018)****, https://doi.org/10.1007/s13202-018-0510-z. Along with the co-authors, Dr. Faisal Khan and Dr. Stephen Butt, I have co-authored this chapter. I conducted the experiment to generate the data and made first attempt to analyze the data. The co-author Faisal Khan helped in analyzing and testing the concepts, reviewed and corrected the data and results, and contributed in preparing, reviewing and revising the manuscript. The co-author Dr. Stephen Butt contributed through assisting in developing and running the experimental setup, generating and analyzing the data, testing and verifying the results and revising the manuscript. Co-authors Drs. Butt and Khan reviewed the revisions and provided feedback which I have implemented. I prepared the first draft of the manuscript and subsequently revised the manuscript based on the co-authors' feedback and the peer review process.*

Abstract

Blowout incidents not only lead to fatalities but also cause loss of assets, expensive clean-up, costly incident investigations and reports, and negative impact on the environment. The 2010 Macondo blowout accident in the Gulf of Mexico was an eye-opener for many oil and gas operators and oilfield service companies; thus, making early kick detection technology research one of the top industry agenda. However, only limited progress has been made in detection technologies that

focus on downhole parameters due to the complexity of offshore drilling operations that is increasingly shifting towards the deepwater. Therefore, the current chapter experimentally explores downhole drilling parameters for kick indication during drilling. The study utilizes a fully instrumented laboratory scale drilling rig coupled with air injection and surface monitoring systems. This study observed a sudden jump in bottomhole pressure, increased volume of the return fluid, decreased density of the return fluid, reduced rate of penetration (ROP), and increased rotary speed as indicators of kick. The most significant new finding, which is also validated with field reports, is the damping effects of the drilling vibrations due to kick. Frequency analysis of the axial bit-rock displacements/vibrations confirms changes of frequencies due to kick induction during drilling. Coupling this important finding with dynamic drilling models, the response of the drilling system at the surface (e.g. standpipe, choke pressures etc.) indicating this change can be predicted.

Keywords: Kick Indicators, Drilling, Axial Bit Vibrations, Early Kick Detection

3.1 Introduction

Early kick detection (EKD) is a vital component of a well control system. The prevention or management of kicks and/or fluid loss occurrence during drilling operations is crucial, particularly in deepwater drilling activities due to the complexity of equipment and operations. Well control failure occurrences could typically cost the oil and gas industry billions of dollars in a year due to non-productive time (NPT) and/or blowout incident and affect the safety of drilling personnel. In addition to the complex operation involved with deepwater drilling, many deepwater wells have greater depths and narrow pressure margins between pore pressure and fracture gradient, which

heighten the risk of unexpected events such as a kick or fluid loss. Given the extent of these challenging drilling operations coupled with today's low oil and gas prices, oil and gas operators are continually striving to improve not only the drilling efficiency but also to understand the behaviour of downhole fluid to survive and grow.

Blowouts can be disastrous, expensive, and cause fatalities; a good example was the dramatic BP Deepwater Horizon blowout in 2010. Several investigative reports indicate a need for more sophisticated EKD technologies among other root causes (Graham et al., 2011). Unfortunately, limited progress has been made due to more reliance on surface detection technologies which are challenged by response time. There is a widely accepted consensus in the industry to explore a bottom-up approach whereby kicks are detected early and can be tracked at multiple points along the wellbore. However, only limited progress has been made on this approach due to the complexity of offshore drilling operations. Velmurugan et al. (2015) presented an automated system for EKD and a control system that monitors and reports the physical conditions inside wellbore annulus instantaneously through time measurements of p-waves' propagation in the annulus. Its performance is questionable for field applications. Nayeem et al. (2016) experimentally investigated kick occurrence based on the changes in mass flow rate, pressure, density and conductivity of fluid downhole and concluded that the parameters have the potential to improve the kick detection system with higher precision than the surface detection system.

Vajargah and van Oort (2015) developed an algorithm that automatically selects the best well control response to influx in a drilling operation running a constant Bottomhole pressure (CBHP) managed pressure drilling (MPD); however, the paper did not clarify how this method will be

implemented while running CBHP MPD operation in the field. Trivedi (2014) proposed an innovative kick detection system that uses a small mud rerouting section consisting of two plates and located just above the BHA. When there is an entrained formation fluid bubbles/droplet in the flow, the medium between the two plates will undergo alteration and form a magnetic impulse registering as an abnormality in fluid flow, hence detecting kick. However, this technology has many limitations, including cuttings intrusion and capacitance limitations due to plate spacing. Ahmed et al. (2016) proposed a new advanced early kick detection method that uses seven parameters data (classified as instantaneous drilling parameters e.g. pit gain, flow rate, ROP etc. and lagging parameters e.g. total gas connection gas etc.) from mud logging while drilling; however, this method was field specific (Offshore Nile Delta field). Schubert and Wright (1998) proposed the use of an acoustic device installed on the casing valve to continuously monitor the liquid level in the annulus of wells experiencing a complete loss of returns; thus, a rise in the liquid level is interpreted as early kick indication.; however, this method has a limitation of lagging time that was not addressed by the authors.

DiFoggio and Duncan (2012) presented, in a patent, a tool and method that measure the acoustic velocity and temperature of borehole fluid from an acoustic sensor and temperature sensor placed in a borehole to detect a gas influx in real-time due to lower bulk modulus and density of the fluid and temperature drop. This is the closest and tested downhole detection methods, but it is only limited to and/or relied on borehole density and temperature parameters. Involving more downhole parameters in early kick detection indicators not only improve the reliability of kick detection but also provides the capability to validate kick occurrence when there are deviations in these parameters.

Thus, this chapter experimentally monitors dynamic drilling parameters, including WOB, rotary speed, drilling vibrations etc. during drilling that give an indication of a gas kick. Many studies on kick detection rely on a flow-loop setup including flow valves, choke valve, and pressure sensors to simulate kick experiments. Therefore, the uniqueness of the current study lies in the utilization of a fully instrumented laboratory scale drilling rig to simulate drilling as the kick is being induced, controlled and monitored.

3.2 Materials and Methods

This section describes the experimental setup, the sample preparation and the procedures implemented to conduct the experiment.

3.2.1 Experimental Setup

The setup consists of two integrated platforms: a fully instrumented laboratory scale drilling rig platform and a surface monitoring equipment and gas injection system platform. The drilling rig is equipped with a rotary head, a fluid circulation system, and a data acquisition system.

3.2.1.1 Laboratory-scale drilling rig

The schematic diagram of the laboratory-scale (scaled-down) drilling simulator is shown in Figure 3.1(a). The rig is powered by an electric drill motor with two rotational speed configurations (300 and 600 rpm) to provide adequate rotary speed and torque to the bit via the drillstring. The loading system consists of a rack-pinion arrangement through which a suspended weight, in addition to a constant weight, can be applied to the bit. The rotary head accounts for the constant weight on bit (WOB) and consists of the drill motor and the drillstring. The drillstring components include a cradle, a swivel, a compliant tool, and a drill pipe. The swivel allows the injection of fluid into the drill pipe down to the drill bit nozzles and the complaint tool, which is configured rigidly for the current experiment, provides relative motion between the top system and the drill pipe using a set

of coned-disc springs and rubber damping elements. The drill pipe connects the drill bit with the top system (i.e. swivel, motor etc.)

A 35 mm OD polycrystalline diamond cutter (PDC) bit with a two-cutter configuration is used as the drill bit in the current experiment. The mud circulation system is equipped with a 1000 L capacity water tank installed over a triplex pump powered by a 20-kW motor with a flow rate and pressure capacities of 150 L/min and 6900 kPa respectively. The pump system also includes a variable frequency drive (VFD) to control the flow rate by adjusting the rotary speed of the motor. The circulation system includes a flow sensor, pressure transducer, and a water tank level meter to monitor and record the circulation conditions Khorshidan (2012). The water-based mud (WBM) is injected into the rig swivel assembly via a hose and then into an enclosed drilling/pressure cell.

The pressure cell, shown in Figure 3.2, is located at the bottom of the rig system to serve as a wellbore and allow application of required bottomhole pressure during drilling. The pressure cell includes a clamping assembly to hold the rock specimen in place during drilling. In other words, the pressure cell serves as a closed wellbore through which confining pressure is applied to the rock specimen during drilling. The drillstring with attached PDC bit is inserted into the pressure cell through a top cap of the cell and rotary seals are placed within the cap to prevent leaks and keep the drillstring centered. The designed pressure of the cell is 2500 kPa with a safety factor of 1.5 (Khorshidan 2012).

3.2.1.2 Integrated surface monitoring equipment and kick injection system

i) Surface monitoring equipment

The surface equipment for monitoring surface parameters consists of a Coriolis flow meter, pressure transducer, P_2, a flow in the choke manifold, and a conductivity sensor. A pressure transducer (P_2) located downstream of the pressure cell and upstream of the Coriolis flow meter,

as shown in Figure 4.1(b), is used to measure the pressure in the return mud entering the surface monitoring equipment.

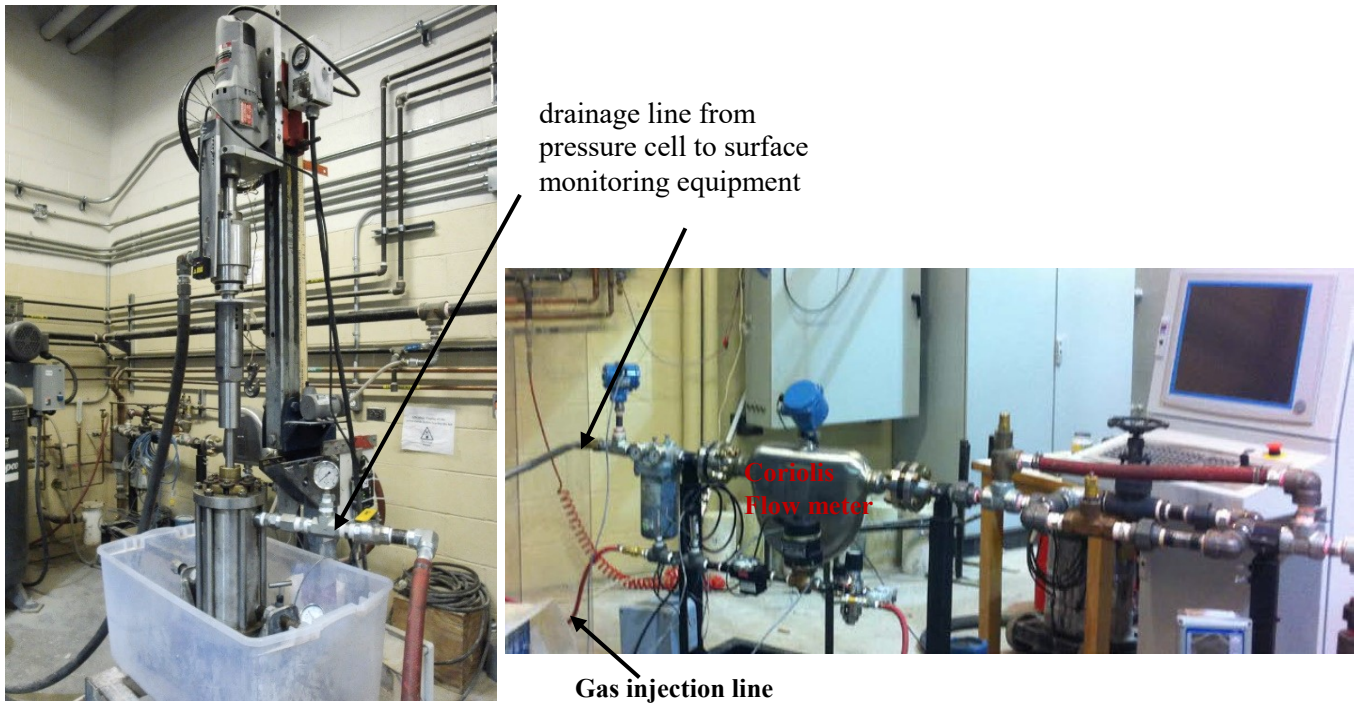

a) Drilling rig simulator

b) Surface monitoring and injection system

Figure 3.1 Equipment setup for a gas-kick simulation experiment

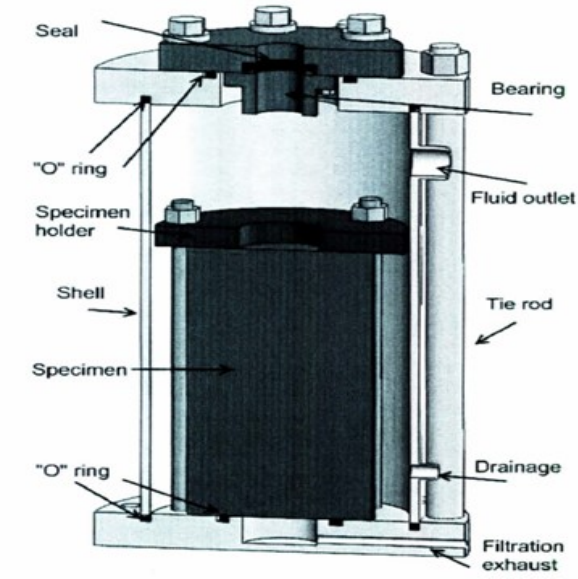

Figure 3.2: Sectional view of a schematic drawing of a Pressure Cell (Source: Khorshidan 2012)

The Coriolis flow meter is equipped with Elite flow sensor to provide good measurement sensitivity and stability when measuring multi-phase flow and it has tolerance for drill cuttings. The Coriolis flow meter is installed such that the tube is in the up orientation or flag up position to allow effective drainage of cuttings and mud from the sensor. The choke manifold consists of three valves: a pressure relief valve installed on the pressure relief loop (line), a needle (or backpressure) valve to adjust backpressure in the downhole pressure in the pressure cell and a manual pressure control valve. In the event of a surge in the pressure cell, a pressure relief valve (PRV), installed upstream of the Coriolis flow meter, diverts flow to the pressure relief (bypass) line. The pressure control and needle valves are mainly used to control the downhole pressure. The conductivity sensor measures the electrolytic conductivity changes in the drilling mud return; however, was not monitored t due to the sensor's incompatibility with drill cuttings.

ii) Kick injection system

The kick injection system is made up of an air compressor supply, a gas flow meter, a pressure sensor, a solenoid valve, and a check valve. The air compressor compresses air into an air pressure vessel and automatically shuts off at a pre-programmed pressure. The pressure vessel is equipped with a valve and a pressure gauge to discharge the pressured air and monitor the pressure in the vessel respectively during the experiment. The air pressure in the vessel is maintained between 120 and 150 psi.

A gas flow meter is used to measure, with accuracies of ±5% in volume flow rate, the air pressure discharged into the pressure cell. The pressure sensor (P_3) on the air line measures the dynamic pressure injected into the downhole pressure cell. A solenoid valve, which is installed just downstream of the compressed air supply, is used to inject compressed air into the downhole pressure cell to simulate gas kick and the check valve installed close to the injection point to throttle any fluid attempting to flow in the reverse direction (Nayeem et al., 2016).

3.2.1.3 Data acquisition system

Two data acquisition (DAQ) systems are used to measure and acquire data for the experiments: a fixed DAQ system termed as DAQ #1 and a portable DAQ system termed as DAQ #2. The DAQ #1 is interfaced with the drilling system to measure and acquire drilling-related parameters, including WOB, axial displacement, motor current etc. All data measured are recorded with a sampling rate of 1000 Hz, which is the required minimum sampling rate to capture the axial displacement signals from the high precision laser sensor. The DAQ #2 (Mobile DAQ system) consists of a power system and a DAQ system. The DAQ system component has NI9188 Chassis built-in and NI9237 and NI9205 for acquiring the data from sensors. The DAQ #2 system measures and captures data from the integrated surface monitoring equipment and kick injection system, including downhole pressure in the pressure cell, gas pressure, mass and density flow etc. Because the DAQ #2 has a 10 Hz sampling rate capacity, the data from the two DAQ systems are compared using a clock synchronization technique.

3.2.2 Rock specimens' preparation

3.2.2.1 Specimen properties

The current experiment is performed on synthetic rock materials modeled by pouring a specified recipe of concrete slurry in 4×4-inch empty cylinders and left to set and harden. The concrete slurry mixture includes sand aggregates, water, cement, and superplasticizer. More information on concrete preparation can be found in Zhang (2017). The physical properties of the rock specimen used in the current study are shown in Table 3.1. The rock specimens are then stored in a controlled-moist environment to maintain their physical properties.

Table 3.1: Physical properties of the synthetic rock specimen (source: Zhang (2017))

Rock Property	Value	Units
Unconfined Compressive Strength (Ucs)	51	MPa
Mohr Friction Angle	40	°
Tensile Strength	5.4	MPa
Young Modulus	29	GPa
Poisson Ratio	0.15	

3.2.2.2 Test specimen preparation

The rock specimens are prepared so that gas injected from the base of the rock can interact with the rotating bit as it cuts through the rock. To accomplish this objective, a hole is drilled through the center of the rock. As shown in Figure 3.3 a-d, the test specimen preparation is completed through the following steps:

a. Step 1– showing the test specimen in its original state, Figure 3.3a
b. Step 2 – the center of the rock is laid out and located as shown in Figure 3.3b.
c. Step 3 – a ¼ inch Masonry bit is used in a drill press to drill a hole through the rock center of the rock as shown in Figure 3.3c.
d. Step 4 – the top and bottom surfaces of the rocks are sanded to smoothly fit into the pressure cell base that will house the specimens during drilling shown in Figure 3.3d.

4.2.3 Bit operation analysis

The bit operation analysis is conducted to ensure that the input parameters set for the experiment are within the operational requirements of the drilling rig simulator. For this experiment, a PDC bit with an outer diameter of 35 mm and two nozzle configurations with a diameter of 5.7/32-in (or 0.178125- in) each is used.

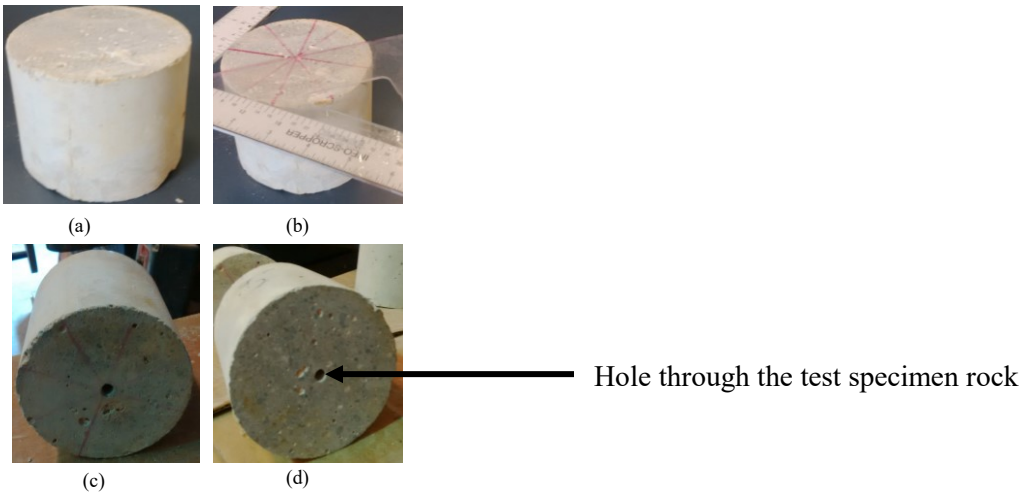

Figure 3.3: Test specimen preparation: steps 1 – 4

The dynamic weight on bit (WOB) is measured directly from the load cell. The WOB measured by DAQ #1 during the experiment is not an effective WOB due to pump-off pressure and force underneath the bit. Hence, the effective WOB can be determined by equation 3.1:

$$WOB_{eff} = (WOB_{measure}) - (pump - off\ force) \qquad (3.1)$$

Hydraulic pump-off force (HPO) can either be measured during a drill off test or estimated by equation 3.2.

$$HPO = 4.1902\ \Delta P_{bit}(d_{bit} - 1) \qquad [N] \qquad (3.2)$$

where: ΔP_{bit} [Pa] is the pressure drop across the bit and d_{bit} [m] is the nozzle diameter in the bit

The pressure drop across the bit can be calculated using equation 3.3.

$$\Delta P_{bit} = \frac{9.523\times10^{-5}\rho q^2}{C_d^2\ A_t^2} \qquad [Pa] \qquad (3.3)$$

Where ρ is the density (kg/m^3); q is the pump flow rate (m^3/s); $\boldsymbol{C_d}$ is the jet nozzle discharge coefficient = 0.95; and $\boldsymbol{A_t}$ is the total nozzle area (m^2). The hydraulic pump-off force obtained using the above equations is **-166.8N**. The negative sign shows that ***HPO*** is a negative weight on bit. Therefore, the effective weight on bit, $\boldsymbol{WOB_{eff}}$, can be calculated using equation (3.1).

Additionally, nozzle jet force $\boldsymbol{F_j}$, which is the impact force developed by the bit, can be calculated using equation (3.4):

$$F_j = 1.0588 \times 10^{-3}\, C_d q\left(\sqrt{\rho \Delta P_{bit}}\right) \qquad \text{[N]} \qquad (3.4)$$

Thus, the nozzle jet force calculated, $\boldsymbol{F_j = 19.35}$ **N.** Another important parameter to be considered is the hydraulic square inch (HSI) which is a function of pump hydraulic horsepower ($\boldsymbol{P_{hp}}$) and bit area and can be determined using equation (3.5) and (3.6) respectively.

$$P_{hp} = \frac{\Delta P_{bit} q}{1714}\ (hp) \qquad (3.5)$$

$$HSI = \frac{P_{hp}}{A_{bit}}\ (\text{hp/ in}^2) \qquad (3.6)$$

$\boldsymbol{P_{hp}}$**= 0.353 hp** and HSI **= 0.238 hp/ in^2 (or 2.75 kW/m^2)** are obtained. Therefore, the bit size and the hydraulic horsepower requirement for this experiment are well within the specifications for the drilling simulator and Table 3.2 provides the summary of the input parameters used in the experiment.

Table 3.2: Summary of input simulation parameters

Parameters	Description	Values	Units
WOB	Applied weight on bit	54.3	kg
Q	Mud pump input flow rate	47.3	L/min
P_I	Initial downhole pressure	30-35	psi
P_G	Compressed gas input pressure	170 - 180	psi
Q	Compressed air input flow rate	8 – 9	SCFM
N	Drilling motor speed	292 - 300	Rpm
$\boldsymbol{\rho_{MUD}}$	Water-based mud density	1000	kg/m^3

3.2.4 Experimental Procedure

The drilling of the test specimens is planned and conducted such that the depth of specimen drilled experiences three consecutive stages of drilling simulation: no kick region 1 (NKR-1), kick region (KR), and no kick region 2 (NKR-2) respectively. Approximately 80% of the test specimen with 4-in total depth is drilled for each run to ensure the test specimen fully interacts with the two PDC cutters and remains intact after drilling simulation. The air is injected into the test specimen via the filtration exhaust of the downhole pressure cell, as shown in Figure 3.4. The test procedure is conducted as follows:

a) The drilling procedure begins by installing the test specimen in the downhole pressure cell, which becomes a closed wellbore.
b) The experiment commences after the test specimen secured in the pressure cell and simulation equipment has been fully set up as shown in Figure 3.4.
c) After drilling about one-third of the test specimen depth (NKR-1), compressed air is injected into the pressure cell at a fixed rate of 8 – 9 SCFM and the pressured air travels from the bottom of the test specimen to the top via the hole through the center of the specimen. This enables the bit-rock-air interactions and simulates the kick region (KR).
d) After drilling approximately another one-third or more of the test specimen during the kick, the air injection is stopped as the drilling continues with no kick (NKR-2). During this operation, downhole parametric data, including rotary angular speed, rate of penetration (ROP), average depth of cut, axial displacement of the bits, motor current and WOB are logged by DAQ #1, while the downhole pressure, inlet pressure into the return line, return mud mass flow and density flow rates are logged by DAQ #2.

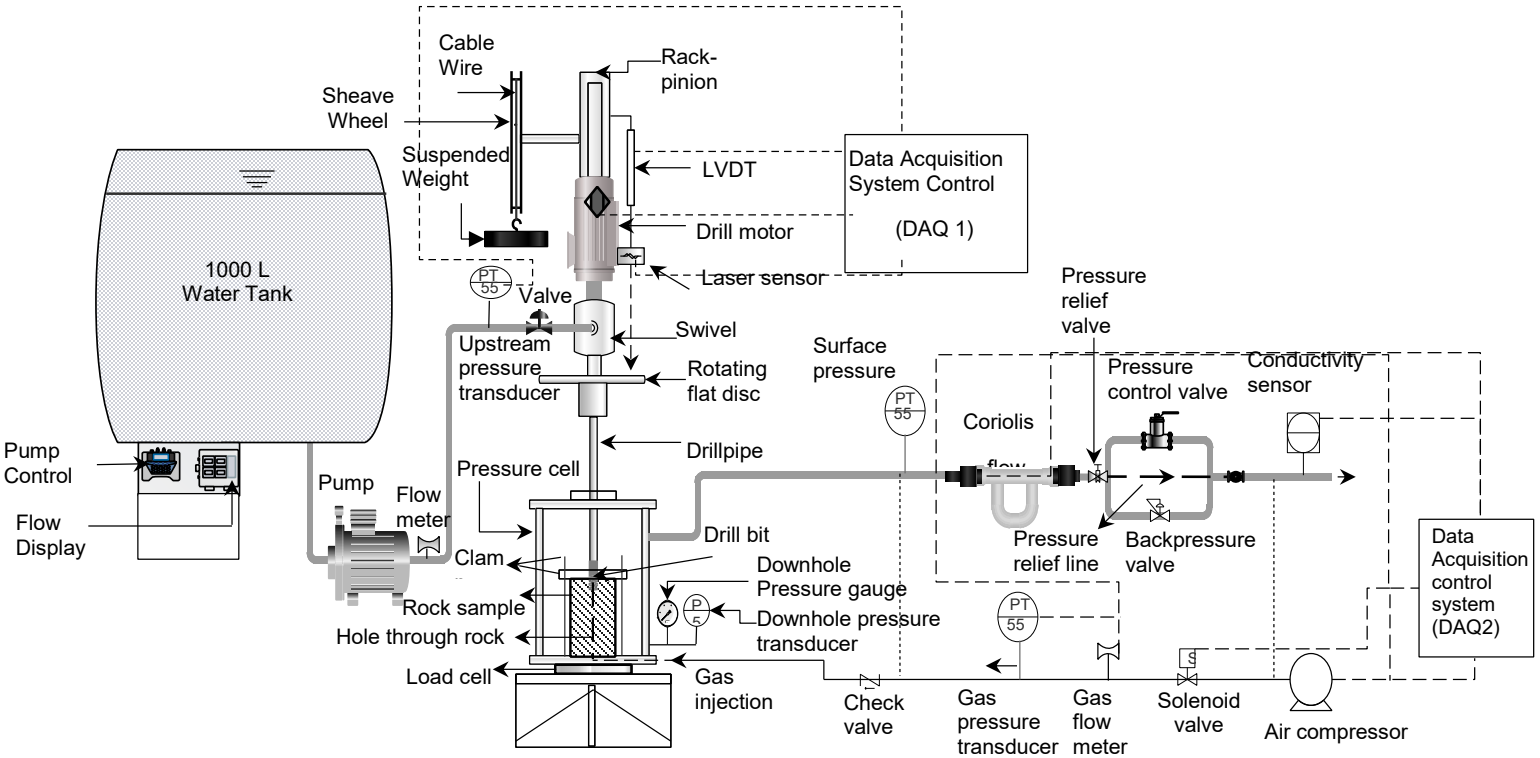

Figure 3.4: Kick Experiment process flow diagram

3.3 Results and discussions

Six downhole dynamic drilling parameters that are measured and calculated during experimental simulations are a weight on bit (WOB), the torque on bit (TOB), downhole pressure, the rate of penetration (ROP), rotary speed and bit-axial displacement (vibrations). In addition to these parameters, four surface parameters are monitored, and these include choke pressure, return fluid mass flow rates, volume flow rates, and density. Two experimental runs are conducted to ensure repeatable and consistent results. The results from these experiments have been compared and found consistent with Aldred et al. (1998) field reports on drilling parameters' response to kick.

Aldred et al. (1998) reports focused on the performance of Annular Pressure While Drilling tools, along with other BHA tools, for monitoring drilling performance and making proactive decisions

during drilling operations. These tools were utilized in the Eugene Island field in the Gulf of Mexico where the formation consisted of sequences of shales and target sands that were likely depleted by the previous production. The drilling contractor, Anadrill, utilized a series of downhole tools, including the Compensated Dual Resistivity, Multi-axis Vibrational Cartridge, Integrated Weight on Bit, and Annular Pressure While Drilling for this well.

Thus, drilling parameters including downhole torque and weight on bit, axial and torsional vibrations, ROP, annulus pressure, equivalent circulating density (ECD) etc., were being measured. When kick was taken in a 12¼-in. hole section, their measurements started to drop in response to kick. These deviations can be observed in Figure 3.5, i.e. ROP, WOB, annulus pressure, torques, vibrations, and ECD dropped due to kick. These responses in drilling parameters indicating kick occurrence are found to have consistent responses with the experimental results that are being presented in this section.

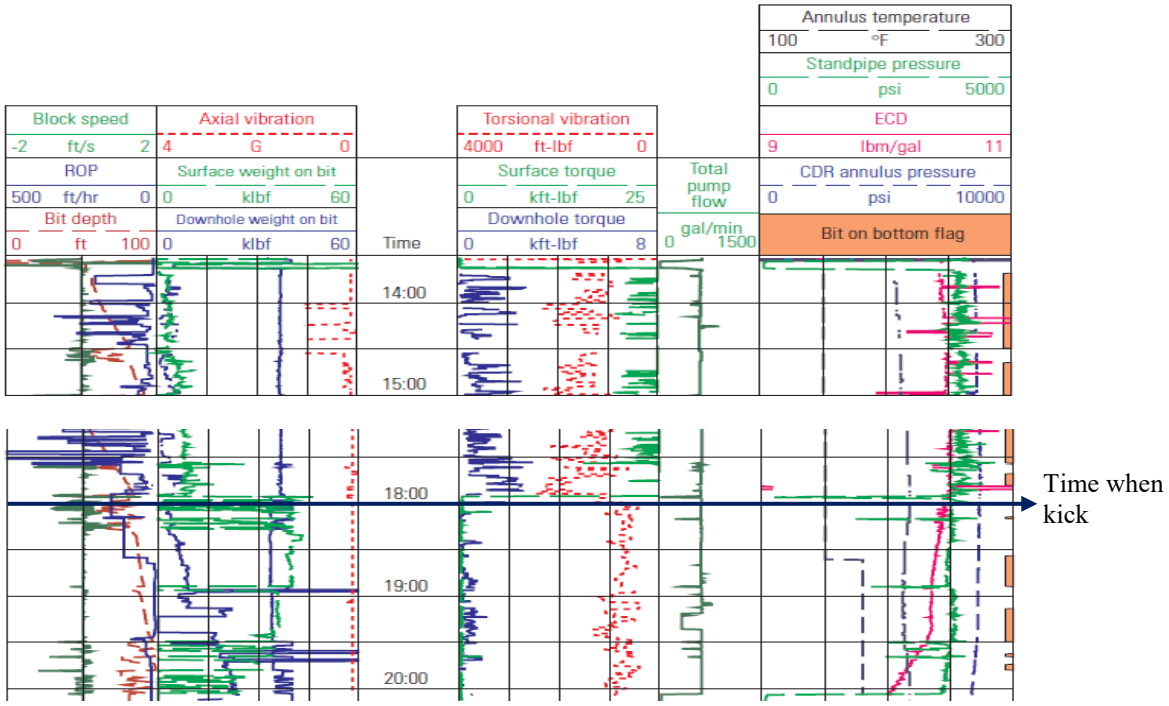

Figure 3.5: Reproduced well log with respect to time showing the kick alert in the GOM well (Source: Aldred et al., 1998)

3.3.1 Kick effects on downhole WOB and pressures

The effects of kick on drilling parameters, such as WOB and bottomhole pressures for both experimental runs are shown in Figures 3.6 – 3.7. Figures 3.6a and 3.6b show the effects of kicks on WOB for both Run_1 and Run_2 respectively. It is observed from both curves that the WOB decreases in magnitude after the kick is initiated. The moment when the kick is injected into the drilling system is consistent with the moment when the downhole and output pressures surge by an average of 25 – 45 psi above the initial downhole pressure, as shown in Figure 3.7a and 3.7b of Run_1 and Run_2 respectively.

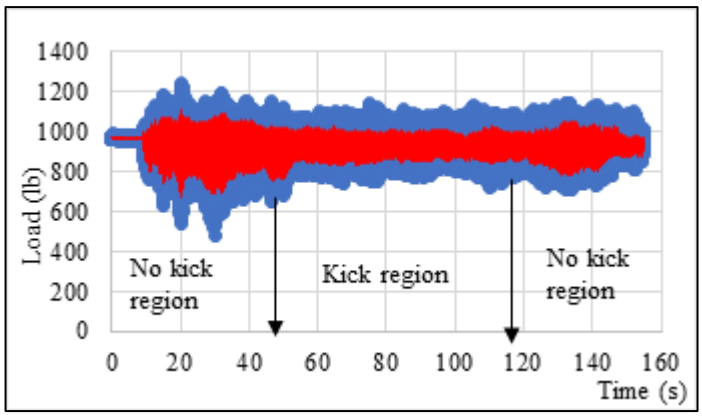

Figure 3.6a: Effects of gas kick on WOB for experimental Run_1

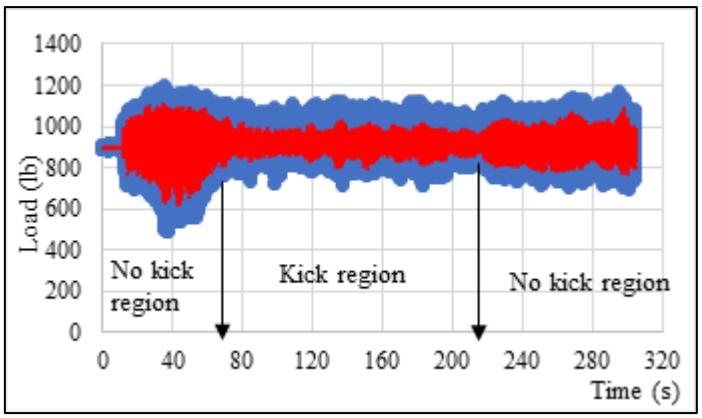

Figure 3.6b: Effects of gas kick on WOB for experimental Run_2

Figure 3.6: Effects of gas kick on WOB

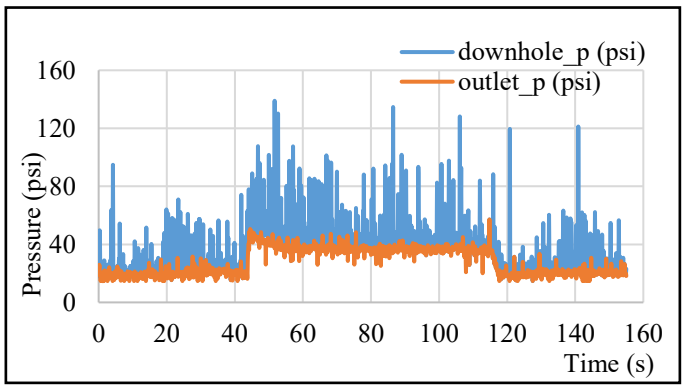

Figure 3.7a: Effects of gas kick on bottomhole pressure for experimental Run_1

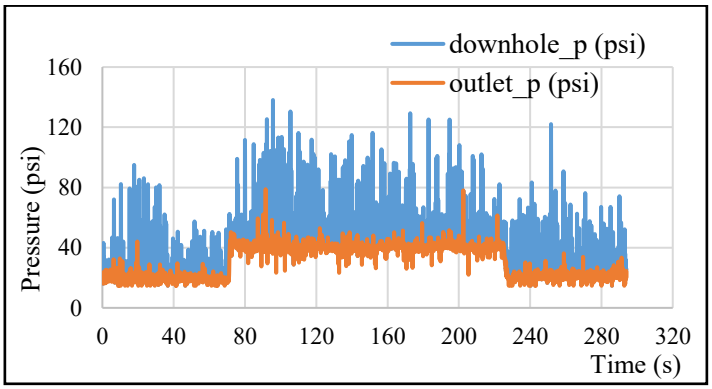

Figure 3.7b: Effects of gas kick on bottomhole pressure for experimental Run_2

Figure 3.7: Effects of gas kick on bottomhole pressure

3.3.2 Kick effects on ROP

The kick effects on the rate of penetration (ROP) can be observed in Figures 3.8a and 3.8b of Run_1 and Run_2 respectively. As shown from point A to point B of the no-kick region 1, the ROP value is 0.055 in/s (1.4 mm/s). As soon as kick occurs (i.e. gas injection into the wellbore) the ROP drops to about 0.04 in/s (1.02 mm/s) from point B to B', which represents about a 27% drop. From point B' to point C, the ROP remains constant in this kick region. When the air injection ceases at point C, the ROP increases to about 0.058 in/s (1.5 mm/s) for Run_1 and 0.055 in/s (1.4 mm/s) for Run_2 from point C to C'. This may be explained by the upthrust force, which creates an air jet between the bit and the core rock specimen, thus lifting the bit and causing minimal bit-rock interactions.

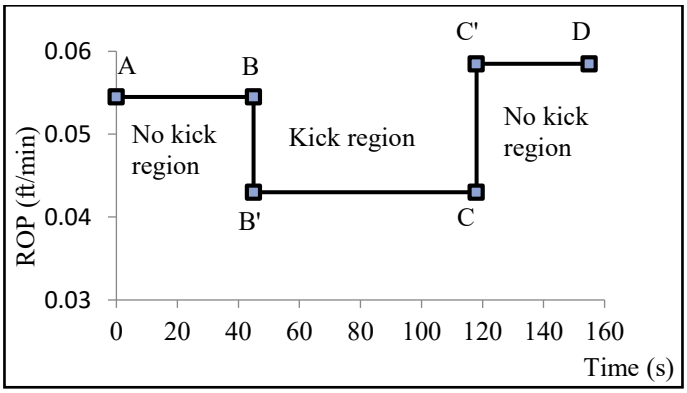

Figure 3.8a: Effects of gas kick on ROP for experimental Run_1

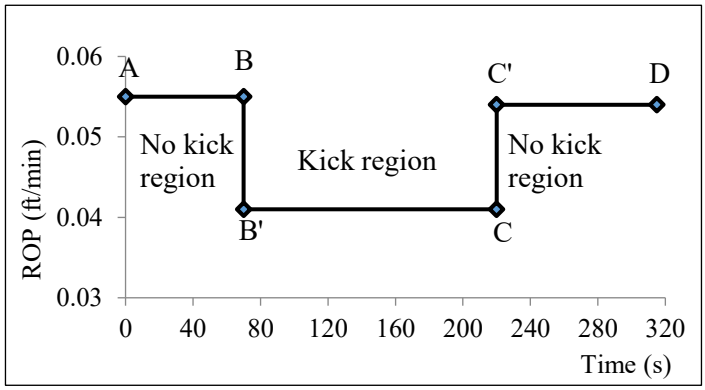

Figure 3.8b: Effects of gas kick on ROP for experimental Run_2

Figure 3.8: Effects of gas kick on ROP

3.3.3 Kick effects on mud return volume flow rate

The effects of kick on the mass flow rate of the mud return for Run_1 and Run_2 are shown in Figures 3.9a and 3.9b respectively. The mass flow rate responds instantaneously to gas influx entering the flow meter as shown by a surge in the mass flow rate of the return mud. The continuous injection of compressed air (influx) into the wellbore then causes erratic readings of the mass flow

rate that, by observation, is on average higher in magnitude than the pre- and post- gas kick readings. The observed increase in the mass flow rate may be due to the increased mass velocity of the fluid caused by the gas influx.

Additionally, the effects of kick on fluid density are shown in Figure 3.10. The fluid density is observed to drop in magnitude due to the gas influx. This can be explained by the low-density fluid (air) injected into the wellbore mud decreasing the bulk density of the return mud. Since the volume flow rate is determined by dividing the mass rate by the combined fluid density, the volume flow rate increases due to gas kick; this effect is shown in Figure 3.11.

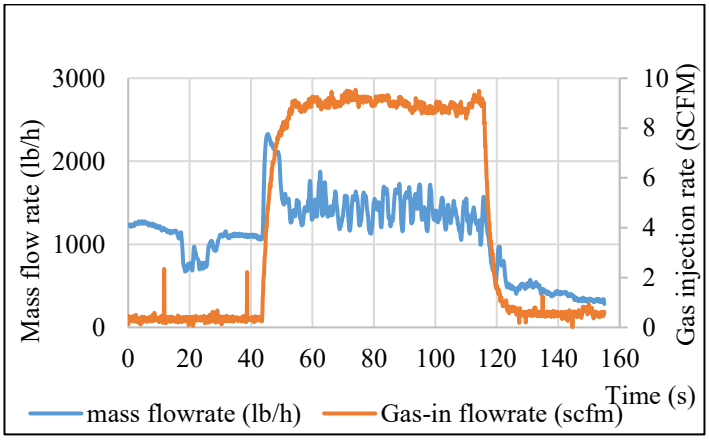

Figure 3.9a: Effects of gas kick on mass flow rate of the return fluid for experimental Run_1

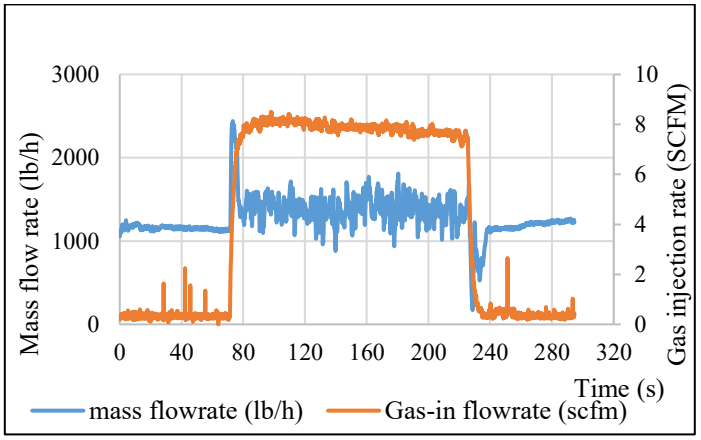

Figure 3.9b: Effects of gas kick on mass flow rate of the return fluid for experimental Run_2

Figure 3.3.9 Effects of gas kick on the mass flow rate of the return fluid

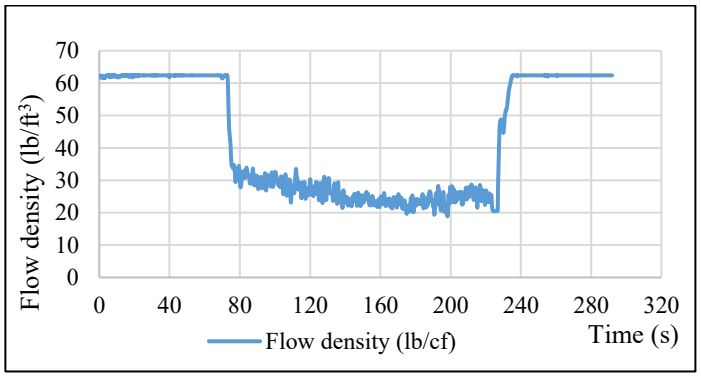

Figure 3.3.10: Effects of gas kick on mud density of the return fluid for experimental Run_2

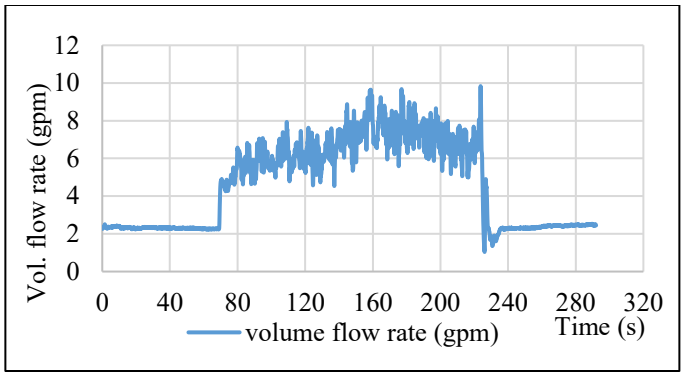

Figure 3.11: Effects of gas kick on the volume flow rate of the return fluid for experimental Run_2

3.3.4 Kick effects on rotary speed

The minimal bit-rock interactions created by the upthrust jet during air injection into the wellbore for Run_1 and Run_2 may also explain the reason for the increase in rotary speed. The rotary speed is calculated from the relative displacement data acquired from the laser sensor projection on a rotating disc by means of counting the number of spikes created by the three grooves located on the plate 120° apart, as shown in Figure 3.12. These grooves are recorded as spikes in the bit-rock axial displacement data as the tool rotates during drilling. These spikes can be noted in Figures 3.13a – 3.15a for Run_1 and Figures 3.13b – 3.15b for Run_2 of the axial bit displacements versus time graphs. The rotary speed for each test condition, is thus calculated by following procedures a) to c) and the results are summarized in Table 3.3:

a) The rotary speed (RPM) calculation can be determined by counting the number of spikes between the two-second period and then calculate the average of spikes per 1-minute revolution.

b) Equation (3.7) is developed to calculate the rotary speed of the drillstring at it experiences drilling phase/region.

c) The rotary speed for each test condition is thus calculated and the results are summarized in Table 3.3.

$$\theta\ (RPM) = \frac{(\#\ of\ spikes)\times 3}{60} \times (\Delta T) \qquad (3.7)$$

where: θ is the rotary speed and ΔT is the time between the first spike and the last spike.

Table 3.3: Summary of calculated rotary speeds during kicks and no-kick drilling simulations

Test Specimen Phase	θ (Rpm) For Run_1	θ (Rpm) For Run_2
No Kick Zone 1	270.8	275.8
Kick Zone	281.6	281.3
No Kick Zone 2	275.9	277.9

Figure 3.13 to 3.15 represent two-second data from each testing region of the test specimen core rock for Run_1 and Run_2. Figures 3.13a – 3.15a show the bit axial displacement data for NKR-1, KR, and NKR_2 respectively for Run_1 while Figures 3.13b – 3.15b show the same for Run_2. It can also be observed that the intensity of the noise in the bit rock displacement data completely dampens out as the test specimen undergoes drilling with no kick and when the gas is injected. These damping effects show the indication of kick, which is evident by a dramatic reduction in axial bit-rock displacements during the kick.

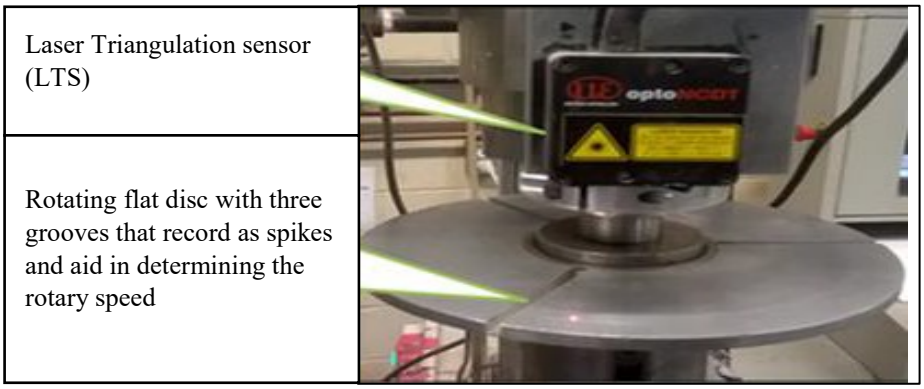

Figure 3.12: An image of a rotating flat disc with three grooves for measuring relative displacement between the motor head and the drill pipe

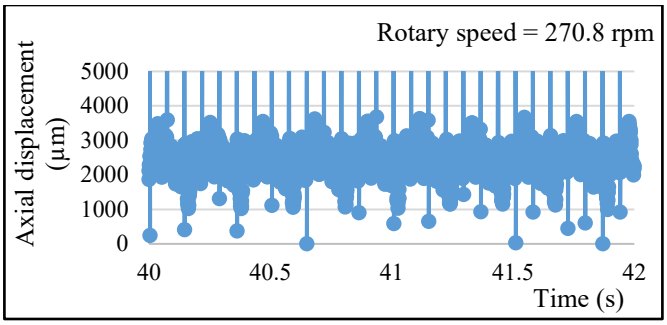

Figure 3.13a: Kick effects on rotary speed - No kick region #1 for Run_1

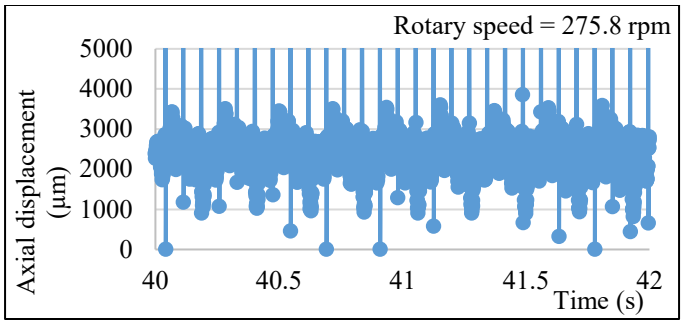

Figure 3.13b: Kick effects on rotary speed - No kick region #1 for Run_2

Figure 3.13: Kick effects on rotary speed - No kick region #1

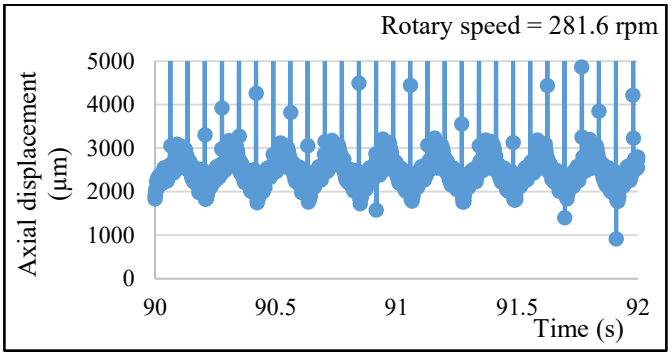

Figure 3.14a: Kick effects on rotary speed - Kick region for Run_1

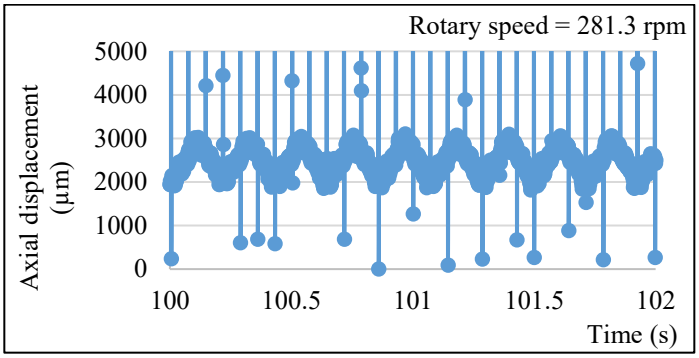

Figure 3.14b: Kick effects on rotary speed - Kick region for Run_2

Figure 3.14: Kick effects on rotary speed - Kick region

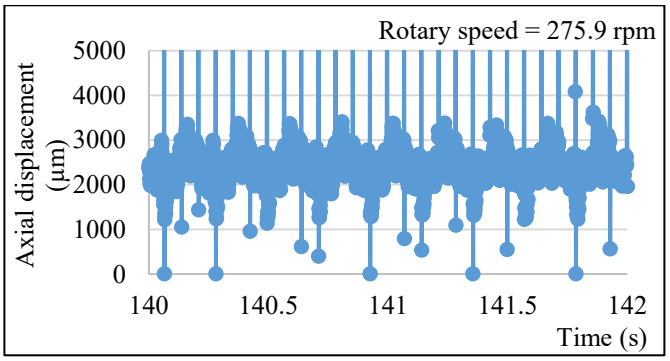

Figure 3.15a: Kick effects on rotary speed - No kick region #2 for Run_1

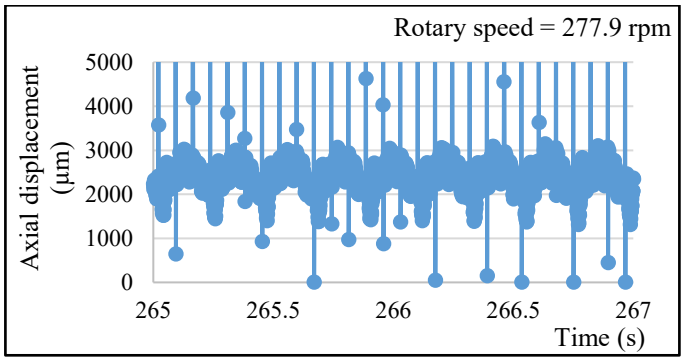

Figure 3.15b: Kick effects on rotary speed - No kick region #2 for Run_2

Figure 3.15: Kick effects on rotary speed - No kick region #2

3.3.5 Kick effects on torque on bit (TOB)

The effects of kick on TOB are also explored, as TOB can be a significant downhole parameter candidate for early kick indicator. Although no direct measurement of TOB is currently installed on the drilling system, Reyes (2017) performed a series of laboratory tests using the drilling system utilized in the current study and a MC6 Load and torque cell equipment to develop a mathematical relationship between TOB, drill motor current, and rotary speed. The motor current and rotary speed are measured using the DAQ #1. The detail procedures are available in Reyes (2017). This formula is given in equation (3.8).

$$TOB(\Omega, i_{rms}) = 59.985 - 0.295\Omega + 26.48 i_{rms} \ \ (N.m) \qquad (3.8)$$

Where: Ω = the angular speed (RPM) and i_{rms} = root mean square of the motor current.

By applying (4.8), the average TOB at each test region (no-kick (1), kick, and no-kick (2)) for experimental Run_1 and Run_2 are determined and summarized in Figure 3.16. It can be observed that the average TOB drops when the kick is experienced in the wellbore (pressure cell). This may be consequential to the lift force exerted by the air jet underneath the bit reducing the interactions between the bit and the core specimen. This reduction in interactions will lower the driving force (or TOB) required to drill the core specimen compared to the higher driving force required when the wellbore is not experiencing kick, which will thus increase the TOB.

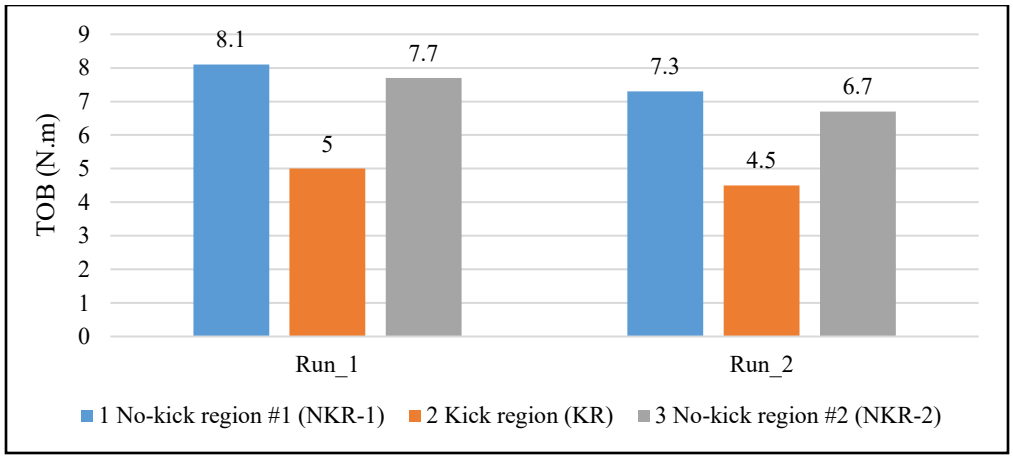

Figure 3.16: Kick effects on TOB for experimental Run_1 and Run_2

These results are consistent with the behaviour of all other drilling / downhole parameters that are explored in this work. For example, the kick region experiences a higher rotary speed, lower TOB and lower ROP compared to a lower rotary speed, higher TOB, and higher ROP for a no kick region. These results are also consistent with the field data reported in Aldred et al., (1998). It can be concluded that a dramatic drop in TOB during drilling can be an indication of kick occurrence downhole.

3.3.6 Bit-rock interaction and analysis

The most significant new finding of this work is the damping effect of drilling vibrations due to kick. These are captured in Figures 3.13a – 3.15a for Run_1 and Figures 3.13b – 3.15b for Run_2. By using a time-scale analysis, two-seconds (precisely 2.048 seconds) data are extracting from Run_1 plots of the test regions in Figures 3.13a – 3.15a and plotted them to place the data response of each test region sequentially for visualization. The result, as illustrated in Figure 3.17, shows significant changes of about 40% reduction in the axial displacement and vibration as the core

specimen experiences kick compared to the no-kick region (1) and region (2). This behaviour may constitute an indication of influx into the wellbore.

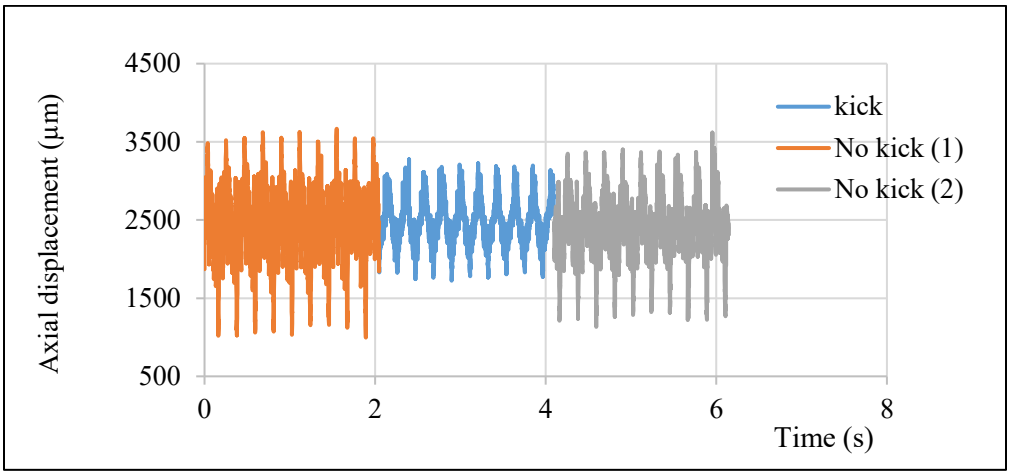

Figure 3.17: Kick effects on axial bit-rock displacement (time domain) – Run_1

Additionally, a frequency analysis is performed using a Fast Fourier Transform (FFT) as a data processing method, which converts the data from time scale domain into the frequency domain. The purpose of performing frequency analysis is to isolate the frequencies in the data caused by axial bit-rock displacement/vibrations and those caused by the rig vibration. By default, the overall bit axial displacement also consists of axial vibration, which is of interest to this analysis. The current work adopts Reyes (2017) methodology to perform the data processing for the overall bit axial vibration frequency analysis by using equation (3.9).

$$U_{vib} = \left(T \times ROP_{Avg}\right) - U \qquad (3.9)$$

where: U_{vib} = axial vibration; T = time; ROP_{avg} = Average ROP; U = axial displacement

By applying this methodology and process, the axial displacement frequencies obtained are signals are shown in Figure 3.18. It can be noted that there is a significant drop (between 33 – 89%) in the bit axial vibration during kick as compared to no-kick conditions.

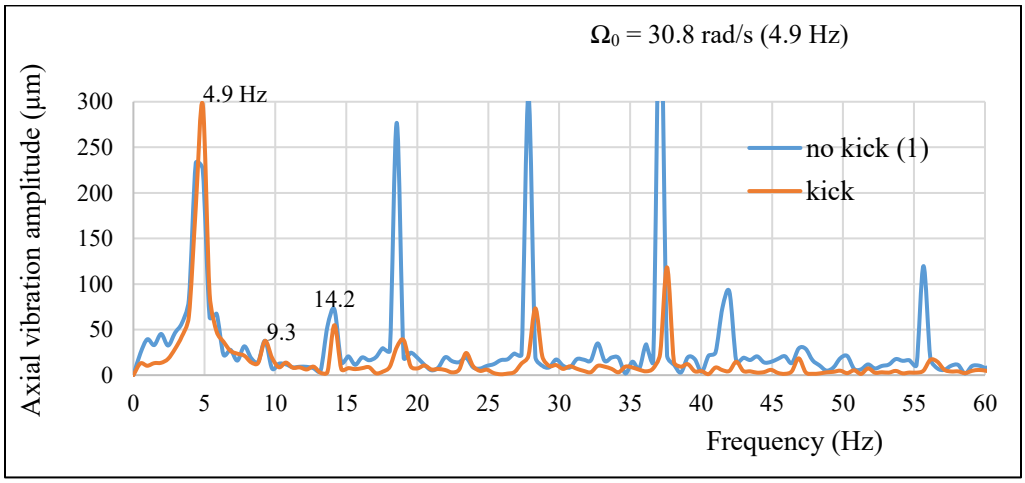

Figure 3.18: Kick effects on axial bit-rock vibration frequency – Run_1

3.4 Conclusions

The current study monitored nine parameters, including dynamic WOB, downhole pressure, ROP, rotary speed, TOB, axial bit-rock interaction vibration, mud density, return mass flow rate, and return volume flow rate. These parameters are measured during lab-scale drilling simulations of synthetic core specimens with a hole drilled through the center to aid bit-rock-gas influx interactions. Each core specimen undergoes three consecutive test stages during drilling: no-kick region (1), kick region (KR), and no-kick region (2). The results from all monitored parameters show that influx indications are consistent with case studies and field reports and are summarized as follows:

a) WOB: The magnitude of WOB decreases in response to the gas influx.

b) Downhole pressure: There is an immediate surge in downhole pressure in response to kick.
c) Mud return flow rate: Mud density drops in response to kick and the volume flow rate increases in response to kick.
d) ROP: The rate of penetration drops during gas influx and this may be explained by less bit-rock interaction due to the air jet exerted below the bit.
e) Rotary speed and TOB: The rotary speed increases when the kick is experienced in the wellbore while the TOB decreases. These behaviours may be explained due to less bit-rock interactions causing the drillstring to rotate faster and with a less driving force.
f) Axial bit vibration: The amplitude of axial bit vibration significantly decreases by about 33 – 89% as the kick is taking in the wellbore.

The most significant new finding of the study is the damping behaviour of drilling vibrations, which ranges between 33 – 89% reduction, due to the gas influx. This is evidenced by a dramatic reduction in axial bit-rock displacement/vibration during the kick and the behaviour are illustrated in both time and frequency scales analyses. The damping effects of drilling vibrations during kick can potentially serve as a new influx indicator during drilling with more large-scale/field investigations. Thus, for most drilling scenarios where temperature and pressure are higher, the kick size, rate, and rising time are expected to be higher; however, these conditions will not change how the drilling parameters will respond to the kick occurrence and detection given that appropriate downhole and surface sensing devices are used. Therefore, the drilling parameters measured and studied in the current chapter are expected to respond consistently to the gas kick in all practices as indicated and concluded.

Chapter 4 Kick Control Reliability Analysis of Managed Pressure Drilling Operation

Preface

This chapter presents a reliability assessment of a managed pressure drilling (MPD) system during a kick control operation. A dynamic annular pressure control (DAPC) system, which is a constant bottomhole pressure MPD technique, is used. A paper version of this chapter has been published in the ***Journal of loss prevention in the processing industry (2018), Vol. 52 pp. 7–20****. Along with the co-authors, Dr. Ming Yang, Dr. Faisal Khan, and Dr. Stephen Butt, I have co-authored this chapter. I developed the conceptual model, made first attempt to perform the model analysis, and interpret the data and results. The co-author Faisal Khan helped in analyzing and testing the concepts, reviewed and corrected the data and results, and contributed in preparing, reviewing and revising the manuscript. The co-author Dr. Ming Yang contributed through assisting in model analysis, data interpretation, verifying the results, and organizing and revising the manuscript. The co-author Dr. Stephen Butt contributed through assisting in analyzing the data, testing and verifying the results and revising the manuscript. Co-authors Drs. Yang, Butt and Khan reviewed the revisions and provided feedback which I have implemented. I prepared the first draft of the manuscript and subsequently revised the manuscript based on the co-authors' feedback and the peer review process.*

Abstract

Offshore drilling involves complex operations and equipment; thus, faces many operational challenges, including well control. Managed pressure drilling has been proved to resolve most of these challenges; however, this technology, for the most part, is still in its infancy. This chapter explores the safety and reliability assessment of a managed pressure drilling operation by investigating the kick control operation of constant bottomhole pressure technique of managed

pressure drilling. In addition, this study seeks to understand the components interactions in an MPD system and their modes of failure. Failure scenarios are first built using a Fault Tree model and then analyzed using a Bayesian Network model. The reliability assessments of kick control operation are performed in two ways: a basic-components approach and a system-barrier elements approach. The analysis identifies communication-related components, including network device damage as the most safety-critical component due to their high-level of influence, while flowline and pump line blockages/rupture are ranked second-most critical but with limited-level of influence. However, the system-barrier element approach ranks the managed pressure drilling control system as the most safety-critical equipment. Further analysis confirms that the monitoring equipment is the most safety-critical components of the managed pressure drilling control system with the Coriolis flow meter and Rig pump exhibiting the most critical monitoring equipment. Additionally, the managed pressure drilling system's components show a high degree of dependencies on one another and exhibit non-sequential modes of failure during kick control operation.

Keywords: Fault tree, Bayesian Network, Reliability, MPD, safety barrier

4.1 Introduction

Offshore drilling involved complex operations and equipment; hence face many operational challenges, including well control. This is even more significant considering that most remaining prospects for hydrocarbon resources are either bringing exploration into deepwater or existing ones are presented with narrow drilling windows between the pore pressure and the fracture gradient. The latter can also be due to depleted reservoirs. The narrow margins are most prominent in deepwater applications where much of the overburden is seawater (Malloy and McDonald, 2008).

These extreme drilling environments heighten geological uncertainty and their complexity are becoming the norm in nowadays drilling operations. Issues, such as well control incidents (e.g. kick) are periodically encountered and can increase operational costs (e.g. lengthy non-productive time - NPT) and risk, especially when drilling using an open hydraulic system (conventional - overbalanced drilling method).

Kick mechanisms, which are a function of formation fluid influx in drilling operations, have been covered explicitly in the literature. The mechanisms can be illustrated based on the relationships between bottomhole pressure (BHP), pore pressure (P_p), and fracture pressure (F_p). During an overbalanced drilling, i.e. when the BHP is maintained above the pore pressure ($BHP > P_p$), influx occurs when the BHP drops below the pore pressure. This unwanted formation influx into the wellbore is defined as a kick. However, when drilling underbalanced (i.e. $BHP < P_p$), the influx of formation fluid is desired to increase the drilling performance (e.g. rate of penetration). However, when the influx size rises above the desired limit, which is usually determined by the topside equipment pressure ratings, then the influx becomes a kick. Conversely, if the BHP rises above the fracture pressure (i.e. $BHP > F_p$), this will result in formation fracture and loss of drilling fluid into the formation causing a drop in BHP and then likely result in a kick (Khakzad et al., 2013).

Thus, when using conventional overbalanced drilling method and maintaining the BHP above the pore pressure in a depleted or an ultra-deepwater formation with narrow pressure window, a small rise in BHP can easily result in a condition where BHP rises above fracture pressure. This can lead to loss of drilling fluid and result in a kick. To avoid or reduce the likelihood of this pressure event,

a constant bottomhole pressure technique of managed pressures drilling (MPD) is implemented to maintain the BHP between the narrow drilling window, i.e. $P_p < BHP < F_p$ (Abimbola et al., 2015).

Managed pressure drilling utilizes specialized equipment and hydraulic control system to maintain the BHP to a near constant within the drilling window when drilling ahead or in a static condition. Managed Pressure Drilling, thus, can be defined per the International Association of Drilling Contractors (IADC) as: "an adaptive drilling process used to precisely control the annular pressure profile throughout the wellbore while ascertaining the downhole pressure environment limits and managing the annular hydraulic pressure profile accordingly. The intention of an MPD is to avoid a continuous influx of formation fluids to the surface."

Contrary to conventional drilling practice that relies primarily on mud weight as the primary safety barrier (Khakzad et al., 2013), managed pressure drilling operation utilizes, in addition to mud weight, special equipment such rotating control device, choke manifold and backpressure pump to adjust annular pressure to meet the BHP requirements. Managed Pressure Drilling (MPD) is operated in a closed loop system, hence improves the safety, efficiency, and economics of drilling operations while avoiding continuous flow to the surface (Gala and Toralde, 2011; Rohani, 2012; Malloy and McDonald, 2008; Kok and Tercan, 2012).

The operational benefits that MPD brings to drilling can be illustrated mathematically. First, considering an open hydraulic system (conventional overbalanced drilling) where the bottomhole pressure (BHP) is maintained by hydrostatic mud weight head (HP) and annular friction pressure (AFP) when circulating or drilling (Birkeland et al., 2009). AFP is maintained by equivalent

circulating density (ECD), which is a function of pump rate and mud rheology. In a static condition, however, ECD is lost, hence the BHP is only controlled by the mud weight head. These conditions can be expressed mathematically below:

$$BHP = HP + ECD(during\ drilling) \quad (4.1)$$

$$BHP = HP\ (during\ static\ condition) \quad (4.2)$$

Meanwhile, in MPD operation, backpressure (BP) can be manually or automatically applied and controlled by MPD control system, via choke manifold, which activates the backpressure pump to precisely maintain the BHP; hence, results in timely mitigation of kicks and mud losses. These can be expressed mathematically as follows:

$$BHP = HP + BP + ECD(during\ drilling) \quad (4.3)$$

$$BHP = HP + BP\ (during\ static\ condition) \quad (4.4)$$

During static condition, the choke is used to add backpressure when drilling stops to maintain the BHP instead of using the heavier mud.

The significance of safety benefits that MPD technologies bring to conventional drilling may be measured or assessed through the improvement in safety barriers of conventional primary well control, especially in deepwater drilling. Gabaldon et al. (2014) used well control barrier envelopes to describe how MPD improves influx management and prevents unnecessary shut-in or blowout due to the additional safety barrier elements in an MPD system compared to the conventional safety barrier elements. These include MPD equipment (e.g. RCD and MPD control system) and the mud weight in the conventional primary barrier element. Zan and Bicke (2014) developed a probabilistic risk analysis model that translated the qualitative assessments in the 2008 Department of Interior Minerals Management Service (DOI MMS) report into a quantitative assessment. Based

on assumed probabilities for each deviation category developed in their model, they obtained a failure probability of 0.0085. This value was reduced by 20% when an MPD system was implemented.

Grayson and Gans (2012) examined the key elements of a closed-loop circulating system (including RCD and MPD influx control) to increase the well control barrier layers and efficiency of drilling operations. They compared the risk levels in an open loop system (conventional well control) to closed loop system (MPD) by using blowout scenarios that include human errors probability (HEP). Their analyses show that the additions of MPD into a well control barrier layer reduced the possible risk of a blowout by almost 500%. Handal A. and Øie (2013) proposed a safety barrier analysis and hazard identification methodology for an MPD system to identify its safety-critical equipment. They used fault tree analysis to illustrate how the failure in an MPD pressure control equipment may be critical to BHP control and how the failure of an MPD control system may lead to a loss of well control.

The operational and economic benefits are well touted by the technology providers, but limited information is available to understand the complexity that an MPD system brings to the drilling operation. There are no clear standards to quantify the acceptable influx that an MPD system can handle to consider the operation safe. Therefore, more research should be devoted to understanding the complexity of MPD operations as this will help to facilitate the development of risk and safety models that will be inclusive. In Abimbola et al., (2015), the safety and risk of MPD study was focused on constant bottomhole pressure technique of MPD operation but did not investigate the operational dependencies of components in the MPD system nor their modes of failure.

Thus, this chapter explores the reliability assessment of an MPD system by investigating the kick control an operational aspect of a constant bottomhole pressure (CBHP) technique of MPD during drilling. The current study is based on the CBHP configuration commonly referred to as dynamic annular pressure control (DACP) and uses an assumption that kick has occurred while drilling. The kick control operation is modeled using a fault tree and analyzed using a Bayesian Network. Additionally, to identify the most critical components in the CBHP kick control operation, sensitivity analysis is performed. The outcomes of the analyses are compared with two related studies.

4.2 Constant Bottomhole Pressure Technique and Kick Control Model Development

4.2.1 Constant Bottomhole Pressure Technique and Operation

Managed pressured drilling (MPD) has many techniques whose operations are well-candidate specific. The four most commonly used MPD techniques are constant bottomhole pressure (CBHD), pressurized mud cap drilling (PMCD), dual-gradient drilling (DGD) method, and return flow control (RFC)-HSE method. Others are controlled mud cap system and continuous circulating system. A constant bottomhole pressure technique of managed pressure drilling (CBHP)-MPD is generally used in a naturally fractured formation with a narrow drilling window where the pore pressure and fracture gradient are very close (Rohani 2013). This MPD technique uses hydraulics models to establish wellhead pressure and maintains a suitable equivalent circulating density (ECD), annulus pressure gradient, and annulus ECD at a selected location in the wellbore.

According to Chustz et al. (2007), the aims of CBHP are to (1) automatically calculate, in real-time, the wellhead pressure required to maintain constant downhole pressure; (2) control the choke

and pump to generate adequate backpressure; (3) provide automatic kick detection. All CBHP systems, which include the dynamic annular pressure control (DAPC) system by Schlumberger, Weatherford MPD technology, and GeoBalance® Managed Pressure Drilling (MPD) by Halliburton, perform these three objectives. Unlike the DAPC control system, Weatherford MPD technology utilizes the Microflux® control system while Halliburton MPD uses the combination of an Automated Choke Control System, a GeoBalance® Sentry™ Data Acquisition and the Halliburton INSITE Anywhere® GeoBalance® system.

As illustrated in Figure 4.1, the DAPC system's pressure control and kick detection operations rely on a rotating control device (RCD) to seal and allow the pressurization of the wellbore annulus. The drilling returns are diverted by the RCD and routed into a choke manifold. The MPD choke manifold is used to apply hydraulic backpressure on the annulus during connections and trips to replace the friction pressure component of ECD. The backpressure pump is used to energize the annular fluid and precisely control the applied backpressure. An MPD control system serves as the control hub for all the entire CBHP equipment. The following are the recommended CBHP-MPD equipment based on Vieira et al. (2008); Elliott et al. (2011); Fredericks and Reitsma (2006); Fredericks (2008); Chrzanowski et al. (2011):

- Rotating Control Device (RCD)
- MPD Choke Manifold
- Flowline
- Downhole Deployment Valve (DDV)
- Non-Return Valves (NRV's)
- MPD Multiphase Separator

- MPD Control System
- Back Pressure Pump (BPP)
- Equivalent Circulation Drilling Reduction Tool (ECD-RT)
- Pressure-While-Drilling (PWD) tools
- Coriolis flow meters

4.2.2 Kick Incident Model

The DAPC system is designed to dynamically keep the BHP constant by using pressure control and other specified equipment. The current analysis assumes that kick has occurred, i.e. the BHP has dropped below the pore pressure. Additionally, the current study only considers a kick occurrence while in drilling-mode. Based on the DAPC operational layout shown in Figure 4.1, the CBHP kick-control operation is illustrated in a schematic diagram shown in Figure 4.2.

4.2.2.1 Equipment Functionality and Operational Dependency

The MPD control system plays significant roles in MPD operations; one of the key roles is to regulate the pressure in the well during drilling or pipe extension. It performs these operations through two control modes: pressure and flow control modes. During pressure control mode, the wellbore pressure is maintained overbalanced and within the bottomhole pressure setpoint. However, when the bottomhole pressure rises above the pressure setpoint due kick, for example, the MPD control system switches to flow control mode by adjusting the choke manifold to increase the backpressure on the well annulus. If there is not enough fluid to apply the appropriate backpressure to control the kick, the MPD controller activates the backpressure pump to generate the needed backpressure.

Additionally, MPD control system needs feedback from the flow measurements from the Rig mud pump (for mud flow-in rate) and Coriolis flow meter (for returns flow rate). These feedback data are

used to detect kick occurrence, which will result due to the deviation between the mud pump flow rates and the return flow rates. The MPD control system needs a power supply and cable-wire connections to ensure communication with other equipment. The accuracies of the PWD tool and Coriolis flow meter depend on the correct calibrations of their sensors. The effectiveness of applied backpressure on the wellbore depends on the rotating control device (RCD) functionality. The non-return valve (NRV) ensures the applied backpressure is effective on the wellbore by preventing fluid from escaping up into the drillstring via the drill bit.

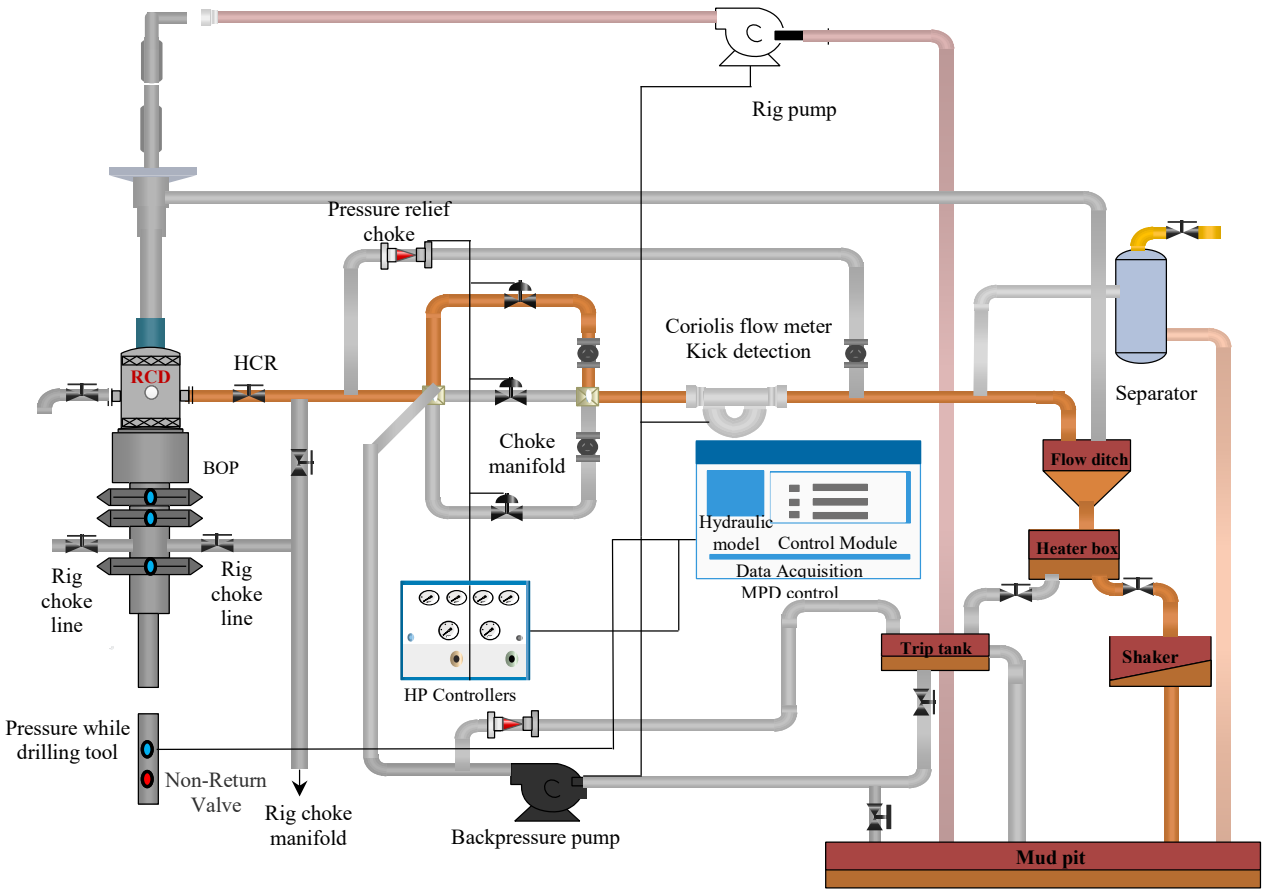

Figure 4.1: CBHP (DAPC) MPD Process Flow Diagram (adapted from Schlumberger's MPD (2016))

The flow pathways indicated in dashed lines of Figure 4.2 signify the power supply and data transmission across the entire system while the pathways indicated in thick lines show the hydraulic movement through the system.

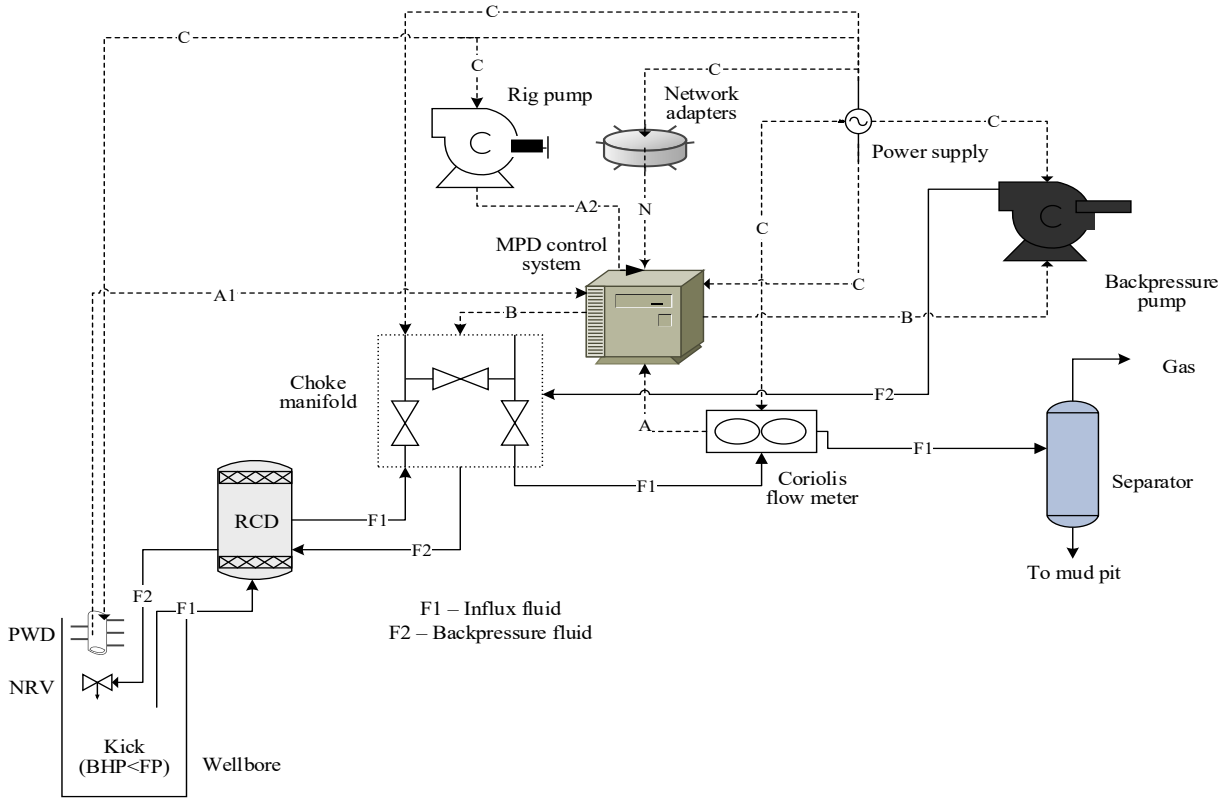

Figure 4.2 CBHP MPD system kick management operational flow – showing equipment dependency and interaction process

The electrical supply/communication to and from the MPD control system in Figure 4.2 is represented by "A1", "A2", "B", "C", and "N" and the hydraulic movements through the choke manifold, Coriolis flow meter, Backpressure pump, RCD, and NRV are represented by "F1" and "F2". These notations are described as follows:

1. "A1" – represents the pressure data inputs required for the integrated pressure management control system to calculate the appropriate hydraulic model.
2. "A2" – represents the flow measurements data inputs required for the MPD control system to determine kick by comparing flow-in and flow-out.

3. “B” – represents the output command signals from the integrated pressure management control system to the choke system and the backpressure pump. The operation of these components depends on these output commands and are sent over a high-speed network connection.
4. “C” – represents the power connection to all devices except RCD, NRV and flowline.
5. “N” – represents the network connection to the integrated pressure management control system, which serves as the hub for all components connected to it as shown in Figure 4.2
6. “F1” – represents the hydraulic movement (or kick) from the wellbore via the RCD and through the choke unit into the Coriolis flow meter and then into the separator.
7. “F2” – represents the hydraulic movement (or backpressure) from the choke unit via the RCD to the wellbore to control or stop influx while the NRV prevents backflow into the drillstring.

4.2.2.2 Kick Incident Scenarios

The kick control operation commences with the entire system becoming energized by the power supply and then uses a network connectivity/cable-wire connection to ensure flow/pressure data transfer to and from the MPD control system. The MPD control system receives inflow data from the rig pump rate and outflow data from the Coriolis flow meter and processes the flow data for kick detection. After kick has been detected, the control system adjusts the choke positions accordingly to apply backpressure to the wellbore.

In the kick control operation diagram shown Figure 4.2, all probable failure scenarios identified cannot occur sequentially; e.g. the choke system is unable to apply the appropriate backpressure to control the influx due to the choke valves not closing or controller not adjusting the valves positions. In addition, the Coriolis flow meter may measure inaccurate flow data due to flow sensor failure or may not send flow data due to connectivity issue etc. Thus, a sequential failure model may be inadequate to account for all these possible scenarios or the CBHP system components’

interactions/dependability. Therefore, the current study utilizes the FT model to identify all possible operational failure scenarios and the BN to analyze the model.

4.3 Models Development

4.3.1 Fault Tree Model

The fault tree model is developed based on kick management operational flowchart in Figure 4.2. The top event (kick control failure) could occur through multiple scenarios of events that could be initiated with the failure of any components in the system. While the power supply may have both a direct and indirect contribution to the kick control failure, the rig pump, Coriolis flow meter, PWD tool, and network connectivity only have indirect contributions. Therefore, the MPD control system, RCD, NRV, backpressure pump, and choke manifold have a direct contribution to the kick control failure.

4.3.1.1 MPD Choke Manifold

The Choke Manifold in this study operates automatically to apply appropriate hydraulic backpressure to the wellbore to neutralize kick. The logical relationships of its components are shown in Figure 4.3. The key components are the *choke valves* which consist of two main valves and one auxiliary valve and the *controllers*, which consist of main and auxiliary controllers. The main controller controls the main choke valves while the auxiliary choke valve is controlled by the auxiliary controller. Hence, the choke valves and the controllers both have redundancy configurations. Another key component of the manifold system is the communication features which are supplied by an electrical power source and network connectivity. The network connectivity relies on cable wire, power supply, and live communication with the satellite. Additionally, since backpressure is applied through the flowline, blockage or rupture of the piping system in the manifold could result in a failure of its operation.

4.3.1.2 Backpressure Pump

The backpressure pump acts as a backup when the MPD choke manifold is unable to provide the required backpressure to control influx into the wellbore. Its operation depends on the fluid level in the system (mud pit), pump line, auxiliary controller, and communication system. These relationships are illustrated in Figure 4.3.

4.3.1.3 Managed Pressure Control System

The MPD control system is designed to coordinate the choke manifold and backpressure pump operations in providing the necessary hydraulic backpressure to keep the BHP constant during drilling or while in a static / circulating condition. More importantly, an MPD control system relies on input flow and pressure data from devices such as the Coriolis flow meter, rig pump rate, and PWD tool to ensure accurate operations. The logical operation of the MPD control system is shown in Figure 4.4. The system consists of four intermediate events, including controller unit failure and monitoring system failure.

The *Controller unit* performs arithmetic and logical operations and consists of:

a) A controller panel – which controls the dynamic MPD pressure control equipment and consists of multiple interfaces including, a dynamic and static pressure control. Its failure may be due to a short-circuited board etc.
b) Hydraulics models – for simulating physical parameters of fluid in the well
c) Mechanistic models – for simulating other relevant operational parameters – such as torque, drag, ROP, formation conditions (Handal and Øie, 2013).

The *monitoring system* supplies the pressure, flow and other hydraulic data to the MPD control system from the Coriolis flow meter, PWD tool, and the rig pump. The logical operation of the Coriolis flow meter, PWD tool, and the rig pump are shown in Figure 4.5 – 4.7 respectively. The Coriolis flow meter failure, for example, could be attributed to the loss of communication to the

controller, blockage in a flowline, or flow sensor malfunction. The loss of communication has multi-level events as shown in Figure 4.7.

4.3.1.4 Rotating Control Device

The hydraulic backpressure is applied through the rotating control device (RCD) to the wellbore. In the current study, the operational dependency of the RCD is limited to its bearing assembly and housing assembly (bowl). These are represented in Figure 5.3.

4.3.1.5 Non-Return Valve

The NRV provides one-way flow of fluid from the surface to the bottom of the well via the drill bit that prevents the backflow of fluid into the drillstring when there is applied backpressure on the annulus (or wellbore). In practice, it is recommended to install two or more NRVs, with at least one located at the top of drilling string to serve as an additional safety barrier element (Stødle et al., 2013).

4.3.2 Bayesian Network

A Bayesian Network (BN) is a graphical model, based on Bayes' theorem for probability reasoning to quantify complex dependencies. It has been widely used in reliability, risk and safety analyses. A BN can also be used to describe the causal influence relationships among variables via a directed acyclic graph (DAG) in which the nodes represent the system variables and the arcs symbolize the dependencies (Bobbio et al., 2001; Khakzad et al., 2011, 2013; Cai et al., 2013; Barua et al., 2016). Additionally, the capability of BN to perform both forward and backward analyses make its models unique in dynamic risk and safety analysis (Abimbola et al., 2015). The forward analysis uses prior probabilities of root nodes and the conditional probabilities to compute intermediate nodes and leaf nodes while the backward analysis instantiates the state of a specified node to update the probabilities of conditionally dependent nodes (Bobbio et al., 2001; Khakzad et al., 2013a; Abimbola et al., 2015).

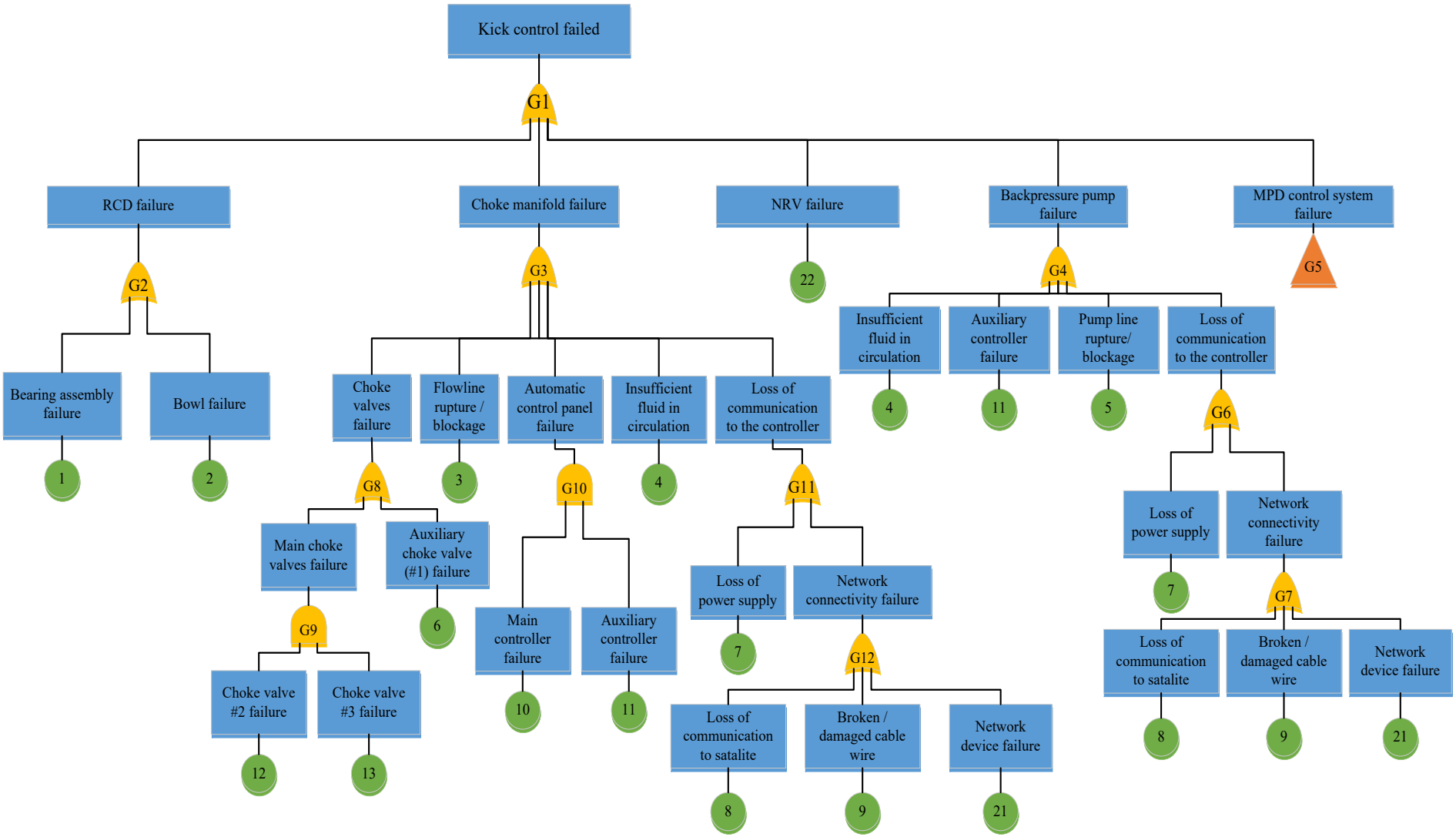

Figure 4.3: Fault tree diagram showing kick handling operation for CBHP

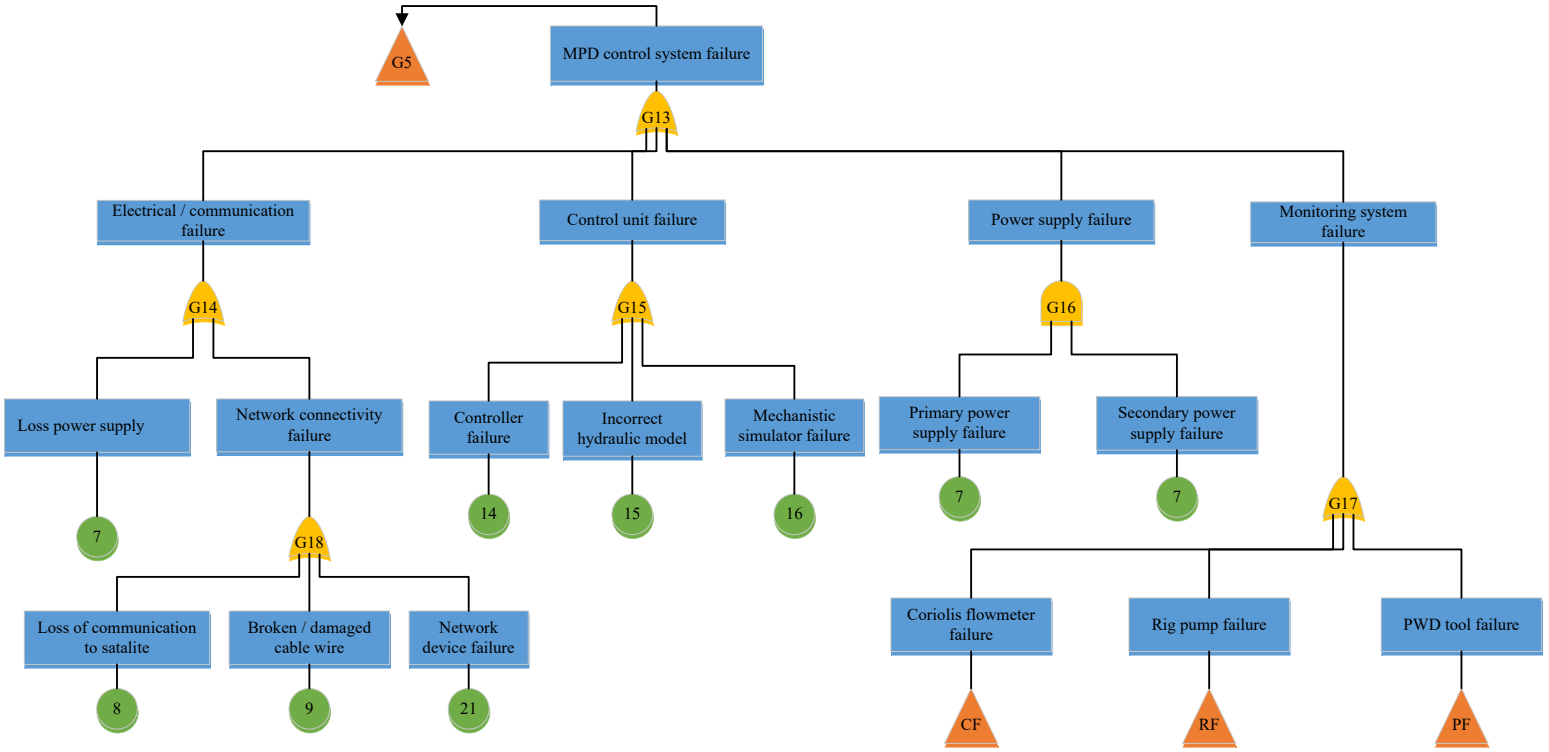

Figure 4.4: Fault Tree diagram of MPD control system in the CBHP kick control operation

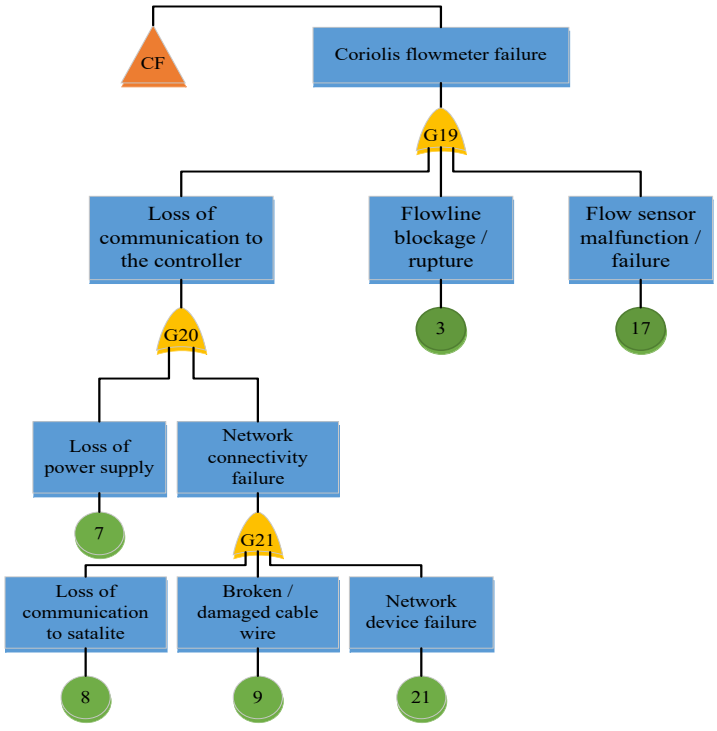

Figure 4.5: Fault Tree diagram of a Coriolis flow meter in the CBHP kick control operation

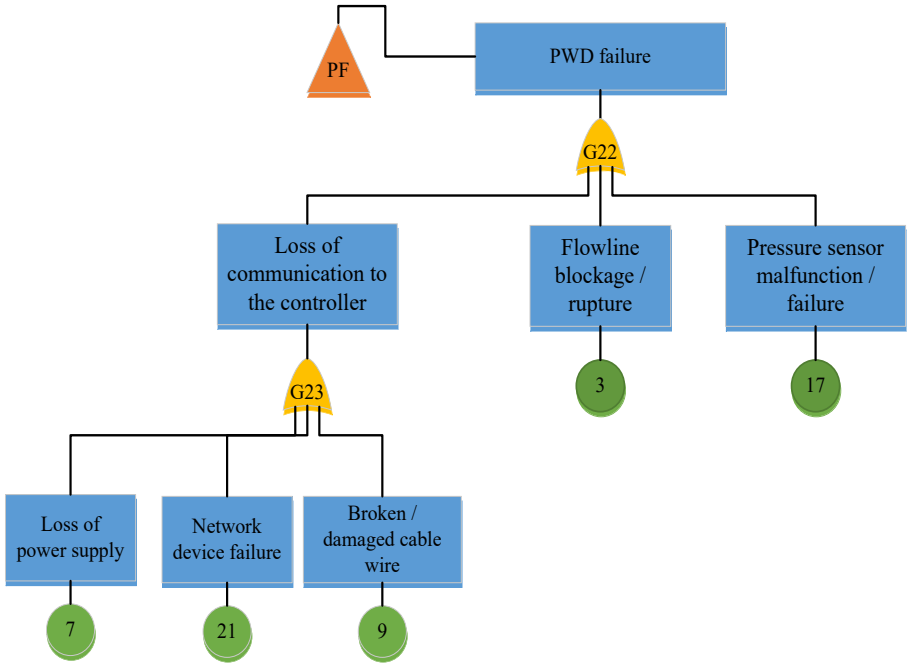

Figure 4.6: Fault Tree diagram of PWD tool in the CBHP kick control operation

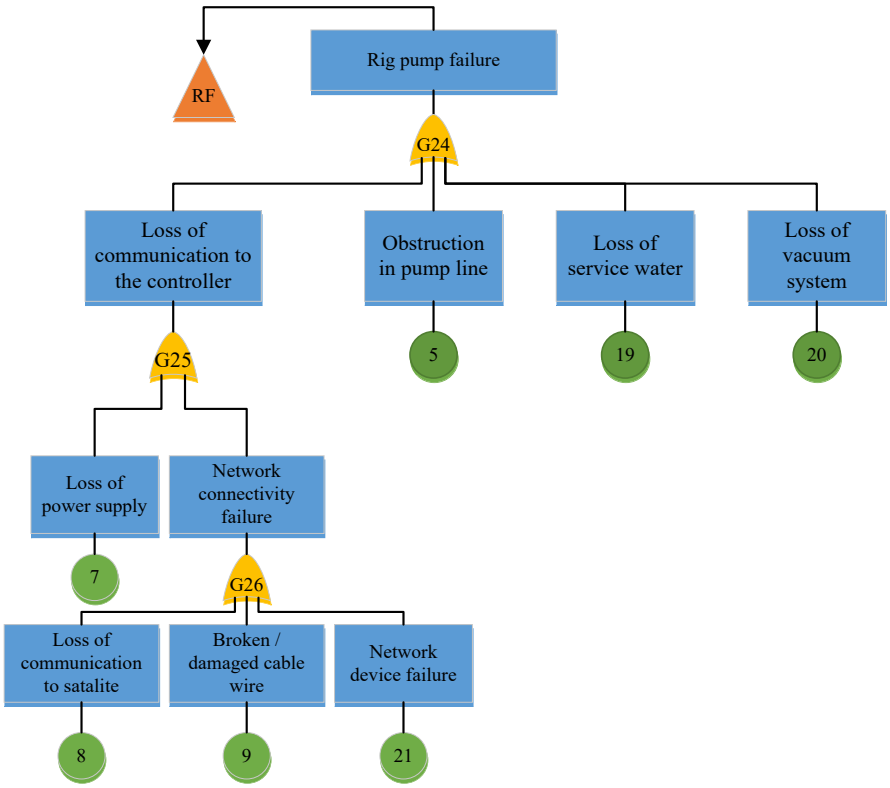

Figure 4.7: Fault Tree diagram of a Coriolis flow meter in the CBHP kick control operation

Thus, BN can reduce parameter uncertainty through probability updating and exploit all the modeling potentials of graphical probabilistic models (Khakzad et al., 2013; Montani et al., 2005).

4.3.2.1 Bayesian Network Model

The BN can be considered as a representation of joint probability distribution with a fundamental assumption that not every node is connected to every other node (Korb and Nicholson, 2011). Assuming a joint distribution of a set of random variables $D_1 \ldots D_n$ is defined as $P(D_1 \ldots D_n)$ for all values of $D_1 \ldots D_n$. Consider the BN showed in Figure 4.8, which consists of deviations D1, D2, D3, and D4 that lead to incident D5. In this illustration, D_1, D_2, and D_4 are root nodes with assigned marginal prior probabilities, D_3 is an intermediate node with defined conditional probability, and D_5 is the leaf node. Hence, using a chain rule, the joint probability distribution of the BN is the product of the conditional probability distributions of the variables $D_1 = d_1$, $D_2 = d_2 \ldots D_5 = d_5$ (Donohue and Dugan, 2003; Jensen and Nielsen, 2007; Korb and Nicholson, 2011; Khakzad et al. 2011). That is:

$$P(d_1, d_2, \ldots, d_5) = \prod_{i=1}^{5} P(d_i | d_{Ai}) \quad (4.5)$$

where *Ai* in equation (4.5) are the parents of node *i* in the DAG and d_1, d_2... d_5 are the states of variables D_1, D_2... D_5. Hence, the joint probability distribution for the BN in Figure 5.8, can be determined by equation (4.6)

$$P(d_1, d_2, \ldots, d_5) = P(d_1)P(d_2)P(d_4|d_1, d_2)\, P(d_5|d_4, d_3) \quad (4.6)$$

Therefore, for conditional probability independents/distributions such as $P(d_4|d_1, d_2)$ can be solved by using equation (4.7).

$$P(d_4|d_1, d_2) = \frac{P(d_1, d_1, d_4)}{P(d_1, d_2)} \quad (4.7)$$

This formulation can be generalized for set *n* random (discrete or continuous) variables with k states, making modeling of complex dependencies be possible and the BN to be robust and reliable for safety and risk analysis tool (Abimbola et al., 2015; Khakzad et al., 2013).

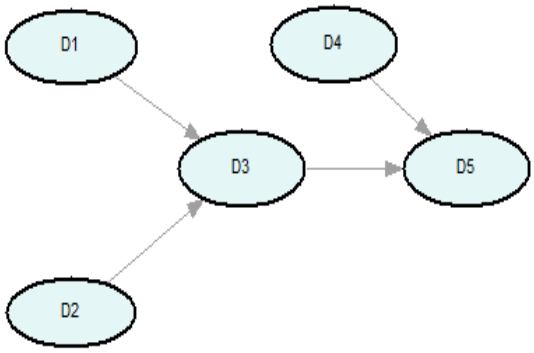

Figure 4.8: Illustrative BN model

4.3.2.2 Model Analysis

The basic events' descriptions in the current FT models are presented in Table 4.1. The failure probabilities of these basic events are adopted from Abimbola et al., 2014; Abimbola et al., 2015; Rathnayaka et al., 2012; Di Natale et al., 2012; Tran et al., 1997; Phillipa et al., 2011. Rathnayaka et al., 2012, for instance, sourced the applicable basic event probabilities from OREDA (2002), Chief Counsel's Report for Macondo incident (2011), experts' opinions, and eight other sources listed in their chapter.

Mapping an FT model into a BN has been performed in many safety and reliability papers. Bobbio et al. (2001) described a methodology for mapping a fault tree into a Bayesian network; Duan and Zhou (2012) mapped a fault tree into a Bayesian Network to develop an innovative method of optimizing fault diagnosis; Khakzad et al. (2011) established a mapping procedure of an FT into a BN in process safety analysis; Leu and Chang (2013) transformed an FT to a BN to create a realistic and accurate safety risk-assessment model for steel building construction (SC) project; Hence, the current model adopts the methods described in Bobbio et al. (2001) for mapping an FT into a BN. Figure 4.9 shows the BN model transformation from the FT model in Section 4.3.1.

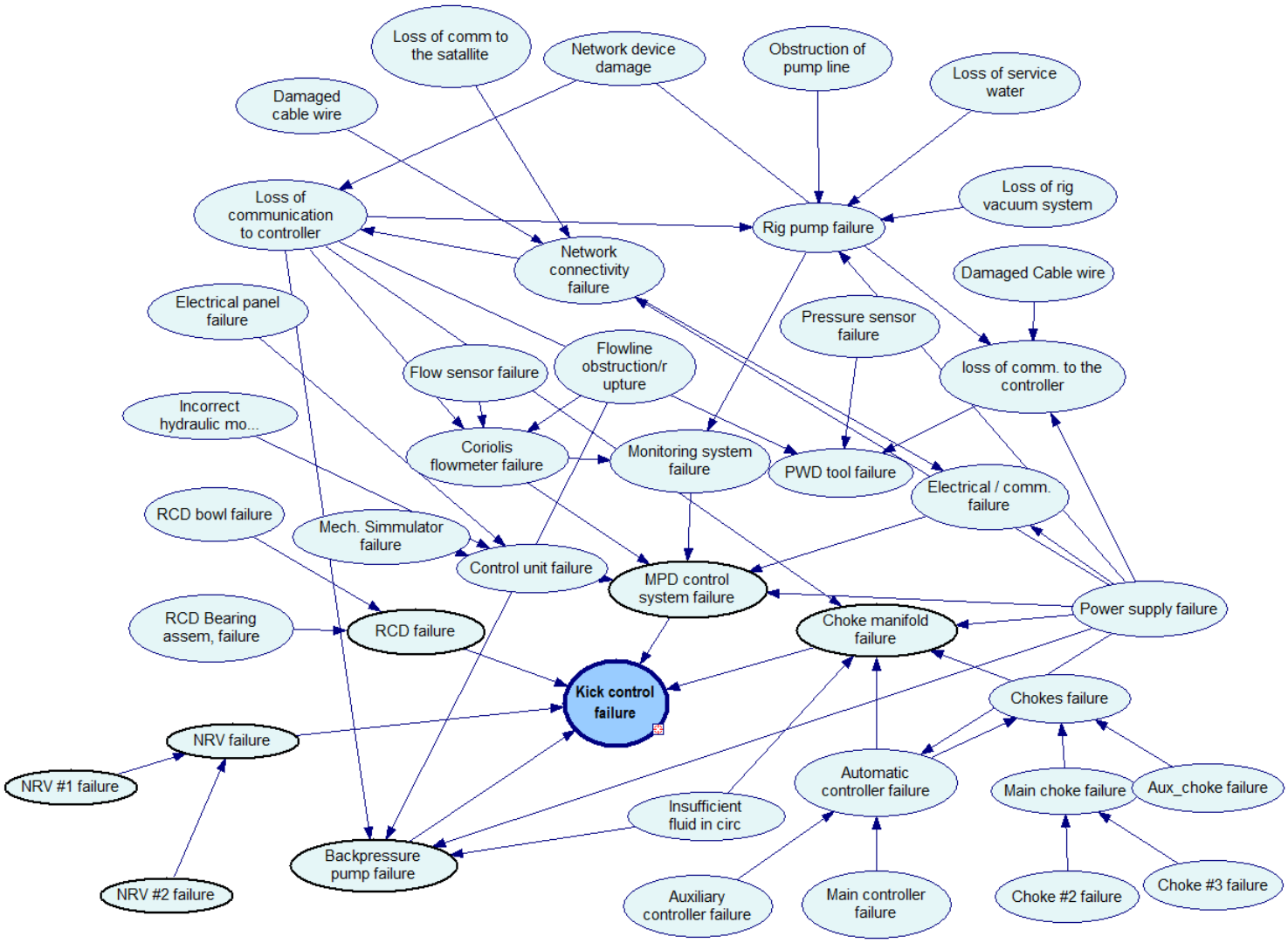

Figure 4.9: Bayesian Network for Kick control incident / Scenario

4.3.3 Sensitivity Study

Sensitivity analysis was performed on both the FT and BN models to find the weakest link in a kick operation system and to identify the system's safety-critical components. Ferdous et al. (2007) used sensitivity analysis comprised of two basic steps in an FT model: cut sets importance determination and improvement index estimation. Ferdous et al. (2007) used equation (4.8) to calculate the Cut set importance.

$$I^{Ci} = \frac{Q_j}{Q_0} \times 100\% \quad (4.8)$$

Where, I^{Ci} = cut sets importance, Q_j = cut sets frequency, and Q_0= top event frequency.

Improvement index estimation observes the contribution of each basic event leading to the top event by eliminating each basic event from the tree and evaluating its weight on the tree (Ferdous et al., 2007; Cheong and Lan-Hui, 2004; Lai et al., 1993). Whereas, Zarei et al. (2016) used the ratio of variation (RoV) to rank minimum cut set (MCS) based on their criticality. The RoV is used to estimate the basic event with the "most contributing factor" (MCF) to top event failure. RoV is calculated by using equation (4.9) and RoV (MCS) by equation (4.10) (Zarei et al., 20016).

$$RoV(C_i) = \frac{\pi(C_i) - \theta(C_i)}{\theta(C_i)} \quad (4.9)$$

$$RoV(MCS) = \frac{\Pi_{i\epsilon MCS}\pi(C_i) - \Pi_{i\epsilon MCS}\theta(C_i)}{\Pi_{i\epsilon MCS}\theta(C_i)} \quad (4.10)$$

Where $\theta(C_i)$ and $\pi(C_i)$ denote the prior and posterior probabilities respectively while $\Pi_{i\epsilon MCS}\theta(C_i)$ and $\Pi_{i\epsilon MCS}\pi(C_i)$ denote prior and posterior minimal cut set probabilities. The comparisons of the results obtained using the RoV (MCS) and I^{Ci} for criticality assessment of an MPD components are performed.

Table 4.1: Basic events and their probabilities (sources: Abimbola et al., 2014; 2015; Rathnayaka et al., 2012; Di Natale et al., 2012; Tran et al., 1997; Phillipa et al., 2011)

Events	Event Description	Prior Probability (Pi)	Posterior probability (Po)	Po/Pi
1	RCD Bearing assembly failure	1.43E-03	5.10E-02	35.66
2	RCD Bowl failure	3.14E-03	1.12E-01	35.66
3	Flowline blockage	3.60E-03	1.28E-01	35.66
4	Insufficient fluid in circulation	2.00E-03	7.13E-02	35.66
5	Pump line blockage / rupture	3.60E-03	1.28E-01	35.66
6	Auxiliary choke valve failure	2.50E-02	2.55E-02	1.02
7	Power supply failure	2.50E-03	8.91E-02	35.66
8	Loss of communication with satellite	2.00E-03	7.13E-02	35.66
9	Cable wire failure	1.00E-06	3.57E-05	35.66
10	Main controller failure	2.52E-04	2.54E-04	1.01
11	Auxiliary controller failure	2.52E-04	2.54E-04	1.01

12	Choke valve #2 failure	2.50E-02	2.55E-02	1.02
13	Choke valve #3 failure	2.50E-02	2.55E-02	1.02
14	Controller panel failure	2.52E-03	8.99E-02	35.66
15	Incorrect hydraulic model	1.00E-03	3.57E-02	35.66
16	Mechanistic simulator failure	2.00E-04	7.13E-03	35.66
17	Flow sensor failure	1.10E-04	3.92E-03	35.66
18	Pressure sensor failure	1.10E-04	3.92E-03	35.66
19	Loss of service water	1.00E-04	3.57E-03	35.66
20	Loss of vacuum system	1.00E-04	3.57E-03	35.66
21	Network device damage	5.00E-03	2.78E-01	59.43
22	Non-return valve failure	3.12E-02	3.47E-02	35.66

4.4 Results and Discussion

4.4.1 Model Results

The BN model is built and analyzed using decision modeling software, GeNIe 2.1, a product of BayesFusion LLC, available at http://www.bayesfusion.com/. By performing a forward propagation, the failure probability of the top event (kick control failure) is obtained as 0.0574. This estimation is based on installing one NRV in the bottomhole assembly. In practice, however, it has been recommended to install more than one NRV in parallel to provide a redundant function, such as installing one NRV above the bit and another above the BHA. Since NRV failure improvement can be easily implemented by installing another NRV in the BHA, further analysis is performed after installing NRV#2 parallel to NRV#1. Thus, the probability of the top event is recalculated and a value of 0.0280 is obtained.

The structural modification decreases the failure probability of the top event by approximately 50%. Although there is currently no knowledge of available literature with which to compare this result, the failure probability seems to be slightly high for an MPD system. For instance, based on the study conducted by Cunningham and O'Banion (2013) of Micro Motion Inc. on Smart Meter Verification, the estimated failure probability a Coriolis flow meter is 2.40E-06. Hence, a conclusion can be drawn that the estimated top event failure probability obtained is high for this MPD system.

To update the probability belief, an assumption was made that kick control failure had occurred by setting the "kick control failure node" (the leaf node) to a failure state and conducting a backward propagation. The posterior failure probabilities of the basic events (parent nodes) are calculated and the results are shown in the 4th column of Table 4.1. The ratio of the posterior probability to prior probabilities of the basic event (shown in Table 4.1) shows that only the "Main controller failure", "Auxiliary controller failure", "Choke valve #1 failure", "Choke valve #2 failure", and Choke valve #3 failure retain their prior probabilities or showing insignificant change. These show that the posterior derivations for these four components have insignificant influence on the kick control failure; this may be due to their redundant configuration in the MPD system structure. The rest of the components, however, have posterior probabilities of about 35 times higher than their prior probabilities, except for Network device damage that has a posterior probability of 59 times the prior probability, making it the most significant basic event.

4.4.2 Sensitivity analyses

The sensitivity analyses are performed using two methods: numerical modeling and GeNIe 2.1 software modeling. The numerical modeling approach uses the models described in section 4.3.3, the cut set importance and rate of variation of MCS to investigate the influence of the basic event components and barrier elements on kick control operation. The GiNIe software approach is direct, more comprehensive, and easy to use. The Sensitivity analysis on GeNIe is performed by setting a node as the target node over which the GeNIe performs the sensitivity analysis.

4.4.2.1 Numerical model approach

Basic event analysis

Using two NRVs installed in parallel to each other within the bottomhole assembly, network device damage achieves the highest cut set importance (I^{Ci}) of 17.44%, followed by flowline

rupture/blockage and pump line blockage with 12.56% apiece, and RCD bowl failure with 10.95%. These results are shown in column #3 of Table 4.2. These results, using the cut set importance, are compared with the RoV MCS method and are shown in Figure 4.10. The results from both methods are consistent with each other and both show that network device damage achieves the most critical basic event. Consequently, in the basic event sensitivity analysis approach, network device damage is the most critical components in the kick control operation.

Table 4.2 Safety-critical assessments of a Kick control system (basic event approach)

MCS	Basic event Components	I^{Ci} *(%)* (with 2 NRVs installed in parallel)
C1	Bearing assembly failure	4.99
C2	Bowl failure	**10.95**
C3	Choke valves failure	0.05
C4	Pressure manager controllers	0.02
C5	Loss communication to satellite	6.98
C6	Cable wire failure	0.003
C7	Network device damage	**17.44**
C8	Power supply failure	8.72
C9	Flowline blockage	**12.56**
C10	Insufficient fluid in circulation	6.98
C11	Auxiliary controller failure	0.88
C12	Pump line blockage / rupture	**12.56**
C13	Electrical panel failure	8.79
C14	Incorrect hydraulic model	3.49
C15	Mechanistic simulator failure	0.70
C16	Flow sensor failure	0.02
C17	Pressure sensor failure	0.38
C18	Loss of service water	0.38
C19	Loss of vacuum system	0.35
C20	Non-return valve failure	3.40

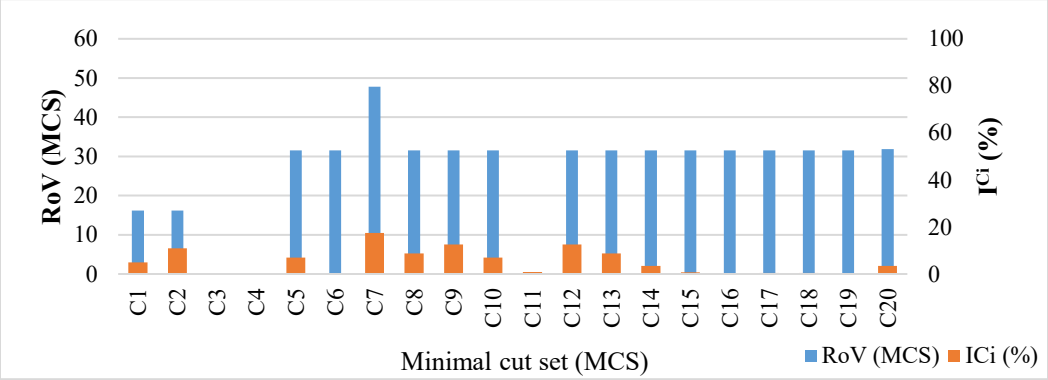

Figure 4.10: Sensitivity Analysis of basic events probabilities

Barrier element analysis

The barrier element approach observes the contributions from the perspective of kick control equipment. This approach gives information on the equipment that is most critically important in the kick control operation. As shown in Table 4.3, **38.47%** of cut set importance is obtained in an MPD control system, followed by 29.1% in backpressure pump and 23.2% in choke manifold. This analysis shows that an MPD control system is the most critical kick control barrier element that receives the most priority for improvement to enhance kick control operation reliability.

Table 4.3: Failure probability data for each kick control barrier elements

Equipment (kick-control barrier elements)	I^{Ci} (%) with 2 NRVs in parallel
MPD control system	**38.47**
MPD choke manifold	23.21
Backpressure pump	29.10
RCD	7.60
NRV	1.62

4.4.2.2 GeNIe software method

Basic event analysis

The sensitivity study is performed by setting the kick control failure node (top event) as the target node. The software performs a complete set of derivatives of the posterior probability distributions

over the target nodes using each of the probability parameters in the BN. The sensitivity rankings are shown in Figure 4.11. Based on the results (Tornado plots), Network device damage is ranked as the most sensitive or critical basic event followed by the flowline rupture/blockage, pump line blockage, and RCD bowl failure. These results are consistent with the numerical model method results.

More comprehensive sensitivity analysis is performed by observing selective parent nodes (basic event) components to see how each influences the entire system's performance in kick control operation. This is done by setting the node to a failure state and conducting a backward propagation. The analysis outputs show that basic events including the loss of communication with the satellite, network device damage, cable wire damage, or power supply failure individually have substantial effects on the kick control operation. This may be due to the equipment's dependence on network connectivity and power supply to transmit data signals and send/receive action commands across an MPD control system, choke manifold, and backpressure pump. These basic events are collectively referred to as "system communication failure" (SCF).

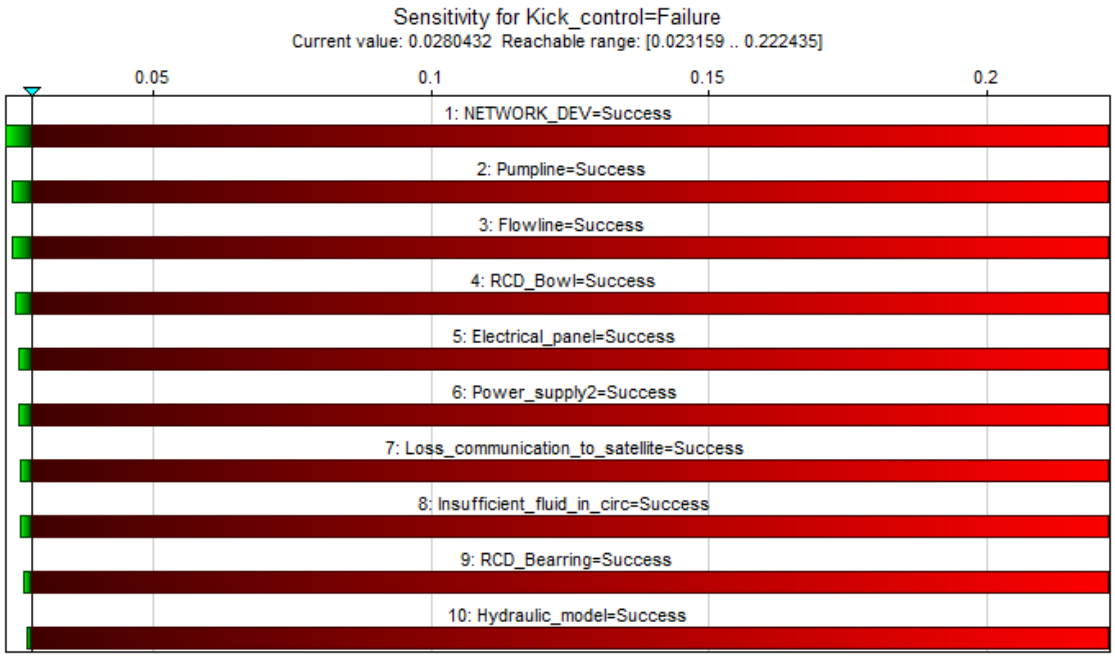

Figure 4.11: Tornado plots showing the top 10 critical basic events for kick control operation

The contribution of system communication failure's occurrence to kick control operation is depicted in Table 4.4. For instance, a "loss communication with satellite" occurrence results in 100% failure occurrence of communication loss to the controllers, network connectivity, Coriolis flow meter, rig pump, monitoring system, MPD control system, choke manifold, backpressure pump, and the top event (kick control operation).

Table 4.4: Effects of loss communication on kick control operation

Kick control operation components	Failure occurrence likelihood	Failure occurrence likelihood	Failure occurrence likelihood	Failure occurrence likelihood
loss comm. to controllers	100%	100%	100%	100%
electrical/comm. Failure	100%	100%	100%	100%
loss comm. to the satellite	*	100%	NA	NA
network connectivity failure	100%	100%	100%	100%
power supply failure	NA†	*	NA	NA
network device damage	NA	NA	*	NA
cable wire failure	NA	NA	NA	*
Coriolis flow meter failure	100%	100%	100%	100%
Rig pump failure	100%	100%	100%	100%
PWD failure	NA	100%	100%	100%
Monitoring system failure	100%	100%	100%	100%
MPD control system failure	100%	100%	100%	100%
Choke manifold failure	100%	100%	100%	100%
Backpressure pump failure	100%	100%	100%	100%
Kick control failure	100%	100%	100%	100%

* Communication components under investigation (setting evident to failure)
† NA denotes component that is not being affected during investigation

These results show the dependency of this equipment on the availability of satellite communication to perform their functions. Power supply failure, network device damage, and cable wire damage shown in Table 4.5 (3rd, 4th, & 5th column respectively) however, influence more components than the loss of communication with the satellite. The influence of power supply failure occurrence and loss of communication with satellite are illustrated in Figures 4.12 and 4.13 for better clarity and comprehension.

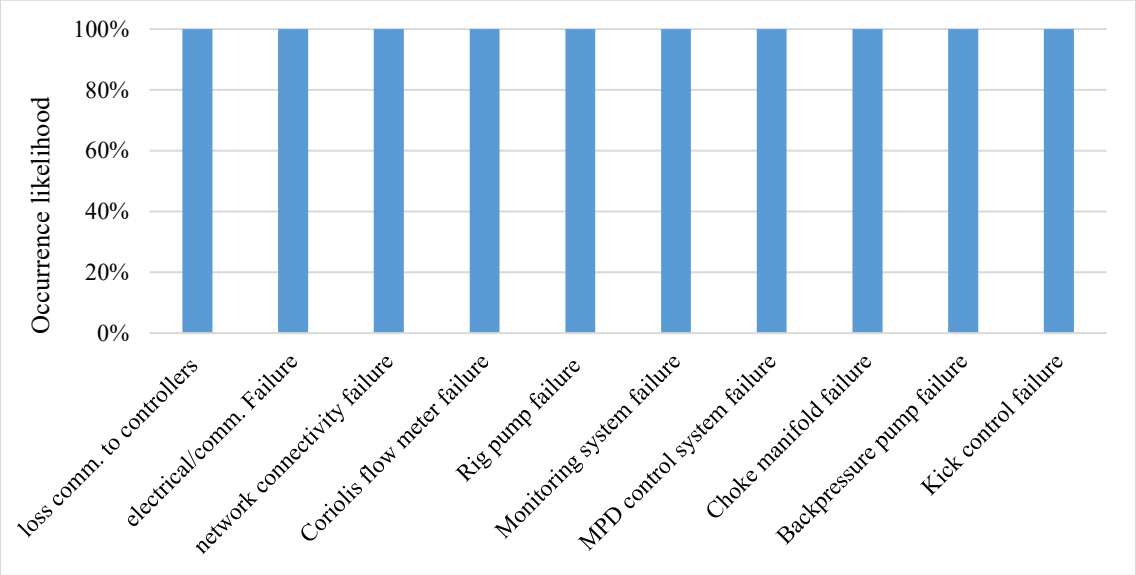

Figure 4.12: Loss of comm. with satellite influence on a kick control operation

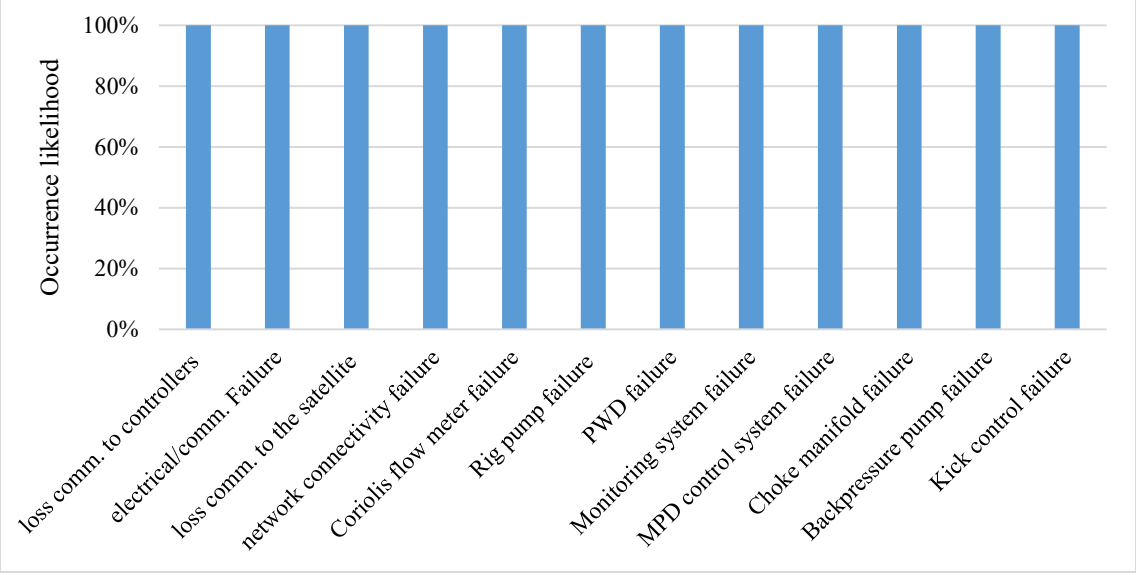

Figure 4.13: Power supply failure influence on a kick control operation

Figure 4.14 shows the limited influence of flowline and pump line rupture/blockage on kick control operation, which only affects the operation of the Coriolis flow meter, Rig pump, monitoring system, MPD control system, choke manifold, and backpressure pump. Thus; an occurrence of flowline and pump line rupture/blockage will cause 100% failure occurrence likelihood of this equipment.

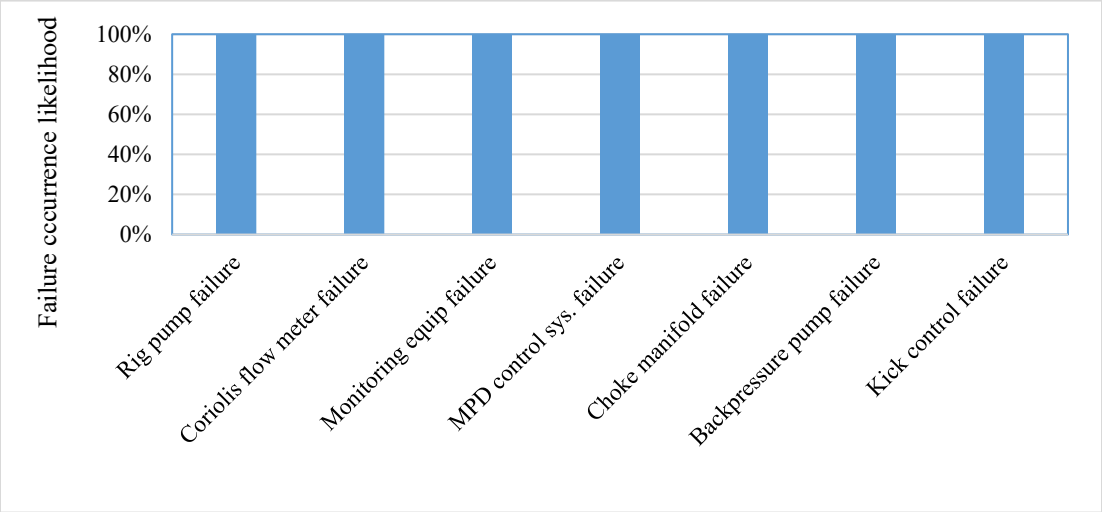

Figure 4.14: Effects flowline rupture/blockage on a kick control operation

Table 4.5 shows the influence of each monitoring equipment component (Coriolis flow meter, rig pump, and PWD tool) on the kick control operations with the Coriolis flow meter exhibiting the most influence. For instance, the effects of the Coriolis flow meter failure on kick control operation depicted in the 3rd column of Table 4.5, shows that failure of Coriolis flow meter will not only propagates to a 100% failure occurrence of the monitoring system, MPD control system, choke manifold and backpressure pump but also increases the likelihood of "loss of communication to the controller" and "rig pump failure" to 67% and those of "network connectivity" and "electrical/communication failure" to 45%. The point here is to emphasize how directly or indirectly a failure of one or more dependable components could affect the functionality of other components. The influence of the Coriolis flow meter and Rig pump failure are better illustrated in Figures 4.15 and 4.16 respectively.

Table 4.5: Effects of monitoring system components failure on a kick control operation

Kick control operation components	Prior Failure occurrence likelihood	Updated Failure occurrence likelihood	Updated Failure occurrence likelihood	Updated Failure occurrence likelihood
loss comm. to controllers	0.7%	67%	66%	98%
electrical/comm. Failure	0.7%	45%	45%	98%
loss comm. to the satellite	0.2%	18%	18%	0.2%
Network connectivity failure	0.5%	45%	53%	66%
power supply failure	0.2%	22%	22%	45%
network device damage	0.5%	38%	38%	66%
flowline obstruction/rupture	0.4%	32%	32%	0.4%
Coriolis flow meter failure	1.1%	*	67%	54%
Rig pump failure	1.1%	67%	*	54%
PWD failure	0.3%	27%	27%	*
Monitoring system failure	1.7%	100%	100%	100%
MPD control system failure	2.1%	100%	100%	100%
Choke manifold failure	1.3%	100%	67%	54%
Backpressure pump failure	1.6%	100%	67%	54%
Kick control failure	5.8%	100%	100%	100%

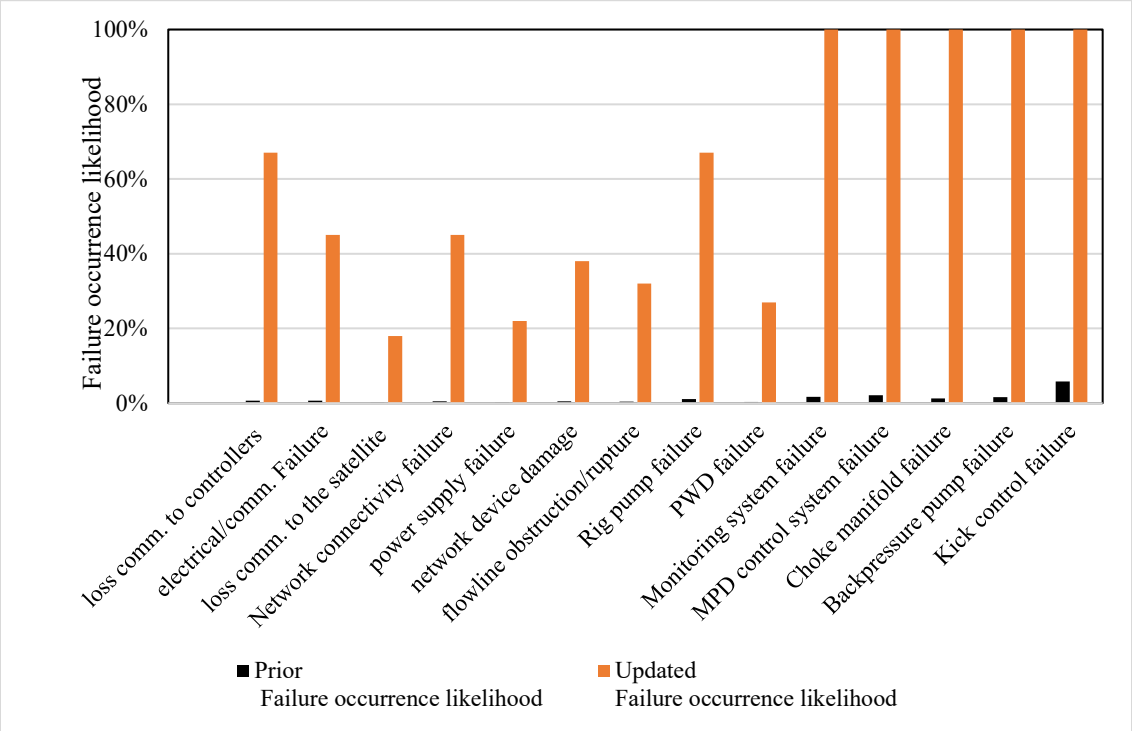

Figure 4.15: Influence of Coriolis flow meter failure on a kick control operation

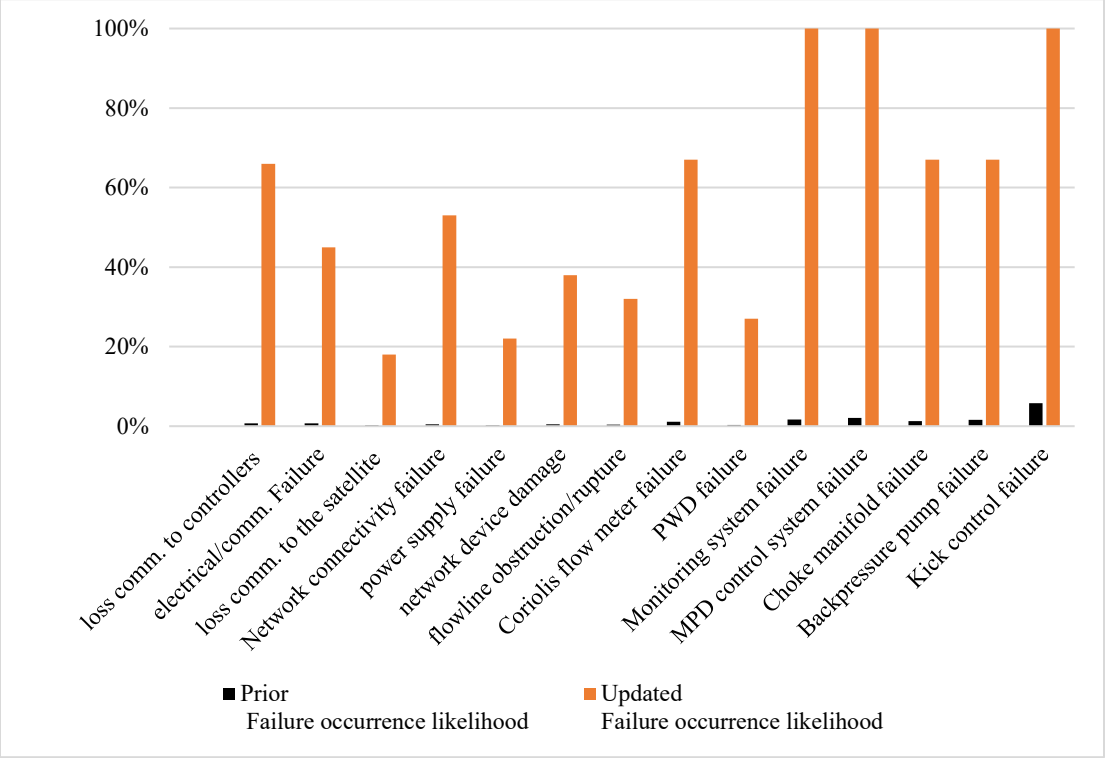

Figure 4.16: Influence of Rig pump failure on a kick control operation

Barrier element approach

The RCD and NRV failures are only limited to their components due to their independencies on other equipment during kick control operation except themselves. For instance, in a scenario when there is an influx during drilling and hydraulic backpressure is applied on the well annulus, the NRV's function prevents upward flow up the drillstring (i.e. U-tube effect). Thus, this specific operation has no relationship with e.g., pump's failure. Hence, the influence of the MPD control system, choke manifold, and backpressure pump is shown in Figure 4.17. It is observed that an MPD control system failure occurrence exhibits most influence in a kick control operation due to its highest number of operational dependencies and interactions with other components to perform its function. For instance, Choke manifold and backpressure pump operations have no dependencies on the functioning of Flow and Pressure sensors, Electrical panel, Mechanistic simulator, Controller unit,

and Hydraulic Model; however, MPD control system does. These inferences are also consistent with those from the numerical model method.

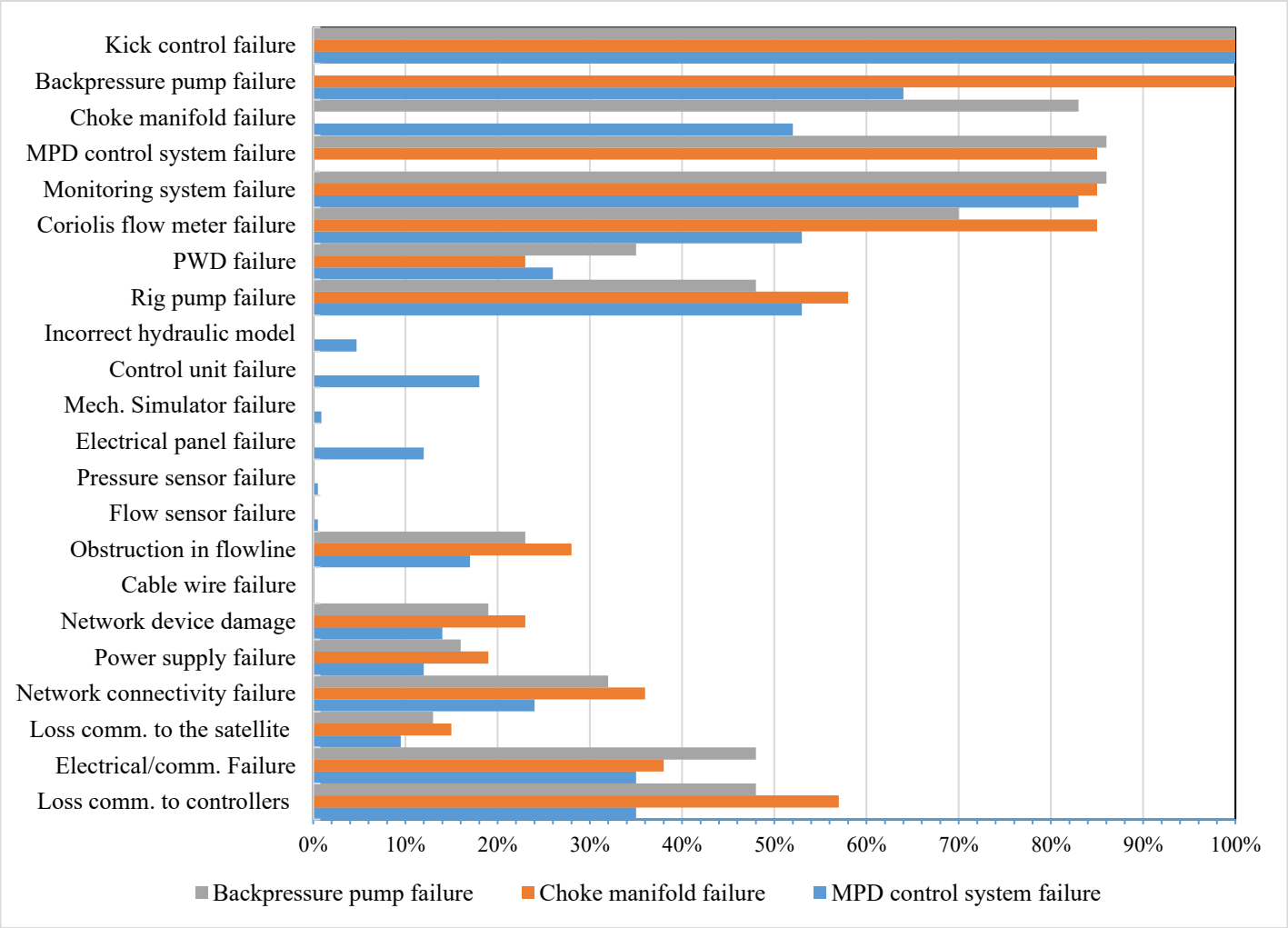

Figure 4.17: Influence of kick control barrier elements on a kick control operation

4.4.3 Discussion

The reliability of constant bottomhole pressure (CBHP) technique of MPD depends on the design of its components and their operational dependencies in managing kick or other abnormal pressure events. While one of the focus of this work is to investigate the reliability of the MPD system, the functionality and operational dependency of all components in the system are also examined. For

the CBHP system utilized in this study, the estimated failure probability to control/mitigate kick occurrence is initially obtained as 0.0574 when the NRV installed in the MPD system setup was only one. However, when the system setup is modified by installing two NRVs in parallel in the drillstring for a redundant configuration, the failure probability of kick control operation decreases to 0.0280 about 50% drop from the previous estimation. The reliability rose from about 94% to 97%. This analysis shows how a modification in the system structure can improve its overall reliability.

Failure of an MPD system to control kick can occur through several scenarios and can be initiated from any component. Failure initiation of any component in the system, excluding those that are redundantly structured, will propagate to a failure of kick control operation. For instance, a failure of one of the three choke valves installed in parallel for redundancy will not propagate to kick control failure; however, when the last choke valve backup fails, the kick control failure occurs. Moreover, a component's failure not only propagates to kick control operation's failure but increases the failure likelihood of other components in the system. This increase in component's failure likelihood depends on the extent of interactions between the failed component and other components in the system. For instance, a network device failure will not only cause kick control operation to fail but also results in loss of communication, monitoring system failure, MPD control system failure, choke manifold failure etc. Additionally, flowline rupture, for example, only influence the functionality of MPD hardware components that process and handle hydraulic control during a kick control operation, and they include Coriolis flow meter, Rig pump, MPD control system, choke manifold, and backpressure pump. These examples show that components have various degree of dependency to each other to perform their functions during kick control operation and that the system failure does not have a sequential approach.

The sensitivity study also provides valuable information about the most critical components or equipment in an MPD system. The criticality assessments of the basic event's components show that network device is the most critical components ahead of the flowline/ pump line rupture, RCD bowl failure, electrical panel failure, and power supply failure. Further comprehensive analysis shows that all components that are associated with communication/data transmission functions collectively exhibit the most influence in kick control operation. This may be due to the reliance of key equipment, such as MPD controller, choke manifold and backpressure pump, on network connectivity to execute their functions during kick control operation. These results are consistent with those of Bhandari et al. (2015) who found the communication failure event to have the highest percentage of contribution to a kick or a blowout occurrence in an MPD operation.

For a kick-control equipment approach, MPD control system is ranked as the most critical equipment. A further investigation shows that the monitoring equipment, i.e. Coriolis flow meter, Rig pump, and PWD, exhibits the most contribution, ~76%, to MPD control system's failure. Among the monitoring equipment, the Coriolis flow meter and the Rig pump exhibit most influence in kick control operation. These findings are consistent with the work of Abimbola et al., (2015) who identified the RCD, Rig pump and MPD control system as the main contributing factors in an MPD hardware system failure. Table 4.6 summarizes the comparisons of the results in this study to those in Bhandari et al. (2015) and Abimbola et al. (2015).

Therefore, the study provides an important insight into how the MPD system's components interact during kick control or pressure management operations. While the operation of several components depends on the functionality of one or more components in the MPD system, the failure scenarios occurrences are non-sequential. Thus, this insight, which was not addressed in Abimbola et al. (2015),

is useful when performing system design improvement for enhanced safety and reliability. Such design improvement may include reducing the excessive dependencies that occur within the system and changing the critical components configurations to be redundant. This study, however, is limited to the operational analysis of dynamic annular pressure control (DAPC) system (a constant bottomhole pressure technique of MPD), whose layout and operational process are different from the Weatherford's MicroFlux® MPD system and the Halliburton's GeoBalance® MPD system. Thus, the outcomes of this study may not broadly apply to all constant bottomhole pressure MPD system. Therefore, the future study may involve the analyses of this MPD system to formulate better conclusions on safety and reliability of MPD operations.

Table 4.6: Summary of outcomes between the FT and BT models on a kick control operation

	Current study	Bhandari et al. (2015)	Abimbola et al. (2015)
Categories	BN model	BN model	BN model
Most safety-critical components	Communication components: e.g. Network device and power supply Flowline / pump line	Communication components	NA
Most safety-critical CBHP equipment	MPD control system	NA	MPD control system, Rig pump, RCD
Most safety-critical component of an MPD control system	Monitoring equipment (Coriolis flow meter, rig pump)	NA	NA

4.5 Conclusions

The current study presents a reliability assessment of kick control operation in a constant bottomhole pressure technique of managed pressure using a dynamic annular pressure control system. A fault tree model is used to develop all possible scenarios and conditions within the system that can lead to a kick control failure and then mapped into Bayesian Network for analyses. Firstly, the estimated reliability of kick control operation of the system increases from 94% to 97% after structural modification of installing two non-return valves in parallel, instead of one, in the bottomhole assembly for a redundancy. Secondly, the top-three most safety-critical components in kick control operation include network device, flowline, and Rig pump line. Further analysis shows that communication related components have the most influence on kick-control operations compared to flowline/Rig pump line rupture whose influence is only limited to equipment that processes hydraulic control e.g., choke manifold. However, at the equipment level, managed pressure drilling control system exhibits the most influence on kick- control operation, making it the most safety-critical equipment. Further analysis of the control system shows that monitoring equipment is the most safety-critical set of equipment (accounting for about 76% of its failures). Lastly, the kick control failure of a managed pressure drilling system can occur in several scenarios and can be initiated from any component in the system. Additionally, due to operational dependencies among components, a failure of any component does not only cause a failure of the kick-control operation but increases the failure likelihood of dependent components. Consequently, these outcomes show that the modes of failure in a managed pressure drilling system are non-sequential. In conclusion, it is recommended that a future study involving the analyses of the Weatherford's MicroFlux® MPD system and the Halliburton's GeoBalance® MPD system be completed to formulate broader conclusions on safety and reliability of MPD operations.

Chapter 5 Nonlinear model predictive control of gas kick in a Managed Pressure Drilling system

Preface

This chapter presents an MPD control model, which consist of a nonlinear model predictive controller (NMPC) and a two-phase flow hydraulic model. for performing numerical simulation of a managed pressure drilling. A paper version of this chapter has been published in the ***Journal of petroleum science and engineering (2019), Vol. 174 pp. 1223–1235****. Along with the co-authors, Dr. Syed Imtiaz, Dr. Faisal Khan, and Dr. Stephen Butt, I have co-authored this chapter. I developed the model, made first attempt to perform the model analysis, and interpret the data and results. The co-author Faisal Khan helped in developing and validating the concepts, reviewed and corrected model results, and contributed in preparing, reviewing and revising the manuscript. The co-author Dr. Syed Imtiaz helped in the model development, improvement, interpretation, and validation, and in organizing and revising the manuscript. The co-author Dr. Stephen Butt contributed through assisting in analyzing the data, validating simulation results and revising the manuscript. Co-authors Drs. Imtiaz, Butt and Khan reviewed the revisions and provided feedback which I have implemented. I prepared the first draft of the manuscript and subsequently revised the manuscript based on the co-authors' feedback and the peer review process.*

Abstract

Managed pressure drilling (MPD) operation utilizes a fully automated control system to manage kick during drilling which typically utilizes a proportional-integral (PI) controller and a single-phase flow model. This study proposes an MPD control system that uses a nonlinear model predictive controller (NMPC) and a two-phase flow model for computing annular pressure and choke valve dynamics during kick control operation. The performance of the proposed model is demonstrated by simulating

kick control operation and compared their results with a single-phase linear model. The results confirm that the single-phase model underestimates key well control parameters (including kick size, bottomhole pressure and choke pressure), which may be due to ignoring gas-phase flow behaviour on mud density and the choke valve performance. Additionally, the performance of the proposed model is tested by validating the gas kick simulation results from a lab-scale MPD setup and a gas kick event from a field's case study based on North Sea drilling operation. The comparison of the control performance between the proposed NMPC model against the PI controller utilized in the field study confirms that the NMPC responds more swiftly to disturbance, such as kick than the PI controller.

Keywords: NMPC; MPD; Kick; Pressure control; Flow control; Drilling

5.1 Introduction

Well control is one of the most significant operations in drilling; more so in offshore exploration and production. It is even more challenging considering that most prospects for hydrocarbon resources are drifting exploration into the deepwater (Graham et al., 2011) or posing operational challenges that range from depleted formations (such as reservoirs with narrow pressure windows) to high-pressured formations. The narrow margins are most prominent in deepwater applications where much of the overburden is the seawater (Malloy and McDonald, 2008). These extreme drilling environments heighten geological uncertainties and their complexity are becoming the norm in nowadays drilling operations. Issues, such as well control incidents (e.g. kick) are periodically encountered and can increase operational costs (e.g. lengthy non-productive time - NPT) and risk, especially when drilling using an open hydraulic system (i.e. conventional - overbalanced drilling method). Some of the associated risks with deepwater drilling are discussed in Bhandari et al., (2015);

Pui et al. (2017), in addition to proposing useful methodologies to assess and reduce the overall risk in an MPD operation.

Kick mechanisms have been covered explicitly in the literature, including in Khakzad et al. (2013). Thus, to avoid or reduce the likelihoods of kick during drilling, managed pressures drilling (MPD) has been implemented to maintain the downhole pressure within the drilling pressure window, even during kick events. MPD operation combines the use of automated drilling and specialized equipment to achieve well control objectives (Godhavn, 2010). Contrary to conventional drilling practice that relies primarily on mud weight as the primary safety barrier element (Khakzad et al., 2013), managed pressure drilling operation utilizes, in addition to mud weight, special equipment such as a rotating control device, choke manifold, backpressure pump, and MPD control system to control the downhole pressure. Because an MPD is operated in a closed loop system, it improves the safety, efficiency, and economic of drilling operations while avoiding continuous flow to the surface (Gala and Toralde, 2011; Rohani, 2012; Malloy and McDonald, 2008; Kok and Tercan, 2012; Sule et al., 2018b).

Sule et al. (2018b) identifies MPD control system as the most safety-critical component; thus, brings MPD control system under the microscope of safety and reliability investigation, which justifies the significance of this study. Automatic control solutions for complex and challenging operations, such as drilling, have been adequately covered in the literature, including its economy and safety benefits (Godhavn 2010; Godhavn et al., 2011; Zhou and Nygaard, 2011). In an automated MPD system, a combination of hydraulic model and control system is used to automatically control downhole pressure during drilling operations (Godhavn 2010; Godhavn et al., 2011). The key objective of an MPD is to accurately control the downhole pressure by regulating the backpressure to compensate

for annular pressure fluctuations. Thus, in an automated MPD system, the automatic operation of the choke manifold is performed by a control system, which typically consists of two main parts: a hydraulic model (to estimate the downhole pressure in real-time) and a controller scheme (to automates the choke manifold to maintain the desired choke pressure). The hydraulic models can be simple or advanced, although the latter is more challenging and complex (Kaasa et al., 2011) and the controller ranges from proportional integral derivative (PID) controller scheme to a non-linear model predictive controller (NMPC).

Automatic pressure control system for an MPD generally adopts the simplified hydraulic model. The detail of its derivations is available in Kaasa et al. (2011). Godhavn (2010) presents a tunable PI controller that utilizes feedback and feed-forward control to control the choke pressure, whereby the feed-forward loop compensates for disturbances gain and the closed loop feedback compensates for error and maintain system equilibrium. To improve the performance and the capabilities of kick estimation and automatic well control system, Zhou et al. (2010) presents adaptive observers for estimating the flow rates through the well and the reservoir pore pressure for improved kick management using a PI controller. Zhou et al. (2011) presents an MPD automatic control procedure, which uses a switched control scheme and a PI controller that, on one hand, regulates the annular pressure in the well during drilling and on the other hand, attenuates kick in the event of a reservoir influx.

Stamnes et al. (2011) presents a method to redesign adaptive observers that use an adaptive law based on delayed observers to give better parameter estimation and robustness properties; however, the method is computationally intensive for the added marginal improvement. Godhavn et al. (2011) presents a nonlinear model-based control scheme and observers to improve pressure control during MPD operations using a feedback linearization method. Hague et al. (2013) utilizes a switched

control concept in controlling bottomhole pressure; whereby an MPD system controller manipulates the choke and backpressure pump by switching between a combination of pressure and flow control when there is no influx, and pure flow control when a kick is detected. Li and Kamel (2016) develops a controller tuning parameter framework for a PI controller that improves the robustness of MPD control system stability and pressure control performance based on the work of Godhavn et al. (2011).

However, most processing systems are nonlinear; thus, in some cases when linear control solutions, such as in PID controller, are insufficient to capture the nonlinearity of a system, the nonlinear controller is sought. Therefore, the nonlinear model predictive controller (NMPC) is one of the advanced and sophisticated nonlinear process controllers that has been a major research focus area within the control community in the recent decades (Godhavn et al. 2011). Its application in drilling automation is only emerging compared to all other industries such as automation, robotics, and aeronautics. Nygaard and Nævdal (2006) presents a nonlinear model predictive control (NMPC) scheme for stabilizing the well pressure during oil well drilling. Breyholtz and Aamo (2008) develops a low-order nonlinear model predictive controller to control bottomhole pressure within specified setpoint during pipe connection operation in MPD setup. Nandan and Imtiaz (2016) proposes a nonlinear model predictive controller for automatic control of an MPD system. Park (2018) presents a new Hammerstein-Wiener nonlinear model predictive controller for bottomhole pressure regulation in controller design.

Another important aspect of an MPD control model is the accuracy estimation of the choke/ bottomhole pressure and kick size. Gas kick incident is particularly severe and challenging to manage, especially in deepwater drilling. Unfortunately, this topic has not been adequately addressed in most MPD control model simulations and only a few studies have sparsely discussed the effects of gas-phase influx in their MPD control simulator. Zhou et al. (2011) noted that because their model does

not account for gas-phase, the estimation of reservoir fluid that contains gas-phase will cause considerable modelling error in influx size. As discussed in Kaasa et al. (2011), an influx of liquid and gas mixture into the annulus will cause the bulk modulus in the annulus to drop; thus, affect the model estimation of influx size and/or the casing pressure. Aarsnes et al., (2016) proposes a simple model of two-phase (gas–liquid) flow based on the drift-flux model to account for gas influx effects on casing pressure transient and to estimate the effective bulk modulus in the annulus. Aarsnes et al. (2014) and Ambrus et al. (2017) propose a choke model for a mixed flow to account for both liquid and gas phase flowing through the choke.

Thus, the current study proposes a two-phase flow nonlinear model predictive controller based on Nandan and Imtiaz (2016) for automatic control of an MPD system. The hydraulic model is a modified Kaasa et al. (2011) model using a simplified transient two-phase flow model proposed in Aarsnes et al. (2014), Aarsnes et al. (2016) and Ambrus et al. (2017). In addition, the study shows the underestimation in influx size and choke pressure from Nandan and Imtiaz (2016), which did not account for the effect of gas phase influx during kick attenuation operations.

5.2 Managed Pressure Drilling (MPD) Control System

It has been shown that the real-time advanced hydraulic model needs calibration data for accurate prediction of downhole pressure. These can be found in Rommetveit and Vefring (1991); Bjørkevoll et al. (2000); Bjørkevoll et al. (2003); Bjørkevoll et al. (2008); Petersen et al. (2001); Petersen et al. (2008a); Kutzensov et al., (2010). However, due to computational challenges and insufficient data to calibrate the physical parameters of an advanced hydraulic model, it falls short of contributing to the overall accuracy of downhole pressure prediction (Kaasa et al., 2011). When a control system is only responsible for low-frequency changes within a bandwidth of its closed-loop instead of high-frequency dynamics, then the system is more robust to disturbances. A control system with simple

and relatively accurate within the bounded frequency of interest can be implemented in an MPD control system (Kaasa et al., 2011; Godhavn, 2010).

Kassa et al. (2011) proposed a simplified hydraulic model using the governing equation of state, continuity (mass transfer) equation, momentum equation, and energy equation. The simplified hydraulic model used in MPD control system is based on a hydraulic flow path categorized into two control volumes: the drill string volume (CV 1) and the annulus volume (CV 2) as shown in Figure 5.1. The drillstring control volume captures the mud flow from the rig pump through the drill pipe to the bit while the annulus control volume captures the mud flow from the bit through the annulus to the choke valve topside. If the reservoir influx does not enter the drill string, the pressure dynamics inside the drill string and the flow rate exiting the bit can be described adequately by a simplified single-phase liquid flow model. Thus, equations (5.1) and (5.2) can be used to compute the pump pressure and flow rates through the bits. The annulus control volume, which is affected by reservoir influx, will be described by the two-phase flow model in this section.

$$\frac{dP_p}{dt} = \dot{P}_p = \frac{\beta_d}{V_d}\left(q_p - q_b\right) \tag{5.1}$$

$$\dot{q}_b = \frac{1}{M}\left(P_p - P_c - F_d {q_b}^2 - F_a(q_{res} + q_b)^2 + (\rho_d - \rho_a) g h_{TVD}\right) \tag{5.2}$$

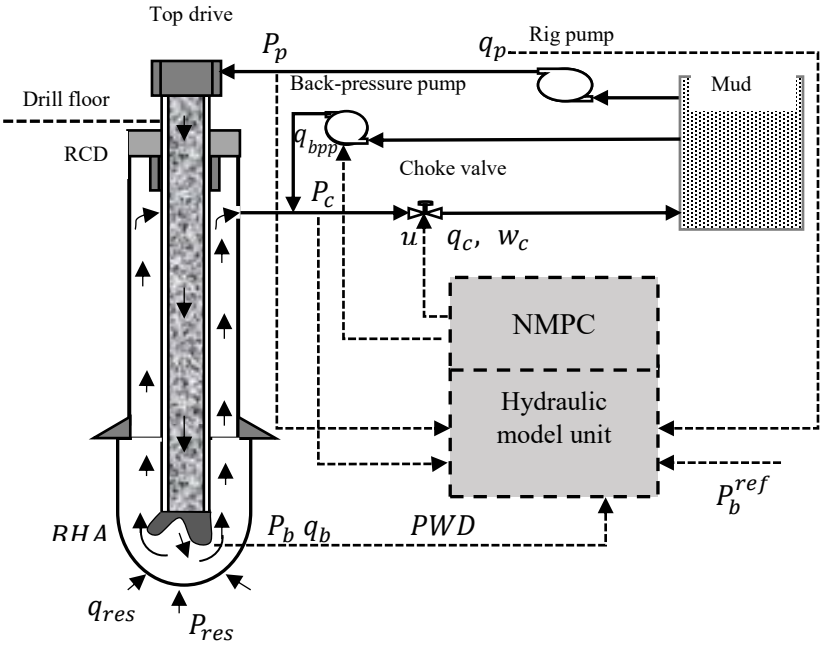

Figure 5.1: Managed pressure drilling control system process flow diagram

5.2.1 Two-phase hydraulic model with choke pressure dynamics

5.2.1.1 Model Assumptions and Limitations

Given the complexity of flow dynamics involved in drilling-fluid hydraulics, a simplified model that removes unnecessary complexity without sacrificing the accuracy of system performance, such as in managed pressure drilling (MPD) control system, is desirable. More so, Kaasa et al. (2011) expressed that in practice, much of the complexities do not contribute to the improvement of the overall accuracy of pressure estimation during MPD operations. Thus, the current model adopts the simplification presented in Aarsnes et al. (2016) and Ambrus et al. (2017) for the drift-flux model with the following assumptions:

a) A steady-state flow with constant temperature profile throughout the length wellbore (i.e. temperature transient is neglected.
b) The variation of liquid density is negligible along the flow path in time and space
c) The velocity of the gas-liquid mixture is uniform in space when calculating the pressure profile

d) The annulus (pipe) is a single control volume (this allows a lumped expression for pressure dynamics in the annulus).

e) The pressure transient terms are neglected when computing the gas and liquid velocities.

Thus, these assumptions limit the model performance to non high-temperature high-pressure well. In a high-temperature high-pressure well, temperature transient effects are significant and cannot be neglected or ignored. Additionally, the model simplification causes the pressure fluctuations to propagate instantaneously; thus, affects the accuracy of the model during fast transients.

5.2.1.2 Two-phase flow in the annulus

Aarsnes et al. (2016) begins the development of a simplified two-phase flow model in the pipe from a classical Drift-Flux Model (DFM) formulation described in Evje and Wen (2015); Gavrilyuk and Fabre (1996). The detail description of the derivation can be found in (Aarsnes et al., 2016; Ambrus et al., 2017). Then applied the model to a pressure dynamic in the wellbore annulus through to choke valve. The two-phase flow model directly affects the choke pressure dynamics in the annulus due to the influx of gas-phase into the control volume, as in Figure 5.1. For simplicity, Aarsnes et al. (2016) lumped the pressure dynamics by treating the annulus (or flow pipe) as one control volume, and applied mass conservation law to define the modified choke pressure dynamic as:

$$\frac{\partial P(x,t)}{\partial t} \approx \frac{\partial P_L}{\partial t} = \frac{\beta_L}{V}(q_L + q_G - q_c + T_{EG}) \qquad (5.3)$$

Where β_L is the bulk modulus of fluid in the annulus, V is volume of the annulus, $q_C, q_G,$ and q_L are flow rate through the choke, flow rates of mixture in gas phase, and liquid phase respectively, and T_{EG} is total gas expansion. T_{EG} is the effect of in-domain gas expansion on the lumped pressure dynamics and given by:

$$T_{EG} = T_{XE} - A\int_0^L \frac{C_0\alpha_G}{\gamma P} dx \frac{\partial P_L}{\partial t} \quad (5.4)$$

The T_{EG} is then divided into two terms, which affects the effective bulk modulus of the gas–liquid mixture, $\bar{\beta}$, and the remaining term, T_{XE}, which accounts for source terms and the gas expansion when propagating through the negative pressure gradient. T_{XE} is determined by equation (5.5) and v_{G0} is initial gas velocity.

$$T_{XE} = A(v_G(L) - v_{G0}) \quad (5.5)$$

By inserting equation (5.5) into (5.3), the choke pressure dynamic becomes:

$$\frac{\partial P_L}{\partial t}\left(1 + \frac{\beta_L}{L}\int_0^L \frac{C_0\alpha_G)}{\gamma P} dx\right) = \frac{\beta_L}{V}(q_L + q_G - q_c + T_{XE}) \quad (5.6)$$

By defining the effective bulk modulus term, equation (6.6) is further simplified as:

$$\frac{dp_c}{dt} = \dot{P}_c = \frac{\bar{\beta}}{V_a}\left(q_b + q_{bpp} + q_{res} - q_c + T_{XE}\right) \quad (5.7)$$

Where the effective bulk modulus is determined by:

$$\bar{\beta} = \frac{\beta_L}{1+\frac{\beta_L}{L}\int_0^L \frac{C_0\alpha_G}{\gamma P} dx} \quad (5.8)$$

The v_G is the velocity of the gas, α_G is the volume fraction of gas in the liquid-gas mixture, C_0 is a drift flux distribution parameter, γ is a gas expansion factor, L is the total vertical depth, and P is the pressure. In Aarsnes et al. (2014) and Aarsnes et al. (2016), the mass conservation law is expressed for the gas and the liquid mixture separately and closure relations are developed to solve the volume fraction α_G and pressure P. Thus, the following equations are defined:

$$\rho_m = \alpha_G \rho_G + \alpha_L \rho_L \quad (5.9)$$

$$v_m = \alpha_G v_G + \alpha_L v_L \quad (5.10)$$

$$\alpha_G + \alpha_L = 1 \tag{5.11}$$

Where ρ_m is the density of the mixture, ($\alpha_G \rho_G = n$) is the mass variable of gas, ($\alpha_L \rho_L = m$) is the mass variable of the liquid, v_m is the mixture velocity, α_G and α_L are the volume fractions of gas and liquid respectively, and v_G and v_L are the velocities of fluid in the gas phase and liquid phase respectively. The sum of volume fractions of gas and liquid must be satisfied as in equation (5.11). The phase densities are defined as a function of the pressure, P and sound velocities $c_{G,L}$.

$$\rho_G = \frac{P}{c_G^2(T)}, \qquad \rho_L = \rho_{L,0} + \frac{P}{c_L^2} \tag{5.12}$$

By combining equations (5.11) and (5.12), the relations for determining the volume fractions from the mass variables are obtained as follows:

$$\alpha_G = 0.5 - \frac{\frac{c_G^2}{c_L^2}n + m + \sqrt{\Delta}}{2\rho_{L,0}} \tag{5.13}$$

$$\Delta = \left(\rho_{L,0} - \frac{c_G^2}{c_L^2}n - m\right)^2 + 4\frac{c_G^2}{c_L^2}n\rho_{L,0} \tag{5.14}$$

The pressure term can then be obtained by equation (5.15).

$$P = \begin{cases} \left(\frac{m}{1-\alpha_G} - \rho_{L,0}\right)c_L^2, & if\ \alpha_G \le \alpha_G^* = 0 \\ \frac{n}{\alpha_G}c_G^2 & otherwise \end{cases} \tag{5.15}$$

Where α_G^* is the condition when the gas phase vanishes and $\rho_{L,0}$ is the reference liquid density. The gas velocity v_G in equation (5.5), can be obtained traditionally by so-called slip relation as given by equation (5.16)

$$v_G = C_0 v_m + v_\infty \tag{5.16}$$

Where v_∞ is the slip velocity, C_0 is the distribution parameters, and v_m is the mixture velocity and is obtained by equation (6.11). The parameters: v_∞ and C_0 can be determined from Bhagwat and Ghajar (2014). However, because of the transition between the single and two-phase flow, a more involved

relation, with state-dependent parameters is needed (Aarsnes et al., 2016); thus, equation (5.17) is proposed.

$$v_G = (K - (K-1)\alpha_G)v_m + \alpha_L S \tag{5.17}$$

Where K and S are positive constants where K ≥ 1 and S ≥ 0.

5.2.1.3 Choke flow model

For a two-phase (liquid-gas mixture) flowing through the choke, the flow rate through the choke can be modeled as a function of choke parameter, choke opening, density, and pressure drop through the choke. By applying a mass conservation law to the total mass flow rate of the two-phase liquid-gas mixture and averaging the density of the two-phase mixture, the mass flow rate through the choke is determined by equation (5.18) from Ambrus et al. (2017).

$$w_c = u_c\, A_o C_d \sqrt{\frac{2(P_c - P_0)}{\frac{\chi_L}{\rho_L} + \frac{\chi_G}{\gamma^2 \rho_G}}} \tag{5.18}$$

Where u_c is the choke control input from the choke valve ranges between position 0% and 100%, i.e. u_c = [0 – 1], w_c is the mas flow rate of the two-phase mixture through the choke, χ_L is the liquid mass fraction, χ_G is the gas mass fraction, γ is the gas expansion factor. With χ_L and χ_G sum up to unity, χ_L or χ_G can be computed as ***f***(volume fraction α, density ρ, and velocity v) as given in equation (5.19):

$$\chi_G = \frac{\alpha_G \rho_G v_G}{\alpha_G \rho_G v_G + \alpha_L \rho_L v_L};\ \chi_L = 1 - \chi_G \tag{5.19}$$

The mass flow rate through the choke in equation (5.19) can be expressed in terms of volume flow rate to obtain a modified two-phase flow choke model given in equation (5.20) as:

$$q_c = w_c\left(\frac{\chi_L}{\rho_L}+\frac{\chi_G}{\rho_G}\right) = u_c\, A_o C_d \left(\frac{\chi_L}{\rho_L}+\frac{\chi_G}{\rho_G}\right)\sqrt{\frac{2(P_c-P_0)}{\frac{\chi_L}{\rho_L}+\frac{\chi_G}{\gamma^2\rho_G}}} \qquad (5.20)$$

5.2.2 Model implementation algorithm

The hydraulic model used in the current study is a modified Kaasa model (Kaasa et al., 2011) equipped with a simplified two-phase flow model that accounts for the gas-phase influx into the wellbore during kick event. The two-phase flow model utilizes drift flux model to describe the choke pressure dynamics in the annulus and the choke flow model at the surface (Aarsnes et al., 2016; Ambrus et al., 2017). Thus, based on the model system in Figure 5.1, the model implementation algorithm in the NMPC operation is given in Figure 5.2.

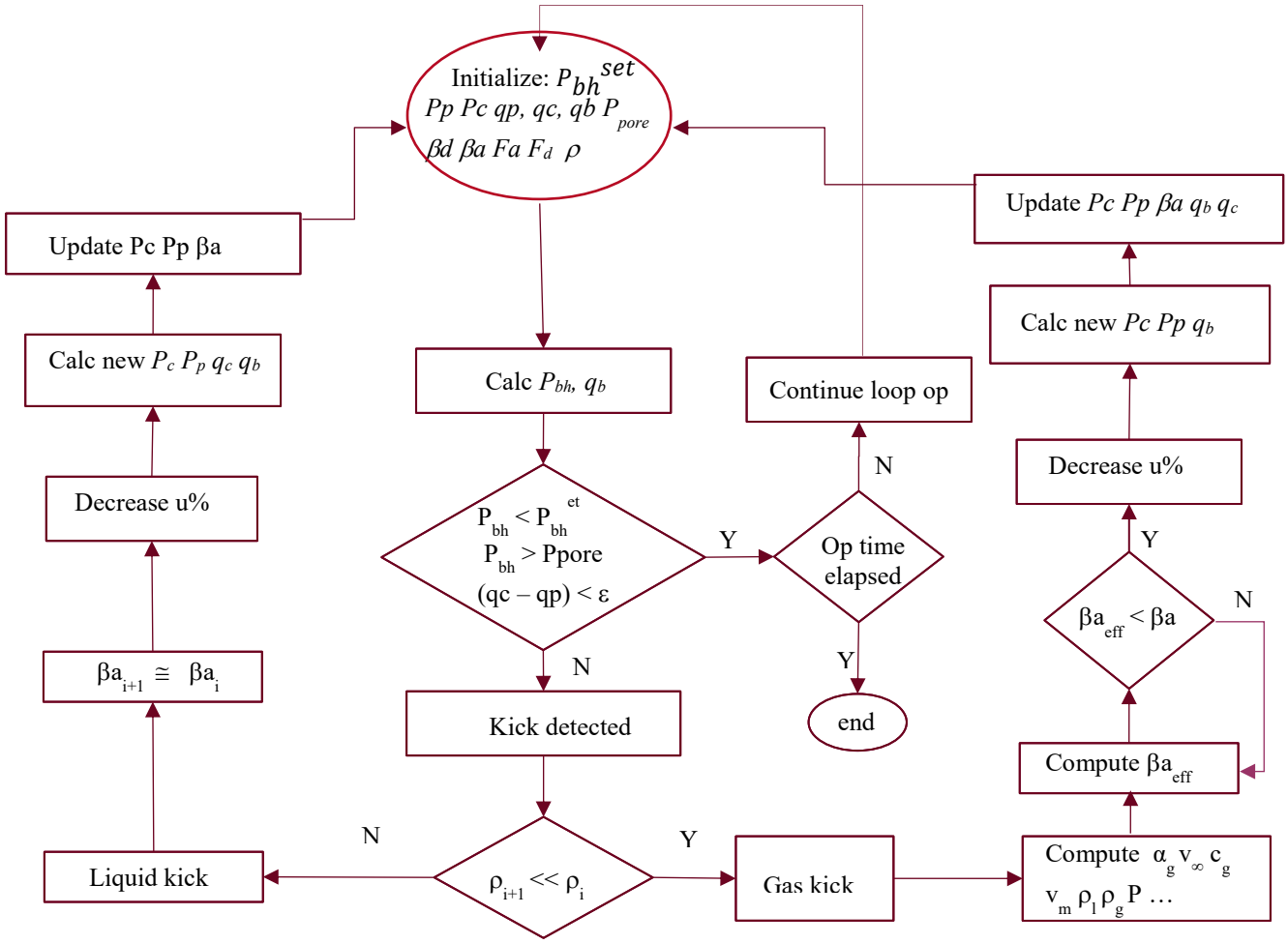

Figure 5.2: The Model implementation algorithm

5.3 The Controller Design Strategy

The main goal of a nonlinear model predictive control, NMPC, is to utilize optimized feedback and predictive control to stabilize and track nonlinear systems. The NMPC block uses plant references, setpoints, known disturbances and current state estimate as inputs to iteratively to solve horizon optimal control problem at each assigned sampling timestep and obtain a fast convergence (Grüne and Pannek, 2017). One common and popular choice to achieve such fast convergence between the reference output and predicted output, is the quadratic function (Grüne and Pannek, 2017), which is utilized in Nandan and Imtiaz (2016). Thus, the control strategy used in the current study is based on Nandan and Imtiaz (2016) nonlinear model predictive control structure, whose core elements include the cost function, prediction model, state constraints, and input constraints. Additionally, the information on NMPC optimization formulation, such as discretization and finite parameterization, optimal control, tuning, and stability can be found in Grancharova and Johansen (2012).

5.3.1 NMPC controller setup

In the current study, a discrete-time nonlinear system optimization is used and is defined as follows:

$$x(t+k) = f(x(t), u(t), d)$$

$$y(t) = Cx(t)$$

Where $x(t), u(t), and\ y(t)$ represent the state, input, and output variables respectively, d represents a bounded disturbance parameter, and f represents the mapping (or state space) function. In the current study, the control variables for the NMPC is setup as follows:

- State vector x, $x = \left[P_p, P_c, q_b\right]^T$ (5.21)
- Control variable u $u = u_c$ (5.22)
- Control output y $y = P_{bh}$ (bottomhole pressure) (5.23)

- Disturbance d $d = q_{res}$ (influx) (5.24)

The nominal state space equation and the output of the system are given by equations 5.25 and 5.26 respectively.

$$\dot{x} = f(x, u) \tag{5.25}$$

$$y = g(x) \tag{5.26}$$

At the initial step of the iteration, the predicted states, given by equation (5.27), is augmented by adding a disturbance d equal to zero ($q_{res} = 0$) and a disturbance integrator (Morari and Maeder, 2012) given by equation (5.28) and (5.29). The prediction model is numerically integrated using explicit Runge-Kutta 4,5 method (Nandan and Imtiaz, 2016):

$$x(k+T) = x(k) + \int_k^{k+T} f(x(\tau))d\tau \tag{5.27}$$

$$x(k+T) = x(k) + \int_k^{k+T} f_{aug}(x(\tau), d(k))d\tau \tag{5.28}$$

$$d(k+T) = d(k) \tag{5.29}$$

Where $x(k)$ is the current state and T is the sampling interval, and f_{aug} is the augmented state function.

The optimization control formulation is given by equation (5.30), where the cost function *j* is set to minimize the error between the equilibrium state targets $\bar{x}$ and system state $x(k)$ and between the equilibrium control input targets $\bar{u}$ and current control input $u(k)$ to achieve offset free tracking of reference input $y(k) = P_{bh}^{ref}$, i.e. the bottomhole pressure setpoint reference. In this work, the cost function set to zero.

$$J = \min_{u} \sum_{\kappa=k}^{k+m} (\hat{x}(\kappa) - \overline{x})^T \lambda_1 (\hat{x}(\kappa) - \overline{x}) \; + \lambda_2 (u(\kappa) - \overline{u})^2 \tag{5.30}$$

Where $\lambda_1 \in \mathbb{R}^{3\times3}$ and $\lambda_2 \in \mathbb{R}^{1\times3}$ are cost function weights and m is the prediction horizon. This optimal control problem is subject to the following constraints:

$$\overline{x} = f_{aug}(\overline{x}, \overline{u}, \hat{d}(k)) \tag{5.31}$$

$$y(k) = g_{aug}(\overline{x}, \hat{d}(k)) \tag{5.32}$$

$$\hat{d}(0) = \hat{q}_{res} \tag{5.33}$$

$$\hat{x} \in \mathbb{X}, \hat{x} \in \mathbb{X}_{NL}, u(k) \in \mathbb{U} \tag{5.34}$$

$$\bar{x} \in \mathbb{X}, \bar{u} \in \mathbb{U} \tag{5.35}$$

Where the state and input constraint set: $\mathbb{X}$ and $\mathbb{U}$ are given by equations 5.36 and 5.37:

$$\mathbb{X} := \begin{bmatrix} P_p^{min} \leq P_p \leq P_p^{max} \\ P_c^{min} \leq P_c \leq P_c^{max} \\ q_{bit}^{min} \leq q_{bit} \leq q_b^{max} \end{bmatrix} \tag{5.36}$$

$$\mathbb{U} := \left[u_c^{min} \leq u_c \leq u_c^{max}\right] \tag{5.37}$$

The main control objectives are to identify and maintain reservoir influx, account for the effects of gas-phase in the reservoir influx mixture and track the output reference $r(k) = P_{bh}^{ref}$. Additionally, a nonlinear state constraint equation to control influx within a defined threshold, in this case, is given by equation (6.38):

$$\mathbb{X}_{NL} := [0 \leq (q_c - \bar{q}_{bit}) \leq \epsilon] \tag{5.38}$$

Where $\bar{q}_{bit}$ is the equilibrium state target for the flow rate through the bit and $\epsilon = 0$.

5.3.2 Flow rates and reservoir pressure estimations

State space parameters consisting of the flow rate through the bit, q_b, reservoir influx flow rate, q_{res}, and reservoir pressure, P_{res}, are usually unknown and are unmeasured parameters during drilling and are required for the NMPC controller to obtain the target equilibrium. For example, the NMPC controller needs a reservoir pressure estimate to compute new pressure setpoint. Thus, the current study adopts the adaptive observers from Zhou et al. (2011) to estimate these state pace parameters. The adaptive observers for estimating the flow rate through the bit, q_b, are given in equations (5.39) and (6.40) below:

$$\dot{\hat{P}}_p = \frac{\beta_d}{V_d}\left(q_p - \hat{q}_b + l_1\left(P_p - \hat{P}_p\right)\right) \tag{5.39}$$

$$\dot{\hat{q}}_b = -\gamma_1\left(P_p - \hat{P}_p\right) \tag{5.40}$$

Where l_1 and $\gamma_1$are positive design constants and $P_p - \hat{P}_p = \bar{P}_p$ and $(q_b - \hat{q}_b) = \bar{q}_b$ are defined as the error variables. The q_{res}, observers are given by equations (5.41 and 5.42).

$$\dot{\hat{q}}_1 = q_p + q_{res} - q_c + l_2(q_1 - \hat{q}_1) \tag{5.41}$$

$$\dot{\hat{q}}_{res} = -\gamma_2(q_1 - \hat{q}_1) \tag{5.42}$$

Where l_2 and $\gamma_2$are positive design constants and $(q_1 - \hat{q}_1) = \bar{q}_1$ and $(q_{res} - \hat{q}_{res}) = \bar{q}_{res}$ are defined as the error variables. Finally, using the reservoir influx model based in equation (5.10), the observer for estimating the reservoir pore pressure can be obtained using equation (5.43 and 5.44), where $\dot{\hat{q}}_2$ is the reservoir adaptive observer.

$$\dot{\hat{q}}_2 = q_p + k\left(\hat{P}_{res} - P_{bh}\right) - q_c + l_3(q_1 - \hat{q}_2) \tag{5.43}$$

$$\dot{\hat{P}}_{res} = \gamma_3(q_1 - \hat{q}_2) \tag{5.44}$$

By applying an adaptively updated law, the reservoir is estimated using equation (5.44); where l_3 and $k$are positive design constants and γ_3 is an adaptation gain. Therefore, $\hat{P}_{res}-P_{bh}$ should converge to zero as the error variable $\bar{P}_{res} = \left(P_{res} - \hat{P}_{res}\right)$ tends to zero.

5.3.3 Controller operation algorithm

The primary goal of an NMPC is to predict the future behaviour of the process control over a finite time horizon and determines an optimal control input that meets the requirement of the cost function at a sampling instant. The NMPC operation algorithm, as illustrated in Figure 5.3, consists of three components: the optimizer, the state estimator, and the target tool and are defined as follows:

i. the ***optimizer*** applies all defined system constraints to compute an optimal open-loop control trajectory that satisfies the system constraints and the minimization cost function.
ii. the ***estimator*** predicts the future outputs of the plant by using the input and output data from the plant, and
iii. the ***target tool*** finds a state and input target to obtain the desired output of the system while applying state and integrated disturbance estimates and setpoint values.

After setting the number of iterations, sampling time, prediction horizon, and initial values (time, t_0, state vector, x_0 and control input, u_0), the NMPC iteration begins by:

a) obtaining new initial values,
b) solving the optimal control problem by applying the defined constraints and cost function to obtain a new control input u_k.
c) applying the control u_k to plant model and compute open loop solution of the system

d) applying control u_k and system output y_k to the estimator, which uses moving horizon estimation to predict the state $\hat{x}$, and disturbance $\hat{d}$ trajectories.

e) applying state $\hat{x}$, $\hat{d}$ and input system reference, y_{ref} in the target state to find the desired output for the system

f) applying the optimal input trajectory to the system until the next sampling instant, during which the horizon is shifted, and the procedure is repeated until the number of iterations set is elapsed.

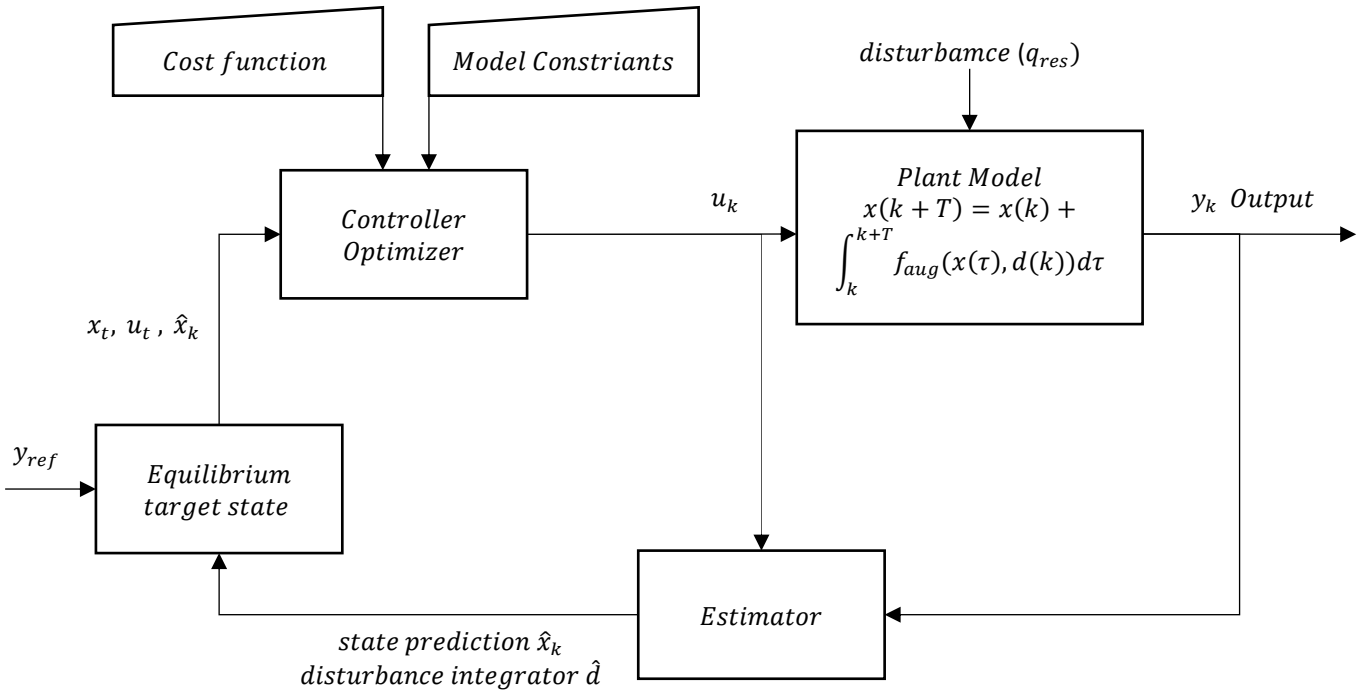

Figure 5.3: NMPC Controller operation loop

5.4 Results and Discussion

In this section, series of simulations are performed to demonstrate the gaps in the model presented in Nandan and Imtiaz (2016) and the errors that result when multi-phase kick fluid (or reservoir influx) is treated as a single-phase liquid flow. In addition, the current NMPC MPD control model is

validated using the results from a lab-scale MPD system simulator and a field case study. The NMPC controller is executed using a MATLAB code based on Grüne and Pannek (2017). The NMPC scheme in the current study is an extension of Nandan and Imtiaz (2016) and uses a sequential discretization method to solve the finite horizon optimization problem. The sampling intervals are set as 5 and 6 seconds based on simulation objectives and controller performance sensitivity in Grüne and Pannek (2017). The pressure window and pump flow capacity, which are used to set the controller bandwidth (or constraints), is based on the reservoir (pore pressure) and a fracture pressure and surface equipment safe operating range. So, the aim of the controller is to safely detect and attenuate kick while maintaining a downhole pressure window.

5.4.1 Effects of the gas-phase influx on kick attenuation

Using a single-phase flow liquid model in an MPD controller may underestimate the kick size or the choke pressure needed to successfully stop the influx due to ignoring gas flow behaviour. The control model presented in Nandan and Imtiaz (2016) only considers reservoir influx as a single-phase liquid; thus, the NMPC scheme does not account for a gas-phase influx behaviour, which is expected when the overpressured zone is encountered during drilling. The following highlights the difference between the proposed model and Nandan and Imtiaz (2016):

a) Nandan and Imtiaz control model implements a single-phase hydraulic flow while the proposed model implements a two-phase liquid-gas hydraulic flow model
b) In Nandan and Imtiaz (2016), the annulus bulk modulus model is fixed, even after influx of reservoir fluid into the well, whereas the proposed model accounts for change in bulk modulus of annulus fluid after reservoir influx is encountered to ensure more accurate estimation of the required choke pressure to stabilize the bottomhole pressure (BHP) set point.

c) The choke model implemented in Nandan and Imtiaz (2016) model ignores the characteristic effects of gas-phase fluid in the reservoir influx, which lead to underestimation of influx size and required surface backpressure to regain wellbore stability; whereas the choke model in the proposed model implements a two-phase (liquid-gas mixture) flow to accounts for the characteristic effects of gas-phase and to improve the accuracy of kick size and surface backpressure required to regain wellbore stability.

Thus, kick control simulations are performed to demonstrate the performance of the proposed model against the Nandan and Imtiaz (2016). The plant state and input constraints used in these simulations are given in Table 5.1.

Table 5.1: Plant parameters (Sources: Nandan and Imtiaz, 2016; Aarsnes et al., 2016)

Parameter	**Value**	**Unit**
Volume of annulus $(\boldsymbol{V_a})$	89.9456	m^3
Volume of drillstring $(\boldsymbol{V_d})$	25.5960	m^3
Mass parameter $(\boldsymbol{M})$	8.04×10^8	kg/m^3
Bulk modulus in annulus $(\boldsymbol{\beta_a})$	2.3×10^9	Pa
Bulk modulus in drillstring $(\boldsymbol{\beta_d})$	2.3×10^9	Pa
Density in drillstring $(\boldsymbol{\rho_d})$	1300	kg/m^3
Density in annulus $(\boldsymbol{\rho_a})$	1300	kg/m^3
Friction factor in drillstring $(\boldsymbol{F_d})$	1.6×10^{10}	s^2/m^6
Friction factor in annulus $(\boldsymbol{F_a})$	2.08×10^9	s^2/m^6
Choke discharge coefficient $(\boldsymbol{C_d})$	0.6	
Choke discharge area $(\boldsymbol{A_0})$	0.002	m^2
Choke downstream pressure $(\boldsymbol{P_0})$	1.013×10^5	Pa
Total vertical depth $(\boldsymbol{H})$	3500	m
Permeability Production index $(\boldsymbol{K_{pi}})$	613.3×10^{-9}	m^3/sPa
Gas mass flow fraction , $\boldsymbol{\chi_G}$	0.1	

Liquid mass flow fraction , χ_L	0.9	
Speed of sound in gas , c_G	345.8	m/s
Density of gas , ρ_g	1.2	kg/m^3
Gas expansion factor , γ	0.3	
Volume flow fraction , α_G	0.1	m^3/s
Slip law constant K	1.2	
Slip law constant S	1	

Sourcing the plant and controller tuning parameters from Nandan and Imtiaz (2016) as shown in Tables 5.2 and 5.3, the effects of gas-phase influx is demonstrated and presented. To estimate the effect of gas-phase inflow to the wellbore, the physical properties of air is assumed for a gas-phase.

Table 5.2: Observer and Controller tuning parameters (Source: Nandan and Imtiaz, 2016)

Parameter	Value	Unit
l_1	1×10^{-7}	
l_2	0.2	
l_3	0.2	
γ_1	2×10^{-6}	
γ_2	0.005	
γ_3	5×10^{6}	
K_0	4.9066×10^{-9}	$m^3/(s \cdot Pa)$
Tuning		
λ_1	$diag[0\ 1\ 0]$	
λ_2	1000	
m (prediction horizon)	4	
T (sampling interval)	$5,6\ s$	

Table 5.3: State and control input constraints (Source: Nandan and Imtiaz, 2016)

Parameter	Value	Unit
Minimum pump pressure, $\boldsymbol{P_p^{min}}$	8×10^5	Pa
Maximum pump pressure, $\boldsymbol{P_p^{max}}$	200×10^5	Pa
Minimum choke pressure, $\boldsymbol{P_c^{min}}$	8×10^5	Pa
Maximum choke pressure, $\boldsymbol{P_c^{max}}$	100×10^5	Pa
Minimum bit flow rate, $\boldsymbol{q_b^{min}}$	-0.002	m^3/s
Maximum bit flow rate, $\boldsymbol{q_b^{max}}$	0.0283	m^3/s
Minimum choke control input, $\boldsymbol{u_c^{min}}$	0	%
Maximum choke control input, $\boldsymbol{u_c^{max}}$	100	%

By applying the model algorithm described in Figure 6.2 and the NMPC controller scheme in Figure 5.3, the well geometry is setup using the data in Table 6.1. At initial condition, the bottomhole pressure tracks the pressure setpoint P_{bh}^{ref} which is set to 480 bars and the pore pressure is set to 475 bars. Prior to the kick event, the rig pump flow rate is running at a fixed rate of 1200 LPM and no backpressure pump is installed. After about 240 s of operation, the kick is initiated by increasing the reservoir pore pressure to 485 bars, resulting in liquid- and gas-phase mixture of reservoir influx. To compare the proposed two-phase flow NMPC controller model to Nandan and Imtiaz (2016), the current controller model was initially configured to obtain single-phase liquid flow model results as in Nandan and Imtiaz (2016).

Figures 5.4a – 5.7a show the bottomhole pressure, choke pressures, reservoir influx, and choke opening plots when implementing a single-phase flow NMPC controller model while Figures 5.4b – 5.7b show similar plots when implementing the proposed model. In both cases, the controller identifies reservoir influx (wellbore instability) at time t = 240 s and responds by closing the choke

valve to apply backpressure on the annulus. Thus, the increase in the choke pressure in Figure 5.5 leads to a corresponding increase in the bottomhole pressure and the estimated reservoir pressure, which is used to set the new bottomhole setpoint as shown in Figure 5.4. This is consistent with choke opening in Figure 5.7. Thus, Figures 5.6 shows the reservoir influx size from the moment kick occurs and kick response time of about 120 s.

Moreover, Figures 5.4 – 5.7 results also show that the single-phase model underestimates the kick size, the choke pressure, and bottomhole pressures setpoint compared the proposed two-phase NMPC model. This is because of gas-phase flow behaviour, which drifts up the annulus with a non-zero slip velocity, expands as it rises to the surface, and causes the bulk modulus of the annulus fluid to drop. This is consistent with the field estimation of effective bulk modulus presented in Manum and Hjulstad (2018) as: $\beta_{eff} = c^2\rho_{bulk}$; where c is the speed of sound and ρ_{bulk} is the bulk density. The increase of kick size shown in Figure 5.6b is also consistent with the influx behaviour due to gas kick simulation in Sule et al. (2018a). Thus, Figures 5.4b – 5.7b show the effects of gas-phase influx behaviour when compared to the results in Figures 5.4a – 5.7a, where bottomhole pressure is higher by 3 bars, choke pressure by 2 bars and influx peak by about 52 LPM - about 90% increase). Similarly, the choke opening plots in Figure 5.7b drops by 10% more than in Figure 5.7a. Consequently, these gas-phase effects are unaccounted when an automated MPD hydraulic model implements a single-phase flow model.

Another important observation is that the NMPC controller can estimate the magnitude of an anticipated disturbance 'kick' and proactively commence the attenuation procedure before the influx is set to occur. These predictive actions can be seen in Figures 5.4b – 5.7b, where the reservoir influx attenuation procedure commences approximately 20 s ahead of the time kick is set to occur.

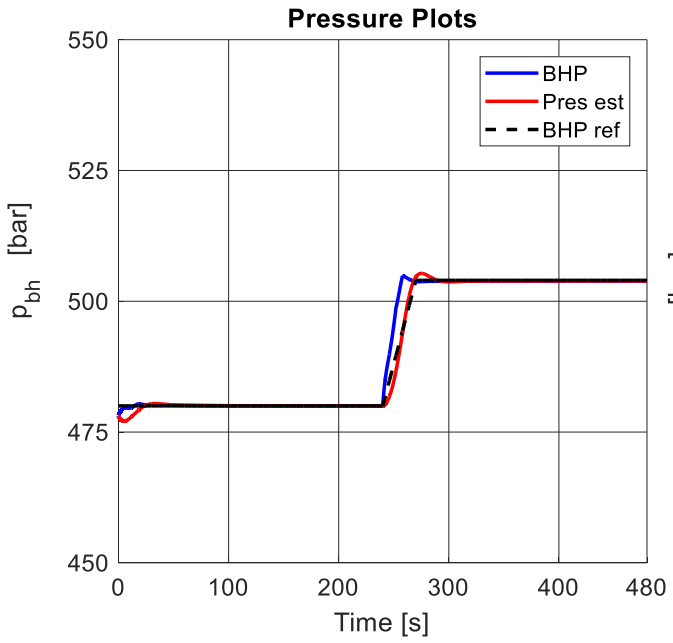

5.4a (single-phase liquid flow model)

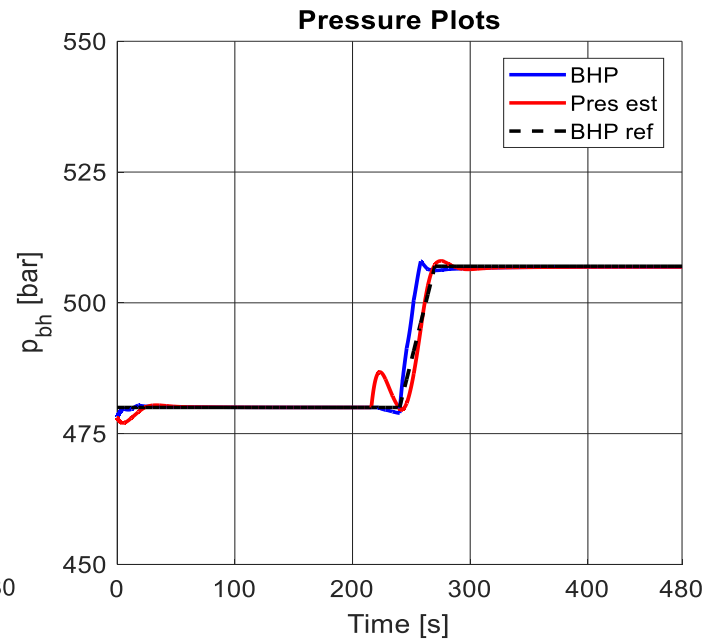

5.4b (two-phase liquid-gas flow model)

Figure 5.4: Effects of the gas-phase influx on Bottomhole pressure estimation

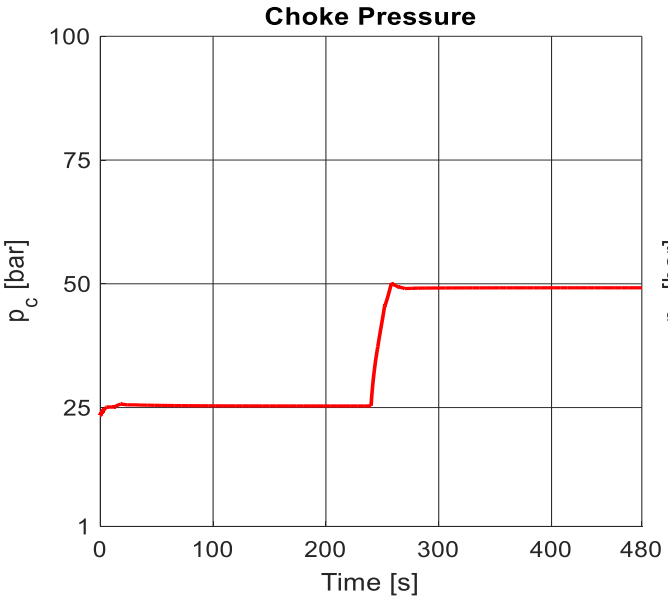

5.5a (single-phase liquid flow model)

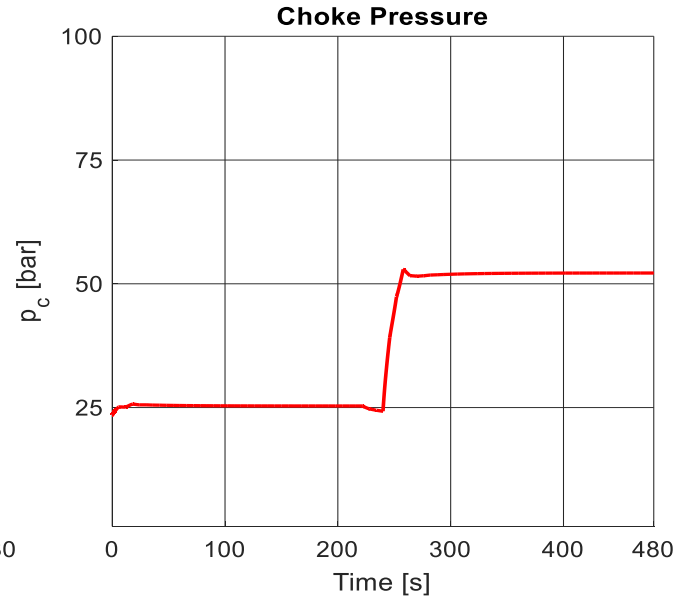

5.5b (two-phase liquid-gas flow model)

Figure 5.5: Effects of the gas-phase influx on choke pressure estimation

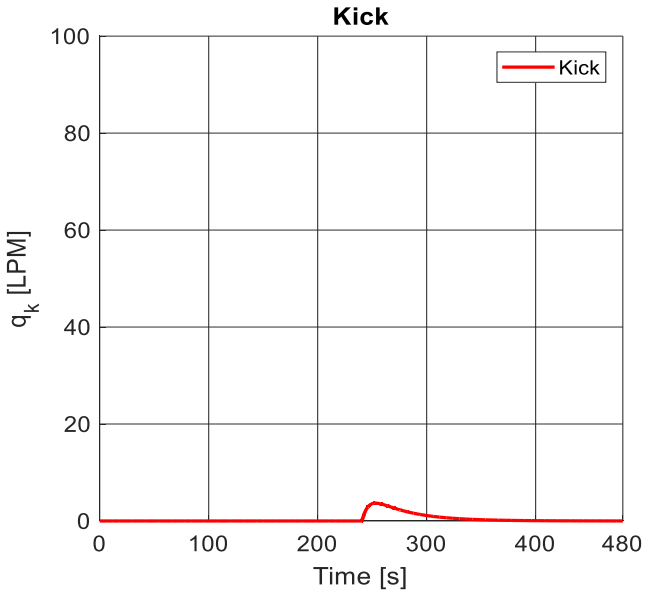

5.6a (single-phase liquid flow model)

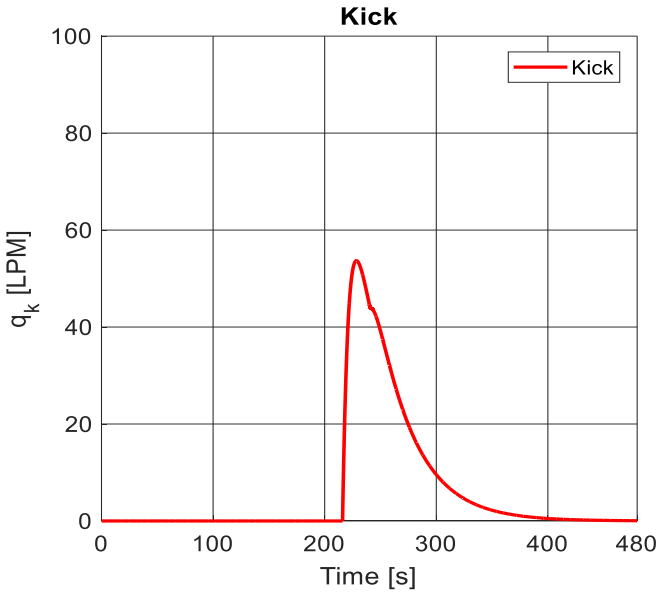

5.6b (two-phase liquid-gas flow model)

Figure 5.6: Effects of the gas-phase influx on an influx size estimation

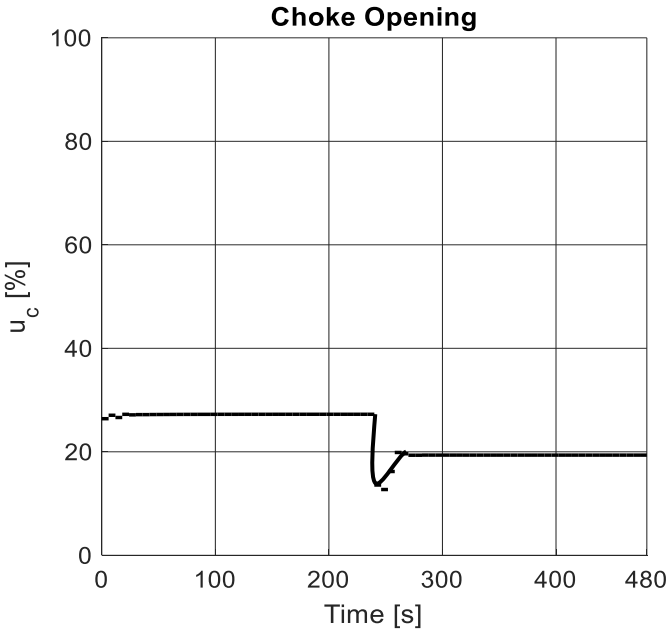

5.7a (single-phase liquid flow model)

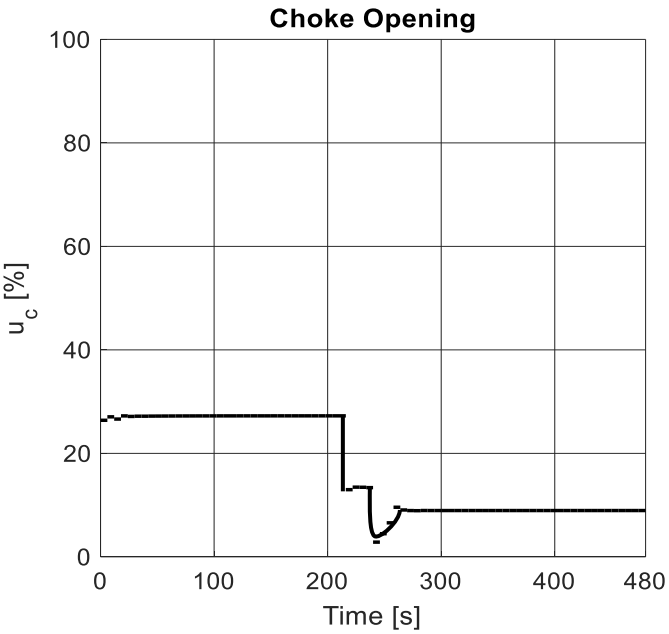

5.7b (two-phase liquid-gas flow model)

Figure 5.7: Effects of the gas-phase influx on the choke valve operation

5.4.2 Model validation

To demonstrate the validity of the proposed two-phase flow NMPC, the proposed model is applied to numerically simulate/calibrate gas kick attenuation operation conducted in a laboratory MPD setup and in a field MPD study.

5.4.2.1 Laboratory experimental setup

Amin (2017) designed and developed a lab-scale automated MPD system setup located in the process engineering facility at Memorial University of Newfoundland. The experimental setup consists of 16.5 ft tall concentric well section in which the inner pipe functions as the drillstring and the outer pipe functions as the annular casing section of a well. The well section is connected to a piping system to replicate the surface return system/circulation loop on a drilling rig and together form a flow loop. The well setup design is installed with several types of pressure transducers, flow meters, and control valves at various points of the flow loop and other fixed equipment including an air compressor and water tank. The automated MPD setup utilizes output feedback NMPC controller with a nonlinear Hammerstein Weinner (H-W) model to maintain the bottomhole pressure at the desired setpoint ($y_{ref} = P_{bh}^{set}$) under various disturbances, such as reservoir kick. Many scenarios are tested during the simulation, including drill pipe extensions and gas kick attenuation. The latter is the focus in the current study. Detail information of the design and NMPC controller setup, equipment specifications, and various drilling scenarios simulated can be found in Amin (2017)

Amin (2017) experimentally simulates gas kick by injecting a pressurized air at 41 psi to the bottomhole section of the setup 140 seconds after starting the operation. The pump flow rate is fixed at 60 LPM and the bottomhole pressure setpoint is set to 40 psi. The results are shown if Figure 5.8, which consists of the pressure and flow rate plots.

Table 5.4: Experimental setup parameters

Parameter	Value	Unit
Volume of annulus & drillstring $(\boldsymbol{V_{a,d}})$	0.0054	m^3
Mass parameter $(\boldsymbol{M})$	8.04×10^8	kg/m^3
Bulk modulus in annulus $(\boldsymbol{\beta_a})$	1.3083×10^5	Pa
Bulk modulus in drillstring $(\boldsymbol{\beta_d})$	1.3083×10^5	Pa
Density in drillstring $(\boldsymbol{\rho_d})$	1000	kg/m^3
Density in annulus $(\boldsymbol{\rho_a})$	1000	kg/m^3
Friction factor in drillstring $(\boldsymbol{F_d})$	5.4025×10^7	s^2/m^6
Friction factor in annulus $(\boldsymbol{F_a})$	5.4025×10^6	s^2/m^6
Choke discharge coefficient $(\boldsymbol{C_d})$	0.6	
Choke discharge area $(\boldsymbol{A_0})$	0.00028	m^2
Choke downstream pressure $(\boldsymbol{P_0})$	1.013×10^5	Pa
Total vertical depth $(\boldsymbol{H})$	4.75	m
Permeability Production index $(\boldsymbol{K_{pi}})$	913.3×10^{-9}	m^3/sPa

It is shown that the NMPC controller is initially tracking the bottomhole pressure until kick occurs and then switches to flow control at t = 140 s by closing the choke valve to apply backpressure until the kick is stopped at t = 225 s. The pressure setpoint after kick attenuation reaches 50 psi and is set as the new bottomhole pressure setpoint after the kick is attenuated.

Using the proposed model, the numerical simulation begins by calculating the required input parameters from the experimental setup in Amin (2017) to run the automated MPD control model developed in section 5.2 and 5.3. Table 5.4 shows the detail of the initial and calculated parameters. The physical properties of air and gas volume fraction of 0.2 are used in this simulation. The numerical simulation results are presented in Figure 5.9a (pressure plots) and Figure 5.9b (the flow rates plots).

As shown in Figure 5.9a, the NMPC controller successfully tracks the bottomhole pressure setpoint within 50 seconds of simulation and this response is replicated in the choke pressure curve. Also, in Figure 5.9b, the rig pump flow rates into the system is set equal to the flow rate out through the choke until at time t = 140 s when the gas kick is initiated. The NMPC controller identifies the gas kick and switches into flow control mode approximately 20 s prior to influx occurring as shown Figure 5.9b. The gas kick is fully attenuated at t = 230 s and the new bottomhole setpoint is estimated at about 52 psi, 2 psi higher than the experimental result.

Thus, the proposed model successfully replicates the experimental results. The kick size, which peaks just below 80 LPM in the experiment compares well with the numerical simulation. Also, the choke pressure and the BHP rise from around 33 psi and 40 psi respectively to around 45 and 50 psi respectively in both the experimental and numerical simulation results. In addition, to demonstrate the effect of gas-phase influx, the proposed model is set to implement a single-phase flow, the kick size results obtained are shown in Figure 5.10a. It is observed that the kick size in Figure 5.10a is significantly underestimated compared to the kick size in Figure 5.9b (also shown in 5.10b), when the NMPC implements a two-phase (liquid-gas) flow hydraulic model.

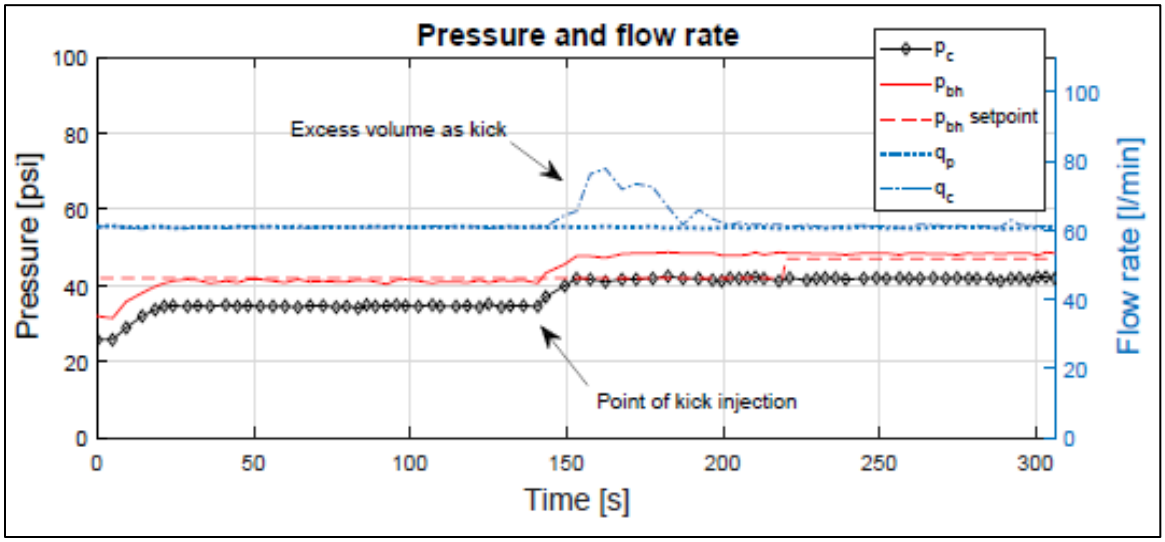

Figure 5.8: Experimental result of gas kick control simulation (Source: Amin, 2017)

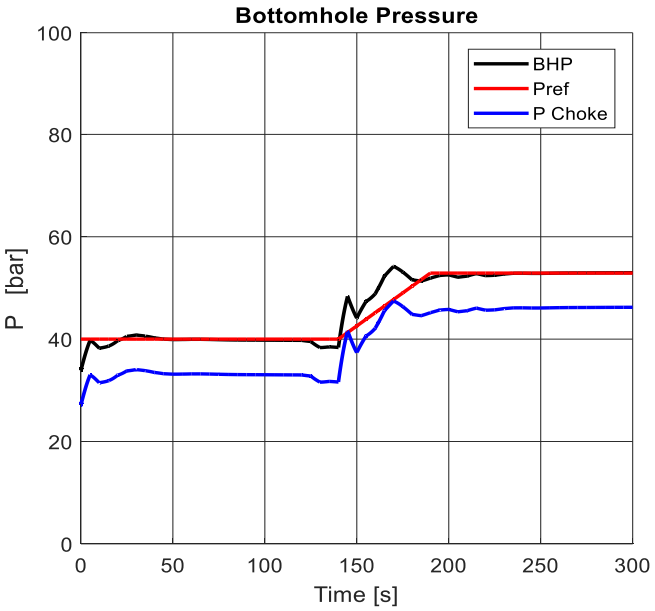

Figure 5.9a

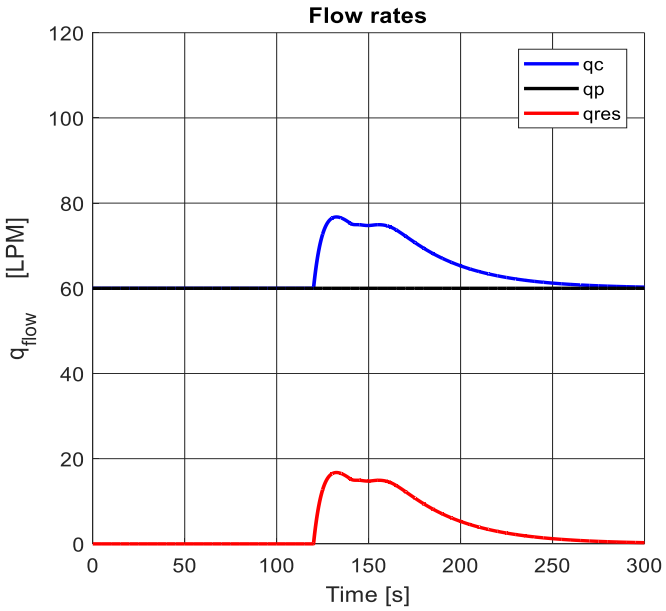

Figure 5.9b

Figure 5.9: Numerical simulation results using proposed NMPC controller model

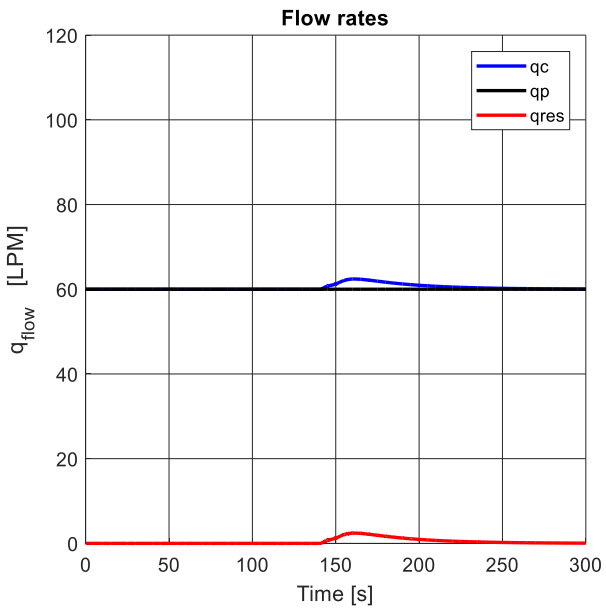

Figure 5.10a (single-phase liquid flow model)

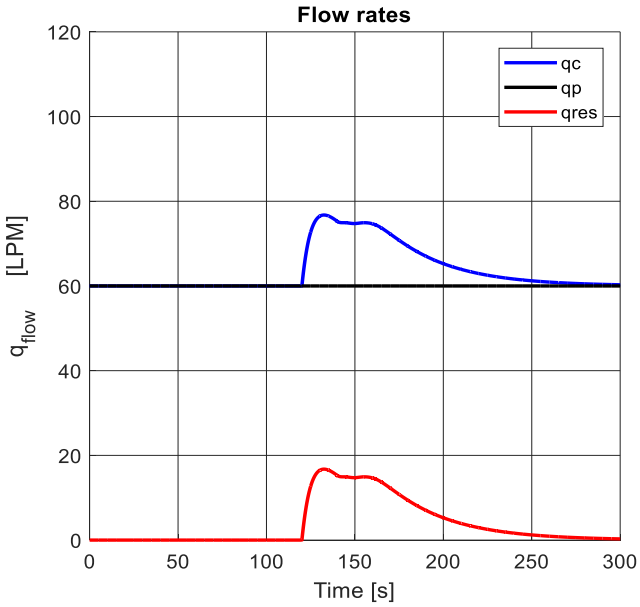

Figure 5.10b (two-phase liquid-gas flow model)

Figure 5.10: Gas-phase flow effect during gas kick event simulated in a lab MPD setup

5.4.2.2 Validation a field case study

Zhou et al. (2016) investigates two alternative well control procedures in an MPD operation: the dynamic shut-in (DSI) procedure and the automatic kick control (AKC) procedure; the current study focuses on the latter procedure. The AKC utilizes a feedback Proportional-Integral controller and a feedforward control scheme. The feedback-feedforward control automatically tunes the choke valve opening in a backpressure MPD setup while the main pump flow and the backpressure pump flow are manually operated. From the equipment side, the AKC utilizes pressure-while-drilling (PWD) tool technology to record pressure measurements at a frequency of 0.5 Hz and transmit them to the surface. A detailed description of the PI controller structure and AKC procedure can be found in their paper (Zhou et al., 2016). The AKC performance is illustrated using two case studies from a North Sea drilling operation; however, for this study, only one case is needed, thus case #1 (Well 1: short well with water-based mud) is used.

The well has a true vertical depth (TVD) of 1720 m and uses a water-based mud of density 1475 kg/m^3. The well geometrical details are given in Table 5.5. Prior to the gas kick incident, the bottomhole pressure and reservoir pore pressure are 261 and 263 bars respectively. The rig pump and backpressure pump flow rates are fixed at 2000 and 400 LPM respectively. The gas kick occurs at t = 300 s. Keeping the rig pump and the backpressure pump flow fixed, the choke responds by controlling the choke valve until the flow rate through the choke equals the rig pump flow rate into the well for pressure stabilization and influx attenuation. The field results are presented in Figures 6.11a (well flow rates plots) and 6.12a (pressure plots).

Table 5.5: Well parameter setup for the numerical simulation of field results

Given well data in Zhou et al. (2016)		Computed data based used for simulation based on given data		
Parameter	**Value**	**Parameter**	**Value**	**Unit**
Measured depth	2300 m	Volume of annulus (V_a)	22.596	m^3
True vertical depth	1720 m	Volume of drillstring $V_d)$	28.945	m^3
Annulus inner diameter	0.2445 m	Mass parameter (M)	8.04×10^8	kg/m^3
Drillpipe outer diameter	0.1397 m	Bulk modulus in annulus (β_a)	1.3×10^9	Pa
Drillpipe inner diameter	0.1183 m	Bulk modulus in drillstring (β_d)	1.3×10^9	Pa
Open hole length	291 m	Density in drillstring (ρ_d)	1475	kg/m^3
Open hole diameter	0.2159 m	Density in annulus (ρ_a)	1475	kg/m^3
Mud density	1.475 sg	Friction factor in drillstring (F_d)	4.36×10^6	s^2/m^6
Reservoir start TD	2290 m	Friction factor in annulus (F_a)	3.6×10^5	s^2/m^6
Reservoir height	2 m	Choke discharge coefficient (C_d)	0.6	
Reservoir pore pressure	263 bars	Choke discharge area (A_0)	0.0056	m^2
		Choke downstream pressure (P_0)	1.013×10^5	Pa
		Total vertical depth (H)	1720	m
		Prod. index (K_{pi})	9.3×10^{-7}	m^3/sPa

To numerically replicate this case study using the proposed two-phase flow NMPC controller model, the given well geometry and initial operating conditions are used compute the required parameters for setting up the hydraulic model and the control objectives presented in Table 5.5. Using the physical properties of air and assuming gas volume fraction of 20%, the numerical simulation of gas kick is performed, and the results are presented in Figures 5.11b and 5.12b. Figures 5.11b shows the flow rate plots of the main pump (q_p)and backpressure pump (q_{bp}) fixed at 2000 and 400 LPM respectively, the flow rate through the choke (q_c), and reservoir influx (q_{res}). While Figure 5.12 shows the bottomhole and choke pressure plots. It can be observed that the numerical model results accurately replicate the field results with q_{res} peaking at 200 LPM and the new choke and bottomhole pressure setpoints around 18 bars and 268 bars respectively after the gas kick is successfully attenuated.

Neglecting any limitations in field processing equipment in the field study, a closer observation of the simulation results shows that the NMPC controller performs better than the PI controller utilized in Zhou et al. (2016) due to faster response to influx disturbance and quicker attenuation of the same gas kick size (i.e. the gas influx is stopped at approximately 100 seconds swifter in the proposed model compared to the field results; see Figure 5.11b).

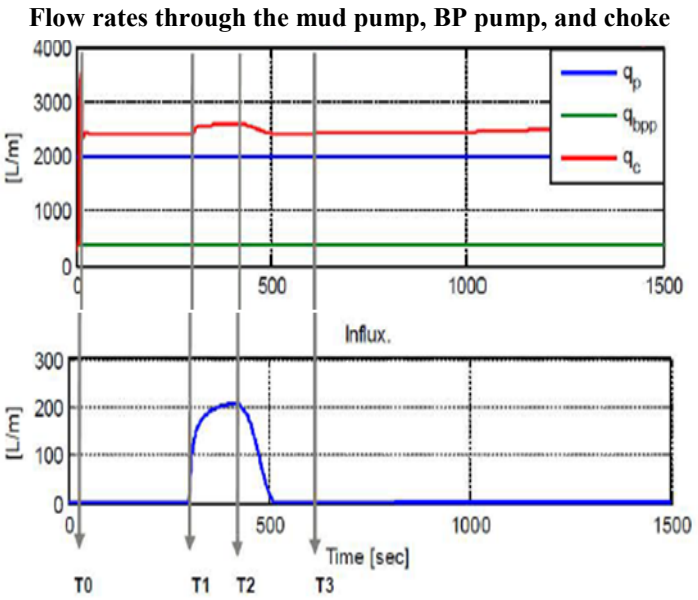

5.11a (Field results from Zhou et al. (2016))

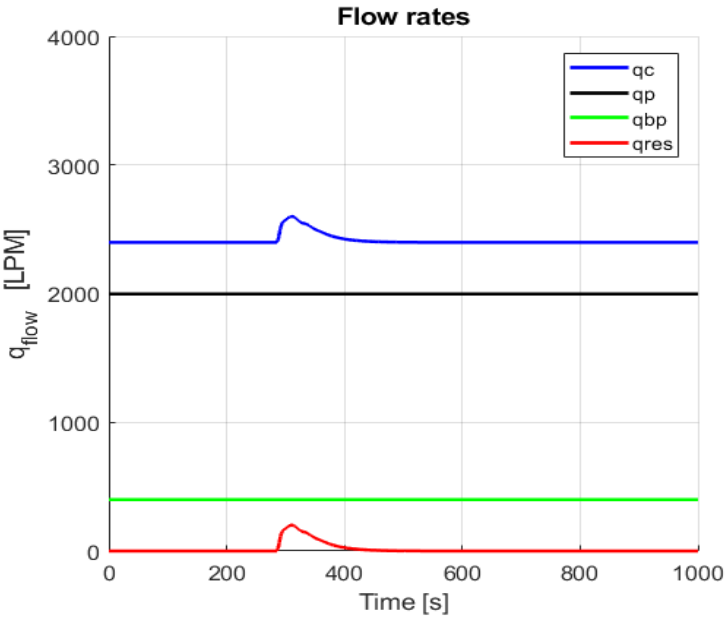

5.11b (Two-phase flow NMPC controller model

Figure 5.11: Field vs model simulation results of well flow rates in automatic kick attenuation operation

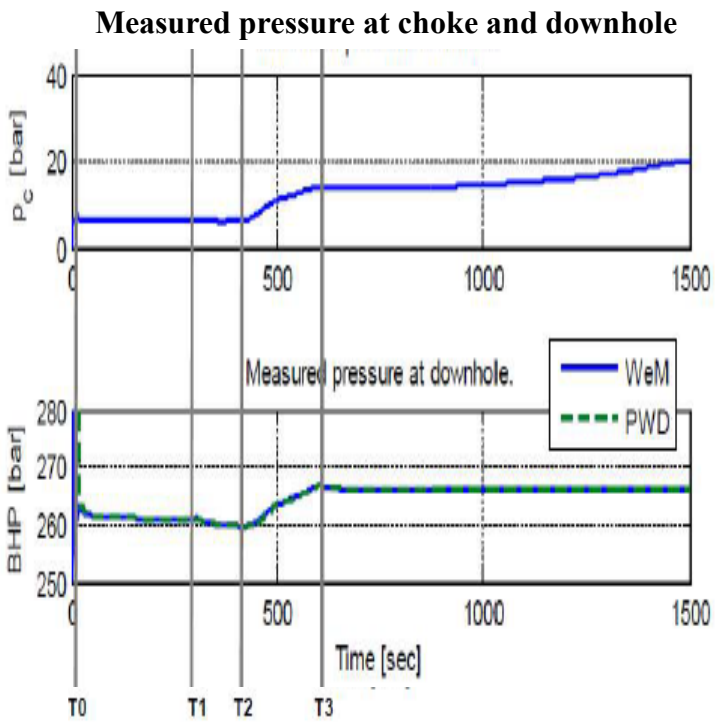

5.12a (Field results from Zhou et al. (2016))

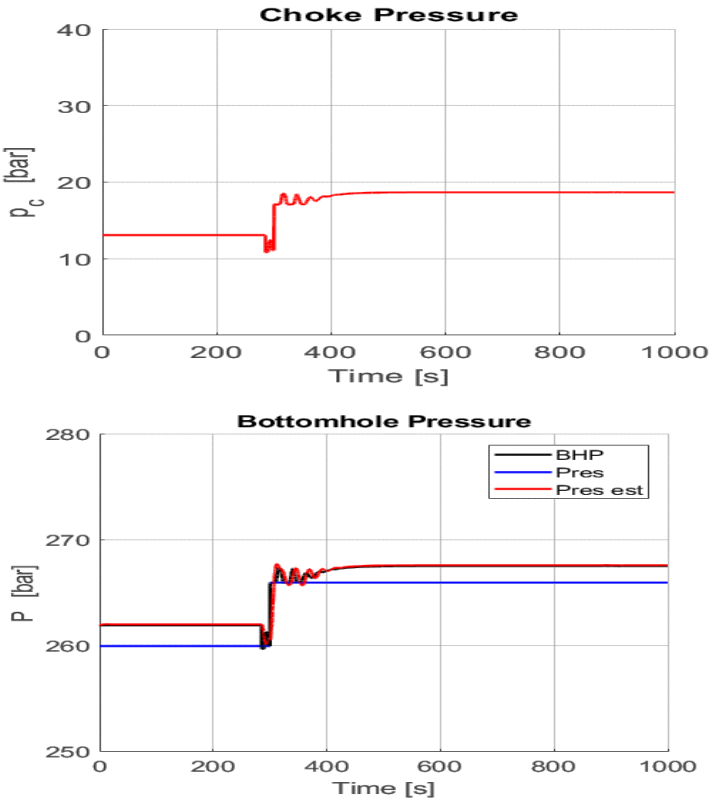

5.12b (Two-phase flow NMPC controller model results)

Figure 5.12: Field vs model simulation results of choke and bottomhole pressures in an automatic kick attenuation operation

5.5 Conclusions and future study

Automated managed pressure drilling operation relies on advanced hydraulic model and control scheme to detect and attenuate kick. It is evident that kick fluid is generally multi-phase, i.e. liquid-gas mixture, and that an MPD system is a nonlinear process; therefore, a PI control scheme is not robust enough and a single-phase liquid flow model will neglect the gas-phase behaviour in the kick fluid. Thus, the current study proposes an MPD control system that utilizes a nonlinear model predictive controller (NMPC) and a two-phase flow model for computing annular pressure and choke valve dynamics during kick control operation. To highlight the control improvement in the proposed model, its performance is compared against a single-phase flow model performance during a multi-phase kick control simulation. The results show that the single-phase model underestimate key well control parameters, including the kick size by about 52 LPM (or ~ 90%), bottomhole pressure by 3 bars and choke pressure by 2 bars compared to the proposed model. These estimation errors in using a single-phase liquid model is attributed to neglecting the characteristic effects of the gas-phase influx.

Furthermore, the proposed model successfully validates gas kick control simulation results from a lab-scale MPD setup and a gas kick case study from a field based in the North Sea MPD operation. For the lab-scale setup, which utilizes an NMPC controller and induces gas kick by discharging air into the bottom of the well, the proposed model accurately replicates the simulation results including the kick size peaking just below 80 LPM and the new bottomhole pressure setpoint of around 50 psi after the kick is attenuated. Meanwhile, for the field case study, which utilizes a PI controller in MPD control system, the proposed control model not only perfectly replicate the field control results (with kick size peaking around 200 LPM and bottomhole pressure around of 268 bars after the gas kick is attenuated), it responds more swiftly to kick disturbance than the PI controller by attenuating the gas kick approximately 100 s faster.

Chapter 6 Risk Analysis of Well Blowout Scenarios during Managed Pressure Drilling Operation

Preface

This chapter presents a dynamic risk assessment model for assessing the safety of a managed pressure drilling operation. A version of this chapter has been submitted for review in the ***Journal of Petroleum Science and Engineering.*** *Along with the co-authors, Dr. Syed Imtiaz, Dr. Faisal Khan, and Dr. Stephen Butt, I have co-authored this chapter. I developed the model, made first attempt to perform the model analysis, and interpret the data and results. The co-author Faisal Khan helped in developing and validating the concepts, reviewed and corrected model results, and contributed in preparing, reviewing and revising the manuscript. The co-author Dr. Syed Imtiaz helped in the model development, improvement, interpretation, and validation, and in organizing and revising the manuscript. The co-author Dr. Stephen Butt contributed through assisting in analyzing the data, validating simulation results and revising the manuscript. Co-authors Drs. Imtiaz, Butt and Khan reviewed the revisions and provided feedback which I have implemented. I prepared the first draft of the manuscript and subsequently revised the manuscript based on the co-authors' feedback and the peer review process*

Abstract

Offshore drilling involves complex operations and equipment; thus, faces many operational challenges, including well control incidents. The managed pressure drilling (MPD) provide a safer alternative; however, this technology, for the most part, is still in its infancy. Potential risks during well control operation in MPD need to be identified, assessed and managed. The current study presents an advanced dynamic blowout risk model (DBRM) to assess the safety during the managed pressure drilling operation. The DBRM involves three key steps: a dynamic Bayesian network (DBN) model, a numerical simulation of an MPD kick control operation, and dynamic risk analysis. The

proposed DBRM implements a novel approach for simulating an MPD failure and assessing blowout risk through varying MPD kick control parameters/variables in a simulated system, which are instrumental for setting the safe/failure operating thresholds for an MPD control system. The proposed DBRM is successfully applied in assessing the dynamic risk of a blowout in an MPD operation based on a case study from the Amberjack field in the Gulf of Mexico. The results show that the presence of drilling hazards, such as depleted formation, increases the likelihood of circulation loss and thus, the kick occurrence, and that an MPD failure likelihood increases as the kick intensity exceed the designed limits of an MPD control system. The increased likelihoods of these two events increase the risk of a blowout. Conversely, MPD failure and blowout risk can be reduced by up to 96% by making the control system robust.

Keywords: Dynamic Bayesian network, Bow-tie, MPD control system, kick, safety barrier, blowout

6.1 Introduction

Well control is one of the most challenging operations in drilling; especially in offshore exploration and production. More so that most prospects for hydrocarbon resources are drifting exploration into the deepwater (Graham et al., 2011) or posing operational challenges that range from depleted formations (such as reservoirs with narrow pressure windows) to high-pressure formations. The narrow pressure margins are most prominent in deepwater applications where much of the overburden is the seawater (Malloy and McDonald, 2008). Well control incidents, such as kick, are frequently encountered and can increase operational costs (e.g. lengthy non-productive time - NPT) and risk. Risk analysis is a vital tool in the process and oil and gas industries to identify and analyze all risks associated with an operation and develop strategies to prevent and mitigate those risks. In drilling operations, the risk of blowout accident is central to well control strategies and overall safety

of the operation due to the catastrophic consequence of a blowout, such as fire and explosion, multiple fatalities, environmental damage, loss of assets, and fines (Graham et al. 2011).

Kick mechanisms and the implementation of managed pressures drilling (MPD) to maintain the downhole pressure in troubled wells, such as in the depleted formations, fractured formations, overpressured formations, or formations with narrow drilling windows have been covered explicitly in the literature (Khakzad et al., 2013; Gala and Toralde, 2011; Rohani, 2012; Malloy and McDonald, 2008; Kok and Tercan, 2012). The safety benefits that MPD technologies bring to conventional drilling may be measured or assessed through the improvement in safety barriers of conventional primary well control, especially in deepwater drilling. Gabaldon et al. (2014) used well control barrier envelopes to describe how MPD improves influx management and prevents unnecessary shut-in or blowout; in Zan and Bicke (2014) MPD implementation reduce failure probability of a well control incident by 20%; in Grayson and Gans (2012), the well control barrier layers provided by MPD system reduced the possible risk of a blowout by almost 500%. However, the safety and reliability assessments of an MPD system have only seen limited focus. In Abimbola et al., (2015) safety analysis of an MPD operation identifies an RCD as the most important critical component. This conclusion is slightly modified in Sule et al (2018b), in which detailed analysis of the MPD system's operational interactions reveals that an MPD control system has the most influence on the success/failure of MPD operation, thus, the most safety critical components.

Many studies have assessed the risk of well control incidents using several risk analysis tools. Conventional risk assessment techniques, including Fault Tree (FT), Event Tree (ET), and Bow-Tie (BT) are incapable of capturing the dynamic effects of operational risks, such as change in well conditions due kick or sudden failure of equipment during drilling operations, and inability to assess

the sequential dependencies among process variables in risk estimations (Barua et al., 2016; Khakzad, et al., 2012;). Bayesian network (BN), is a more flexible modelling approach that can perform both forward and backward analyses and suitable for dynamic risk and safety analyses (Bobbio et al., 2001; Langset and Portinale, 2007; Khakzad et al., 2011, 2013; Cai et al., 2013; Barua et al., 2016; Sule et al.,2018b). However, these BN models are only restricted to one-step posterior analysis and are not capable of explicitly modeling the changes in events likelihood or relationship over time.

Thus, a dynamic Bayesian Network (DBN), which is a temporal extension of BN capable of modeling influences over time, has been developed to address the dynamic restrictions in the BN models (Murphy, 2002; Cai et al., 2013). The DBN models have been used in many probabilistic analyses of dynamic systems and operations across many industries, including oil and gas, process, manufacturing, computing etc. For instance, DBN has been used by Cai et al., (2013) in quantitative risk assessment of human factors on offshore blowouts; Wu et al., (2016) in prediction and diagnosis of offshore drilling incidents; Dong and Yue (2016) in identification of functional connections in Biological neural networks; Amin et al., (2018) in dynamic availability assessment of safety-critical systems; Zhu et al., (2019) in Fatigue damage assessment of orthotropic steel deck; Luque and Straub (2019) in optimal inspection strategies for structural systems.

Thus, the present study proposes an advanced dynamic blowout risk model (DBRM) for assessing the risk in managed pressure drilling kick control operation. The model integrates a numerically simulated MPD kick control model to a dynamic blowout risk methodology using a dynamic Bayesian Network (DBN) model. The main objective is to develop a risk assessment model for numerically simulating and assessing the safety of a managed pressure drilling operation as well control barrier element during drilling. Given the dynamic nature of a drilling operation, the current study uses a DBN model to give the model capability to update the risk during drilling when latest

information is available and to evaluate the influence of an MPD control failure propagation to a blowout incident. A brief discussion of MPD control model, BN and DBN model will be presented in section 6.2; the dynamic risk methodology in section 6.3; the application of the dynamic blowout risk model will be demonstrated in section 6.4 using a field case study, and the results and discussion are presented in section 6.5.

6.2 Modeling concepts

6.2.1 A managed pressure drilling control operation

Managed pressured drilling (MPD) has many techniques whose applications are based on well specific conditions. One of the most commonly used MPD techniques is a constant bottomhole pressure (CBHP) technique, which is suitable for a naturally fractured or depleted formation with a narrow pressure margin between the pore pressure and fracture gradient (Rohani 2013). This MPD technique uses hydraulics models to establish wellhead pressure and maintains a suitable equivalent circulating density (ECD) and annulus pressure gradient in the wellbore. One of the common commercially available CBHP system is a dynamic annular pressure control (DAPC) system by Schlumberger, which is adapted for the current study. A detailed description of the DAPC system operation, components operational interactions and modes of failure can be found in the author's previous work (Sule et al., 2018b). The DAPC system consists of a rotating control device (RCD), MPD choke manifold, backpressure pump, MPD control system integrated with a real-time hydraulic simulator, non-return valve (NRV), pressure relief valves (PRV), and monitoring equipment (pressure while drilling (PWD) tool, Coriolis flow meter, and rig pump.

The DAPC system's pressure control relies on RCD to seal and allow the pressurization of the wellbore annulus and to divert the mud returns into the choke manifold. The MPD choke manifold is used to apply hydraulic backpressure on the annulus to manage the bottomhole pressure. When

needed, the backpressure pump is activated to supplement annular fluid required to apply precise backpressure and the NRV prevents the backflow of mud into the drillstring. Figure 6.1 illustrates the system's kick control operation, where the flow pathways indicated in dashed lines signify the power supply and data transmission across the entire system while the pathways indicated in thick lines show the hydraulic movement through the system. The detailed analysis of the DAPC system in kick control operation from the authors' previous work, (Sule et al., 2018b), identifies an MPD control system as the most safety critical component.

The subsequent work by the authors (Sule et al., 2019) proposes an advanced nonlinear model predictive control (NMPC) model for an MPD control system that can capture the dynamic and nonlinear process of an MPD system and the multiphase behaviour of kick fluid during drilling. The MPD control model, which is an integral part of the dynamic blowout risk model methodology described in section 6.3, has been tested and validated using laboratory experiments and a field case study in Sule et al., (2019).

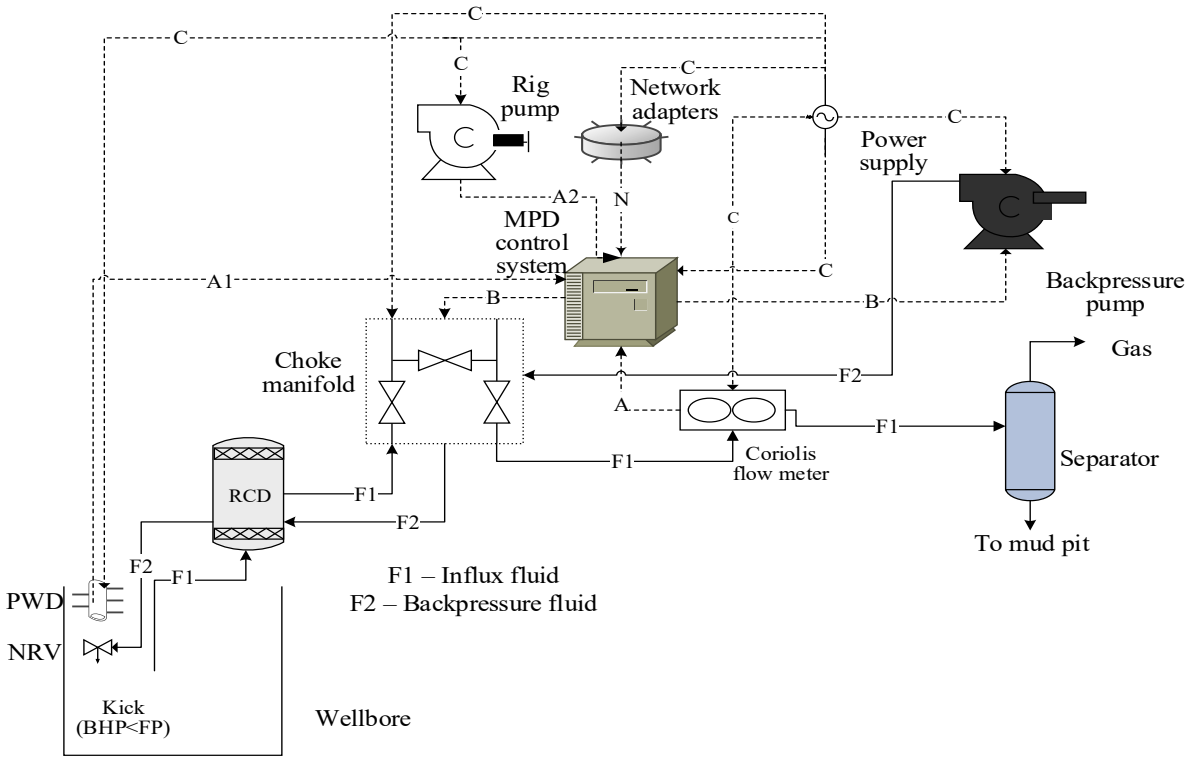

Figure 6.1: CBHP MPD system kick management operational flow – showing equipment dependency and interaction process (Source: Sule et al., 2018b)

6.2.2 Bayesian network and dynamic Bayesian network

6.2.2.1 Bayesian network model

Bayesian Network (BN) describes the causal relationships among variables via a directed acyclic graph (DAG) in which the nodes represent the system variables and the arcs symbolize the dependencies. The capability of BN to perform both forward and backward analyses make it unique in dynamic risk and safety analysis (Bobbio et al., 2001; Khakzad et al., 2013a; Abimbola et al., 2015). BN can be considered as a representation of joint probability distribution (JPD) with a fundamental assumption that not every node is connected to every other node (Korb and Nicholson, 2011). For instance, assuming a joint distribution of a set of random variables $D_1 \ldots D_5$ is defined as $P(D_1 \ldots D_5)$ where D1, D2, D3, and D4 that lead to incident D5 (Figure 6.2). In this illustration, D_1, D_2, and D_4 are root nodes with assigned marginal prior probabilities, D_3 is an intermediate node with defined conditional probability, and D_5 is the child node. Hence, using a chain rule, the JBD of the

BN is the product of the conditional probability distributions of the variables $D_1 = d_1$, $D_2 = d_2$ … $D_5 = d_5$ (Korb and Nicholson, 2011; Khakzad et al. 2011). That is:

$$P(d_1, d_2, \dots, d_5) = \prod_{i=1}^{5} P(d_i | d_{Ai}) \quad (6.1)$$

where *Ai* in equation (1) are the parents of node *i* in the DAG and d_1, d_2... d_5 are the states of variables D_1, D_2... D_5. Hence, the JPD for the BN in Figure 6.2, can be determined by equation (6.2)

$$P(d_1, d_2, \dots, d_5) = P(d_1)P(d_2)P(d_4|d_1, d_2)\, P(d_5|d_4, d_3) \quad (6.2)$$

Therefore, for conditional probability independents/distributions such as $P(d_4|d_1, d_2)$ can be solved by using equation (6.3).

$$P(d_4|d_1, d_2) = \frac{P(d_1, d_1, d_4)}{P(d_1, d_2)} \quad (6.3)$$

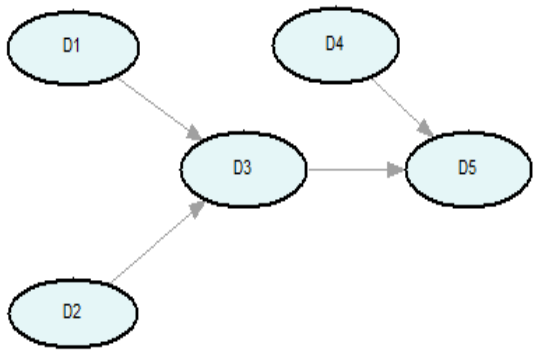

Figure 6.2: Illustrative BN model

6.2.2.2 Dynamic Bayesian Network

A dynamic Bayesian network (DBN) is a BN extended with a time dimension to model the behaviour of dynamic systems, whereby the dynamic extension does not mean the network structure or parameters changes dynamically but a dynamic system is modeled (Murphy, 2002; Hulst, 2006). A DBN model consists of time-slices with each time-slice containing its own variables. The DBN formalism based on Murphy (2002) conform to two assumptions: a DBN model is defined as a first-order Markov model (i.e. $P(Z_t|Z_1, \dots, Z_{t-1}) = P(Z_t|Z_{t-1})$) and the transition model $P(Z_t|Z_{t-1})$ remain the same for all time-slices, t (Murphy, 2002; Hulst, 2006). Thus, a DBN is defined by a pair $(B_1, B_{\rightarrow})$. Where $B_1$is a BN that defines the prior distribution of the state variables $P(Z_1)$ and $B_{\rightarrow}$ is a two-slice temporal Bayesian network (2TBN) that defines the transition model $P(Z_t|Z_{t-1})$ as follows:

$$P(Z_t|Z_{t-1}) = \prod_{i=1}^{N} P(Z_t^i|Pa(Z_t^i)) \qquad (6.4)$$

Where Z_t^i is the i-th node at time-slice t of components variables, $Pa(Z_t^i)$ are the parents of Z_t^i at same time-slice t or previous time-slice $t-1$, and N is the number of random variables in Z_t^i (Hulst, 2006). While the nodes in the first time-slice have no parameters associated with them, the nodes in the second time-slice of the 2TBN have a conditional probability tables (CPT). Thus, for a DBN with a sequence of length T slices, the joint probability distribution can be obtained by *unrolling* the 2TBN network (Hulst, 2006) as:

$$P(Z_{1:T}) = \prod_{t=1}^{T} \prod_{i=1}^{N} P(Z_t^i|Pa(Z_t^i)) \qquad (6.5)$$

However, to improve the DBN modeling power, Hulst (2006) developed *extended DBN formalism* from the *Murphy (2002) DBN formalism* as *k*th-order Markov processes where $B_{\rightarrow}$ is defined as $(k+1)TBN$ instead of 2TBN. Thus, the transition model $P(Z_t|Z_{t-1}, Z_{t-2}, \dots, Z_{t-k})$ for a *kth*-order Markov process is defined:

$$P(Z_t|Z_{t-1}, Z_{t-2}, \dots, Z_{t-k}) = \prod_{i=1}^{N} P(Z_t^i|Pa(Z_t^i)) \qquad (6.6)$$

This *extended DBN formalism* is distinguished from Murphy's definition in that the set of parents is not restricted to nodes in previous or current time-slice but can also contain nodes in time-slices further in the past. Thus, unrolling the (*k* + 1)TBN and then multiplying all the CPTs can obtain the JPD for a sequence of length T slice, which ends up with the same definition in eq (6.5).

Graphical representation of a *k*th-order Markov process with a (*k* + 1)TBN is simplified by using *temporal arc*, which is an arc between a parent node and a child node with an index that denotes the temporal order or time-delay k > 0 (Hulst, 2006). Figure 6.3 shows two graphical visualizations of second-order DBN, in which Figure 6.3a illustrates the graphical representation without temporal arc; thus, can appear complex and cumbersome with higher order, i.e. many variables and different temporal orders per time-slice. However, in a visualization shown in Figure 6.3b, it is immediately clear that the DBN has three temporal arcs ($X_{t-2} \rightarrow X_t$, $X_{t-1} \rightarrow X_t$, and $Y_{t-1} \rightarrow Y_t$) and two non-temporal arcs ($U_t \rightarrow X_t$, $Xt \rightarrow Y_t$), where this is less obvious from the (k + 1)TBN visualization.

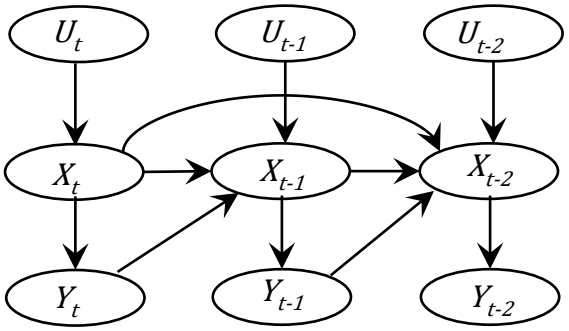

Figure 6.3a: DBN structure 3 time slices without temporal arc

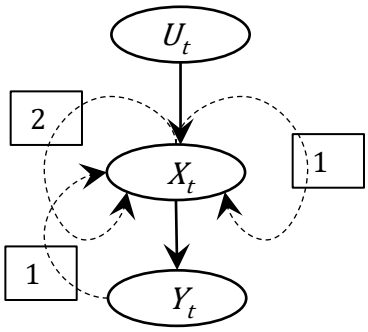

Figure 6.3b: DBN structure with temporal arc

Figure 6.3: Comparison of visualization of a second-order DBN between using (a) t = 3 time-slices and (b) using temporal arcs (Source: Hulst, 2006).

In addition to introducing the *temporal arc*, Hulst (2006) introduced *temporal plate* in the *extended DBN formalism* to avoid every node to be copied to every time-slice when unrolling the DBN for inference as in the case of Murphy (2002) DBN formalism due to its memory waste and higher computational power requirement. So, all nodes outside the temporal plate are not copied when unrolling but their arcs are, meaning that they will remain constant over time. These nodes are termed *contemporal nodes* on the DBN.

Thus, DBN models in the *extended DBN formalism* by Hulst (2006) is implemented in the DBN of the proposed model via the GeNIe modeling software by BayesFusion (available at https://www.bayesfusion.com). Additionally, several inference algorithms, such as filtering (or monitoring), prediction, and smoothening are available (Murphy, 2002; Hulst, 2006) and their goal in a DBN is to calculate $P(X_t|y_{1:\tau})$. The filtering (where $t = \tau$) is to keep track of the current state for rational decision making; the prediction (where $t < \tau$) is to evaluate the effect of possible actions on the future state; and smoothing (where $t > \tau$) is useful to get a better estimate of the past state, because more evidence is available at time *t* than at previous time-step $(t - 1)$. All these inferences are supported in the GeNIe software.

6.3 Methodology to Develop Dynamic Blowout Risk Model (DBRM)

The proposed dynamic blowout risk model (DBRM), shown in Figure 7.4, is to assess the safety of managed pressure drilling (MPD) operation during kick control operation. A blowout incident can lead to disastrous consequences as evident in the deepwater horizon accident in 2010 (Graham et al., 2011). In the current work, undesired pressure is recognized as the gas kick and a blowout is considered as the undesirable consequence due to failure of an MPD (a primary well control safety barrier) in preventing and/or containing kick and failure of the BOP system (secondary well control safety barrier) to contain the well.

The DBRM framework in Figure 6.4, begins with identifying drilling hazards (step 1); identifying the safety system, equipment, process barrier (step 2); collecting incident analysis reports to identify: root causes to system or operational failure, drilling events (kick or circulation loss), escalation analysis and underlying failure consequences, including blowout (step 3); developing the FT and ET models of top and pivoting events to establish BT (step 4); mapping BT into BN to develop a DBN model for dynamic risk assessment (step 5); and performing model analysis and probability updating using data collected from simulations and from an expert or outside source (step 6). The extension of step 2 (i.e. the safety barrier components) identifies MPD system as the initial safety barrier element in well control operation and it proceeds to numerical simulation phase for kick control operation using an advanced NMPC MPD control model. As shown in Figure 6.4, the numerical kick control simulation loop is designed with failure/safe operating thresholds for four kick control parameters (backpressure, bottomhole pressure, kick size, and surface equipment) relevant during an MPD operation.

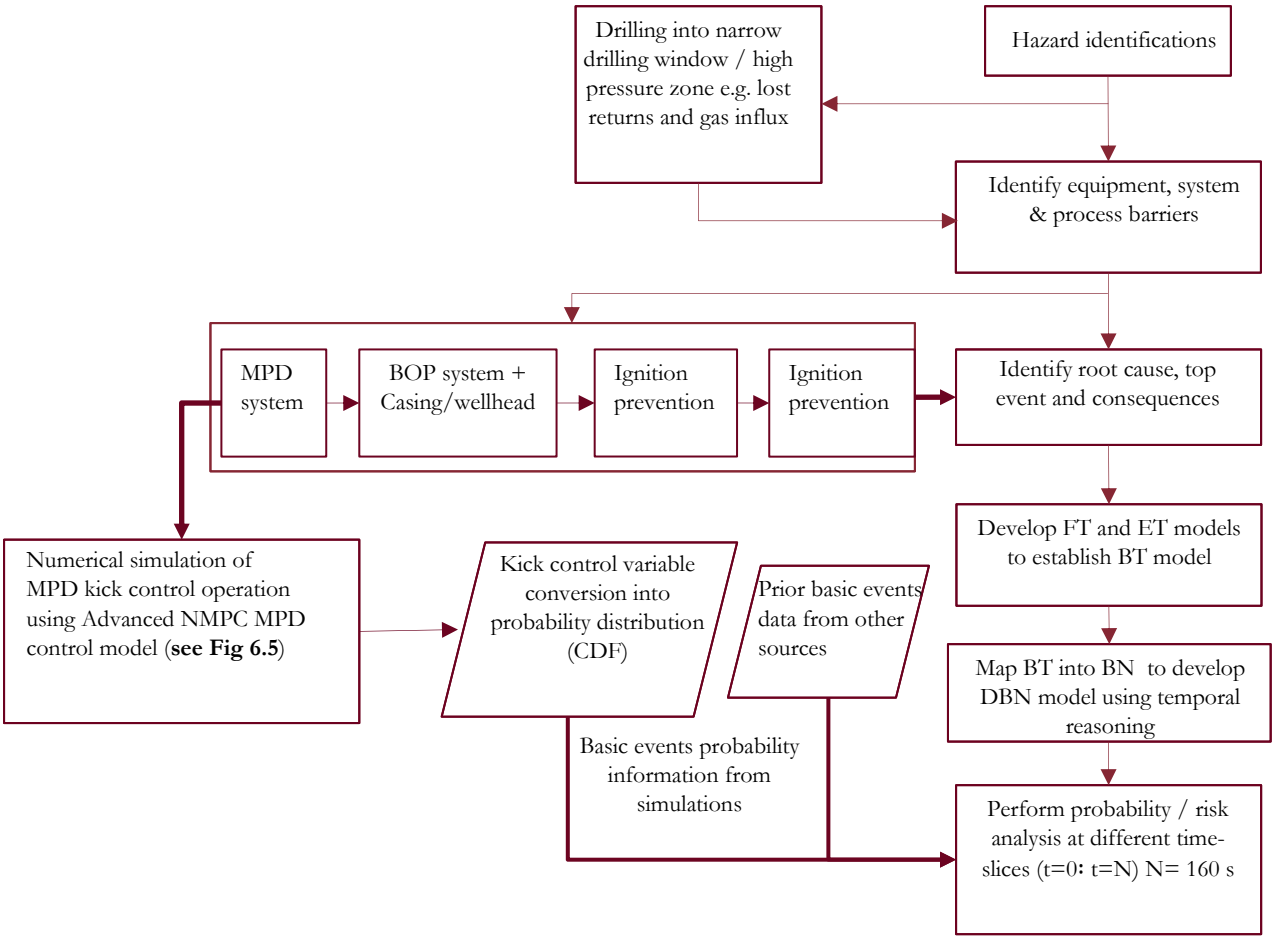

Figure 6.4: Dynamic blowout risk model framework for an MPD kick control operation

The operation ends if any of these safe operating thresholds are violated or operation time is elapsed. Finally, the simulation data collected is converted into probability distribution and then fed into the DBN for phase 3 operation, which is the risk assessment of the drilling operation.

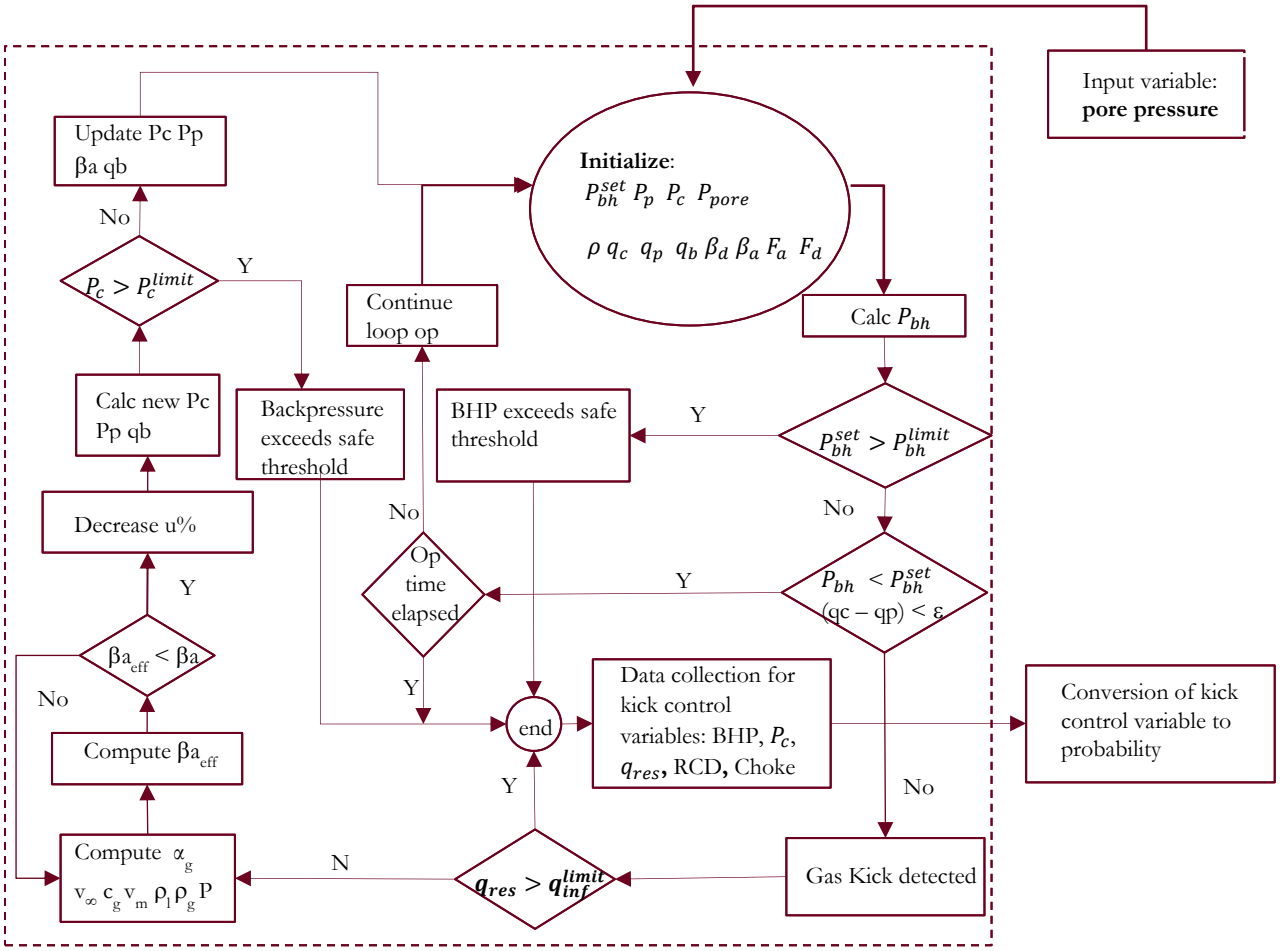

Figure 6.5: Numerical simulation model process flow diagram for the DBRM framework in Fig. 6.4

7.3.1 Hazard identification by Bow-Tie model

This is the phase There are many techniques available to perform hazard identification; however, one of the most intuitive techniques is the Bow-Tie model, which provides one of the best graphical representation of a complete accident scenario progression and the effectiveness of the various safety barriers (Wu et al., 2016; Khakzad et al., 2013). A simplified BT model is composed of an FT diagram on the left-hand side identifying the basic events leading to the top event and located at the middle of the BT and an ET on the right-hand side identifying possible consequences of the top (investigating) event given the effects of the safety barriers. A more complex BT may involve more

than one FTs in which at least one of the FT top event will be an initiating event of the ET (located at the center of BT) and other FTs top events may fault analysis of the safety barriers in the ET section of the BT. The BT also help identify logical relationships among basic and intermediated events leading to top event and illustrate the sequential failure of safety barriers due to the escalation of the top event (Khakzad et al., 2013). A simplified BT model is illustrated in Figure 6.6a.

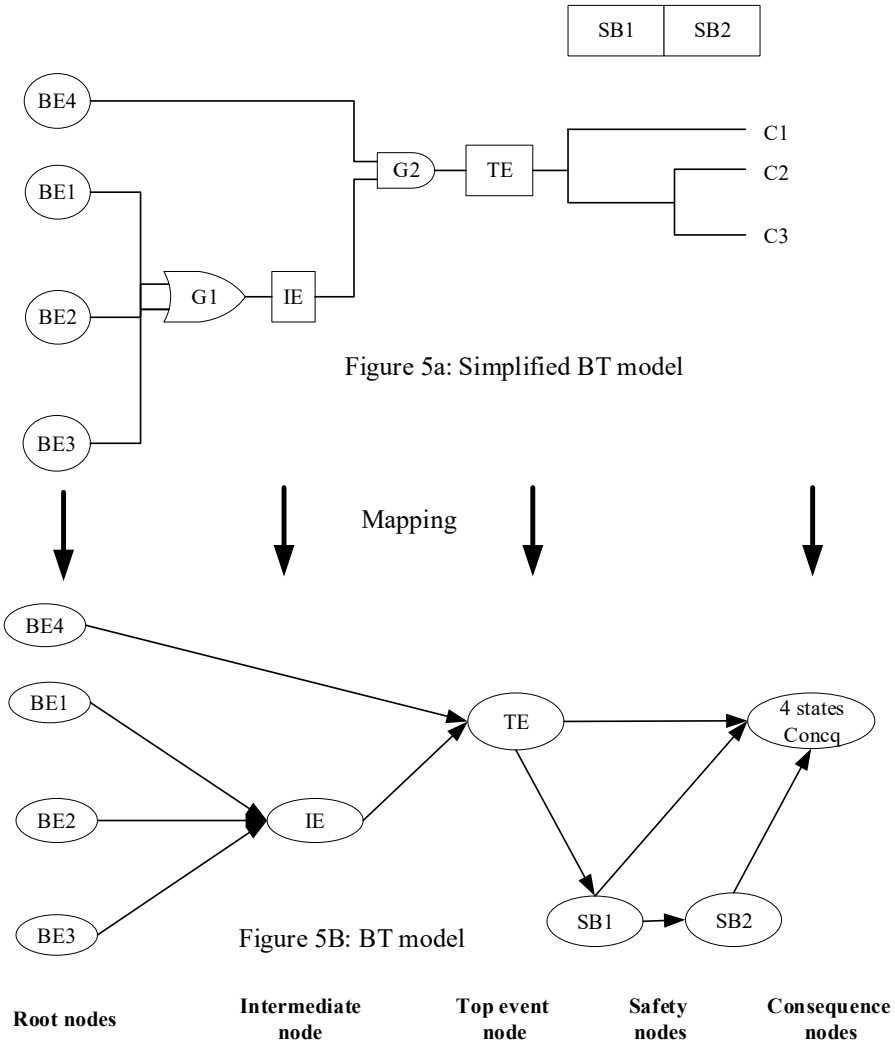

Figure 5a: Simplified BT model

Figure 5B: BT model

Figure 6.6: Creating a BN model from the BT model

6.3.2 DBN model development

6.3.2.1 BT to BN Mapping

The BN model mapping and construction is developed using a decision modeling software, GeNIe 2.3, available at http://www.bayesfusion.com/. The transformation of BT to the BN model is performed using the mapping algorithm proposed in Khakzad et al. (2013). Figure 6.6b shows the BN model version of the BT model after mapping algorithm has been implemented. The mapping of BT to BN illustrated in Figure 6.6 is a simplified example, whereby the basic events (BE) of the FT are mapped as the root nodes, intermediate event as intermediate node, top event as pivot node, and the safety barriers (SB) and consequence as the safety and consequence nodes respectively. Unlike BT, the BN can capture the dependency of safety barriers on the top event and among safety barrier elements by means of drawing causal arcs as shown in Figure 6.6b; where the influence of top event on the SB1 and that of SB1 on SB2 nodes can be analyzed. Lastly, the gate relationships, such as "OR" and "AND" gates, among the BT components, are used to define the conditional probability relationships among the nodes in the BN.

6.3.2.2 Developing DBN model

The GeNIe software is used to create the DBN model in the current work. The GeNIe software implements the *extended DBN formalism* based on Hulst (2006) discussed in section 6.2.2 of this chapter. The temporal extension of BN to develop the DBN model is initiated by enabling the temporal plate on the GeNIe Network. The DBN model in GeNIe does not focus on time-slices but rather on variables; thus, allows for compact modeling of higher order temporal influences. This is possible due to the *temporal arc* that imposes temporal influences on the DBN model and the number within the arc denotes their order.

For instance, as shown in Figure 6.7, an influence of zero-order, which is a normalized temporal arc, signifies instantaneous influence, the first order, marked by [1] represents an influence spanning over one time-step, and an influence of higher order span over multiple time-steps, e.g., [2] represents slower influences that span over two time-steps. Furthermore, a looping influence, as shown in Figure 6.7, which originates and ends at the same node TE, gives the DBN model the capability to analyze the TE impacts on itself in future (i.e. first-order influence). The probability inference is performed by updating temporal beliefs to obtain marginal posterior probability distributions as a function of time or by setting temporal evidence from historical data and updating the temporal beliefs.

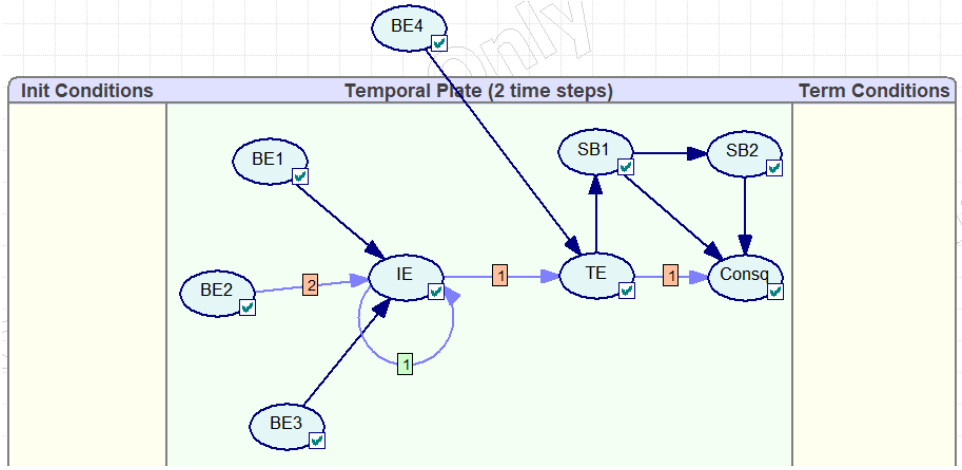

Figure 6.7: Simplified case illustration of a DBN model using GeNIe

6.3.3 Numerical simulation of MPD kick control operation

This is the phase 2 of the DBRM framework. The numerical model simulation implements an MPD control model proposed in earlier work by the authors (Sule et al., 2019) that utilizes a nonlinear model predictive controller (NMPC) and a two-phase hydraulic flow model for computing annular pressure and choke valve dynamics during kick control operation. The NMPC controller is executed using a MATLAB code based on Grüne and Pannek (2017). The sampling intervals are set as 5

seconds based on simulation objectives and controller performance sensitivity in Grüne and Pannek (2017).

The pressure window and pump flow capacity, which are used to set the controller bandwidth (or constraints), is based on the reservoir (pore) pressure, the fracture pressure and the surface equipment safe operating range. While the aim of the controller is to safely detect and attenuate kick while maintaining a downhole pressure window, the numerical simulation will push the controller beyond its safe operating thresholds for the purpose of the current work.

The MPD control plant model implemented in the numerical simulation is described by equations (6.7 – 6.12) below and are based on the process flow diagram in Figure 6.8. A detailed description of the hydraulic model and the NMPC controller scheme can be found in Sule et al. (2019).

$$\frac{dP_p}{dt} = \dot{P}_p = \frac{\beta_d}{V_d}\left(q_p - q_b\right) \qquad \text{(pump pressure dynamics)} \tag{6.7}$$

$$\dot{q}_b = \frac{1}{M}\left(P_p - P_c - F_d {q_b}^2 - F_a(q_{res} + q_b)^2 + (\rho_d - \rho_a) g h_{TVD}\right) \quad \text{(bit flow dynamics)} \tag{6.8}$$

$$\frac{dP_c}{dt} = \dot{P}_c = \frac{\bar{\beta}}{V_a}\left(q_b + q_{bpp} + q_{res} - q_c + T_{XE}\right) \qquad \text{(choke pressure dynamics)} \tag{6.9}$$

$$where\ \bar{\beta}\ (effective\ bulk\ modulus) = \frac{\beta_L}{1+\frac{\beta_L}{L}\int_0^L \frac{C_0 \alpha_G}{\gamma P} dx}\ ,\ \alpha_G + \alpha_L = 1 \tag{6.9b}$$

$$q_c = u_c\, A_o C_d \left(\frac{\chi_L}{\rho_L} + \frac{\chi_G}{\rho_G}\right) \sqrt{\frac{2(P_c - P_0)}{\frac{\chi_L}{\rho_L} + \frac{\chi_G}{\gamma^2 \rho_G}}} \qquad \text{(two-phase choke flow model)} \tag{6.10}$$

$$where\ \ \rho_G = \frac{P}{c_G^2(T)}\ , \rho_L = \rho_{L,0} + \frac{P}{c_L^2} \qquad \text{(gas and liquid densities)} \tag{6.10b}$$

$$P_b = \begin{cases} P_c + F_d {q_b}^2 + \rho_a g h_{TVD} \\ P_p - F {q_p}^2 + \rho_a g h_{TVD} \end{cases} \qquad \text{(bottomhole pressure)} \tag{6.11}$$

$$q_{res} = k_p(P_{res} - P_{bh}) \quad \text{(reservoir influx)} \quad (6.12)$$

Where P_p, is the rig pump pressure, q_p is rig pump flow rate, V_d and V_a are the volume of the drillstring and annulus respectively, β_d and β_a are the bulk moduli of mud in the drill string and annulus respectively, q_b is the flow through the bit, P_c is the upstream choke pressure, q_c is the flow through the choke, q_{res} is the reservoir influx flow rate, $F_d$and F_a are frictional pressure loss in the drillstring and annulus respectively, χ_L is the liquid mass fraction, χ_G is the gas mass fraction. and $u_c \in [0,1]$ is the choke opening (or choke control input).

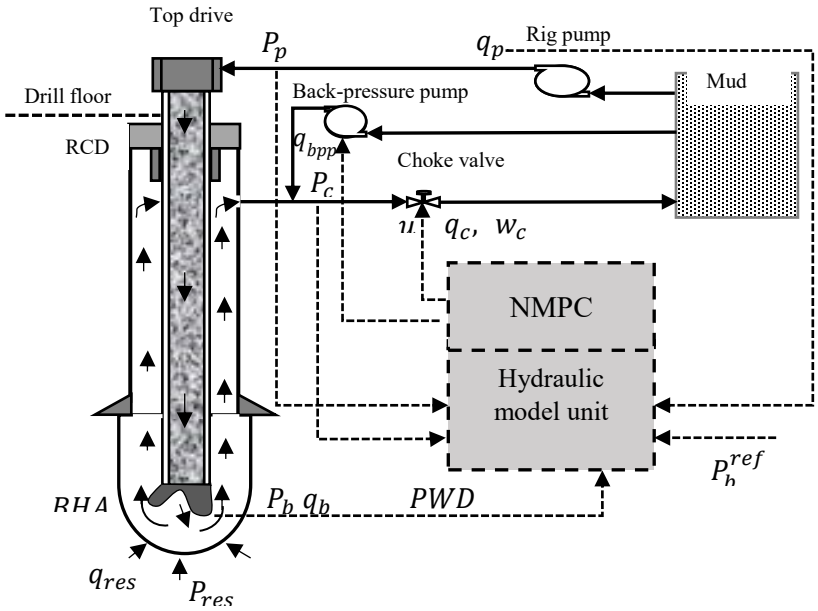

Figure 6.8: Managed pressure drilling control system process flow diagram

6.4 Application of proposed risk model framework

6.4.1 Case study background

The Amberjack field, located 32 miles off the coast of Louisiana in Mississippi Canyon Block 109 in 1030 ft of water, is discovered by BP in 1983 and by 1992 38 wells had been completed and were producing oil and gas from various sand packages. A redevelopment program initiated with the A16

ST1 and A25 ST1 wells in 1999 after about 10 years of production encountered significant challenges, including, reduced fracture gradient, unmanageable equivalent circulation density (ECD), and wellbore instability through the overburden and depleted reservoir sands above the target formation. These resulted in undesirable drilling events, including gas influx. However, with the implementation of Schlumberger DAPC constant bottomhole pressure MPD technique to drill the troubled reservoir section, the operator successfully managed the bottomhole pressure windows, within ± 0.16 ppg while drilling, ± 0.12 ppg while tripping, and ± 0.05 ppg while rolling over the mud from 14.8 to 15.0 ppg, to reach the target depth. In this drilling operation, the influx was limited to 2.5 bbl and shut-in-casing-pressure to 150 psi. Detail information of this case study can be found in Fredericks et al. (2011).

6.4.2 MPD kick control simulations

6.4.2.1 Plant and control model development

An MPD system that meets the downhole drilling operating requirements for the Amberjack case study and key surface equipment, including the RCD and the MPD choke manifold is developed. This is done using the operational limits set in the Amberjack MPD case study for influx rate of 2.5 bbl./min, surface casing pressure of 150 psi and target formation fracture and pore pressures of 8353.8 psi (15.3 ppg) and 8080.8 psi (14.8 ppg) respectively. Using these operational requirements, M-I SWACO RCD 3† and AUTOCHOKE† drilling choke are selected for the Schlumberger DAPC system. The RCD 3† has a maximum static pressure of 3000 psi and a dynamic pressure of 1000 - 1500 psi at 100 - 80 rpm respectively and the AUTOCHOKE† is available in 3000, 10000 and 15000 psi models.

Consequently, a further model analysis is achieved by developing "*MPD kick control variables*" to assess the success/failure of the kick control operation. The MPD kick control variables consist of *surface backpressure* P_c*, bottomhole pressure* BHP*, kick size ,* q_{res}*, and allowable surface pressure for RCD* (RCD_P_{lim}) *and drilling choke* $(Choke\_P_{lim})$.

Table 6.1 presents the failure thresholds for kick control variables, based on the drilling operation limitations, which determines when control operation may fail. The controller/ model error listed as category 3 is not numerically defined; thus, the study considers the failure probability database available to describe its contribution to MPD control system failure. The numerical model begins by using the well geometry and the pressure profiles described in the Amberjack field MPD case study to compute the required kick control parameters for setting up the hydraulic model and the control objectives for gas kick control numerical simulations. The narrow pressure margins between the pore pressure/minimum BHP setpoint (14.8 ppg) and fracture pressure/maximum BHP setpoint (15.3 ppg) in the target formation section are used to set the controller pressure constraints (boundaries) for the MPD system, i.e.

$$\left[P_{pore} \leq BHP^{ref} \leq P_{frac} = 14.8\ (ppg) \leq BHP^{ref} \leq 15.3\ (ppg)\right] \tag{6.13}$$

The BHP^{ref} is computed using the given mud weight of 14.85 (ppg) to maintain the required ECD.

Table 6.1: Operational limits for an MPD control model simulation

Category 1: drilling parameters	Failure threshold
Gas kick rate (size)	> 2.5 bbl./min
Formation fracture pressure (Fp)/maximum BHP setpoint	> 8353.8 psi (576 bars)
Formation pore pressure (Ppore)/minimum BHP setpoint	< 8080.8 psi (557 bars)
Bottomhole pressure setpoint	8190 psi (565 bars)
Category 2: surface equipment allowable pressure	

RCD 3†‡	> 1500 psi
AUTOCHOKE†	> 10000 psi
Category 3: controller / model error	

6.4.2.2 Kick control simulations in an automated MPD control system

Normal operating condition

The simulations are performed using a MATLAB code based on Grüne and Pannek (2017) and the detail control model setup can be found in Nandan et al. (2016); Sule et al. (2019). The first step of the numerical simulations is tuning the model to calibrate the field data reported in the Amberjack case study (Fredericks et al., 2011) when implementing the operational limits of rig pump flow fixed at 398 GPM, BHP setpoint = 15 ppg (565 bars), casing pressure below 150 psi (10.3 bars), minimum BHP setpoint not exceeding 14.8 ppg (557 bars) and maximum BHP setpoint not exceeding 15.3 ppg (576 bars) set in the study. Table 6.2 summarizes well parameter used in setting up the MPD control model.

The results are shown in Figure 6.9 (a and b). Figure 6.9b shows the results of an unplanned fire drill for testing the MPD system in the case study. As seen in the plot, while pumping at around 398 GPM, and maintaining the BHP setpoint of 15 ppg and backpressure (Pc), the rig pump is intentionally stopped to see how the MPD system will respond in maintaining the ECD and moments later, the pump is restarted, and the operation went back to normal. The goal for this study, however, is to set the normal operating conditions for the control model before running failure simulations. Figure 6.9a shows the model tuning results, in which the controller swiftly tracks the BHP setpoint (within 40 s),

‡ Trademark

to set system's normal control operation without any disturbance while the pump flow rate is fixed at around 398 GPM.

Table 6.2: Well parameter for MPD control simulation based on Amberjack case study

Parameter	Value	Unit
Volume of annulus $(\boldsymbol{V_a})$	180.95	m^3
Volume of drillstring $\boldsymbol{V_d}$)	74.86	m^3
Mass parameter $(\boldsymbol{M})$	8.04×10^8	kg/m^3
Bulk modulus in annulus $(\boldsymbol{\beta_a})$	2.3×10^9	Pa
Bulk modulus in drillstring $(\boldsymbol{\beta_d})$	2.3×10^9	Pa
Density in drillstring $(\boldsymbol{\rho_d})$	1779.5	kg/m^3
Density in annulus $(\boldsymbol{\rho_a})$	1779.5	kg/m^3
Friction factor in drillstring $(\boldsymbol{F_d})$	6.29×10^7	s^2/m^6
Friction factor in annulus $(\boldsymbol{F_a})$	6.39×10^6	s^2/m^6
Choke discharge coefficient $(\boldsymbol{C_d})$	0.6	
Choke discharge area $(\boldsymbol{A_0})$	0.0022	m^2
Choke downstream pressure $(\boldsymbol{P_0})$	1.013×10^5	Pa
Total vertical depth $(\boldsymbol{H})$	3200 (10500)	m (ft)
Prod. index $(\boldsymbol{K_{pi}})$	6.833×10^{-7}	m^3/sPa
Gas mass flow fraction, $\boldsymbol{\chi_G}$	0.2	
Liquid mass flow fraction, $\boldsymbol{\chi_L}$	0.8	
Speed of sound in gas, $\boldsymbol{c_G}$	345.8	m/s
Density of gas, $\boldsymbol{\rho_g}$	1.2	kg/m^3
Gas expansion factor, $\boldsymbol{\gamma}$	1.4	
Volume flow fraction, $\boldsymbol{\alpha_G}$	0.2	m^3/s
Slip law constant K	1.2	
Slip law constant S	1	

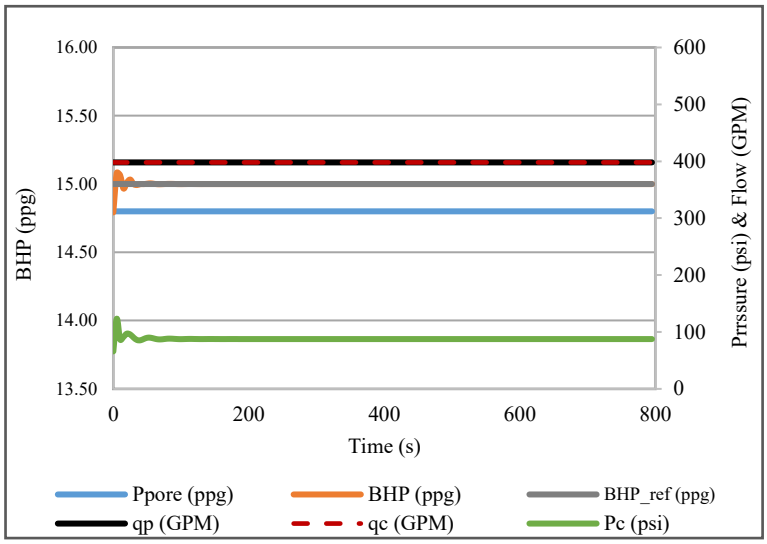

Figure 6.9a: Tuning operation to set the normal operating condition for simulation

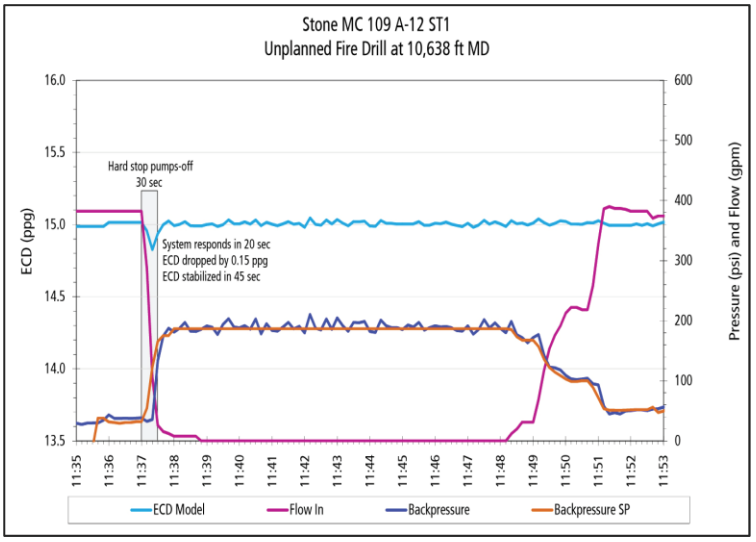

Figure 6.9b: Result of unplanned fire drill for the MPD control operation

Figure 6.9: Model tuning results to set the normal operating conditions vs the field results.

Failure simulations

The required objective of an MPD control system is to detect and attenuate the kick. Using the operational limitations and the failure thresholds presented in Table 1, kick control failure simulations are numerically performed by initiating kick through pore pressure increase above the BHP setpoint of 15 ppg (565 bars or 8190 psi) while maintaining the mud pump flow at 398 GPM. Because the goal is to simulate kick control failure that consequently leads to a blowout scenario, the pore pressure is initially increased to 566.5 bar (8207 psi) just above the BHP setpoint to run the first simulation, and then increased incrementally by 0.5 bar until failure thresholds of the kick control variables are exceeded. As shown in Table 6.3, a total of eight kick simulations are numerically performed and the drilling parameters including BHP, backpressure (P_c), choke flow rate (q_c), reservoir influx (q_{res}), and choke valve opening (u_c) are computed and plotted.

For example, to initiate the gas kick scenario for run #1, the reservoir pore pressure is increased to 566 bars at time T = 240 s while keeping the rig pump flow rate constant at 398 GPM. As soon as

controller detects the kick, the choke opening, which have an operating range of $[0-1]$, automatically starts to decrease to deliver corresponding choke pressure (backpressure) on the annulus to increase the BHP setpoint until the kick is attenuated and a new BHP setpoint is set. The simulation is repeated for the remaining runs until the kick control operation starts to fail due to the kick control variables exceeding their failure thresholds.

Table 6.3: Kick simulation runs for MPD control failure

	Run #	Pore pressure (bars)	Pore pressure (psi)
Successful simulations	0	557 [initial]	8080.8 [initial]
	1	566	8207
	2	566.5	8214.25
	3	567	8221
	4	567.5	8228.75
Failed simulations	5	568	8236
	6	568.5	8243.25
	7	569	8250.5
	8	569.5	8257.75

6.4.3 Failure probability distributions for MPD kick control variables

The failure probability estimations of MPD kick control variables are performed by transforming the failure data obtained from kick control simulations into probability data. The control variables are described based on drilling parameters (allowable BHP, backpressure, and kick size/ flow rate), the surface equipment pressure containment rating of an RCD and a drilling choke, control model failure. The numerical simulation results obtained for each kick control variable are used to generate their cumulative probability distributions. P represents the probability of failure at any observation

obtained using equation (6.14), i.e. each computed value of the kick control variable x, including BHP setpoint, backpressure, influx size, and RCD-drilling choke pressure at a discrete time. Where a mean μ and standard deviation σ are determined by equations (6.15) and (6.16). Thus, the failure probability of each kick control variable is estimated from the cumulative distribution curve, i.e. the probability from the point where the control variable exceeds the failure threshold.

$$P = F(x|\mu,\sigma) = \frac{1}{\sigma\sqrt{2\pi}}\int_{-\infty}^{x} e^{-\frac{(t-\mu)^2}{2\sigma^2}}dt \tag{6.14}$$

$$\mu = \frac{1}{N}\sum_{i=1}^{N} x_i \tag{6.15}$$

$$\sigma = \sqrt{\frac{1}{N-1}\sum_{i=1}^{N}(x_i-\mu)^2} \tag{6.16}$$

6.4.4 Dynamic Bayesian Network model development

The BN model is developed by mapping the BT model into a Bayesian network using the illustrated example shown in Figure 6.6. In this study, two fault trees top events (kick event as the initiating event and MPD failure as the first safety barrier element of the event tree) are developed. The kick event FT (Figure 6.10) is developed based on the history of drilling challenges in the case study (Fredericks et al. (2011). Meanwhile, the MPD kick control failure FT model in Figure 6.10, (a primary well control safety barrier), is developed based on the operational interactions and dependencies among the MPD system components illustrated in Figure 6.1. The ET model in Figure 6.10 consists of the kick event as the initiating event, the well control safety barrier elements, and the consequences. The safety barrier elements include: an MPD, a BOP system, and escalation barriers preventers (casing and wellhead, ignition prevention, and emergency response plan (ERP). Detail discussion on ignition prevention barriers and emergency response plan can be found in Rathnayaka et al., 2013; *IADC Deepwater Well control guidelines, 2015*.

The DBN model in Figure 6.11 is an extension of BN model is set up in a *temporal plate* with 160 time-slices for dynamic analysis using a *Normal arc*, which assumes that any occurring event will have an instantaneous influence on the system operation. For instance, drilling into a high-pressure zone where $P_{pore} > BHP$ provides instantaneous effect of kick occurrence. The 160 time-steps is based on the simulation time set for the MPD kick control operation. Furthermore, the consequence node consists of a total of seven states outcomes, a safe state plus six others described in Table 6.4. A safe state outcome named "no kick" is added to the consequence node state account for no kick event. To assess the impacts of kick control variable nodes on themselves in the future, i.e., $p(Z_t|Z_{t-k})$, the temporal arc from each node is looped back to itself as shown in Figure 6.11. This can be interpreted as how the prior node event impacts the occurrence of the node event on the present day. The probability of kick event or blowout, for example, is evaluated by forward analysis, and the posterior probability given the occurrence of these events is evaluated by backward analysis.

Table 6.4: Consequences resulting from well control failure

Consq.	Outcomes	Description
C1	Kick controlled	The MPD control system successfully attenuate kick
C2	Kick uncontrolled	MPD failed but the kick is contained by BOP system
C3	Blowout contained	BOP system failed but Wellhead/casing prevent release to surface
C4	Blowout	Wellhead and casing failed to contain kick event escalation to blowout
C5	Fire and explosion	Ignition prevention failed to prevent fire and explosion escalation
C6	Catastrophic accident	Emergency response plan failed causing fatalities, loss of asset, environment damage, monetary losses etc.

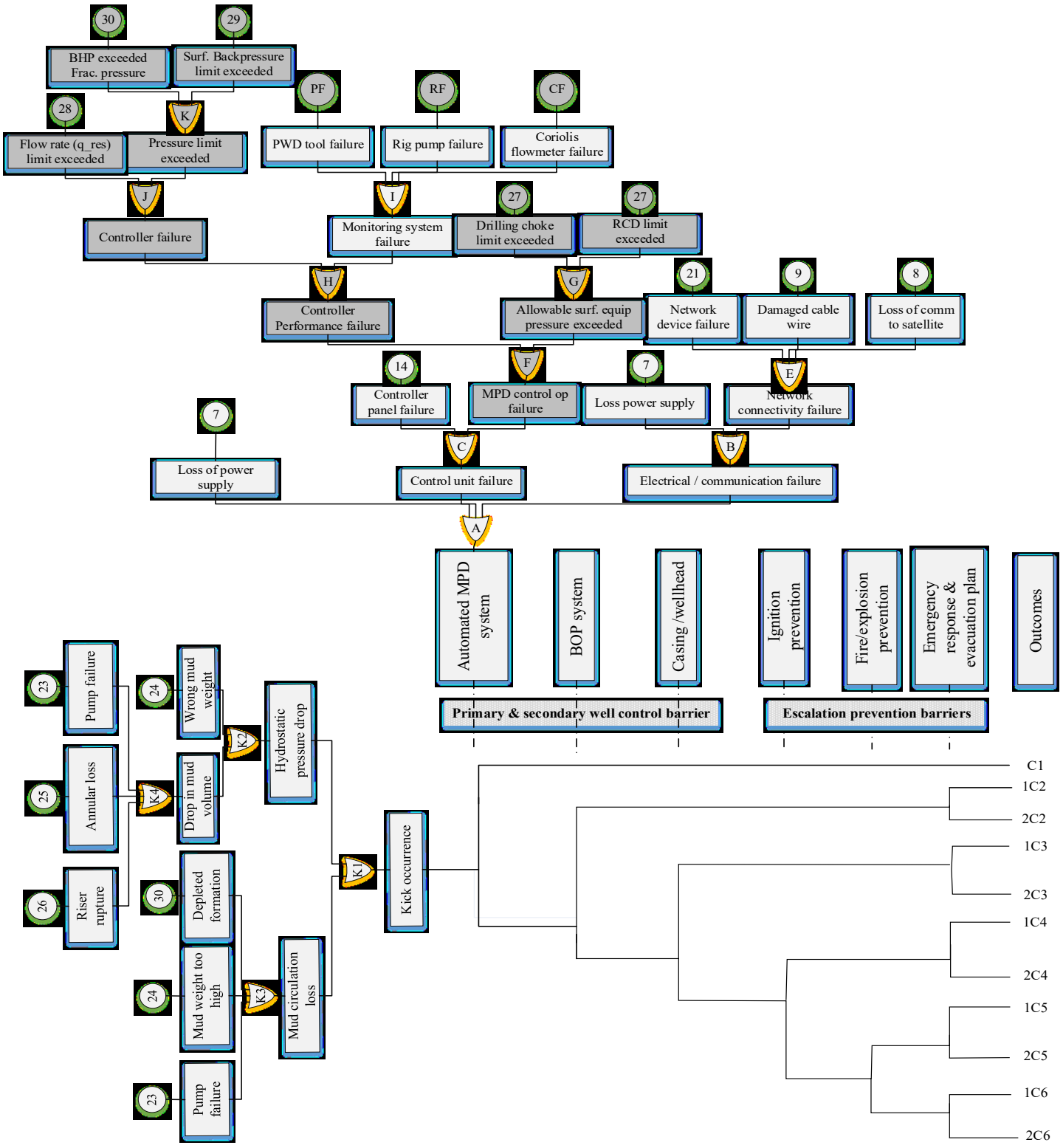

Figure 6.10: Bow-tie model for loss of well control in an MPD operation

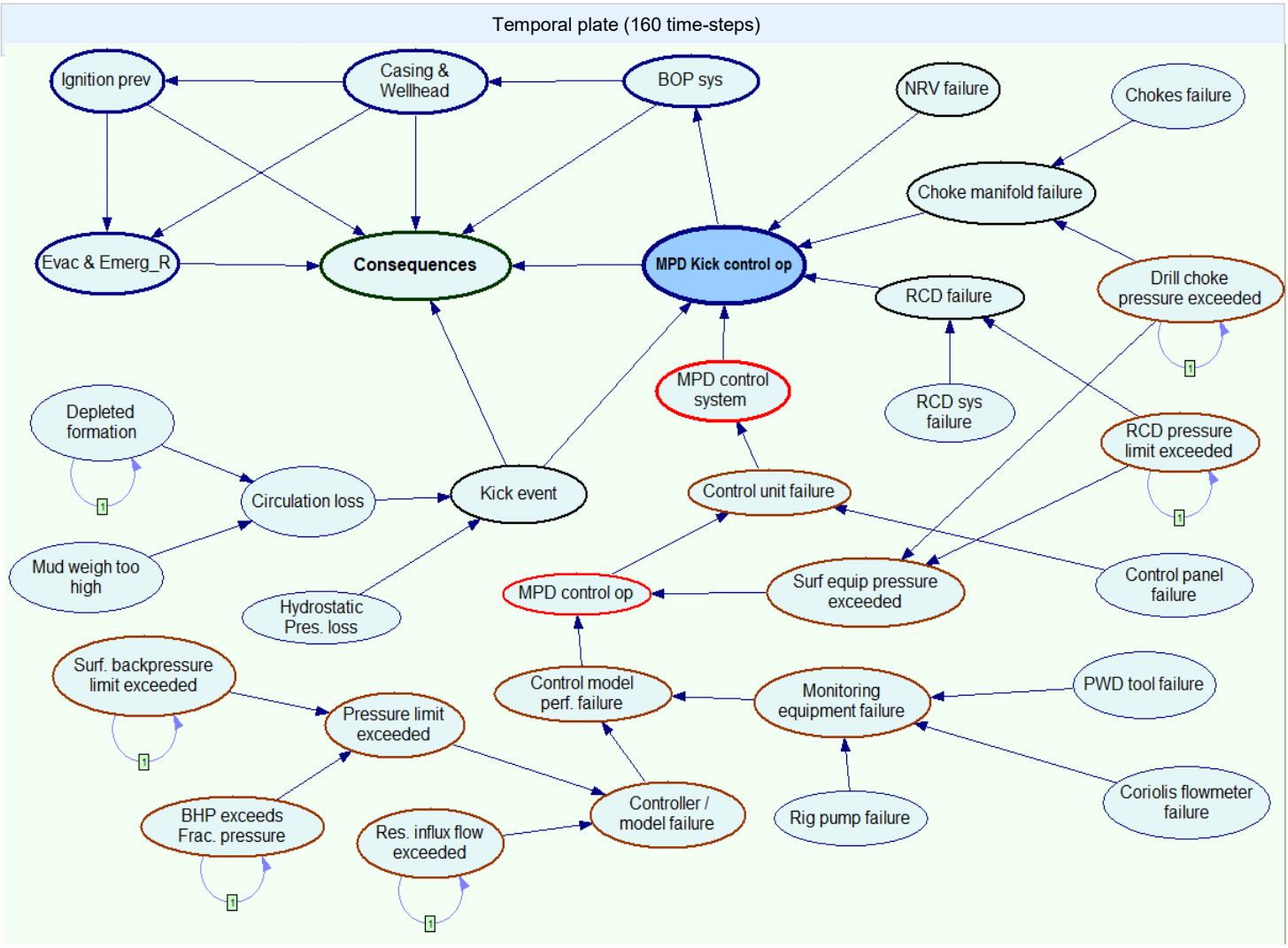

Figure 6.11: DBN model for risk analysis of loss of well control in an MPD operation

6.5 Results and discussions

The simulation results, including kick control simulations, probabilities distribution of kick control variables, and dynamic analysis of blowout consequence are presented. The failure probabilities of basic events used are presented in Table 6.5.

6.5.1 MPD control failure simulations

For each kick control simulation run, all kick control variables are computed at every 5 seconds of sample time defined in the control model. The results for backpressure, BHP setpoint, and influx size (q_{res}) are presented in Figures 6.12, 6.13, and 6.14 respectively. As shown in Figures 6.12 – 6.14, the controller automatically identifies reservoir influx at time t = 240 s and responds by applying backpressure on the annulus. Thus, the increasing backpressure leads to a corresponding increase in the BHP setpoint in attempt to attenuate the kick. It can also be noted, in Figures 6.12 – 6.14, that the backpressure, BHP and kick size increases with higher pore pressure (P_p) of the formation until the MPD kick control variables exceed their failure thresholds defined in Table 6.1.

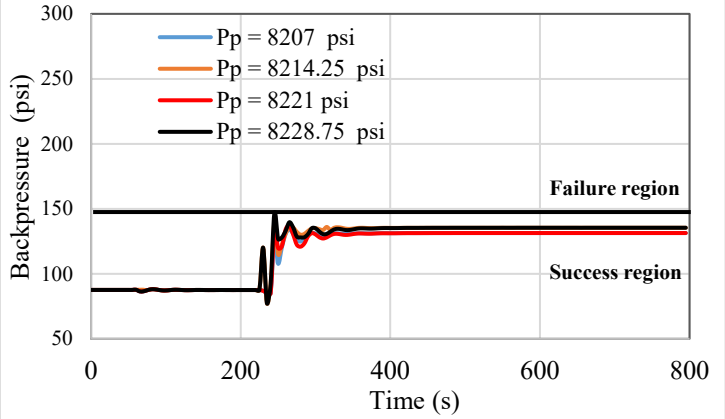

Figure 6.12a: Sim. results of backpressure plots for successful kick-control op

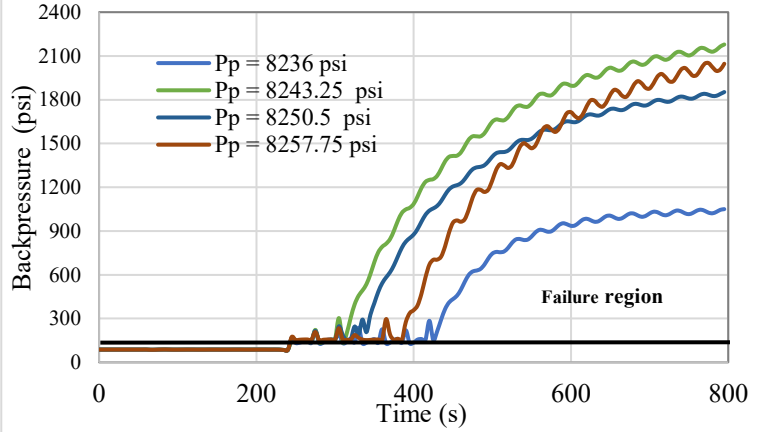

Figure 6.12b: Sim. results of backpressure plots for failed kick control op

Figure 6.12: Simulation results of backpressure for successful/failed kick control operations

For the backpressure results, Figure 12a shows that the formation pore pressure, P_p, of up to 8228.75 psi (567.5 bars) will not exceed the backpressure failure threshold of 150 psi; thus, the MPD control system will result in a successful kick control operation. However, when the formation pore pressure rises to 8236 psi (568 bars) and beyond, as shown in Figure 6.12b, the applied backpressure will

exceed failure threshold of 150 psi; thus, results in failure of kick control. The same explanations apply to the BHP results shown in Figures 6.13 a and b. However, the kick size does not exceed its failure threshold of 2.5 bbl/min until the formation pore pressure increases to 8257.75 psi (569.5 bars) as shown in Figure 6.14.

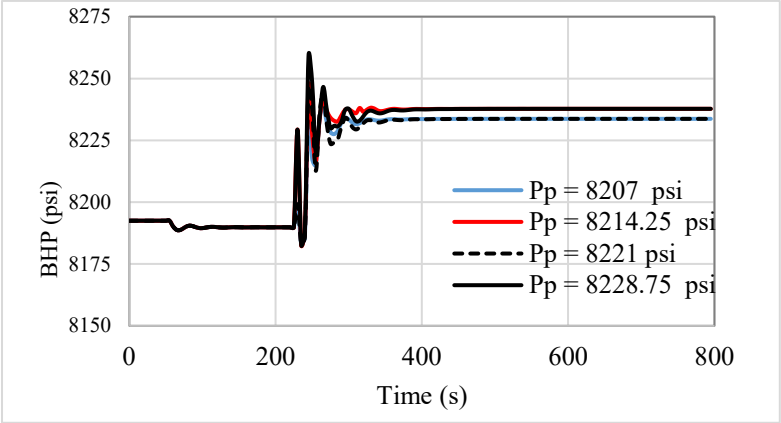

Figure 6.13a: Simulation results of BHP plots for successful kick control operation

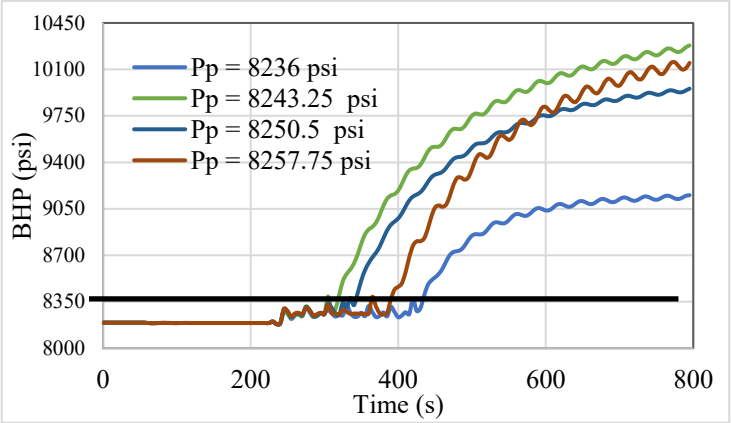

Figure 6.13b: Simulation results of BHP plots for failed kick control operation

Figure 6.13: Simulation results of BHP for successful/failed kick control operations

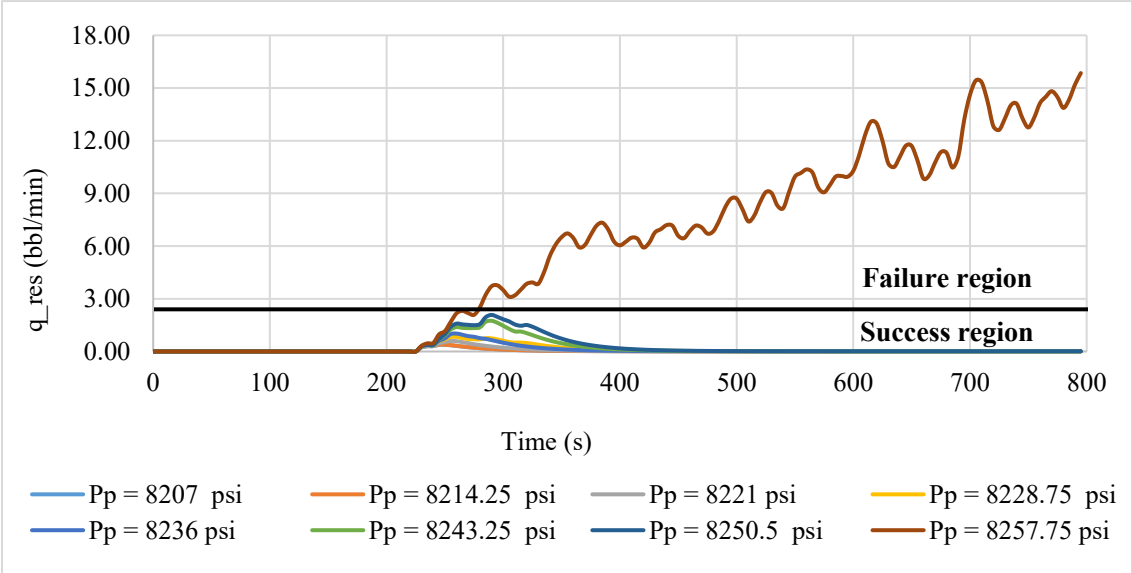

Figure 6.14: Simulation results of kick size for successful/failed kick control operations

6.5.2 Failure probability results

The cumulative distribution obtained for the kick control variables, including backpressure, BHP, kick size, and allowable pressure of RCD and drilling choke, are presented in Figures 6.15 – 6.18 respectively. The RCD failure probability analysis is performed using the results obtained for backpressure operation. This is because an MPD system can only apply surface backpressure within the available pressure control rating of an RCD (Hannegan et al., 2017). Furthermore, because the allowable working pressure of the surface equipment will be based on the equipment with the least pressure rating, the failure probability of the drilling choke will be equal to the failure probability obtained for the RCD. Thus, the failure probability of the RCD and drilling choke is estimated from the simulated backpressure results exceeding the RCD failure threshold of 1500 psi. The failure probabilities of each MPD kick control variable are computed from their respective cumulative distribution curve. For instance, in the case of backpressure, the probability that the backpressure exceeds the failure threshold, i.e. $P = [P_c > 150\ (psi)]$ is computed. The computed probabilities for all MPD kick control variables are presented in Table 6.5 and implemented in the failure and blowout analysis of MPD operation.

These computed failure probabilities are reasonable considering the drilling challenges in the case study. Thus, because of the narrow pressure margin between the pore pressure and the fracture pressure of the target formation in the Amberjack case study, approximately 2% increase in the pore pressure may result in about **75.5%, 72.9%, 75.3%,** and **15.4%** likelihoods that the backpressure, BHP setpoint, kick size, and RCD respectively will exceed their safe operating thresholds.

Table 6.5: Failure probabilities of MPD control variables in a kick control operation

MPD control variables	Failure probability			
	Pp = 8243.25 (psi)	Pp = 8250.5 (psi)	Pp = 8257.75 (psi)	Average
Backpressure	0.7636	0.7513	0.7496	0.755
BHP setpoint	0.7458	0.7191	0.7230	0.729
Kick size	No data	No data	0.7534	0.753
RCD/Drilling choke	0.2080	0.1144	0.1401	0.154

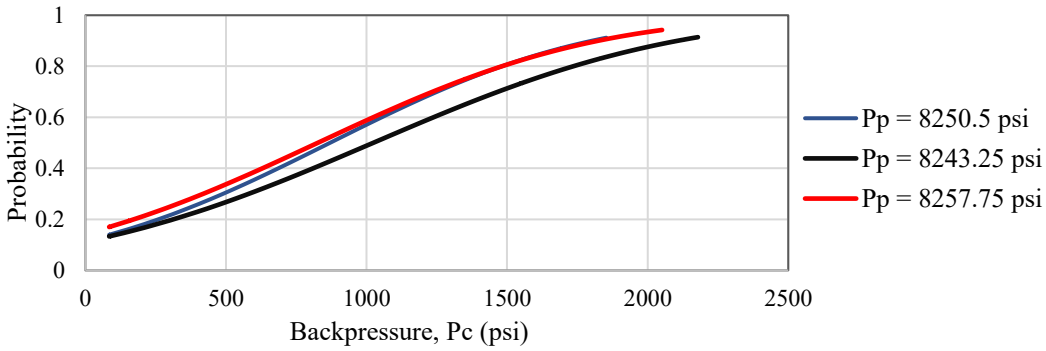

Figure 6.15: Cumulative distribution of backpressure obtained in MPD kick control simulation

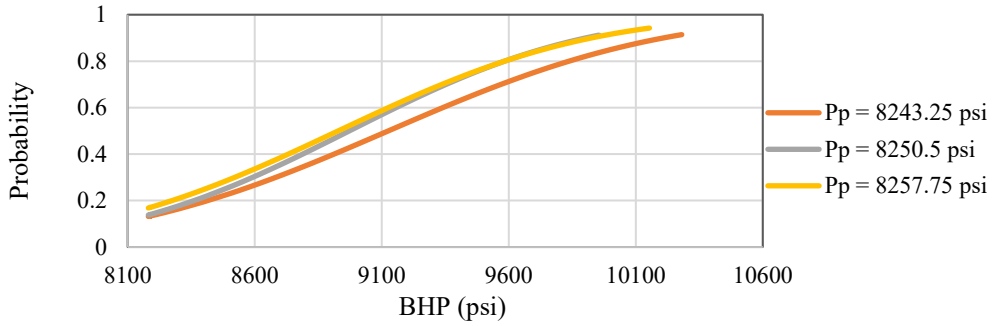

Figure 6.16: Cumulative distribution of BHP setpoint obtained in MPD kick control simulation

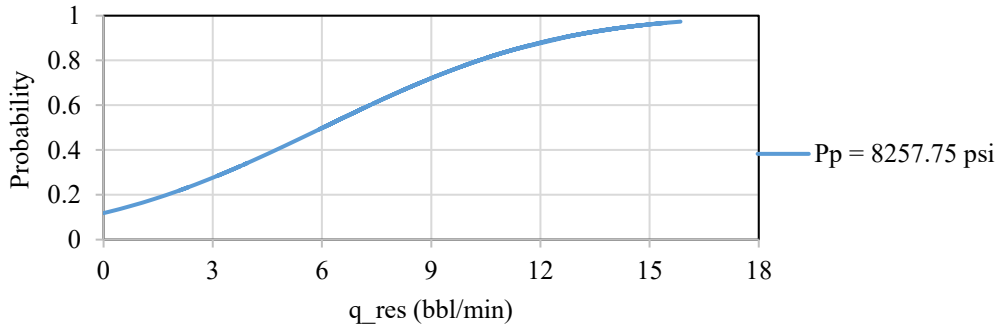

Figure 6.17: Cumulative distribution of reservoir influx obtained in MPD kick control simulation

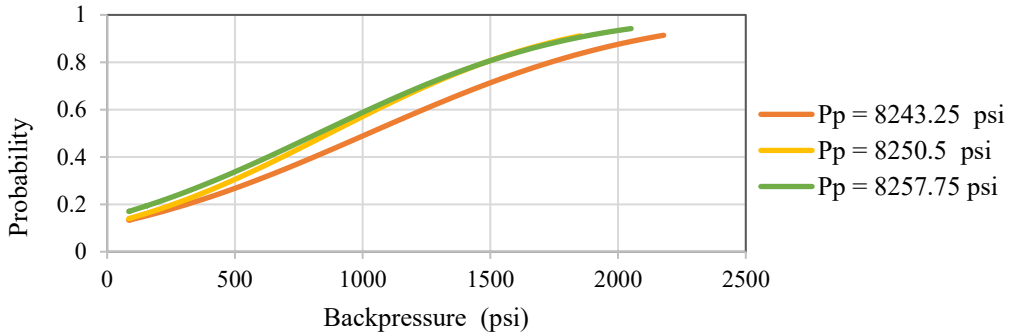

Figure 6.18 Cumulative distribution of RCD obtained in MPD kick control simulation

6.5.3 Failure and risk analysis of an MPD and blowout inferences

6.5.3.1 Forward analysis of the DBN model

Using the prior probabilities of basic events presented in Table 6.6 and performing a forward analysis on the DBN model for the given 160 time-slices provides one-step Bayesian updating of the network variables and outputs probability observations for the entire times-steps (i.e. from $t = 0 - t = 159\ s$). The results for the 159th time-slice are shown in Figure 6.19. The probability of kick event occurring, given 74% chance of circulation loss and 9% chance of hydrostatic pressure loss, is estimated as 0.760. It is shown here that the 74% likelihood of circulation loss is due to a high chance of fractured formation given a 73% likelihood of formation depletion, as indicated in the case study. Moreover, the failure probability of an MPD kick control operation is estimated as 0.752. About 73% of MPD kick control failure is contributed by an MPD control system failure, which has a failure likelihood of 98.9% due to MPD kick control variables exceeding their safe operating thresholds. The MPD control operation accounts for the operational limits of the surface equipment and the robustness of an MPD control model whose failure occurrence probability is estimated as 98% in this case. The control model execution, which depends on the control design limits, is highly influenced by the severity of the disturbance, such as kick, due to wellbore/formation instabilities.

The probabilities of these two nodes (kick event and MPD system) propagate through other operational safety barriers nodes in the model to estimate the likelihood of risk. The results are shown in Figure 6.19. For instance, given the 76% likelihood that kick event occurs results in no kick consequence likelihood of 24%. Additionally, the high probability of 75% that the MPD system safety barrier fails, results in about 1% likelihood consequence that kick is controlled. Thus, the chances that kick escalation is uncontrolled, a blowout is contained, or blowout incident occur depends on the failure probabilities of the BOP system and wellhead/casing safety barriers. In this case, the chance of well control incident leading to blowout risk is estimated as 32% and the risk of blowout escalation, including fire explosion and catastrophic accidents are estimated as about 7% and 2% respectively.

Furthermore, to assess the influence of kick control events occurrence on itself in relation to the DBN analysis, the conditional probability table (CPT) for each kick control event is defined with respective prior probabilities of occurrence at t = 0 and updated (posterior) probabilities of occurrence at t = 1 (i.e. a time prior), and perform temporal probability updating. These analyses increase the failure likelihoods of kick occurrence, MPD failure, and blowout risk by 29%, 29%, and 50% respectively as shown Figure 6.20, compared to analysis with no prior evidence as shown in Figure 6.19. This is highly useful for risk prediction and diagnostic analyses of an MPD operation when evaluating the safety of the operation

Table 6.6: Basic events and their probabilities (Sources: Khakzad et al., 2013; 2013a; Abimbola et al., 2015; Rathnayaka et al., 2012; Di Natale et al., 2012; Tran et al., 1997; Phillipa et al., 2011; OREDA, 2002; Sule et al., 2018b)

Events	Event Description	Prior Probability (Pi)	Posterior probability (Po)	Po/Pi
1	RCD Bearing assembly failure	1.43E-03	1.44E-03	1.01
2	RCD Bowl failure	3.14E-03	3.17E-03	1.01
3	Flowline blockage	3.60E-03	3.63E-03	1.01
4	Insufficient fluid in circulation	2.00E-03	2.02E-03	1.01
5	Pump line blockage / rupture	3.60E-03	3.63E-03	1.01
6	Auxiliary choke valve failure	2.50E-02	2.50E-02	1.01
7	Power supply failure	2.50E-03	2.52E-03	1.01
8	Loss of communication with satellite	2.00E-03	2.02E-03	1.01
9	Cable wire failure	1.00E-06	1.01E-06	1.01
10	Main controller failure	2.52E-04	2.52E-04	1.00
11	Auxiliary controller failure	2.52E-04	2.52E-04	1.00
12	Choke valve #2 failure	2.50E-02	2.50E-02	1.00
13	Choke valve #3 failure	2.50E-02	2.50E-02	1.00
14	Controller panel failure	2.52E-03	2.54E-03	1.01
15	Incorrect hydraulic model	1.00E-03	1.11E-04	1.01
18	Pressure sensor failure	1.10E-04	1.11E-04	1.01
19	Loss of service water	1.00E-04	1.01E-04	1.01
20	Loss of vacuum system	1.00E-04	1.01E-04	1.01
21	Network device damage	5.00E-03	5.04E-03	1.01
22	Non-return valve failure	3.12E-02	3.12E-02	1.00
23	Pump failure	4.00E-02	5.20E-02	1.30
24	Wrong mud density	3.00E-02	3.90E-02	1.30
25	Annulus losses	1.00E-02	1.30E-02	1.30
26	Riser rupture	1.00E-02	1.30E-02	1.30
Computed failure probability of kick control variables from an MPD control failure simulations				
27	Depleted formation	7.29E-01	9.47E-01	1.30
28	Drilling choke / RCD limit exceeded	1.54E-01	1.61E-01	1.05
29	Flow rate (q_res) limit exceeded	7.53E-01	7.84E-01	1.05
30	Surf. Backpressure limit exceeded	7.55E-01	7.89E-01	1.05
31	BHP exceeded Frac. pressure	7.29E-01	7.63E-01	1.05

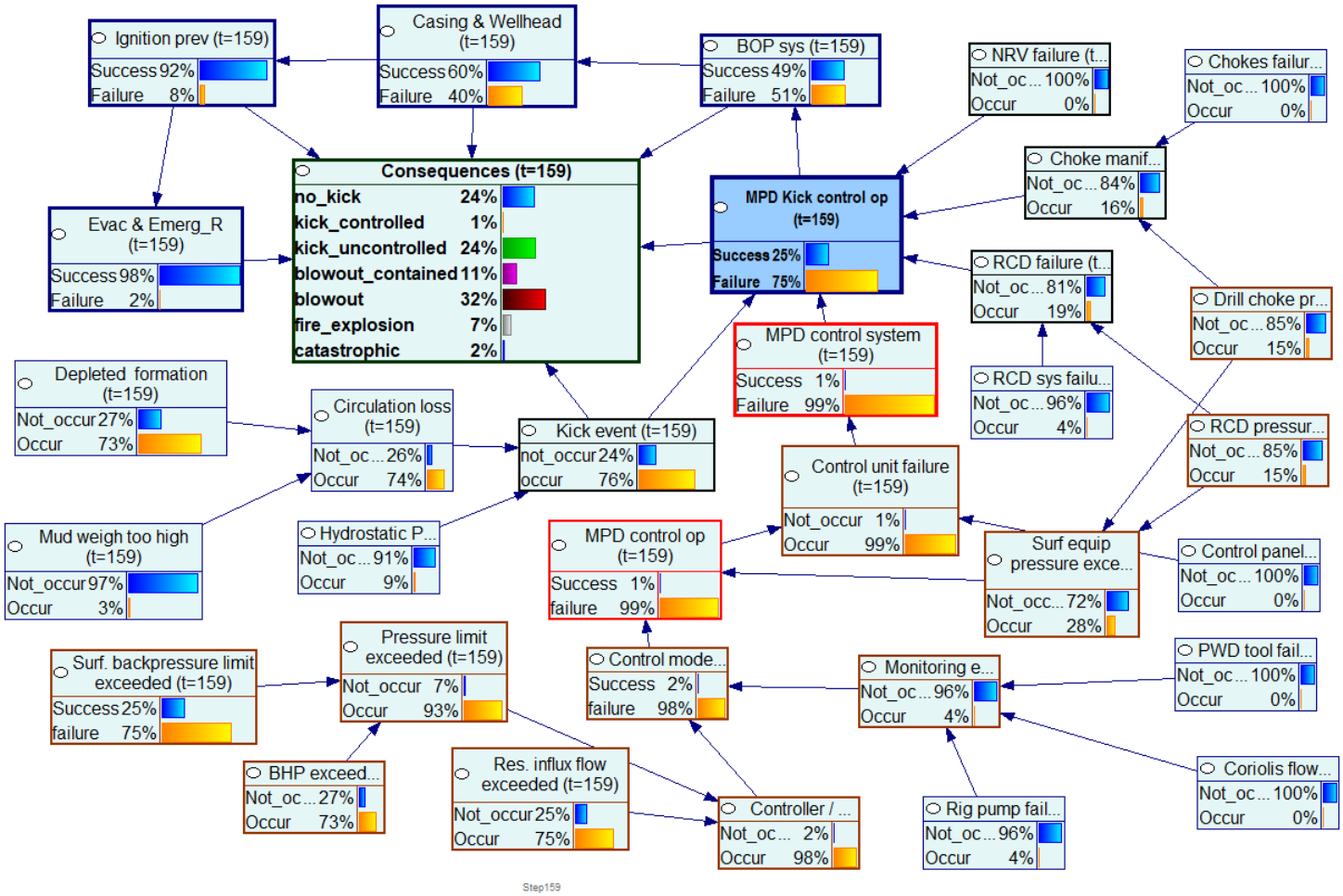

Figure 6.19: Unrolled DBN results representing the 159th time-slice of the blowout risk evaluation

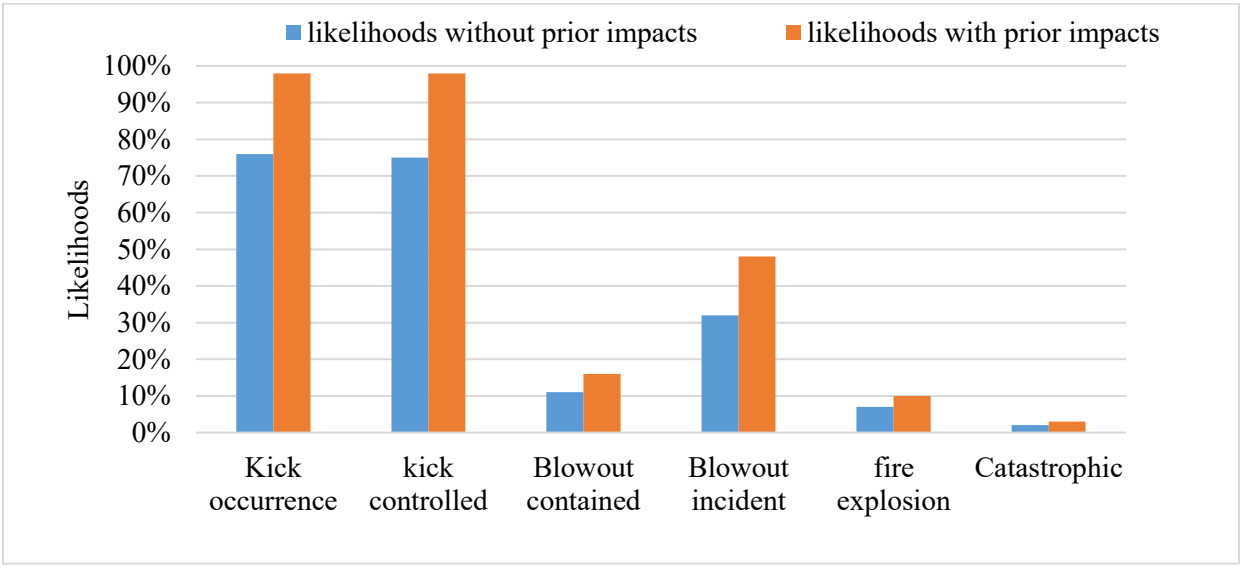

Figure 6.20: Risk comparisons of prior and posterior probability analysis of @ 159th time-slice

6.5.3.2 Backward analysis of the DBN model

The probability distributions computed for kick control variables are fed into the DBN model as temporal evidence to assess and monitor the physical behaviour of the kick control operation simulation. These involve six temporal root nodes (6-TRN), including *BHP setpoint exceed maximum BHP limit, surface backpressure limit exceeded, depleted formation, reservoir influx limit exceeded, and RCD/ drilling choke pressure limits exceeded*. The backward analysis (i.e. updating the temporal beliefs) is performed to obtain marginal posterior probability distributions as a function of time. The results shown in Figure 6.21 gives a better picture of the dynamic operation involved in well control events, such as kick and blowout consequences. As shown in Figure 6.21, the probability distribution inference for kick occurrence follows that of the depleted formation and while that of an MPD kick control failure follow those of the MPD kick control variables.

For instance, the chances of formation collapse due to depletion is low at the beginning and gradually increases with operation time. This in turns increases the chances of circulation loss and consequently a risk of kick occurrence. Because the circulation loss event has about 90% contribution to kick event occurrence, an inference that is consistent with the Amberjack case study background, the risk of kick event follows the probability distribution of circulation loss event. Similarly, as the likelihood of the nodes *BHP set point, choke pressure, kick size, RCD* and *drilling choke equipment pressure limits* exceeding their safe operating thresholds increase, given the limitations of narrow pressure margins in the target depth of the Amberjack redevelopment well, the risk of failure of an MPD kick control operation increases. Simultaneously, these results are propagated through the operational safety barrier components for dynamic risk evaluation.

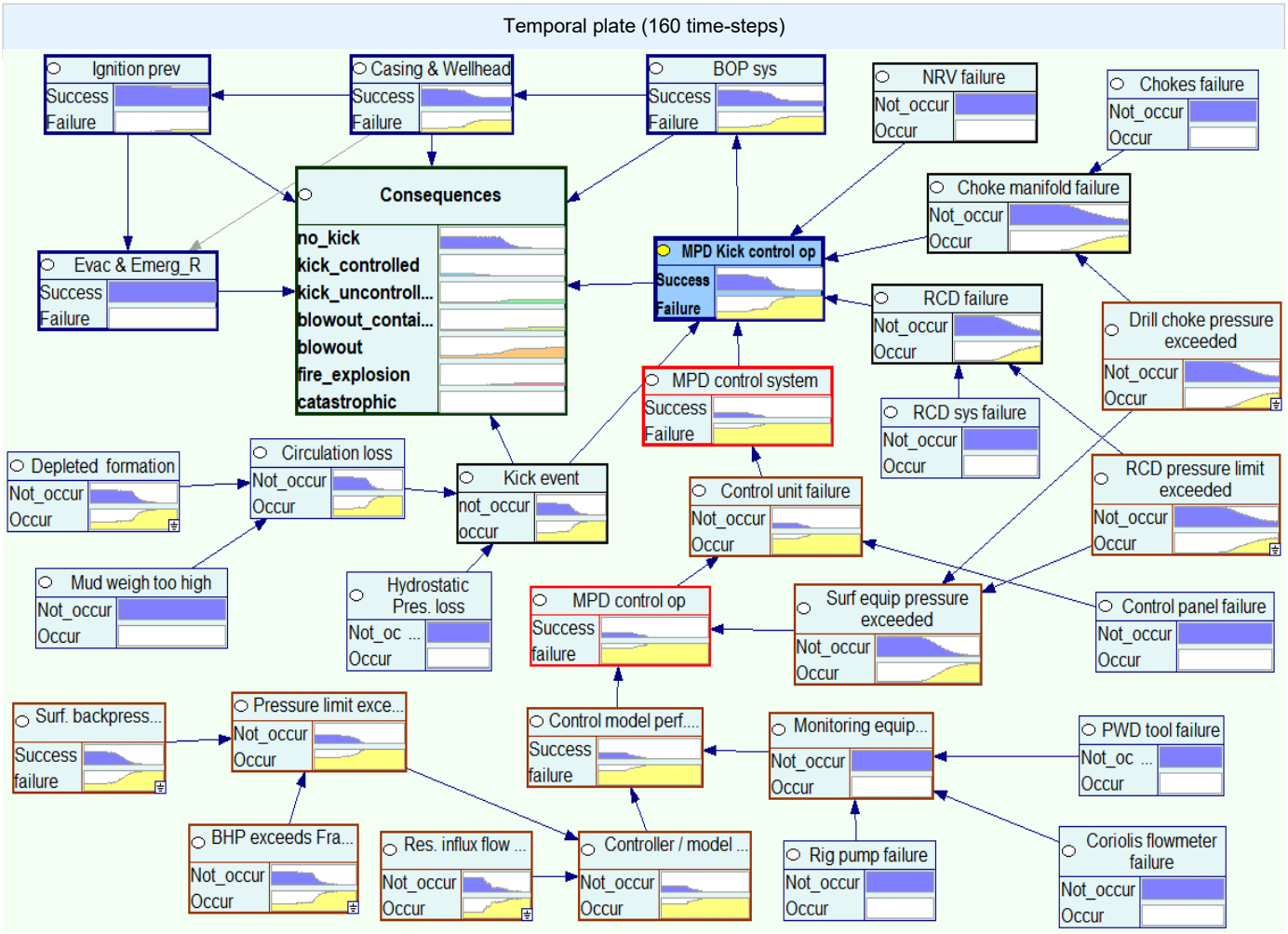

Figure 6.21: Results of kick control simulation during an MPD well control operation

The dynamic risk probability distributions of the key well control events discussed thus far are clearly presented in Figures 6.23 and 6.23. Figure 6.22 mirrors the drilling events demonstrated in the numerical simulation of an MPD kick control operation whereby gas kick is initiated after a period of incident-free operation and then followed by a period with an increasing chance of MPD kick control variables exceeding their failure thresholds. Figure 6.23 presents the resulting dynamic changes of operational risk as a function of time. For instance, as shown in Figure 6.22, the risk of blowout can be expressed in three phases, when it is initially below 20% during the initial periods of operation, then the risk slowly increases after kick occurrence but with MPD kick control variables

still within operating safe limits, and then suddenly spikes to about 50% after MPD control system has failed. Also shown, is an increase in the likelihood of an escalation event, such as fire and explosion.

Further analysis is performed by setting the temporal evidence of an MPD control system and circulation loss nodes to 100% success and 100% "not_occur" respectively and updating the temporal beliefs. In the case of MPD control system, though given the evidence of kick event occurring, the likelihood of MPD kick control failure reduced to about 2% from 75%; thus, improves the likelihood of "kick controlled" consequence to about 94% from 1% and reduces the risk of blowout to 2% from about 50% at the 159th time-slice. This confirms the MPD control system as the most safety-critical component in an MPD system (Sule et al., 2018b) due to its dominant influence on the success of an MPD operation. Moreover, a 100% likelihood of non-occurrence circulation loss not only increases the likelihood of "no kick" consequence to about 91% but also reduces the risk of a blowout to about 4% and the chance of MPD failure to about 9%. The significance of circulation loss to kick occurrence and blowout risk in these results are consistent with the drilling challenges experienced in the Amberjack case study.

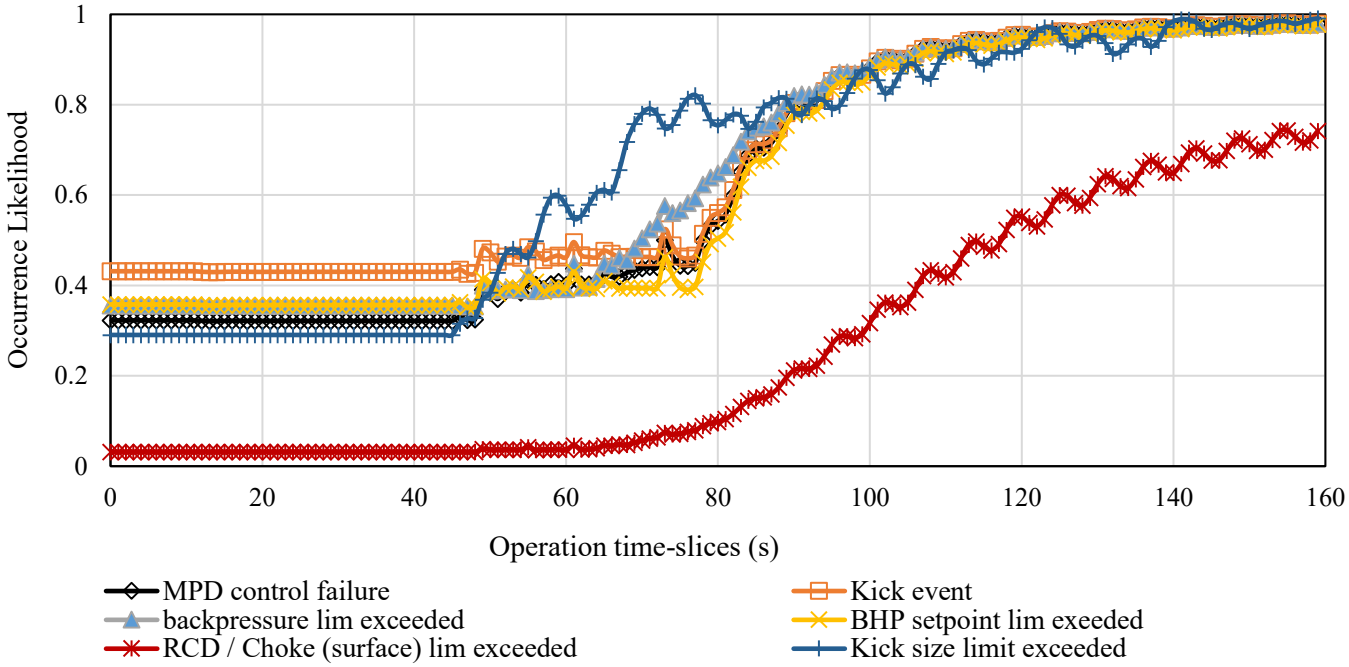

Figure 6.22: Dynamic failure probability analysis of MPD kick control operation

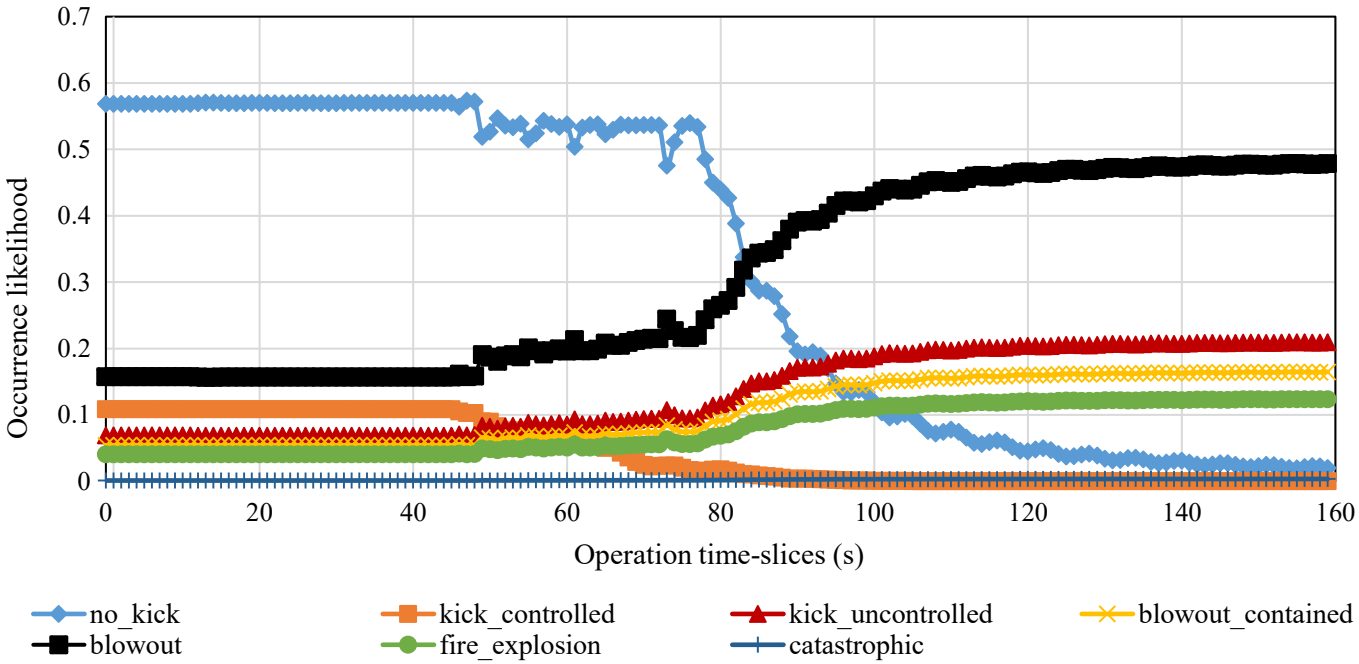

Figure 6.23: Dynamic operational risk analysis of blowout during an MPD kick control operation

6.6 Conclusions

The current study focuses on developing a dynamic risk assessment model for assessing the safety on MPD operation. Thus, this chapter proposes an advanced dynamic blowout risk model (DBRM) framework for a managed pressure drilling operation, which involves three phases of operation: a dynamic Bayesian network (DBN) risk model development, numerical simulation an MPD kick control operation, and dynamic risk analysis. One of the advanced features of the proposed DBN model is the ability to model complex processes with time-delay without copying nodes across multiple time-slices and modeling power of up to 1000 time-slices. The DBRM model integrates a numerical simulation of a kick control operation performed using an MPD control model presented in Sule et al. (2019) to the proposed DBN model. Another important novelty feature of the proposed model is the introduction of an MPD kick control parameters/variables, which are instrumental in setting safe/failure operating thresholds for an MPD control operation and performing numerical simulations of an MPD failure and blowout risk analyses. These parameters include *BHP setpoint*, *backpressure, kick size, and RCD/drilling choke limits*.

The proposed model has been applied to a case study from the Amberjack field in the Gulf of Mexico where the drilling hazards include depleted formation and narrow pressure margins between pore and fracture pressure. Analyses of the logical causal relationships leading to kick occurrence and MPD system failure are established to develop a dynamic risk model based on DBN. Series of numerical simulations are performed, and the data collected based on the MPD kick control variables are transformed into a probability distribution for dynamic risk analysis. The results show that the likelihood of kick occurrence increases with an increasing likelihood of circulation loss due to the increasing likelihood of depleted formation resulting in the fractured formation. Simultaneously, this is causing an increasing likelihood of MPD failure as primary well control barrier due to an MPD

kick control variables exceeding their safety thresholds; consequently, increasing the risk of a blowout. Further analysis shows that 100% success of an MPD control system increases the likelihood of MPD kick operation success by 96% and reduces the risk of a blowout by about 96% while circulation loss occurrence is significant to the chances of well control event, such as kick. These results consistently mirror the drilling scenarios experienced in the Amberjack case study.

Chapter 7 Conclusions and Recommendations

7.1 Conclusions

This thesis presents a comprehensive and novel approach, illustrated in Figure 7.1, to enhance the safety of well control operation by advancing the kick detection technique and assess the reliability and safety of managed pressure drilling (MPD) system.

From this research, it has been found that downhole drilling parameters, such as the weight on bit, the torque on bit, rotary speed, and axial-bit vibrations, can be implemented as kick-indicators for earlier kick-detection techniques The most significant new finding of the study is the damping behaviour of drilling vibrations, which ranges between 33 – 89%, due to the gas influx. These kick-indicator parameters may be coupled with surface systems, such as a standpipe, to enhance, validate and confirm gas kick occurrence during drilling. These findings not only advance the reliability of kick detection operation but can be used to validate a flow-detection technique, such as in an MPD early kick detection system. A Bayesian network (BN) model is developed to assess the reliability of an MPD during a kick-control operation using a dynamic annulus pressure control (DAPC) system. It is found that: the estimated reliability of kick control operation increases from 94% to 97% after structural modification of the system; a failure of a managed pressure drilling system can be initiated by any of its components due to their operational interactions and dependencies to function; the failure of any component does not only cause a failure of the kick-control operation but increases the failure likelihood of the dependent components; the modes of failure of an MPD system/operation are non-sequential; and finally, an MPD control system is the most safety-critical components of the system.

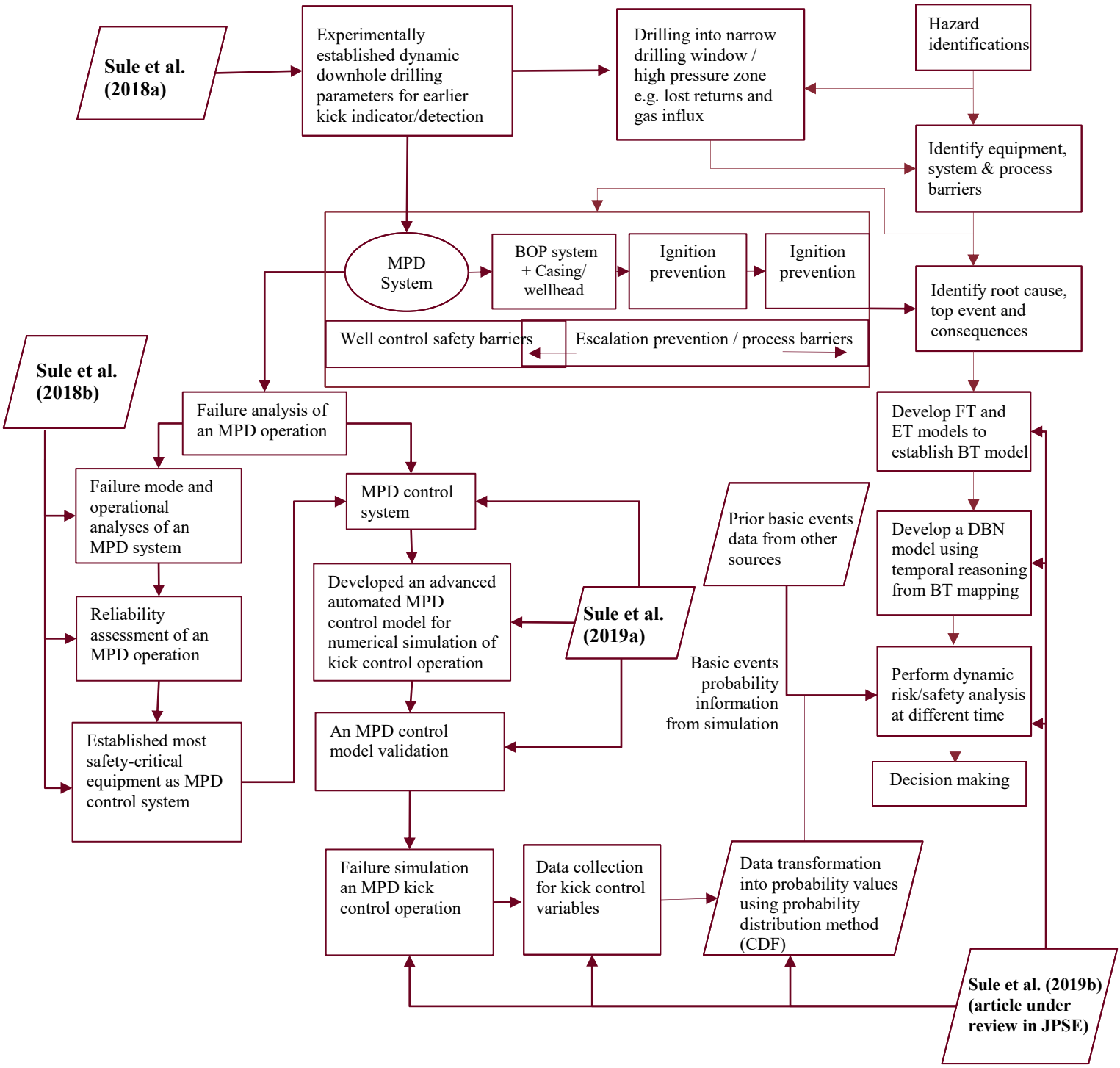

Figure 7.1: Integrated kick detection enhancement with safety and reliability assessment model for a managed pressure drilling in well control operation

Another key novel contribution of this research is a development of a modeling approach to numerically simulate the safety and reliability of an MPD operation to identify, assess, and make a decision that enhances the safety of drilling operation. a two-phase hydraulic flow model is developed

and validated using experimental work and field reports. The improvement in this MPD control model is highlighted by comparing its hydraulic model performance against a single-phase flow hydraulic model and the results show that the single-phase model underestimate key well control parameters, including the kick size, bottomhole pressure, and choke pressure. The kick size is underestimated by about 52 LPM (or ~ 90%), the bottomhole pressure by 3 bars and choke pressure by 2 bars. This is because its two-phase hydraulic model captures the essential aspects of multiphase flow dynamics in reservoir influx. An advanced model predictive controller (NMPC) was implemented on the MPD system. Results show that NMPC structure has a better performance over a proportional integral (PI) controller due to its predictive ability, as well as ability to handle nonlinearity of an MPD system process. The controller also offers enhanced safety to the system by implementing operational constraints on the system.

The MPD system equipped with NMPC was used to simulate the failure and risk scenarios of an MPD control operation. Thus, the simulated MPD system was used in developing a dynamic blowout risk model (DBRM) to simulate blowout scenarios and assess the safety of the well control during a managed pressure drilling operation.

The DBRM involves three key modeling processes: a dynamic Bayesian network (DBN) model, a numerical simulation of an MPD kick control operation, and dynamic risk analysis. The DBN is a temporal extension of a static BN that explicitly capture the modeling changes in events likelihood or relationship over time. Furthermore, the DBRM implements a novel approach for simulating an MPD failure and blowout risk assessment through varying MPD kick control parameters/variables in a simulated system. These are instrumental for setting the safe/failure operating thresholds for an MPD control system. The kick-control variables include the *BHP setpoint*, *backpressure, kick size,*

and RCD/drilling choke pressure limits. This is a highly useful risk assessment tool to run a prediction and a diagnostic analysis of an MPD operation over time for a safe decision making. The DBRM has been successfully applied to assess the dynamic risk of blowout scenarios in an MPD operation based on a case study from the Amberjack field in the Gulf of Mexico, and the results consistently mirror the drilling scenarios experienced in the case study.

7.2 Recommendations

Following future studies are recommended:

i. **Early kick detection system:** In this Ph.D. research, several downhole drilling parameters have been found to confirm a gas kick occurrence in real-time, given their unique responses to a gas kick. For example, when a gas kick is experienced in the wellbore, a rotary speed is seen to increase while the weight on bit, torque on bit and axial vibration of the bit are seen to decrease. Another important gas kick-indication is the damping effects of the drilling vibrations due to a gas influx. Thus, incorporating these downhole drilling parameters data, in real-time, to the flow data being processed in the MPD control system may not only enhance the earlier kick detection operation but also may be used to validate kick occurrence. Figure 7.2 illustrates the architecture of this recommended concept, whereby the downhole drilling parameters being monitored are interfaced with the flow monitoring at the surface and then fed into the MPD control module to perform the analysis. The conceptual illustration presented in Figure 7.2 is only focusing on the data transmission components of an MPD operation. This enhanced kick detection system may involve a redesign of the control algorithm in the MPD controller to implement both the downhole drilling parameters and flow data information to evaluate kick detection operation. Thus, the controller may base its kick-

detection evaluation primarily on the downhole drilling parameters or on both the downhole drilling parameters and flow data.

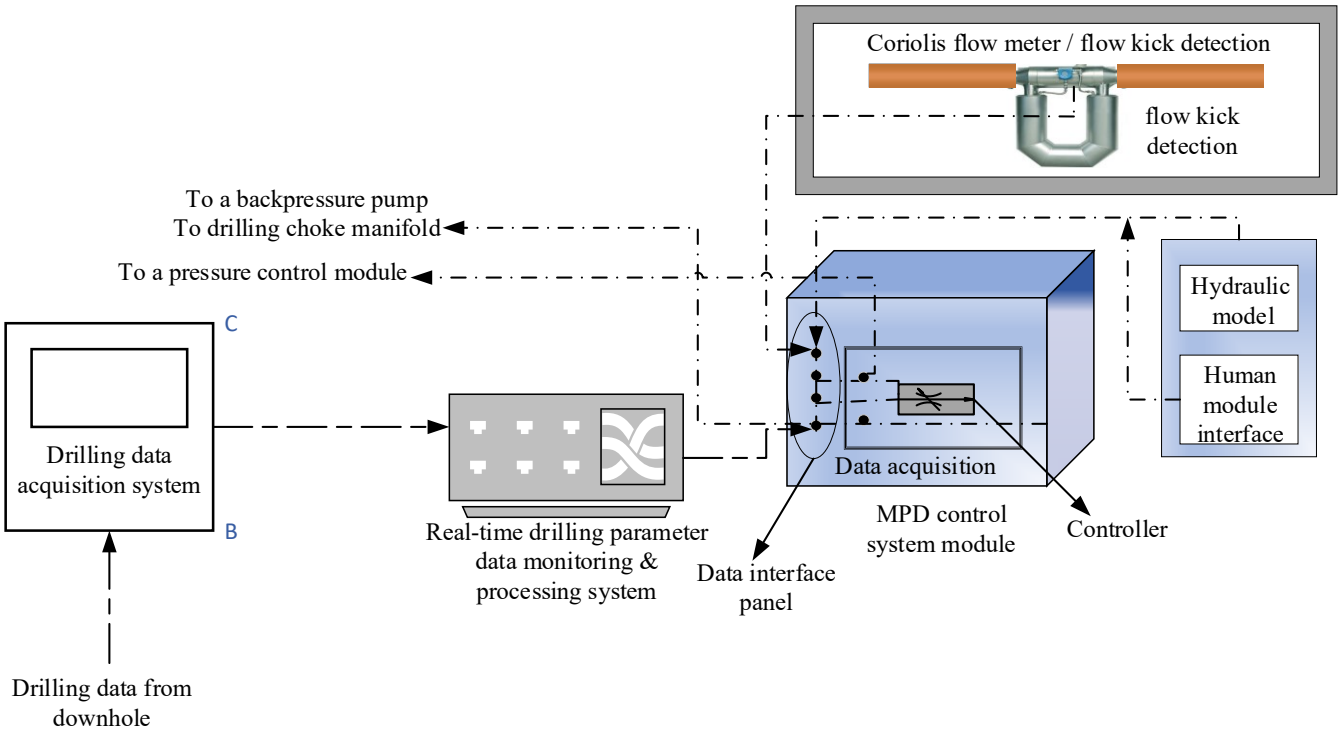

Figure 7.2: A recommended concept for an enhanced earlier kick detection (EKD) in an MPD system

ii. **Investigation of a PMCD and DGD operations for safety and reliability assessment**. Given the efforts to develop a safety and a reliability assessment tool for a managed drilling operation, this research has focused only on the constant bottomhole pressure (CBHP) technique of an MPD. Although other MPD techniques, including pressurized mud cap drilling (PMCD) and dual gradient drilling (DGD), implement the DAPC system described in this work, with additional specified tools and design configurations suitable to accomplish their applications. For instance, the PMCD technique, which is suited for a fractured carbonate reservoir where a total mud loss is expected, relies on all MPD key equipment, including an RCD and MPD control system, but also requires different operation and configuration

compared to the CBHP technique. Therefore, the work that has been done in this research may be built upon to investigate the PMCD and DGD operations in a future study.

iii. **Reliability assessment of the Weatherford's MicroFlux® MPD system and the Halliburton's GeoBalance® MPD system**

Because the DAPC system, which uses @balance control service, is a Schlumberger MPD system, a future study involving the analyses of the Weatherford's MicroFlux® MPD system and the Halliburton's GeoBalance® MPD system may be desirable to formulate broader conclusions on safety and reliability of MPD operations.

iv. **Field testing and implementation of the NMPC control model developed in this research work**

The nonlinear model predictive controller (NMPC) is still evolving in drilling automation where a PID controller, which is best suited for a linear system, is still a commonly use controller scheme for an MPD control system. Therefore, a future study focusing on performing field testing and implementation of an NMPC control model developed in this research work may be explored.

v. **Implementation of two-phase hydraulic and heat transfer models in an MPD control model.**

Because the MPD hydraulic model implemented in this research assumed that the heat transfer process is negligible in the well, its application is limited to a non-high temperature high-pressure well. Therefore, a future study on hydraulic model that does not neglect or

ignore the temperature transient effects in the well may be explored so that the MPD control model can be applied in high-temperature high-pressure wells.

References

Aarsnes U.J.F., Açıkmeşe B., Ambrus A., and Aamo O.M. (2016). Robust controller design for automated kick handling in managed pressure drilling. Journal of Process Control. Vol. 47. Pp 46-57. https://doi.org/10.1016/j.jprocont.2016.09.001

Aarsnes U.J.F., Ambrus A., Di Meglio F., Vajargah A.K., Aamo O.M., and van Oort E. (2016). A simplified two-phase flow model using a quasi-equilibrium momentum balance. International Journal of Multiphase Flow, Vol. 83. Pp 77-85. https://doi.org/10.1016/j.ijmultiphaseflow.2016.03.017

Aarsnes U.J.F., Di Meglio F., Evje S., Aamo O.M., (2014). Control-oriented drift-flux modeling of single and two-phase flow for drilling. ASME. Dynamic Systems and Control Conference, San Antonio, Texas, USA, October 22–24, Vol. 3. http://dx.doi.org/10.1115/DSCC2014-6121

Abimbola, M., Khan, F., and Khakzad, N. (2014). Dynamic safety risk analysis of offshore drilling. Journal of Loss Prevention in the Process Industries, 30, 74-85.

Abimbola, M., Khan, F., Khakzad, N., and Butt, S. (2015). Safety and risk analysis of managed pressure drilling operation using Bayesian network. Safety Science, 76, 133-144. https://doi.org/10.1016/j.ssci.2015.01.010

Ahmed, M. A., Hegab, O.A., Sabry, A. (2016). Early detection enhancement of the kick and near-balance drilling using mud logging warning sign. Egyptian Journal of Basic & Applied Science. 3 (1), 85–93. http://dx.doi.org.qe2a-proxy.mun.ca/10.1016/j.ejbas.2015.09.006

Aldred, W., Cook, J., Bern, P., Carpenter, B., Hutchinson, M., Lovell, J., Rezmer-Cooper, I., Leder, P.C. (1998). Using Downhole Annular Pressure Measurements to Improve Drilling Performance. Oilfield Review. URL: http://www.slb.com/~/media/Files/resources/oilfield_review/ors98/win98/using.pdf [Accessed: November 12, 2016].

Ambrus A.M., van Oort E., and Fernandez B. (2017). Modeling and Control of Managed Pressure Drilling Operations. Ph.D. Dissertation, The University of Texas at Austin. URL: https://repositories.lib.utexas.edu/handle/2152/54113 [Accessed: June 20, 2018]

Amin A. (2017). Design, Development and Control of a Managed Pressure Drilling Setup. Master's Thesis. Faculty of Engineering and Applied Science, Memorial University of Newfoundland. URL: http://research.library.mun.ca/12806/1/thesis.pdf

Amin M.T., Khan F., and Imtiaz S. (2018). Dynamic availability assessment of safety critical systems using a dynamic Bayesian network. Reliability Engineering & System Safety. Vol. 178, pp 108-117. https://doi.org/10.1016/j.ress.2018.05.017

Barua S., Gao X., Pasman H., and Mannan M.S. (2016). Bayesian network based dynamic operational risk assessment. Journal of Loss Prevention in the Process Industries. Vol. (41), pp 399-410. https://doi.org/10.1016/j.jlp.2015.11.024.

Bhagwat S.M. and Ghajar A.J. (2014). A flow pattern independent drift flux model based void fraction correlation for a wide range of gas–liquid two phase flow. International Journal of Multiphase Flow. Vol. 59, pp 186-205. https://doi.org/10.1016/j.ijmultiphaseflow.2013.11.001.

Bhandari J., Abbassi R., Garaniya V., and Khan F. (2015). Risk analysis of deepwater drilling operations using Bayesian network, Journal of Loss Prevention in the Process Industries, Vol.38, pp 11-23. https://doi.org/10.1016/j.jlp.2015.08.004.

Birkeland T., Kårstad E., and Vaishampayan R. (2009). Automated Well Control Using MPD Approach. Master's Thesis. Faculty of Science and Technology, University of Stavanger, Norway

Bjørkevoll K.S., Anfinsen B.-T., Merlo A., Eriksen N.-H. and Olsen E. (2000). Analysis of extended reach drilling data using an advanced pressure and temperature model. Paper

SPE/IADC 62728 Asia Pacific Drilling Technology, Kuala Lumpur, Malaysia, September 11–30, 2000

Bjørkevoll K.S., Molde D.O., Rommetveit R. and Syltøy S. (2008). MPD operation solved drilling challenges in a severely depleted HPHT reservoir. Paper IADC/SPE 112739 presented at the IADC/SPE Drilling Conference, Orlando, Florida, March 4–6, 2008.

Bjørkevoll K.S., Rommetveit R., Aas I.B., Gjeraldstveit H., and Merlo A. (2003). Transient gel breaking model for critical wells applications with field data verification, Paper SPE/IADC 79843 presented at SPE/IADC Drilling Conference, 19-21 February 2003, Amsterdam, Netherlands

Bobbio, A., Portinale, L., Minichino, M., Ciancamerla, E. (2001). Improving the analysis of dependable systems by mapping fault trees into Bayesian networks. Reliability Engineering & System Safety, 71, 249-260.

Breyholtz Ø., Nygaard G., and Nikolaou M. (2011). Managed pressure drilling using model based predictive control to improve the pressure control during dual-gradient drilling. SPE-124631. SPE Drilling & Completion, 2011. pp 184 -197

Cai B., Liu Y., Liu Z., Tian X., Dong X., and Yu S. (2012). Using Bayesian networks in reliability evaluation for subsea blowout preventer control system. Reliability Engineering & System Safety. Vol. 108. pp 32-41. https://doi.org/10.1016/j.ress.2012.07.006.

Cai B., Liu Y., Zhang Y., Fan Q., Liu Z., Tian X. (2013). A dynamic Bayesian networks modeling of human factors on offshore blowouts, Journal of Loss Prevention in the Process Industries, Vol. 26 (4) pp 639-649. https://doi.org/10.1016/j.jlp.2013.01.001

Center for Chemical Process Safety. (2000). Guidelines for Chemical Process Quantitative Risk Analysis. 2nd ed. American Institute of Chemical Engineers. 3 Park Ave. NY, USA

Chrzanowski W.S., Hergaard A., and Hoffman M. (2011). Managed Pressure drilling from Floaters: Feasibility Studies for Applying Managed Pressure Drilling from a floater on the Skarv/Idun field on the Norwegian continental Shelf by PGNiG Norway AS. Master's Thesis, 2011. Faculty of Science And Technology, University of Stavanger

Chustz M.J., May J., Reitsma D., Fredericks P., Dickinson S., and Smith L.D. (2007). MPD with DAPC system proves successful on Auger TLP redevelopment program in GOM. Drilling Contractors. URL http://www.drillingcontractor.org/dcpi/dc-julyaug07/DC_July07_Auger.pdf [Accessed on February 13, 2016]

Contini, S., Scheer, S. and Wilikens, M. (2000). Sensitivity analysis for system design improvement. Joint Research Centre, Institute for Systems, Informatics and Safety, T.P. 210, I-21020 Ispra (VA) Italy.

Cunningham T.J. and O'Banion T. (2013). Allow Smart Meter Verification to Reduce your Proving and Proof-Test Costs." Micro Motion, Inc. 2013. URL: http://www2.emersonprocess.com/siteadmincenter/PM%20Micro%20Motion%20Documents/Improving-Proof-Test-WP-001540.pdf [Accessed: April 5, 2016]

Deyab S.M., Taleb-berrouane M., Khan F. and Yang M. (2018). Failure analysis of the offshore process component considering causation dependence. Process Safety and Environmental Protection. Vol. 113, pp 220-32. https://doi.org/10.1016/j.psep.2017.10.010.

DiFoggio. R., Blue, D.D. (2012). Early kick detection in an oil and gas well. US Patent 2012/0170406 A1, published July 5. URL: http://www.google.com/patents/US20120170406 [Accessed: November 16, 2016].

Dikis K. and Lazakis I. (2016). Dynamic Risk and Reliability Assessment of Ship Machinery and Equipment. International Society of Offshore and Polar Engineers

Dong C. and Yue H. (2016). Identification of Functional Connections in Biological Neural Networks Using Dynamic Bayesian Networks. IFAC-PapersOnLine. Vol. 49 (26), 178-183. https://doi.org/10.1016/j.ifacol.2016.12.122

Driedger D. J., Kelly S. P., Leggett C., Thain J., and Silva M. (2013). Managed Pressure Drilling Technique Applied in a Kurdistan Exploration Well. Society of Petroleum Engineers. https://doi:10.2118/164403-MS

Duan R. and Zhou H. (2012). A New Fault Diagnosis Method Based on Fault Tree and Bayesian Networks. Energy Procedia,17, Part B, 1376-1382

Evje S. and Wen H. (2015). Global solutions of a viscous gas-liquid model with unequal fluid velocities in a closed conduit. SIAM J. Math. Anal. 47 (1), 381–406. https://doi.org/10.1137/140959353

Ferdous R., Khan F., Veitch B., and Amyotte P.R. (2007). Methodology for Computer-Aided Fault Tree Analysis. Process Safety and Environmental Protection, 87, 217-226

Fredericks P. (2008). Constant Bottom-Hole Pressure with Pressure as a Primary Control. Managed Pressure Drilling. Editors: Rehm B., Schubert J., Haghshenas A., Paknejad A.S., and Hughe J. Gulf Publishing Company, Houston, Texas, USA

Fredericks P. D., Smith L., and Moreau K. J. (2011). ECD Management and Pore Pressure Determination with MPD Improves Efficiency in GOM Well. Society of Petroleum Engineers. doi:10.2118/140289-MS

Fredericks P.D. and Reitsma D. (2006). MPD automation addresses drilling challenges in conventional, unconventional resources. Well Control, Drilling Contractors. URL: http://www.drillingcontractor.org/dcpi/dc-novdec06/DC_Nov07_fredericks.pdf [Accessed on February 13, 2016]

Gabaldon O., Culen M., and Brand P. (2014). Enhancing Well Control Through Managed Pressure Drilling. Offshore Technology Conference. https://doi:10.4043/25256-MS

Gala D.M. and Toralde J.S. (2011) Managed Pressure Drilling 101: Moving Beyond "It's Always Been Done That Way". The Way Ahead. Vol. 7 (1)

Gavrilyuk S. and Fabre J. (1996). Lagrangian coordinates for a drift-flux model of a gas-liquid mixture. Int. J. Multiph. Flow, Vol. 22 (3), pp 453–460.

Godhavn J-M. (2010). Control Requirements for Automatic Managed Pressure Drilling System. SPE-119442-PA, SPE. Vol. 25 (3), pp 336-345

Godhavn J-M., Pavlov A., Kaasa G-O., Rolland N.L (2011). Drilling seeking automatic control solutions. IFAC Proceedings Volumes, Vol. 44 (1), pp 10842-10850

Graham, B., Reilly, W.K., Beinecke, F., Boesch, D.F., Garcia, T.D., Murray, C.A., Ulmer, F. (2011). Deep Water, The Gulf Oil Disaster and the Future of Offshore Drilling. National Commission on the BP Deepwater Horizon Oil Spill and Offshore Drilling. URL: https://www.gpo.gov/fdsys/pkg/GPO-OILCOMMISSION/pdf/GPO-OILCOMMISSION.pdf [Accessed on December 21, 2016].

Grancharova A. and Johansen T.A. (2012) Nonlinear Model Predictive Control. In: Explicit Nonlinear Model Predictive Control. Lecture Notes in Control and Information Sciences, vol. 429. Springer, Berlin, Heidelberg. https://doi.org/10.1007/978-3-642-28780-0_2

Grayson B. and Gans A.H (2012). Closed Loop Circulating Systems Enhance Well Control and Efficiency With Precise Wellbore Monitoring and Management Capabilities. SPE/IADC Conference and Exhibition, Milan, Italy, 20 –21 March 2012

Grüne L. and Pannek J. (2017). Nonlinear Model Predictive Control. Theory and Algorithms. 2nd Ed. Springer International Publishing Switzerland. ISBN 978-3-319-46024-6

Haghshenas, Arash & Saman Paknejad, Amir & Rehm, Bill & Schubert, Jerome. (2013). The Why and Basic Principles of Managed Well-Bore Pressure. Managed Pressure Drilling. 1-38. https://10.1016/B978-1-933762-24-1.50007-3

Halliburton, Customer Guide to Managed Pressure Drilling (2014). URL: https://www.halliburton.com/content/dam/ps/public/ts/contents/Brochures/web/GBA-CustomerGuide.pdf [Accessed on October 21, 2017].

Handal A. and Øie S. (2013). Safety Barrier Analysis and Hazard Identification of Blowout Using Managed Pressure Drilling Compared with Conventional Drilling. SPE/IADC Conference and Exhibition, San Antonio, USA, 164564

Hannegan D. M. (2006). Case Studies-Offshore Managed Pressure Drilling. Society of Petroleum Engineers. https://doi:10.2118/101855-MS

Hannegan D.M., Bailey T.F. , Jacobs M.T. , and White N.A. (2017). *US Patent No US 9845653B2*. Retrieved from Google Patent. URL: https://patentimages.storage.googleapis.com/a7/6d/01/066b2daf5bf4b8/US9845653.pdf [Accessed: October 3, 2018]

Hauge E., Aamo O.M., and Godhavn J.-M. (2012). Model-based estimation and control of in/out-flux during drilling. American Control Conference (ACC), Montreal, QC. pp. 4909-4914. doi:10.1109/ACC.2012.6315027

Hauge E., Aamo O.M., Godhavn J.-M., Nygaard G. A. (2013) novel model-based scheme for kick and loss mitigation during drilling, Journal of Process Control, Vol. 23 (4). pp 463-472

Haver, S., Larsen, K., & Meling, T. S. (20010). Reliability Assessment of a Mooring System. International Society of Offshore and Polar Engineers.

Hulst J. (2006). Modeling physiological processes with dynamic Bayesian networks. Master Thesis. Faculty of Electrical Engineering, Mathematics and Computer Science, Delft University of Technology.

IADC Drilling Manual (2014). Sample pages available on URL: http://www.iadc.org/wp-content/uploads/2015/08/preview-mpub.pdf [Accessed on June 21, 2016]

International Association of Drilling Contractors (2015). IADC Deepwater Well Control Guideline. 2nd edition. Houston, Texas USA

Jon Espen Skogdalen J.E. and Vinnem J.E.(2011). Quantitative risk analysis offshore-Human and organizational factors, Reliability Engineering & System Safety, Vol. 96 (4), pp 468-479, https://doi.org/10.1016/j.ress.2010.12.013.

Kaasa G., Stamnes O.N., Imsland L., Aamo O.M. (2011), Intelligent Estimation of Downhole Pressure Using a Simple Hydraulic Model. IADC/SPE Managed Pressure Drilling and Underbalanced Operations Conference and Exhibition held in Denver, Colorado, USA, Apr 5–6

Khakzad N., Khan F., and Amyotte P. (2013). Dynamic safety analysis of process systems by mapping bow-tie into Bayesian network. P. Saf. and Env. Protec. 91(1-2), pp 46-53.

Khakzad N., Khan F., and Amyotte P. (2013). Quantitative risk analysis of offshore drilling operations: A Bayesian approach. Safety Science,7, 108-117

Khakzad, N., Khan, F., and Amyotte, P. (2011). Safety analysis in process facilities: Comparison of fault tree and Bayesian network approaches. Reliability Engineering & System Safety, 96(8), 925-932. https://doi.org/10.1016/j.ress.2011.03.012

Khan F.I, Sadiq R., and Husain T.(2002). Risk-based process safety assessment and control measures design for offshore process facilities. Journal of Hazardous Materials. Vol. 94 (1), pp 1 – 36. https://doi.org/10.1016/S0304-3894(02)00004-3.

Khan, F. (2001). Use of maximum credible accident scenarios for realistic and reliable risk assessment. Chemical Engineering Progress, Volume 11, pp. 56-64.

Khorshidan, H. (2012). Phenomena Affecting Penetration Mechanisms of Polycrystalline Diamond Compact Bits. Master Thesis, Faculty of Engineering and Applied Science, Memorial University of Newfoundland, St. John's, NL. http://research.library.mun.ca/id/eprint/2357

Kok M. V. and Tercan E. (2012). Managed Pressure Drilling Techniques, Equipment, and Applications. Energy Sources, Part A: Recovery, Utilization, and Environmental Effects, 34 (7), 591-601. https://doi.org/10.1080/15567036.2010.516319

Korb K.B. and Nicholson A.E (2011). Bayesian Artificial Intelligence. 2nd Ed. Computer Science and data Analysis Series. CPC Press, Taylor and Francis Group. FL, USA 37-38.

Kuznetsov D.S., Cheremisin A.N., Chesnokov A.A., and Golovin S.V. (2010) Advanced Horizontal Well Model. Paper SPE 127742 presented at SPE North Africa Technical Conference and Exhibition, Cairo, Egypt, February 14-17.

Lage A. C. V. M., Nakagawa E. Y., and Cordovil A. G. D. P. (1994). Well Control Procedures in Deep Water. Society of Petroleum Engineers. doi:10.2118/26952-MS

Lai, F.S., Shenoi, S. and Fan, T.L. (1993). Fuzzy fault tree analysis theory and applications, Engineering Risk and Hazard Assessment, 1, 117–137.

Langseth, H. and L. Portinale (2007). Bayesian networks in reliability. Reliability Engineering and System Safety 92 (1), 92–108. https://doi.org/10.1016/j.ress.2005.11.037

Leu S.S. and Chang C.M. (2013). Bayesian-network-based safety risk assessment for steel construction projects. Accident Analysis & Prevention, 54, 122-133

Li Q. and Kamel M. (2016). Robustness Analysis and Tuning for Pressure Control in Managed Pressure Drilling. IFAC-PapersOnLine. Vol. 49 (7). pp 556–561

Luque J. and Straub D. (2019). Risk-based optimal inspection strategies for structural systems using dynamic Bayesian networks, Structural Safety. Vol. 76 pp 68-80. https://doi.org/10.1016/j.strusafe.2018.08.002

Malloy K.P and McDonald P. (2008). A Probabilistic Approach to Risk Assessment of Managed Pressure Drilling in Offshore Applications. DOI MMS report - Joint Industry Project DEA155.

Manum H. and Hjulstad Å.(2018). *US Patent No US 20180245412*. Retrieved from Google Patent. URL: https://patentimages.storage.googleapis.com/18/41/79/d82b9b1ee7c578/US20180245412A1.pdf [Accessed: September 3, 2018]

Montani S., Portinale L., and Bobbio A. (2005). Dynamic bayesian networks for modeling advanced fault tree features in dependability analysis. European Safety and Reliability Conference. Tri City Polland 27-30 June 2005. p 1414-1422.

Morari M. and Maeder U. (2102) Nonlinear offset-free model predictive control. Automatica. Vol. 48 (9). pp 2059-2067. https://doi.org/10.1016/j.automatica.2012.06.038

Murphy K. (2002). Dynamic Bayesian Networks. Representation, Inference and Learning. PhD Thesis, UC Berkley

Nandan A. and Imtiaz S. (2016). Nonlinear Model Predictive Controller for Kick Attenuation in Managed Pressure Drilling. IFAC-PapersOnLine, Vol.49, (7) pp 248-253. https://doi.org/10.1016/j.ifacol.2016.07.268.

Nas S. W. (2010). Deepwater Managed Pressure Drilling Applications. Society of Petroleum Engineers. https://doi:10.2118/132049-MS

Nayeem, A.A., Ramachandran, V., Khan, F. (2016). Monitoring of down-hole parameters for early kick detection. Journal of Loss Prevention in the Process Industries. Vol. 40, 43-54. http://dx.doi.org.qe2a-proxy.mun.ca/10.1016/j.jlp.2015.11.025

Nygaard, G., Nævdal, G. (2006). Nonlinear model predictive control scheme for stabilizing annulus pressure during oil well drilling. J. Process Contr. 16 (7), 719–732. https://doi.org/10.1016/j.jprocont.2006.01.002.

OREDA (Offshore Reliability Data Handbook), 2002. SINTEF Industrial Management.

Oyovwevotu J., Low E., and Nas, S. (2014). Improving Drilling-Operations Efficiency on an Ultranarrow-Margin High-Pressure/ High-Temperature Managed-Pressure-Drilling Well With Use of a Mud Cap. Society of Petroleum Engineers. https://doi:10.2118/167985-PA

Park, J., 2018. Nonlinear Model Predictive Control for a Managed Pressure Drilling with High-fidelity Drilling Simulators. All Theses and Dissertations. Brigham Young University. https://scholarsarchive.byu.edu/etd/6792.

Petersen J., Bjørkevoll K.S. and Lekvam K. (2001). Computing the danger of hydrate formation using a modified dynamic kick simulator. Paper PSE/IADC 67749 presented at the SPE/IADC Drilling Conference, Amsterdam, Netherlands, February 27 – March 1

Petersen J., Rommetveit R W., Bjørkevoll K.S. and Frøyen J. (2008). A general dynamic model for single and multi-phase flow operations during drilling, completion, well control and intervention. Paper IADC/SPE 114688 presented at Jakarta, Indonesia, August 25–27

Phillipa G., Navendu J., and Nachiappan N. (2011). Understanding Network Failures in Data Centers: Measurement, Analysis, and Implications. SIGCOMM'11, August 15-19, 2011, Toronto, Ontario, Canada. URL: http://research.microsoft.com/en-us/um/people/navendu/papers/sigcomm11netwiser.pdf [accessed December 12, 2016]

Pui G., Bhandari J., Arzaghi E., Abbassi R., Garaniya V. (2017). Risk-based maintenance of offshore managed pressure drilling (MPD) operation, Journal of Petroleum Science and Engineering, Vol. 159, pp 513-521. https://doi.org/10.1016/j.petrol.2017.09.066.

Rathnayaka, S., Khan, F., and Amayotte, P. (2013). Accident modeling and risk assessment framework for safety-critical decision-making: Application to deepwater drilling operation. Proceedings of the Institution of Mechanical Engineers, Part O: Journal of Risk and Reliability, 227(1), 86-105

Rausand M. and Høyland A. (2004) System Reliability Theory: Models, Statistical Methods, and Applications, 2nd Ed. John Wiley & Sons, Inc

Reyes N. R. (2017). Bit-rock Interaction in Rotary Drilling: Numerical and Experimental Study. Master Thesis, Faculty of Engineering and Applied Science, Memorial University of Newfoundland, St. John's, NL.

Rice W. E., Burris G. D., and Johnson B. C. (1987). Well Control Insurance: An Overview and Outlook. Society of Petroleum Engineers. doi:10.2118/16095-MS

Rohani M.R. (2012). Managed-pressure drilling; techniques and options for improving operational safety and efficiency. Petroleum & Coal, 54 (1), 24-33

Rommetveit R. and Vefring E.H. (1991). Comparison of results from an advanced gas kick simulator with surface and downhole data from full scale gas kick experiments in an inclined well. Paper SPE 22558 was presented at the 66th Annual Technical Conference and Exhibition, Dallas, Texas, October 6–9.

Schubert, J.J., Wright, J.C. (1998). Early Kick Detection Through Liquid Level Monitoring in the Wellbore. Presented at IADC/SPE Drilling Conference held in Dallas, Texas. 3-6 March. https://doi-org.qe2a-proxy.mun.ca/10.2118/39400-MS

Smith K.L., Gault A.D., Witt D.E., and Weddle P.E (2001). SubSea MudLift Drilling Joint Industry Project: Delivering Dual Gradient Technology to Industry. Presented at the SPE. Annual Technical Conference and Exhibition, New Orleans, Louisianna, USA, 30 September–3 October. SPE-71357. https://doi.org/10.2118/71357-MS

Stamnes Ø.N., Aamo O.M., Kaasa G.(2011).Redesign of adaptive observers for improved parameter identification in nonlinear systems. Vol. 47 (2). pp 403-410 https://doi.org/10.1016/j.automatica.2010.11.005.

Stamnes Ø.N., Zhou J., Kaasa G-O., and Aamo O.M. (2008). Adaptive Observer Design for the Bottomhole Pressure of a Managed Pressure Drilling System. Proceedings of the 47th IEEE Conference on Decision and Control Cancun, Mexico, Dec. 9-11, . pp 2961-2966

Stødle T.O., Nygaard G.H, and BG Norge S.N. (2013). Managed Pressure Drilling from Floaters – Existing Technology & Where do we go from here. Master Thesis. Faculty of Science and Technology, University of Stavanger. URL: http://brage.bibsys.no/xmlui/bitstream/handle/11250/183534/Stodle.pdf?sequence=1 [Accessed on February 5, 2016]

Sule I., Imtiaz S., Khan F., Butt S. (2019). Nonlinear model predictive control of gas kick in a managed pressure drilling system, Journal of Petroleum Science and Engineering, Vol. 174 pp 1223-1235. https://doi.org/10.1016/j.petrol.2018.11.046

Sule, I.O., Khan, F. & Butt, S. (2018a). Experimental investigation of gas kick effects on dynamic drilling parameters. J Petrol Explor Prod Technol. https://doi.org/10.1007/s13202-018-0510-z

Sule, I.O., Khan, F. Yang M., & Butt, S. (2018b). Kick control reliability analysis of managed pressure drilling operation. J. Loss Prev. Pro Ind. Vol. 52 pp. 7–20. https://doi.org/10.1016/j.jlp.2018.01.007

Terwogt J. H., Mäkiaho L. B., van Beelen N., Gedge B. J., and Jenkins J. (2005). Pressured Mud Cap Drilling from A Semi-Submersible Drilling Rig. Society of Petroleum Engineers. https://doi:10.2118/92294-MS

Trivedi, P.P (2014). Innovative Kick Detection System for HP/HT Ultradeepwater Wells Using a Section of the BHA. Paper presented at the Offshore Technology Conference held in Houston, Texas, USA. 5–8 May. https://doi-org.qe2a-proxy.mun.ca/10.4043/25074-MS

Vajargah, A.K, van Oort, E. (2015). Early kick detection and well control decision-making for managed pressure drilling automation. Journal of Natural Gas Science and Engineering. 7 (1), 354–366. http://doi.org.qe2a-proxy.mun.ca/10.1016/j.jngse.2015.08.067

Velmurugan, N., Bansal, G., Sharma, T., Gandhi, R. (2015). WellCON: An Early Kick Detection System. SPE. Paper presented at Abu Dhabi International Petroleum Exhibition and Conference held in Abu Dhabi, UAE, 9-12 November. https://doi-org.qe2a-proxy.mun.ca/10.2118/177670-MS

Vesely W., Stamatelatos M., Dugan J., Minarick J., and Railsback J. (2002). Fault Tree Handbook with Aerospace Applications. NASA office of Safety and Mission Assurance, Washington D.C., USA

Vieira P., Arnone M. A., Cook I., Moyse K., Haojie H. W., Qutob H. H., Yuesheng C., and Qing, C. (2008). Constant Bottomhole Pressure: Managed-Pressure Drilling Technique Applied in an Exploratory Well in Saudi Arabia. Society of Petroleum Engineers. https://doi:10.2118/113679-MS

Wu S., Zhang L., Zheng W., Liu Y., and Lundteigen M.A. (2016). A DBN-based risk assessment model for prediction and diagnosis of offshore drilling incidents. Journal of Natural Gas Science and Engineering. Vol.34, pp 139-158. https://doi.org/10.1016/j.jngse.2016.06.054

Zan K. and Bicke J.E (2014). Managed Pressure Drilling Probabilistic Risk Analysis: An Illustration. OTC-25290-MS, Houston, Texas, USA, 5–8 May 2014.

Zarei E., Azadeh A., Khakzad N., Aliabadi M.M., and Mohammadfam I. (2017). Dynamic safety assessment of natural gas stations using Bayesian network. Journal of Hazardous Materials. Vol. 321, 830–840

Zhang Z. (2017). Development and characterization of synthetic rock-like materials for drilling and geomechanics experiments. Master Thesis, Faculty of Engineering and Applied Science, Memorial University of Newfoundland, St. John's, NL.

Zhou J. and Nygaard G. (2011). Automatic model-based control scheme for stabilizing pressure during dual-gradient drilling. Journal of Process Control Vol. 21. pp 1138–1147

Zhou J., Gravdal J.E., Strand P., and Hovland S. (2016). Automated Kick Control Procedure for an Influx in Managed Pressure Drilling Operations by Utilizing PWD. Modeling, Identification and Control, Vol. 37 (1), pp. 31-40, ISSN 1890-1328 https://doi:10.4173/mic.2016.1.3

Zhou J., Nygaard G., Godhavn J-M, ¬Breyholtz Ø., and Vefring E.H. (2010). Adaptive Observer for Kick Detection and Switched Control for Bottomhole Pressure Regulation and Kick Attenuation during Managed Pressure Drilling. American Control Conference, pp.3765-3770

Zhu J., Zhang W., and Li. X. (2019). Fatigue damage assessment of orthotropic steel deck using dynamic Bayesian networks. International Journal of Fatigue, Vol. 118. pp 44-53. https://doi.org/10.1016/j.ijfatigue.2018.08.037

Zhu J., Zhang W., and Li. X. (2019). Fatigue damage assessment of orthotropic steel deck using dynamic Bayesian networks. International Journal of Fatigue, Vol. 118. pp 44-53. https://doi.org/10.1016/j.ijfatigue.2018.08.037